Self-Assembled Structures of Stimuli Responsive Polymers and Their Controlled Release Applications

by

Elda Beruhil Adatoz

A Dissertation Submitted to the Graduate School of Sciences and Engineering in Partial Fulfillment of the Requirements for the Degree of Doctor

of Philosophy

in

Biomedical Science and Engineering

KOÇ ÜNİVERSİTESİ

June 16, 2020

Dedicated to my lovely son, Mark Moris Adatoz

ABSTRACT

Self-Assembled Structures of Stimuli-Responsive Polymers and Their Controlled Release Applications

Elda Beruhil Adatoz

Doctor of Philosophy in Biomedical Science and Engineering

June 16, 2020

Self-assembled nanostructures of stimuli-responsive polymers combine the advantages of responding to environmental changes with specific properties of the nano-systems. Effect of various physicochemical factors on self-assembly process is important in designing nano-systems for controlled release applications. This thesis reports the formation and controlled release applications of hydrogen-bonded (H-bonded) self-assembled structures (layer-by-layer (LbL) films or fibers) consisting of a thermo-responsive polymer, poly(2-ethyl 2-oxazoline) (PEOX), and pH-responsive molecules, tannic acid (TA) or malonic acid (MA).

pH-responsive H-bonded LbL assemblies of PEOX and TA restructure in acidic phosphate buffer into pH-responsive fibers. Since H-bonds between PEOX and TA are stable in acidic solutions, the restructuring was attributed to hydrophobicity increase of PEOX in time by $H_2PO_4^-$ ions.

A systematic investigation of the influence of Hofmeister series of salts on the properties of PEOX/TA multilayers was presented. pH stability of the films increased and the film thickness decreased with the anion type in Hofmeister series in direction from kosmotropic (dehydration of polymer chains) to chaotropic anions (direct binding of ion on the chain).

PEOX/TA multilayers as controlled release platforms were demonstrated by using Rhodamine 6G dye molecule. Release was pH and temperature-responsive depending on the ionization of TA and cloud point temperature (T_{cp}) of PEOX. Effect of chemical structure of H-accepting polymer on release was studied by forming poly(N-isopropylacrylamide) (PNIPAM)/TA multilayers which exhibited faster release due to more hydrophobic structure.

Hollow fibers of PEOX/MA formed in aqueous solutions by slow self-assembly. At pH2, hollow fibers formed by H-bonding while at pH4, electrostatic bridging of PEOX chains by MA was dominant. Fiber formation was temperature-responsive depending on T_{cp} of PEOX. The effect of three salts (Na_2CO_3, NaCl, NaSCN) on fiber formation was studied. The potential of fibers in controlled release applications was demonstrated by the release of Ciprofloxacin, a broad-spectrum antibiotic, at pH7.4.

ÖZETÇE

Uyarana Duyarlı Polimerlerin Kendiliğinden Yapılanarak Oluşturduğu Yapılar ve Bu Yapıların Kontrollü Salınım Uygulamaları

Elda Beruhil Adatoz

Biyomedikal Bilimler ve Mühendislik, Doktora

16 Haziran, 2020

Uyaranlara duyarlı polimerlerin kendiliğinden yapılanarak oluşturduğu nano yapılar, çevredeki değişikliklere yanıt verme veya nano-sistemlerin kendilerine ait spesifik özellikleri gibi faydaları birleştirirler. Çeşitli fiziko kimyasal faktörlerin kendiliğinden yapılanma sürecine olan etkisi, kontrollü salınım uygulamalarında kullanılacak olan nano sistemlerin tasarlanabilmesi açısından önemlidir. Bu tez çalışmasında, kendiliğinden yapılanan, hidrojen-bağlı, içeriğinde sıcaklığa duyarlı- poli (2-etil 2-oksazolin) (PEOX)- ve pH'ya duyarlı moleküller - tanik asit (TA) veya malonik asit (MA)- bulunan yapıların (çok katmanlı film veya fiber) oluşumu ve bu yapıların kontrollü salınım uygulamaları rapor edilmiştir.

pH'ya duyarlı, hidrojen bağlı, PEOX ve TA'in oluşturduğu çok katmanlı film yapıları asidik fosfat tampon çözeltisi içerisinde yeniden yapılanarak pH'ya duyarlı fiberlere dönüşür. PEOX ve TA arasındaki hidrojen bağları asidik çözeltilerde stabil olduklarından, yeniden yapılanma çözeltideki $H_2PO_4^-$ iyonlarının PEOX'un hidrofobikliğini zaman içerisinde arttırmasıyla açıklanmıştır.

Hofmeister serisindeki tuzların PEOX / TA çok katmanlı filmlerinin özellikleri üzerindeki etkisi sistematik şekilde araştırılmış ve sunulmuştur. Filmlerin pH'ya karşı olan dayanıklıkları artarken, film kalınlığı, Hofmeister serilerindeki anyon tipine bağlı olarak kosmotropikten

(polimer zinirlerinin dehidrasyonu) kaotropik anyonlara (iyonların polimer zincirlerine direkt bağlanması) doğru azaldı.

Kontrollü salınım platformu olarak PEOX / TA çok katmanlı filmler, Rhodamine 6G boya molekülü kullanılarak gösterildi. Salınım, TA'in iyonizasyonuna ve PEOX 'un kritik sıcaklığına (T_{cp}) bağlı olarak pH ve sıcaklığa duyarlıdır. Hidrojen alıcısı olan polimerin kimyasal yapısının salınım üzerine olan etkisi, poli (N-propil izoakrilamit) (PNIPAM) / TA çok tabakalı filmler oluşturularak inceledi ve bu filmlerin daha hidrofobik yapısından dolayı daha hızlı salınım yaptığı görüldü.

PEOX / MA den oluşan içi boş fiberler, sulu çözeltide yavaşça kendiliğinden yapılanarak oluştu. pH 2 'de içi boş fiberler, hidrojen bağı etkileşimleriyle oluşmuşken, öte yandan pH 4'te bu fiberler MA moleküllerinin köprü görevi görerek, PEOX zincirlerini elektrostatik olarak bağlamasıyla oluşmuştur. Fiber oluşumu, PEOX'un kritik sıcaklığına bağlı olarak sıcaklığa duyarlıdır. Fiber oluşumuna üç tane tuzun (Na_2CO_3, NaCl, NaSCN) etkisi incelenmiştir. Bu fiberlerin kontrollü salınım uygulamalarında olan kullanım potansiyeli, Ciprofloxacin'in, -geniş spektrumlu bir antibiyotiğin, pH 7.4'te salınımıyla gösterilmiştir.

ACKNOWLEDGEMENTS

In this part, I would like to express my gratitude to all people who stand with me and supported me with an eternal sympathy for completing this thesis and important stage of my life.

One of the biggest gratitude goes to my dear advisor of this thesis, Prof. Levent Demirel. I met him in 2016 Spring, in the course taught by himself, “Surface and Interface Properties of Materials”. Together with that one, his course “Physical Chemistry of Polymer Science”, triggered me to take a decision which was one of the most important one in my life. His attitude towards his students and his deep knowledge motivated me to change my PhD thesis topic, even though I passed Qualifier exam in Chemical Engineering. As a result, I pursued my PhD of Biomedical Science and Engineering in his research group and somehow restarted my PhD journey. Prof. Levent Demirel is a great scientist, his questions and perfectionist attitude towards science has shaped my scientist personality and improved me a lot. In that sense, he is “the idol” as a scientist for me. He is not only a great scientist, but also one of the kindest and fairest man that I have met in my life. I am grateful to him for accepting to be my advisor and his continuous support- both professional and emotional- and I feel lucky for doing scientific work together with him.

I would like to thank Dr. Annamaria Miko for her belief in me and continuous motivation to complete my work. In my hard times, whenever I feel worried, she encouraged me a lot. I would like to thank Dr. Pınar Tatar for her productive scientific discussions with me. I would like to thank Dr. Aatif Ijaz for making my contact angle and AFM measurements, but more importantly, his company and joyful friendship in this journey. I would like to thank Dr. Zerrin Altıntaş for her help from the first moment I have joined the group, sincerity and her good heart. She always “got my back” like a bigger sister would do whenever I forget something. Our memories in San Sebastian conference is unforgettable and valuable for me. I would like to thank Dr. Saman Hendessi for the moments that burst us into laugh during those “nights” in lab. We overcame hard times but we also had too much fun together. I am very glad that I have a friend like her. I also thank Dr. Hanan Fael for providing me help whenever I need. Finally, I would like to thank Dr. Gökhan Topçu, Ghazaleh Azizi Saadetlou and Kubilay Şahin for listening me during my thesis presentation rehearsals and giving me recommendations to make my presentation better.

I thank to Dr. Barış Yağcı and Dr. Amir Motallebzadeh for their help to complete the characterization part of my thesis.

I am also grateful to my thesis jury members, Dr. Seda Kızılel, Dr. Uğur Ünal, Dr. Cleva W. Ow-Yang and Dr. Hüseyin Deligöz for accepting to be in my thesis committee, evaluating my thesis and being always very kind to me and responding quickly my countless emails. Especially, Cleva Hoca's SEM analysis of my fibers contributed to my work and my first article a lot.

In this part, I would like to thank all my friends. Without you, I would not be able to "make it" and life would be harder. However, I would like to express my deepest appreciation to Yasemin Demir. She is not only a friend, but even closer than a sister for me. I thank to the day I decided to pursue my undergraduate education in Koc University in 2007 and passed TOEFL in one semester so I could meet her. She is the best thing that Koç University has contributed to me for 12 years. She was always with me in all my important stages and moments of my life (I can't count here all the countless memories), supported me unconditionally and I am grateful for her existence and just being "her". Yasemin's lovely husband, Aral Can Kaymaz, is one of the most intelligent man that I have met in my life. I would be always glad to see their happiness as a couple and believe that in future, we will be sharing best moments together.

Finally, I would like to thank my dear family. I am extremely and eternally appreciative to my parents, Sara and Viktor Beruhil, for their eternal and unconditional love and support. In my whole life, I always feel your support and love deepest in my heart. Your existence always made me to stand strong and confident. You would be always best "mom and dad" to me and I am grateful everyday to be your daughter. I love you too much and I hope that I will do things in life that you would feel proud of me.

Final "thank you" goes to my "other half", soulmate, and my husband, Yasin Adatoz. Without his support, literally I would neither be able to write down these words nor achieve one of the biggest challenging aim of my life, completing this PhD in the times of pandemic. Besides being a great father of our child, he is the most rightful and decent man that I have met in my life. In 15 years, his unconditional and every day growing love made me who I am and even in the darkest times, he never lost faith in me. There are not enough words to describe his contributions in me or the appreciation that I felt because of his existence and love. I love him eternally and my

only hope is that one day, our son Mark, became a man like him. I know that, we will overcome every difficulty in our life together and I will always feel secure and happy beside him.

TABLE OF CONTENTS

Chapter 1: Introduction 1
2.1 Stimuli-responsive polymers 7
2.1.1 pH responsive polymers 8
2.1.2 Tannic acid: a pH responsive polyphenol 10
2.1.3 Temperature responsive polymers 12
2.1.3.1 Polymers exhibiting UCST behavior in water 15
2.1.3.2 Polymers exhibiting LCST behavior in water 17
2.1.4 PNIPAM: a LCST polymer 20
2.1.5 Poly (2-alkyl 2-oxazoline)s (PAOX): LCST polymers 23
2.2 The effect of Hofmeister salt series on the properties of stimuli-responsive polymers 25
2.2.1 Hofmeister salt series 26
2.2.2 Hofmeister salt series and the stability of proteins and macromolecules in aqueous solution 28
2.2.3 Effect of Hofmeister salt series on the LCST of thermo-responsive polymers 32
2.2.4 Hofmeister Salt series and the biological processes 36
2.3 Self-Assembly of polymeric structures 38
2.3.1 Polymeric self-assembled structures 38
2.3.2 Self-assembly via hydrogen bonding 41
2.4 Layer-by-Layer (LbL) Self-Assembly of Stimuli-Responsive Polymers 42
2.4.1 Properties and Methods of LbL Assembly 43
2.4.2 Molecular Interactions Driving LbL Assembly 46
2.4.2.1 Electrostatically Bonded LbL Assembly 46
2.4.2.2 Hydrogen-Bonded (H-bonded) LbL Assembly 51
2.4.2.3 Role of Hydrophobic Interactions in LbL Assembly 60
2.5 Controlled Release Applications of Self-Assembled Systems Based on Hydrogen Bonding 63
2.5.1 Objectives of Controlled Drug Release 63
2.5.2 Drug Release Mechanisms 65
2.5.3 Controlled Drug Release from Hydrogen Bonded LbL Assembly 67
2.5.3.1 pH Triggered Release from Hydrogen Bonded LbL Films 68
2.5.3.2 Temperature Triggered Release from Hydrogen Bonded LbL Films 71

2.5.4 Controlled Drug Release from Electrospun Fibers 73
Chapter 3: Materials and Methods 78
3.1 Chemicals 78
3.2 Characterization Methods 78
3.2.1 Ellipsometer 78
3.2.2 Optical Microscope (OM) 79
3.2.3 Atomic Force Microscopy (AFM) 79
3.2.4 Field Emission Scanning Electron Microscopy (FESEM) 80
3.2.5 Thermogravimetric Analysis (TGA) 81
3.2.6 X-ray Photoelectron Spectroscopy (XPS) 81
3.2.7 Fourier Transform Infrared Spectroscopy (FTIR) 82
3.2.8 Ultra-Violet Visible (UV-Vis) Spectroscopy 82
3.2.9 Contact Angle Measurements 84
3.2.10 Differential Scanning Calorimetry (Nano-DSC) 85
3.2.11 Isothermal Titration Calorimetry (ITC) 87
Chapter 4: Self Assembly and Restructuring of PEOX and TA into Layer-by-Layer Multilayers 90
4.1 Overview 90
4.2 Experimental Details 91
4.2.1 Preparation and Characterization of PEOX / TA Multilayers 91
4.2.2 Preparation and Characterization of PEOX / TA Aqueous Complexes and Aggregates 92
4.2.3 Characterization of Fibers Formed by Restructuring of PEOX / TA Multilayers 92
4.3 Results and Discussion 92
4.3.1 Restructuring of PEOX/ TA LbL Films into Fibers 92
4.3.2 Characterization of Fibers 104
4.4 Conclusion 114
Chapter 5: Effect of Hofmeister Series of Salt on the Properties of Hydrogen Bonded PEOX / TA Multilayers 116
5.1 Overview 116
5.2 Experimental Details 117
5.2.1 Preparation and Characterization of PEOX / TA Multilayers 117
5.2.2 Cloud Point Measurements by Differential Scanning Calorimetry 118
(Nano-DSC) 118

5.2.3 Determination of Interaction Parameters between PEOX and TA by ITC 119
5.3 Results and Discussion 120
5.3.1 Effect of Hofmeister Series of Salts on the Growth of PEOX / TA Multilayers 120
5.3.2 Effect of Hofmeister Series of Salts on the Morphology of PEOX / TA Multilayers ... 131
5.3.3 Nature of Interaction Between PEOX and TA in the Presence of Hofmeister Series of Salts 135
5.3.4 Effect of Hofmeister Series of Salts on the Stability of PEOX / TA Multilayers 138
5.4 Conclusions 146
Chapter 6: Controlled Release Applications of H-Bonded PEOX/TA and PNIPAM/TA Multilayers 148
6.1 Overview 148
6.2 Experimental Details 149
6.2.1 Preparation and Loading of Rhodamine 6G into PEOX/TA and PNIPAM/TA Multilayers 149
6.2.2 Characterization of Release of Rhodamine 6G from PEOX / TA and PNIPAM /TA Multilayers 150
6.3 Results and Discussion 151
6.3.1 Loading of Rhodamine 6G into PEOX / TA Multilayers 151
6.3.2 pH Triggered Release of Rhodamine 6G from PEOX/TA Multilayers 154
6.3.3 Temperature Triggered Release of Rhodamine 6G from PEOX/TA Multilayers 159
6.3.4 Effect of Polymer Hydrophobicity on Release Mechanism for Hydrogen Bonded LbL Films 166
6.3.5 Effect of Number of Bilayers (Film Thickness) on the Release Profile of Rhodamine 6G from PNIPAM / TA and PEOX / TA Multilayers 180
6.4 Conclusions 182
Chapter 7: Self-Assembled PEOX and Malonic Acid Hollow Fibers in Aqueous Solutions 184
7.1 Overview 184
7.2 Experimental Details 186
7.2.1 Formation of Fibers through Self-Assembly of PEOX and Malonic Acid 186
7.2.2 Characterization of Fibers 188
7.3 Results and Discussion 189
7.3.1 Hydrogen Bonded PEOX / Malonic Acid Fibers at pH $<pKa_1 < pKa_2$ 189
7.3.2 Effect of pH on the Formation of Hydrogen Bonded PEOX and Malonic Acid Fibers 193

7.3.3 Effect of Temperature on the Formation of Hydrogen Bonded PEOX and Malonic Acid Fibers 198
7.3.4 Effect of Salt Type on the Formation of Hydrogen Bonded PEOX and Malonic Acid Fibers 201
7.4 Conclusions 205
Chapter 8: Encapsulation and Release of Ciprofloxacin from PEOX / Malonic Acid Fibers 207
8.1 Overview 207
8.2 Experimental Details 208
8.2.1 Preparation of PEOX / MA Fibers 208
8.2.2 Loading and Release of Cipro from PEOX / MA Fibers 209
8.3 Results and Discussion 210
8.3.1 Encapsulation of Ciprofloxacin into PEOX / MA Fibers 210
8.3.2 Release of Ciprofloxacin from PEOX / MA Fibers 215
8.4 Conclusions 218
Chapter 9: Conclusion 220

LIST OF TABLES

Table 2.1**:** Properties of kosmotropic and chaotropic anions and their effects on proteins and macromolecules ……27

Table 4.1: Elemental composition of the fibers as atomic weight % determined by XPS……105

Table 5.1**:** Average BL thickness of PEOX / TA films prepared in the presence of chaotrpic salt solutions as a function of concentration of the salt solutions…….127

Table 5.2**:** T_{cp} of PEOX/TA aqueous solutions with changing TA concentration according to the ratio of PEOX carbonyl groups to TA phenol groups……...142

Table 6.1**:** Summary of the release mechanisms of dye molecules (Rhodamine 6G) from PEOX/ TA multilayers at different pH values……...157

Table 6.2: Thickness (nm) data of Rhodamine 6G loaded PEOX/TA LbL films before and after release……..158

Table 6.3: Summary of the release mechanisms of dye molecules (Rhodamine 6G) from PEOX/ TA multilayers at different pH values at 37°C…….160

Table 6.4: Summary of the release mechanisms of dye molecules (Rhodamine 6G) from PNIPAM/ TA multilayers at different pH values……...172

Table 6.5: Thickness data of Rhodamine 6G loaded 18 BL PNIPAM/TA LbL films before and after release……..174

Table 6.6**:** Thickness data of Rhodamine 6G loaded PNIPAM/TA LbL films before and after release at different conditions……...179

Table 6.7**:** R^2 values for linear fit for the release profile of Rhodamine 6G from PEOX / TA or PNIPAM/TA multilayers having different number of bilayers…….181

Table 7.1: Observation of fiber formation from PEOX and MA solutions prepared at different temperature based on LCST of PEOX (X= no fiber formation)……198

Table 7.2: Thermodynamic parameters (ΔH, ΔS and ΔG) of the interaction between PEOX and MA at different temperature……200

Table 7.3**:** Observation of fiber formation from PEOX and MA mixed solutions prepared in different 0.1 M salt solutions……201

Table 7.4: Thermodynamic parameters (ΔH, ΔS and ΔG) of the interaction between PEOX and MA in the presence of different sodium salts at 25°C……...204

LIST OF FIGURES

Figure 2.1: Chemical structure of tannic acid (TA)……...10

Figure 2.2: Thermodynamic map that predicts the solubility and temperature dependent behavior of polymers in aqueous solution based on the signs of ΔH_{mix} and ΔS_{mix} values……13

Figure 2.3: A sample phase diagram of a polymer which exhibits UCST behavior……15

Figure 2.4: A sample phase diagram of a polymer which exhibits LCST behavior……18

Figure 2.5: Chemical structure of PNIPAM……...21

Figure 2.6: Chemical structure of poly (2-ethyl 2-oxazoline)……...23

Figure 2.7**:** Illustrated scheme of LbL dip coating (immersive assembly) method……45

Figure 3.1: A drop of water on a solid substrate and contact angle (Ɵ) is shown geometrically with Υ_{SV}, Υ_{SL}, Υ_{L} [239]……...84

Figure 4.1: Thickness of PEOX/TA LbL films as a function of number of bilayers for four different films grown to a final thickness of 10 BL (squares), 15 BL (circles), 20 BL (up triangles) and 30 BL (down triangles) at pH 3 in the presence of NaH_2PO_4 solution, together with a 30 BL film grown at pH 3 without NaH_2PO_4 (stars)……94

Figure 4.2: (a) Optical microscope image of the 20 BL PEOX/TA film (5480 mm x 4110 mm), (b) optical microscope image of the 20 BL PEOX/ TA film (548mm x411 mm), (c) atomic force microscope (AFM) height image of the 20 BL PEOX /TA film. Detached part of the film from the surface is shown (d) height profile of the detached part in (c)……95

Figure 4.3: (a) Optical microscope image (5.48 mm x 4.11 mm) of the fibers that were collected from rinse solution (phosphate buffer at pH 3) after PEOX adsorption (b) Optical microscope image (5.48 mm x 4.11 mm) of the fibers that were collected from rinse solution (phosphate buffer at pH 3) after TA adsorption……...96

Figure 4.4: (a), (c) SEM images of 30 BL PEOX/TA film prepared in the presence of $H_2PO_4^-$ anions (b), (d) SEM images of 30 BL PEOX/TA film prepared in the absence of $H_2PO_4^-$ anions...97

Figure 4.5: Optical microscopy images of 30 BL PEOX/TA films grown and kept at various conditions: a-c) 30 BL PEOX/TA film prepared at pH3 phosphate buffer and observed at pH3 in the absence of $H_2PO_4^-$ anions: a) after preparation, b) after 1 day at pH3, c) after 2 days at pH3; d-f) 30 BL PEOX/TA film prepared at pH3 in the absence of $H_2PO_4^-$ anions and observed at pH3 in the presence of H2PO4 - anions: d) after preparation, e) after 1 day at pH3, f) after 2 days at pH3; g-i) 30 BL PEOX/TA film prepared at pH3 in the absence of $H_2PO_4^-$ anions and observed at pH3 in the absence of $H_2PO_4^-$ anions: g) after preparation, h) after 1 day at pH3, i) after 2 days at pH3. All images are 2.74 mm x 2.05 mm ……99

Figure 4.6: Optical microscope images of detached parts of PEOX/ TA LbL film and fibers restructured around these regions. (a) A flaked region of the film and the attached fibers around it (2740 mm x2055 mm). (b) Fibers that were restructured at the gap between the two parts of a uniform film (2740 mm x 2055 mm)……100

Figure 4.7: SEM images of 30 bilayer PEOX/TA LbL film and fiber formed. Scale bar for (a) and (c) are 10 μm. Scale bar for (b) and (d) are 2μm……101

Figure 4.8: pH stability of 30 BL PEOX/TA LbL films grown at pH 3 in the presence (down triangles) and the absence (stars) of NaH_2PO_4. pH stability is shown and plotted as the fraction of the film remained on the substrate as a function of pH of the phosphate buffer…….102

Figure 4.9: Optical microscopy images of restructuring of a PEOX/TA LbL sheet into fibers at pH3 buffer solution: (a) initial sheet, (b) after 1 day, (c) after 2 days, (d) after 3 days, (e) after 4 days, (f) after 5 days. All images are 5480 mm x 4110 m……..103

Figure 4.10: TGA of PEOX (dashed line), TA (dashed dotted line) and dried fibers (solid line)……..104

Figure 4.11: XPS spectrum of dried PEOX/TA fibers. The peaks correspond to C 1s at 286 eV, O 1s at 533 eV and N 1s at 400 eV……....105

Figure 4.12: (a) FTIR data of 30 BL PEOX / TA LbL film (solid line), PEOX (dashed line) and TA (dashed dotted line). (b) FTIR data of dried fibers from restructuring of PEOX / TA multilayers (solid line) with PEOX (dashed line) and TA (dashed dotted line)……...106

Figure 4.13: FTIR spectrum of PEOX/TA complexes with changing PEOX monomer ratio at a fixed concentration of TA showing the shifts in carbonyl (C=O) group of both PEOX and TA…108

Figure 4.15: UV-Visible spectrum of dissolved PEOX/TA fibers at pH 10 (solid line) which confirms the presence of ionized TA in pH 10 solution. The dashed line is the UV Visible spectrum of TA at pH3 (non-ionized) showing a single peak at 276 nm……109

Figure 4.16: FESEM images of dried fibers from restructuring of PEOX / TA multilayers collected from the rinse solutions of 30 BL PEOX / TA LbL film…….110

Figure 4.17: (a), (b) Optical microscopy images of 30 BL PEOX / TA LbL films before putting in under vacuum at 50°C (c), (d) Optical microscopy images of 30 BL PEOX / TA LbL films after putting in under vacuum at 50°C. All images are 5480 mm x 4110 m……...111

Figure 4.18: (a) Contact angle measurements of PEOX / TA LbL films as a function of number of bilayers (b) AFM height image of 10 BL PEOX / TA LbL film (c) AFM height image of 15 BL PEOX / TA LbL film (d) AFM height image of 20 BL PEOX / TA LbL film (e) AFM height image of 30 BL PEOX / TA LbL film……113

Figure 5.1: **(a)** Thickness of PEOX/TA LbL films as a function of number of bilayers for nine different films grown to a final thickness of 10 BL and prepared in the presence of 0.01 M different sodium salts (**b)** Final thickness of 10 BL PEOX/TA LbL films prepared in the presence of 0.01 M different sodium salts……...121

Figure 5.2: Thickness of PEOX/TA LbL films as a function of number of bilayers for nine different films grown to a final thickness of 10 BL. **(a)** Prepared in the presence of Na_2CO_3 at different concentrations **(b)** Prepared in the presence of NaH_2PO_4 at different concentrations **(c)** Prepared in the presence of NaCl at different concentrations……...124

Figure 5.3: Thickness of PEOX/TA LbL films as a function of number of bilayers for nine different films grown to a final thickness of 10 BL. **(a)** Prepared in the presence of $NaNO_3$ at different concentrations **(b)** Prepared in the presence of NaSCN at different concentration……...126

Figure 5.4: Optical microscope images of 10 BL PEOX / TA LbL films prepared in the presence of different salt solutions **(a)** prepared in the presence of 0.05 M Na_2CO_3 **(b)** prepared in the presence of 0.1 M Na_2CO_3 **(c)** prepared in the presence of 0.5 M Na_2CO_3 **(d)** prepared in the

presence of 0.05 M NaH_2PO_4 **(e)** prepared in the presence of 0.1 M NaH_2PO_4 **(f)** prepared in the presence of 1 M NaH_2PO_4 **(g)** prepared in the presence of 0.05 M NaCl **(h)** prepared in the presence of 0.1 M NaCl **(i)** prepared in the presence of 0.5 M NaCl……..128

Figure 5.5: Optical microscope images of 10 BL PEOX / TA LbL films prepared in the presence of different salt solutions **(a)** prepared in the presence of 0.05 M $NaNO_3$ **(b)** prepared in the presence of 0.1 M $NaNO_3$ **(c)** prepared in the presence of 0.5 M $NaNO_3$ **(d)** prepared in the presence of 1 M $NaNO_3$ **(e)** prepared in the presence of 0.05 M NaSCN **(f)** prepared in the presence of 0.1 M NaSCN **(g)** prepared in the presence of 0.5 M NaCl **(h)** prepared in the presence of 1 M NaSCN…….129

Figure 5.6: **(a)** DSC thermogram of PEOX aqueous solution showing LCST transition **(b)** T_{cp} of PEOX solutions as a function of concentration of salt solutions measured by NanoDSC……130

Figure 5.7: FESEM images of 10 BL PEOX/TA LbL films prepared in the presence of salt solutions with different concentrations **a)** 0.05 M Na_2CO_3 **b)** 0.1 M Na_2CO_3 **c)** 0.5 M Na_2CO_3 **d)** 0.05 M NaH_2PO_4 **e)** 0.1 M NaH_2PO_4 **f)** 0.5 M NaH_2PO_4 **g)** 0.05 M NaCl **h)** 0.1 M NaCl **i)** 0.5 M NaCl **j)** 0.05 M $NaNO_3$ **k)** 0.1 M $NaNO_3$ **l)** 0.5 M $NaNO_3$ **m)** 0.05 M NaSCN **n)** 0.1 M NaSCN **o)** 0.5 M NaSCN……...133

Figure 5.8: AFM height image of 10 BL PEOX/TA LbL film **(a)** prepared in the presence of 0.5 M Na_2CO_3 **(b)** prepared in the presence of 0.5 M NaH_2PO_4 **(c)** prepared in the presence of 0.5 M NaCl **(d)** prepared in the presence of 0.5 M $NaNO_3$ **(e)** prepared in 0.5 M NaSCN……134

Figure 5.9: **(a)** ITC data of raw heat rate (µJ/s) with time (s) for the injection of TA (0.0587 mM) to PEOX (0.05 mM) in the absence of any salt **(b)** ITC thermodynamic data of binding of TA at various concentrations (0.294 mM, 0.176 mM and 0.0587 mM) to PEOX (0.05 mM) in the absence of salt……136

Figure 5.10: ITC thermodynamic data of binding of TA (0.0587 mM) to PEOX (0.05 mM) in the absence or presence of various salts (100 mM)…… 138

Figure 5.11: **(a)** pH stability of 10 BL PEOX/TA LbL films grown in the presence of 0.01 M sodium salt solutions that contain different ions from Hofmeister series of salts **(b)** Critical

disintegration pH of the films prepared in the presence of 0.01 M sodium salt solutions that contain different ions from Hofmeister series……...139

Figure 5.12: Critical disintegration pH of 10 BL PEOX/TA multilayers as a function of concentration of sodium salt solutions used during the preparation of films……140

Figure 5.13: pH stability of 10 BL PEOX/TA LbL films grown in the presence of sodium salt solutions at various concentrations **(a)** in the presence of Na_2CO_3 solution at various concentrations **(b)** in the presence of NaH_2PO_4 solution at various concentrations **(c)** in the presence of NaCl solution at various concentrations **(d)** in the presence of $NaNO_3$ solution at various concentrations **(e)** in the presence of NaSCN solution at various concentrations……..141

Figure 5.14: Measured T_{cp} of the PEOX/TA mixture solutions prepared in different 0.1 M salt solutions as a function of pH…….144

Figure 6.1: Calibration curve of aqueous Rhodamine 6G solution in terms of absorbance at 525 nm as a function of concentration as measured by UV-Vis Spectroscopy……152

Figure 6.2: **(a)** UV -Vis spectra of Rhodamine 6G loaded PEOX/TA multilayers having different number of bilayers **(b)** Absorbance at 525 nm of PEOX/TA film on quartz substrate versus number of bilayers of PEOX/TA films……..153

Figure 6.3: pH triggered release profile of Rhodamine 6G from PEOX/TA LbL films formed on quartz substrate at room temperature **(a)** Concentration of the dye (mg/cm^3) remained in the PEOX / TA multilayers versus time (min) **(b)** Fraction of cumulative release of the dye versus time (min)…….155

Figure 6.4: **(a)** FESEM image of the 10 BL PEOX / TA LbL film after Rhodamine 6G is loaded (**b)** FESEM image of the Rhodamine 6G loaded 10 BL PEOX / TA film after release of dye molecules is completed at pH 7 **(c)** FESEM image of the Rhodamine 6G loaded 10 BL PEOX / TA film after release of dye molecules is completed at pH 7.4 **(d)** FESEM image of the Rhodamine 6G loaded 10 BL PEOX / TA film after release of dye molecules is completed at pH 8.5……157

Figure 6.5: Release of Rhodamine 6G from 10 BL PEOX/TA LbL films at 37°C, at pH 6.5, 7.4 or 8.5 **(a)** Concentration remained (mg/cm^3) on film versus time **(b)** Fraction of cumulative release versus time……...160

Figure 6.6: Release of Rhodamine 6G from 10 BL PEOX/TA LbL films at 42°C, at pH 6.5, 7.4 or 8.5 **(a)** Concentration remained (mg/cm^3) on film versus time **(b)** Fraction of cumulative release versus time……...161

Figure 6.7: Release of Rhodamine 6G from 10 BL PEOX/TA LbL films at 62°C, pH 6.5, 7.4 or 8.5 **(a)** Concentration remained (mg/cm^3) on film versus time **(b)** Fraction of cumulative release versus time……...162

Figure 6.8: Release of Rhodamine 6G from 10 BL PEOX/TA LbL films at 75°C, pH 6.5 **(a)** Concentration remained (mg/cm^3) on film versus time **(b)** Fraction of cumulative release versus time……..163

Figure 6.9**:** Release of Rhodamine 6G from 10 BL PEOX/TA LbL films at pH 6.5, different temperatures in terms of fraction of the cumulative release of the dye……..164

Figure 6.10: **(a)** FESEM image of the Rhodamine 6G loaded PEOX / TA film after 180 minutes of release at 37°C, pH 6.5 **(b)** FESEM image of the Rhodamine 6G loaded PEOX / TA film after 180 minutes of release at 37°C, pH 7.4 **(c)** FESEM image of the Rhodamine 6G loaded PEOX / TA film after 180 minutes of release at pH 8.5, 37°C **(d)** FESEM image of the film after 180 minutes of release at 42°C, pH 6.5 **(e)** FESEM image of the film after 180 minutes of release at 42°C, pH 7.4 **(f)** FESEM image of the film after 180 minutes of release at 42°C, pH 8.5. Scale bar is 200 nm for all images……165

Figure 6.11: Thickness of PNIPAM/TA LbL film as a function of number of bilayers grown to a final thickness to 18 BL……167

Figure 6.12**: (a)** UV-Visible spectra of Rhodamine 6G loaded 18BL PNIPAM/TA multilayers as a function of post-treatment time **(b)** Absorbance at 540 nm (maximum peak) of Rhodamine 6G in 18 BL PNIPAM/TA multilayers as a function of loading (post-treatment) time……168

Figure 6.13: **(a)** UV -Vis spectra of Rhodamine 6G loaded PNIPAM/TA multilayers having different number of bilayers **(b)** Absorbance at 530 nm of PEOX/TA films and PNIPAM/TA films deposited on quartz substrate versus number of bilayers that the films have…….169
Figure 6.14: pH triggered release profile of Rhodamine 6G from PNIPAM / TA LbL films formed on quartz substrate at room temperature **(a)** Concentration of the dye (mg/cm^3) remained in the PNIPAM / TA multilayers versus time (min) **(b)** Fraction of cumulative release of the dye versus time (min)……..171

Figure 6.15: pH stability of 18 BL PNIPAM/TA films and 15 BL PEOX/TA films. The fraction of the film remained on the substrate is plotted as a function of pH of phosphate buffer……173

Figure 6.16: (**a)** FESEM image of the 18 BL PNIPAM / TA LbL film after Rhodamine 6G is loaded (**b)** FESEM image of the Rhodamine 6G loaded 18 BL PNIPAM / TA film after release of dye molecules is completed at pH 6.5 **(c)** FESEM image of the Rhodamine 6G loaded 18 BL PNIPAM / TA film after release of dye molecules is completed at pH 7.4……174

Figure 6.17**:** Release of Rhodamine 6G from 18 BL PNIPAM/TA LbL films at 15°C , pH 6.5, 7.4 or 8.5 **(a)** Concentration of the dye (mg/cm^3) remained in the PNIPAM / TA multilayers versus time (min) **(b)** Fraction of cumulative release of the dye versus time (min)……..175

Figure 6.18: (**a)** FESEM image of the 18 BL PNIPAM / TA LbL film after release of Rhodamine 6G is completed at 15°C, pH 6.5 **(b)** FESEM image of the 18 BL PNIPAM / TA LbL film after release of Rhodamine 6G is completed at 15°C, pH 7.4 **(c)** FESEM image of the 18 BL PNIPAM / TA LbL film after release of Rhodamine 6G is completed at 15°C, pH 8.5. Scale bar is 200 nm for all images……176

Figure 6.19: Release of Rhodamine 6G from 18 BL PNIPAM/TA LbL films at 32°C , pH 6.5 or 7.4 **(a)** Concentration of the dye (mg/cm^3) remained in the PNIPAM / TA multilayers versus time (min) **(b)** Fraction of cumulative release of the dye versus time (min)……178
Figure 6.20: Release of Rhodamine 6G from 18 BL PNIPAM/TA LbL films at 37°C , pH 6.5 or 7.4 **(a)** Concentration of the dye (mg/cm^3) remained in the PNIPAM / TA multilayers versus time (min) **(b)** Fraction of cumulative release of the dye versus time (min)……178

Figure 6.21**:** Release profile of Rhodamine 6G from PEOX/ TA or PNIPAM/TA LbL films having different number of bilayers formed on quartz substrate at RT, pH 7.4 **(a)** Concentration of dye remained on the film versus time **b)** Fraction of cumulative release versus time……181

Figure 7.1: **(a)** Chemical structure of poly (2-ethyl 2-oxazoline) (PEOX) **(b)** Chemical structure of malonic acid (MA) **(c)** Schematic bridging of PEOX and MA via H-bonds…….186

Figure 7.2: **(a) and (b)** Optical microscope images of PEOX / MA fibers formed at pH 2 after 21 days **(c)** SEM images of the fibers shown in (a) and (b) scale bar= 1 µm **(d)** IR data of PEOX, MA and dried fibers of PEOX / MA formed at pH 2……190

Figure 7.3: **(a)** IR data of PEOX/MA blends. PEOX/MA mole ratio was changed from 1:0.1 to 1:1 (the direction of the curved arrows). **(b)** TGA data of PEOX/MA fibers formed in aqueous solution at pH 2, PEOX and MA…….....191

Figure 7.4: **(a), (b), (c)** ITC data of the interaction between MA (2.4 mM, pH2.5) to PEOX (0.05 mM, pH2.5) at 25^{o}C. **(a)** Raw data **(b)** Independent Model fit (solid line) corresponding to n = 4.06; ΔH = -49.39 kJ/mol; ΔG = -24.83 kJ/mol; ΔS = -82.37 J/mol-K. **(c)** Heat in kJ/mol of injectant. **(d)** ITC data for addition of MA (2.4 mM, pH2.5) to pH 2.5 HCl (aq) at 25 ^{o}C…….193

Figure 7.5: **(a)** SEM image of the PEOX/MA fibers at pH 2 (**b)** SEM image of the PEOX/MA fibers at pH 4 **(c)** SEM image of the PEOX/MA fibers at pH 7. Scale bar of (a) and (b) is 200 nm and (c) is 1 µm. **(d)** AFM height image of the PEOX/MA fibers at pH 2 **(e)** AFM height image of the PEOX/MA fibers at pH 4 **(f)** AFM height image of the PEOX/MA fibers at pH 7 **(g)** AFM height profiles of the fibers in (d), (e) and (f)……195

Figure 7.6: **(a)** IR data of dried PEOX/MA fibers formed at pH 2 and at pH 4 together with that of PEOX and MA **(b)** TGA data of dried PEOX/MA fibers formed at pH 2 and at pH 4 together with that of PEOX and MA…….....196

Figure 7.7: **(a)** Raw ITC data of the interaction between MA (2.4 mM, pH2.5) to PEOX (0.05 mM, pH2.5) at 6^{o}C. **(b)** Released heat versus mole ratio (MA / PEOX) of the interaction between MA (2.4 mM, pH2.5) and PEOX (0.05 mM, pH2.5) at 6^{o}C. Curve fitting is made according to independent binding model and ΔH, ΔS and ΔG values are -37.26 kJ/mole, -39.42 J / mole K and -26.25 kJ/ mole…….200

Figure 7.8: **(a), (b)** SEM images of the fibers formed in 0.1 M NaSCN solution at pH 2. Scale bar for (a) and (b) is 1 µm. **(c)** SEM images of the fibers formed in 0.1 M Na_2CO_3 solution at pH 4 **(d)** SEM images of the fibers formed in 0.1 M NaCl at pH4 **(e)** SEM images of the fibers formed in 0.1 M NaSCN at pH 4. Scale bar for (a) and (b) is 1 µm. Scale bar for (c), (d) and (e) is 2 µm….202

Figure 7.9: **(a), (b) and (c)** Raw ITC data of the interaction between MA (2.4 mM, pH2.5) to PEOX (0.05 mM, pH2.5) in the presence of Na_2CO_3 (a), NaCl (b) and NaSCN (c). **(d), (e) and (f)** Released heat versus mole ratio (MA / PEOX) of the interaction between MA (2.4 mM, pH2.5) and PEOX (0.05 mM, pH2.5) in the presence of Na_2CO_3 (a), NaCl (b) and NaSCN (c)……204

Figure 8.1: Chemical structure of Ciprofloxacin……..208

Figure 8.2: Calibration curve of aqueous Ciprofloxacin solution in terms of absorbance at 275 nm as a function of concentration measured by UV-Vis Spectroscopy……..210

Figure 8.3: **(a)** Ciprofloxacin loading to sample set 1 in terms of concentration of cipro loaded (µg / mL) versus time (hours). Sample set 1 contains PEOX (5 mg/mL) / MA fibers (0.0220 g) and PEOX (0.4 mg/ mL) / MA fibers (0.0222 g). **(b)** Ciprofloxacin loading to sample set 2 in terms of concentration of cipro loaded (µg / mL) versus time (hours). Sample set 2 contains PEOX (5 mg/mL) / MA fibers (0.0118 g) and PEOX (0.4 mg/ mL) / MA fibers (0.0120 g) and PEOX fiber (0.0118 g)…….212

Figure 8.4: **(a), (b)** ITC data of the interaction between MA (0.3 mM, pH 4) to PEOX (0.05 mM, pH 4) at 25°C. **(a)** Raw data **(b)** Independent Model fit (solid line) corresponding to ΔH = -100 kJ/mol; ΔG = -25.98 kJ/mol; ΔS = -248.3 J/mol-K **(c), (d)** ITC data of the interaction between MA (0.6 mM, pH 4) to PEOX (0.05 mM, pH 4) at 25°C. **(a)** Raw data **(b)** Independent Model fit (solid line) corresponding to ΔH = -39.66 kJ/mol; ΔG = -23.32 kJ/mol; ΔS = -54.79 J/mol-K……214

Figure 8.5: **(a)** SEM image of PEOX (0.4 mg/mL) / MA fibers before Ciprofloxacin loading. Scale bar is 200 nm. **(b)** SEM image of PEOX (0.4 mg/mL) / MA fibers before Ciprofloxacin loading. Scale bar is 1 µm. **(c)** SEM image of PEOX (5 mg/mL) / MA fibers before Ciprofloxacin loading. Scale bar is 2 µm. **(d)** SEM image of PEOX (0.4 mg/mL) / MA fibers after Ciprofloxacin loaded into them. Scale bar is 200 nm. **(e)** SEM image of PEOX (0.4 mg/mL) / MA fibers after Ciprofloxacin loaded into them. Scale bar is 1 µm. (**f)** SEM image of PEOX (5 mg/mL) / MA fibers after Ciprofloxacin loaded into them. Scale bar is 1 µm……..215

Figure 8.6: **(a)** Release profile of Ciprofloxacin from PEOX / MA fibers in PBS, at pH 7.4 in terms of concentration of released drug versus time **(b)** Release profile of Ciprofloxacin from PEOX / MA fibers in PBS, at pH 7.4 in terms of fraction of released drug versus time……..217

NOMENCLATURE

Poly (acrylic acid) (PAA)

Poly (methacrylic acid) (PMMA)

Poly (N, N'dimethyl aminoethyl methacrylate) (PDMAEMA)

Poly (N, N'diethyl aminoethyl methacrylate) (PDEAEMA)

Tannic acid (TA)

Layer-by-layer (LbL)

Poly(vinylpyrrolidone) (PVP)

Poly(ethylene) glycol (PEG)

Poly (styrene sulfonate) (PSS)

Poly (diallyldimethylammonium chloride) (PDDA)

Poly (N-isopropylacrylamide) (PNIPAM)

Upper critical solution temperature (UCST)

Lower critical solution temperature (LCST)

Critical temperature (T_c)

Combinational entropy (ΔS_{com})

Ideal gas constant (R)

n_i = molar number of the component i

Θ_i = volume fraction of the component i

Flory-Huggins interaction parameter (λ_{12})

Temperature (T)

Cloud point (T_{cp})

Gibbs free energy (ΔG)

Free energy of mixing (ΔG_{mix})

Poly (ethylene oxide) (PEO)

Poly (vinyl methyl ether) (PVME)

Poly (vinyl alcohol) (PVA)

Poly (hydroxyethylmethacrylate) (PHEMA)

Poly (2-vinylpyridine) (P2VP)

Poly (*N*-acryloyl glycinamide) (PNAGA)

Poly (N-vinyl caprolactam) (PVCL)

Poly (oxazoline)s (POX)

Poly (N,N-diethylacrylamide) (PDEAAm)

Poly(N-vinylisobutyramide) (PNVIBA)

Volume phase transition (VPT)

Poly (2-alkyl 2-oxazoline) (PAOX)

Alkyl group (R)

Poly (2-methyl 2-oxazoline) (PMeOX)

Poly (2-ethyl 2-oxazoline) (PEOX)

Poly (2-isopropyl 2-oxazoline) (PIPOX)

Poly (n-isopropyl 2-oxazoline) (PnPOX)

Critical micellar concentration (CMC)

Critical micellar temperature (CMT)

Packing parameter (p)

Glass transition temperature (T_g)

Poly (vinyl phenol) (PVPh)

Poly (ε-caprolactone)-block-poly(methacrylic acid) (PCL-block-PMMA)

Langmuir-Blodgett (LB)

Self-assembled monolayers (SAM)

Polyelectrolyte multilayers (PEM)

Poly (allylamine) hydrochloride (PAH)

Polyaniline (PAni)

Poly (N-vinylpyrrolidone) (PVPON)

Poly (4-vinylpyridine) (P4VP)

Poly (l-aspartic acid) (PLAA)

Block copolymer micelle (BCM)

Poly (2-diethylamino) ethyl methacrylate)-*block*-poly (N-isopropyl acrylamide) (PDEA-*b*-PNIPAM)

Poly (styrene-*alt*-maleic acid) (PSMA)

Bovine Serum Albumin (BSA)

Doxorubicin (DOX)

Phenyl Boronic Acid (PBA)

Polyacrylamide (PAAD)

Polyacrylonitrile (PAN)

Minimum effective concentration (MEC)

Minimum toxic concentration (MTC)

Enhanced permeability and retention (EPR)

Rose Bengal (RB)

5,10,15,20-tetraphenyl-21H,23H-porphinetetrasulfonate (TPPS)

Carboxyl terminated poly(amidoamine) (PAMAM-COOH)

Rhodamine B (Rb)

Poly (2-(*N*-morpholino) ethyl methacrylate (PMEMA)

2-(diisopropylamino) ethyl methacrylate (PDPA)

Phosphate buffer saline (PBS)

Poly (L-lactic acid) (PLLA)

Poly (lactide-co-glycolide) (PLGA)

Poly (lactic acid) (PLA)

Poly (ethylene glycol)-b-poly (lactide) (PEG-b-PLA)

Poly (ethylene-co-vinyl acetate) (PEVA)

Poly (N-isopropylacrylamide-co-methacrylic acid) (PNIPAM-co-MAA)

Optical microscope (OM)

Atomic force microscopy (AFM)

Scanning tunnel microscopy (STM)

Field emission scanning electron microscopy (FESEM)

Thermogravimetric analysis (TGA)

X-ray photon spectroscopy (XPS)

Kinetic energy (KE)

Binding energy (BE)

Photoelectric work function (Θ)

Fourier transform infrared spectroscopy (FTIR)

Ultra-violet visible spectroscopy (UV-Vis)

Absorbance (A)

Molar absorptivity (ε)

Intensity of the light passing through the reference cell (I_0)

Transmitted intensity of light (I)

Contact angle (Θ)

Solid-vapor interfacial tension (Υ_{SV})

Solid-liquid interfacial tension (Υ_{SL})

Surface tension of liquid (Υ_L)

Advancing contact angle (ACA)

Receding contact angle (RCA)

Differential scanning calorimetry (DSC)

Specific heat of solute (C_2)

Specific heat of solvent (C_1)

Specific heat of solution (C_{sol})

Mass fraction of solute (m_2)

Specific calorimetric enthalpy (Δh)

Isothermal titration calorimetry (ITC)

Root mean square (rms)

Bilayer (BL)

Binding constant (K_a)

Dissociation constant (K_{diss})

Malonic acid (MA)

Ciprofloxacin (Cipro)

Chapter 1: Introduction

Stimuli-responsive polymers are macromolecules that exhibit a specific physical, chemical or biological behavior that changes according to their environment, such as these parameters like pH, temperature or the existence of a molecule or enzyme. Polymers that are in this group are especially useful in biomedical applications, since it gives the opportunity to tune their response by regulating the changes in their environment and their reversible response upon these changes. The scope of the work in this thesis is limited to pH and temperature responsiveness of macromolecules, since pH and temperature changes in body conditions are most discriminating ones when dealing with biomedical applications like drug release or delivery, drug therapy. For this reason, we selected biocompatible, uncharged and either pH or temperature responsive polymers for the studies being presented in this thesis work.

Temperature responsive polymers are commonly used in biomedical applications, especially the ones that exhibit critical temperatures around physiological conditions. These polymers exhibit volumetric phase transitions upon temperature changes. According to the phase volume transition behavior upon temperature change, temperature responsive polymers are categorized into two groups: Upper critical solution temperature (UCST) polymers, lower critical solution temperature (LCST) ones or those that exhibit both LCST and UCST. In this work, temperature responsive polymers exhibiting LCST behaviour were chosen. For biomedical applications, poly (N-isopropylacrylamide) (PNIPAM) is the most frequently used polymer in biomedical area since LCST of this polymer is close to physiological temperature, at ~32°C. In this thesis work, poly (2-ethyl 2-oxazoline) (PEOX) was used. PEOX is also a temperature-responsive polymer exhibiting an LCST around ~62°C, depending on the molecular weight. Although the LCST temperature of PEOX polymers is much higher than physiological temperature, this temperature responsive behavior can be tailored easily by changing environmental conditions like pH or ionic strength of salts. In addition to that, PEOX has advantages compared to PNIPAM like higher biocompatibility, lack of toxic products, versatility and absence of hydrogen donating groups.

pH-responsive polymers have ionizable groups that donate protons or accept protons according to the pH of the environment. pH-responsive polymers can be polyacids or polybases. In this thesis, pH responsive polyacids were used. For polyacids, when the pH of the environment exceeds the pKa of the acid, pH responsive groups are ionized. For this work, tannic acid (TA) is selected as a pH-responsive component. TA is a polyphenol, which has anti-microbial, anti-cancer and antioxidant properties. Besides its biological activity, the most beneficial property of TA is its high pKa value since it is very close to the physiological pH of the body. This makes TA to be widely used in biomedical applications, especially the ones that deal with physiological conditions. In this work, not only polyacids but also a small dicarboxylic acid like malonic acid that have two pKa values were used to form pH responsive structures.

In this thesis work, the focus is on "self-assembled structures of stimuli-responsive polymers through hydrogen bonding". Self-assembly, by its nature, is a spontaneous process and through this process, ordered supramolecular structures can be formed. When these structures are formed via hydrogen bonding, the formed structures exhibit beneficial properties like reversibility, dynamic nature, being orientational and directional. In addition, self-assembly process via hydrogen bonding can be easily controlled adjusting the environmental conditions like pH, temperature or ionic strength, especially when stimuli-responsive components are used.

Self-assembled structures that are formed by stimuli-responsive polymers are various. In this work, layer-by-layer (LbL) films and fibrous structures were formed by using PEOX and an acidic component that donates protons to PEOX amide groups via hydrogen bonds. LbL assembly depends on alternating and sequential deposition of species through complementary interactions. On the other hand, fibers are solid structures that are in nano to micro scale. In the literature, fibers are generally formed electrospinning process. In this work, for the first time, fibrous structures via hydrogen bonds are formed via a very simple method. Controlled release applications of both hydrogen bonded LbL films and fibers were demonstrated.

For both self-assembled structures, hydrogen bonded LbL films and fibers, , effect of Hofmeister series of salt has an important role, especially when the biomedical applications of the self-assembled structures are considered. Since the physiological serum of the body itself is a mixture of salts, the effect of these salts on the polymeric structures that are designed to be used

in cell applications should be understood very well. For this reason, the influence of Hofmeister series of salts on self-assembled polymeric structures was emphasized. In the Hofmeister series of salts, ions were ranked based on their ability to precipitate proteins, and they were classified as either “salting-out” or “salting-in” ions. Prior studies about Hofmeister series of salts mostly discuss the working mechanism of these ions and how they affect the protein stability. Different from the previous work in the literature, the effect of “Hofmeister series of salt” was discussed in detailed on the H-bonded self-assembled structures.

In the first part of the thesis, hydrogen bonded LbL films of PEOX and TA were fabricated via dip coating. As PEOX is a temperature responsive polymer exhibiting LCST and TA is a pH-responsive polyphenol, deposited films were both pH and temperature responsive. For the first time, it was shown that PEOX / TA multilayers restructured into fibers in acidic phosphate buffer. In this specific condition, hydrogen bonds between PEOX and TA were still intact, so they formed fibers that were both pH and temperature responsive. These fibers were characterized with different methods to clarify their chemical and physical structure. This first part of the thesis work contributes to an understanding of the stability of LbL multilayers in different chemical conditions. In addition, this work shows the different ways to modify the structure of LbL films and how the transition from one self-assembled structure to another is possible. pH responsive fibers obtained from LbL multilayers have potential biomedical applications such as controlled release and biosensors.

Restructuring of LbL multilayers into fibers in phosphate buffer also opens for questioning a the effect of Hofmeister salts on the stability of LbL films. In the literature, the effect of Hofmeister series of salts on the properties of polyelectrolyte multilayers was broadly investigated. A few studies also deal with the effect of Hofmeister salts on the hydrogen bonded multilayers, but these studies are limited with either the salt annealing or post-treatment of multilayers through salt solutions. Thus, the effect of Hofmeister salts on the structure and properties of hydrogen-bonded LbL films and their working mechanism is not yet well-understood. In this part of the thesis, the influence of Hofmeister series of salts on the properties of H-bonded PEOX/TA films was demonstrated. This work shows that by understanding the working mechanism of Hofmeister series of salts and their influence on the properties of hydrogen bonded polymeric films, it is possible to tune the properties like film thickness, stability and morphology of the multilayers. In

particular, the nature of the interaction between PEOX and TA in the presence of salt solutions was emphasized. As indicated, this part of the study is especially important for biomedical applications, such as drug encapsulation or drug release, since physiological serum of the body itself is a salt solution. In addition, when the influence of the salt on the properties of LbL films are elucidated, biomedical applications that were indicated above would be successfully implemented.

After analyzing the restructuring of PEOX/TA multilayers as a self-assembly process and analyzing the effect of salts on the properties, controlled release applications of these multilayers was also demonstrated. Controlled release systems increase the efficiency of the administered drug in terms of site-specific delivery and dosage of the administered drug, so that concentration of the drug could be within therapeutic window. In a controlled release system, the release kinetics of the administered drug should be regulated. Most of drug release systems have kinetics, in which the release of drug is fast in the first few hours, but this subsequently extended. Fast then slow" release could have problems like side effects and reduced therapeutic effect. For this reason, the objective of the controlled release applications studied in this work is to have a "zero order release kinetics". With zero order release kinetics, the amount of the drug released within specific time intervals remains same and independent of the starting concentration of the drug. The objective of this part of the work is to induce the zero-order release of a hydrophilic model molecule, Rhodamine 6G, from hydrogen-bonded PEOX/TA multilayers. Achieving controlled release of a hydrophilic small molecule is a particular challenge due to its high solubility in body fluids. LbL films are good platforms for controlled-release applications with their nanoscale higher order structure, ease and low-cost of fabrication and versatile surface chemistry. However, there is a vast amount of studies in the literature demonstrating controlled release applications from electrostatically bound polyelectrolyte multilayers. When electrostatically bound LbL multilayers are used for the controlled release applications, the applications are limited to charged molecules. On the other hand, hydrogen bonded PEOX/TA multilayers have advantages like being pH-responsive and thermo-responsive at the same time, in addition opening possibilities for release applications. The objective of this part of the study is to show the potential of hydrogen-bonded PEOX/TA multilayers as a model system for the zero-order release of Rhodamine 6G at the specific conditions in terms of pH and temperature. pH and temperature responsiveness of the

PEOX / TA multilayers make the release simultaneously both stimuli responsive and degradation controlled.

After demonstrating the potential application of PEOX/TA multilayers, the objective of the seventh chapter of this work is to show that through hydrogen bonding between PEOX and a small dicarboxylic acid, malonic acid (MA), well-defined and hollow fibers can be formed. In addition to that, the effect of pH, temperature and ionic strength on the properties of the fibers were examined. Understanding the effect of these factors would be beneficial to tailor the properties of the fibers. Especially, pH responsivity of these fibers is emphasized. In addition, the formation of hollow fibers is beneficial for using them as templates for various applications, due to their high surface-area-to-volume ratio and protection of the drug for site-specific delivery.

In the final part of this thesis study, the aim is to demonstrate a controlled-release application of hollow PEOX/MA fibers under physiological conditions. Ciprofloxacin, a broad-spectrum antibiotic, is selected as a drug since it is a hydrophilic, broad-spectrum antibiotic. Obtaining controlled release kinetics of this broad antibiotic is especially crucial since the burst release of this drug can result in very harmful side effects. Thus, PEOX/MA fibers with their hollow morphology can be great candidates for the encapsulation and release of this antibiotic. As a reference, the encapsulation and release performance of PEOX/MA fibers with PEOX content was compared with PEOX fibers that had formed as a result of crystallization above the cloud point.

As a whole and as the title of this thesis suggests, the ultimate objective of this work is to demonstrate the formation of self-assembled polymeric structures through hydrogen-bonding and their controlled release applications. PEOX, as a temperature-responsive polymer, was used in two self-assembled structures: first, in LbL multilayers with tannic acid and in hollow fibers with malonic acid. Reversibility, pH/temperature responsivity and simplicity of fabrication are common properties of the formed structures. Different from previous literature works, the self-assembly mechanism of the formed structures was shown in terms of the molecular interactions, specifically the interplay between hydrogen-bonding and hydrophobic interactions, and thermodynamic driving forces, additionally, giving special emphasis on the effect of Hofmeister series of salts.

With the knowledge gained in the first part, properties of the self-assembled structures could be tailored for the various biomedical applications, so controlled release applications demonstrated.

Chapter 2: Literature Review

2.1 Stimuli-responsive polymers

Polymers or macromolecules are essential components of living systems and they have vital operational functions in the most basic unit of life, simply in cells. The need to mimic biological polymers essential to life like proteins, nucleic acids, carbohydrates and to regulate interaction the functional groups of these polymers for different applications led researchers to produce responsive polymers. In this sense, "stimuli-responsive polymers" are defined as the polymers which exhibit different chemical, physical or biological behaviors as a response upon changes or "stimuli" in their environment [1] ,[2] [3].

The stimuli that a polymer responds can be categorized into physical, chemical or biological stimuli. Examples of chemical stimuli are pH, ionic strength and various chemical agents while physical stimuli can be temperature, electrical or magnetic field, light, mechanical stress… etc. Biological stimuli are generally very specific, they signal generally via enzymatic action or change in overall biological environment such as overexpressed intracellular enzymes, bacterial enzymes, inflammation signaling molecules [4]. Stimuli producing changes in polymer behavior can be also classified as external stimuli which are externally and artificially controlled or internal stimuli which are naturally controlled through physiological conditions [5]. Basically, stimuli-responsive polymers recognize these stimuli as signals and adapt their chain conformation as a response [1]. The response of these polymers can be observed via a change in their surface characteristics, solubility, sol-gel transition etc…

Stimuli-responsive polymers share some common characteristics. A very important feature of these kind of polymers is that their reversibility, the ability to go back to their initial state when stimuli is not applied anymore, so that they produce a non-linear response to the stimuli [6]. When a stimuli is applied, these polymers usually undergo from hydrophilic to hydrophobic state or vice versa [7]. They can be also classified into three groups according to their physical forms: linear free chains in solutions, covalently cross-linked gels or physical gels and polymer adsorbed on a surface or grafted form. Linear free polymer chains collapse in the solution via application of

external stimuli [7]. Polymers that fall into this category should contain both hydrophilic and hydrophobic parts so that when the polymer collapses, they can form separate phases in the solution [7]. Similarly, for the polymers adsorbed on a surface, depending on whether the stimuli is applied or reverted, the polymer can reversibly swell when in hydrophilic state or collapse or aggregate in hydrophobic state. Polymers in gel form usually contain hydrogels that swells in water.

Versatility and tunable sensitivity of these polymers let them to be used in many applications [5] [8] [9]. Especially, applications of stimuli-responsive polymers in biology and medicine are many: controlled drug release and delivery [5, 10] [11, 12], sensors [13], actuators that convert energy to mechanical forces [14] ,[15] and tissue-engineering [16]. In order to tune the properties of stimuli-responsive polymers for all the applications that are listed above, it is essential to control them kinetically and thermodynamically and understand the structure-property relationship [1]. Among stimuli-responsive polymers, especially pH and temperature responsive ones have been gaining importance in biomedical applications due to their convenience for physiological conditions.

2.1.1 pH responsive polymers

pH responsive polymers are polymers that have ionizable groups which can accept or donate protons and show tunable physiochemical properties upon pH change in their environment [1], [7] , [17]. The key property of pH-responsive polymer is that the presence of ionizable groups which are attached to the hydrophobic backbone of the polymer [18]; since at the specific pH in which the polymer behavior changes depends on the pKa, the logarithmic value of acid dissociation or the pH value, of these ionizable groups. In other words, pKa is critical for pH-responsive polymers since pKa is the pH value where half of these groups are ionized. The physicochemical properties which are altered via pH change in the environment are solubility, volume, configuration, chain conformation or surface activity [17] ,[19]. The change in the physicochemical behaviors with pH is due to the modified balance between electrostatic interactions, hydrogen bonding and hydrophobic interactions which this modified balance results in a micro-phase separation and different self-assembly behavior [19]. For example, depending on the degree of ionization, conformation and hydrodynamic volume of the polymer may change due

to the domination of electrostatic repulsion between generated charges over hydrophobic interactions [1],[7],[17], [18]. The degree of the ionization of these groups also influence the solubility of the polymer: Increased ionization leads to the increased solubility in aqueous environment. Similarly, for polymer gels, the delicate balance between electrostatic repulsion and hydrophobic interactions influences swelling / de-swelling behavior.

pH responsive polymers are classified into two groups: Polyacids which can form polyanions and polybases which can form polycations in aqueous solutions. Polyacids generally have carboxylic or sulfonamide groups so that they accept protons at low pH and donate protons at high pH depending on pKa [1], [7] . pKa value depends on the composition, molecular weight or length of alkyl side chains since these parameters affect the hydrophobicity of the polymer [7]. Most common polyacids are poly (acrylic acid) (PAA) and poly (methacrylic acid) (PMAA). From natural biopolymers, most common examples are alginate, carboxymethyl cellulose, pectin, hyaluronic acid or poly (glutamic acid). Polybases contain amine, imidazole or pyridine groups which accept protons at high pH but donate protons at low pH. [1], [7]. Most common polybases are poly (N, N'dimethyl aminoethyl methacrylate) (PDMAEMA) and poly (N, N'diethyl aminoethyl methacrylate) (PDEAEMA) and chitosan is the only polycationic sachharide among natural biopolymers. pH responsive polymers can have linear, branched or network structures while different architectures of these polymers can be linear homopolymers, amphilic, double hydrophilic block copolymers, star, branched, hyper-branched, brushes, gels or hydrogels… [17]. Among these different polymeric architectures, double hydrophilic block copolymers are interesting structures and they share similar characteristics of amphiphilic block copolymers which have two different polymer segments with different hydrophilicity and self-assemble micellar structure consisting of hydrophobic core and hydrophilic corona in aqueous solutions. Double hydrophilic block copolymers form micellar structures due to difference in pH responsiveness of different polymeric block [17] since with pH change hydrophilicity of the blocks are altered.

Biomedical applications of pH-responsive polymers are many; these applications include but not limited to controlled drug release and site specific delivery [20], [21], [22], [23] gene therapy and delivery [24], [25], non-biofouling or cell-adhesive surfaces [26], [27] protein separation [28]... In order to design a pH sensitive system for any application, either polymer with a critical pH matching the desired pH range for the application should be selected or polymer selected can be

modified for the desired pH range [18]. This modification can be achieved via introducing hydrophobic moiety into polymer backbone which increases critical pH for polyacids and decreases critical pH for polybases. These pH responsive polymers are especially central to drug release and delivery applications due to the pH variations in the body which can be found in organ level (gastrointestinal track), tissue level (cancer tissue vs. normal tissue) and in subcellular level (different organelles) [18]. pH responsive polymers ease the delivery of DNA since they are able to screen the negative charge of DNA [3]. Zwitterionic polymer surfaces have a mixed charge due to quaternary amines and negative carboxylic acid residues which are useful for bacteria adhesive/resistance transition [17]. All these different applications underline the importance of the pH responsive polymers.

2.1.2 Tannic acid: a pH responsive polyphenol

Tannic acid (TA) is a high-molecular and biodegradable polyphenol and it has a central glucose core with gallic acids connected through ester bonds with hydroxyl groups of that central glucose (Chart 1) [29], [30].

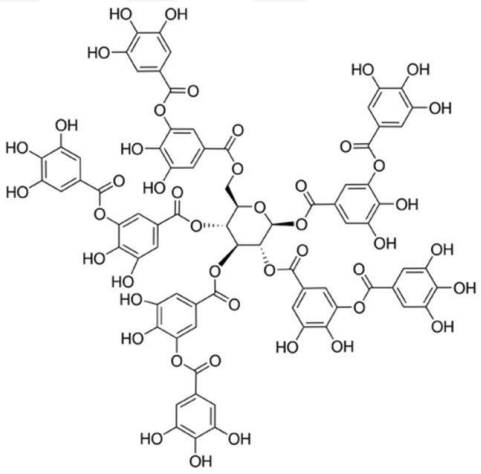

Figure 2.1: Chemical structure of tannic acid (TA)

Polyphenols are secondary metabolites of the plants and they play a significant role in plants' defense mechanism against UV radiation or pathogenic invasion, are responsible from oxidative stability, and exhibit properties like pigmentation, flavoring, free radical scavenging, metal coordination… [31], [32]. These group of polyphenols, including TA, are anti-oxidant due to their ability to take part as a reducing agent in redox reactions and, are anti-bacterial since they

prevent bacterial growth, and also exhibit anti-tumor and anti-inflammatory activities [31]. All these useful properties led their usage in bio-based engineering areas and tune the surface properties of different materials through diverse intermolecular interactions.

The main intermolecular interactions that TA can participate into are hydrogen bonding, hydrophobic interactions, electrostatic interactions, metal complexation or covalent interactions [31]. TA can act as a hydrogen donor due to many available hydroxyl (-OH) in the phenol groups. Above its pKa, (~8.5), due to the deprotonation of the hydroxyl groups, TA carries negative charge and involves in electrostatic interactions. Planar aromatic rings of TA induce hydrophobic interactions and these interactions are especially important when TA non-covalently interacts with hydrophobic moiety of the proteins [30]. Polyphenols, including TA, are able to cross-link and interact many different macromolecules through this diverse interactions and phenolic based functional materials are produced with realization of the versatile interactions that TA.

These phenolic based functional materials are classified into three categories: Thin films, including layer-by-layer films, metal-phenolic networks, particles, including capsules, nanoparticles, micelles etc.., and bulk materials, including gels, plastics and elastomers [32]. TA can be assembled with various polymers via hydrogen bonding or electrostatic interactions in layer-by-layer (LbL) fashion. Metal-phenolic films are useful in terms of pH-responsiveness and low toxicity [29]. For the preparation of phenolic particles, especially pH-responsive TA-Fe^{3+} capsules are considered by taking advantage of metal-coordination bonds [29]. Hydrogel formation with TA is a challenge due to the all of these multiple interactions result in coacervation formation, however, Fan *et al.* successfully produced hydrogels based on TA and different polymers such as poly(vinylpyrrolidone) (PVP), poly(ethylene) glycol (PEG), poly(styrene sulfonate) (PSS) and poly(diallyldimethylammonium chloride) (PDDA) via hydrogen bonding or electrostatic interactions and further cross-linked with metal ions [33].

Applications of TA and polyphenols include but not limited to adhesives, self-healing or self-sealing films, drug delivery, sensing and imaging applications for the recognition of proteins, catalysis due to chelating ability etc… [32]. Especially for the bio-applications, ability to coordinate macromolecules through different interactions, anti-microbial or anti-tumor activities, high pKa around physiological pH and pH responsive behavior have led TA to be used in many different categories.

2.1.3 Temperature responsive polymers

Temperature responsive polymers are a class of stimuli responsive polymers which exhibit different behavior upon temperature change [34]. This different behavior as a response to temperature change is usually accompanied with a volume phase transition, which we observe as either conformational change or solubility change of the free polymer chains [35]. Especially, temperature-responsive polymers exhibit temperature dependent miscibility / solubility gap in aqueous solutions in which phase diagram of the polymer clearly shows this transitional behavior [36]. The boundary curve, which is called bimodal, separates one-phase region from two phase region in which the polymer and the solvent is immiscible. The extremum point of the curve is called the critical temperature (T_c).

To predict the thermo-responsive behavior of the polymer, one needs to understand the thermodynamic picture. Flory-Huggins theory can be used to understand the entropic and enthalpic contributions for the temperature-responsive behavior. The enthalpic contribution to the free energy of mixing is always positive since, the contact of the polymer chain with the solvent increases the number of microscopic configurations [37].

$$\Delta S_{com} = -R\,(n_1 \ln\Theta_1 + n_2 \ln\Theta_2) \qquad (1)$$

where R is the ideal gas constant, n_1 and n_2 are the molar number of solvent and the polymer respectively and Θ_1 and Θ_2 are the volume fraction of the solvent and the polymer respectively. The mixing enthalpy of the polymer in the solvent is given:

$$\Delta H_{mix} = R\,T\,\lambda_{12}\,n_1\,\Theta_2 \qquad (2)$$

where T is the temperature, λ_{12} is the Flory-Huggins interaction parameter between the polymer and the solvent. Since the Gibbs free energy (ΔG) of the system is always determined by

$$\Delta G = \Delta H - T\Delta S \qquad (3)$$

then, the free energy of mixing (ΔG_{mix}) becomes

$$\Delta G_{mix} = R\,T\,(n_1 \ln\Theta_1 + n_2 \ln\Theta_2 + \lambda_{12}\,n_1\,\Theta_2) \qquad (4)$$

According to the above equations, polymer will be always soluble in a solvent if it has a negative ΔH_{mix} and positive ΔS_{com} and polymer will be always insoluble in the solvent vice versa. If the

ΔH_{mix} and ΔS_{com} are both positive and both negative, then temperature is very critical and this will determine the temperature-responsive behavior of that polymer [37]. Hence, T_c is defined as:

$$T_c = \Delta H_{mix} / \Delta S_{com} \qquad (5)$$

Temperature responsive polymers are gathered in two groups: Polymers that exhibit upper critical solution temperature (UCST) behaviour or UCST polymers, and polymers that exhibit lower critical solution temperature (LCST) behaviour or LCST polymers. According to the ΔH_{mix} and ΔS_{com} values, Zhao *et al.* prepared a thermodynamic map which shows the polymer solubility and temperature dependent behavior in water, shown in Figure 2.2 [37].

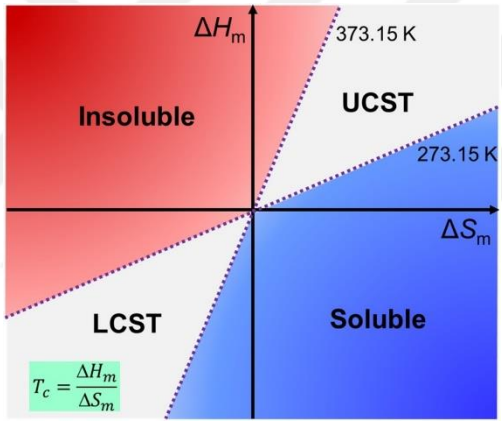

Figure 2.2: Thermodynamic map that predicts the solubility and temperature dependent behavior of polymers in aqueous solution based on the signs of ΔH_{mix} and ΔS_{mix} values [37].

Thermo-responsive behavior is due to the competing intermolecular and intramolecular interactions between polymer-solvent and polymer-polymer segments [34], [35]. In terms of H-bonds, there are three competing interactions: polymer-polymer, water-water and polymer-water. These competing interactions determine the solubility, ΔH_{mix} (polymer-polymer and water-water interactions have a positive contribution to ΔH_{mix}) and the transition temperature [37]. At the transition temperature, which is also de-mixing temperature, hydrogen bonds with water are weakened, water molecules are expelled from polymer structure so polymer chains are dehydrated and phase separation from water occurs due to the interaction between polymer chains among themselves and aggregation of them in one phase [36], [38]. In other words, the phase transition temperature of thermo-responsive polymers is determined by the balance between interactions

between polymer-solvent and polymer-polymer. The first reported temperature-responsive polymer was poly (N-isopropylacrylamide) (PNIPAM) in 1967 [39].

Phase transition temperature can be influenced by many factors. The main factors are additives such as salt, surfactants, co-solvents or co-solutes etc... The effect of these additives generally is due to their ability to change the solvent quality of the solution, and as a result polymer-solvent interactions including hydrogen bonding capability of the polymer [34]. Especially, amphiphilic molecules like surfactants, adsorb onto polymers and change the hydrophilicity of the polymer. Introducing hydrophobic moieties or introducing functional groups to polymers that would enhance the polymer-polymer interaction, entanglements, crosslinking or branching would affect ΔS_{mix} and ΔH_{mix} and consequently, thermo-responsive behavior of the polymer [37].

Using thermo-responsive polymers in biomedical applications is advantageous because body temperature is set to 35-37°C, regardless of specific tissue or organ so no special consideration is required [36]. Main biological applications of thermo-responsive polymers include but not limited to drug delivery, gene delivery and tissue engineering. In drug delivery applications, polymer chains loaded with drug or functional molecules expand as a result of temperature change and drug molecules diffuse to the targeted site [40]. In tissue engineering applications, these polymers are either used as substrates for cell growth, migration and proliferation or as injectable gels to be used as *in situ* scaffolds so that cells can be encapsulated in the 3D structured body [38] ,[40]. Other biomedical applications are bio-separations, filtrations, imaging, regulating enzyme activity, smart surfaces etc… [41].

Temperature responsive polymers can be also classified based on the architecture: Hydrogels, interpenetrating networks, micelles, films, particles are only few examples. Hydrogels produced from thermo-responsive polymers are useful in terms of swelling in response to temperature, while physical gels show sol-gel transition depending on temperature [34], [40]. Thermo-responsive micelles with hydrophobic core are used to encapsulate hydrophobic drugs, while polymersomes, self-assembled block copolymers with a hydrophilic exterior and interior, are used to encapsulate hydrophilic drugs. In addition, thermo-responsive colloidal cores are hydrophobic part of the colloids and its hydrophobicity can be changed with temperature [35].

Thermo-responsive smart nanofibers are also commonly used in biomedical applications due to its high surface area and high drug loading capacity [36].

2.1.3.1 Polymers exhibiting UCST behavior in water

Polymers which exhibit UCST behaviour in aqueous solutions are simply polymers which phase separate from water upon cooling [42]. In the phase diagram, UCST is the maximum point of the binodal curve as observed in Figure 2.3 [42], [43] which means that below UCST, there is a miscibility gap or polymer and solvent are immiscible within a range of polymer composition [42]. Other points on the curve are cloud point (T_{cp}) or de-mixing temperature which can be determined using turbidity measurement or calorimetric or light scattering methods which are described in Section 2.1.3.2.

UCST behaviour mainly stems from the enthalpic interactions like H-bonding or electrostatic interactions between polymer segments [37], [42], [44]. In other words, UCST is an enthalpy driven process unlike LCST behaviour where hydrophobic interactions are considered, so polymer-polymer interactions and water-water interactions are crucial. For UCST polymers, ΔH_{mix} and ΔS_{mix} are both positive and the relative contribution of enthalpic intramolecular interactions in ascending order varies from Van der Waals interactions to ion-ion interactions [37], [42].

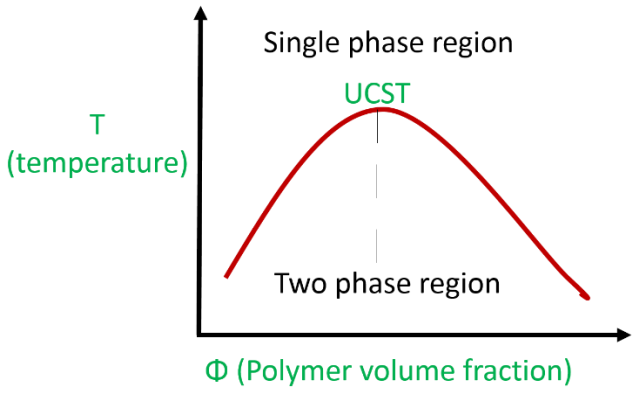

Figure 2.3: A sample phase diagram of a polymer which exhibits UCST behavior

Research on UCST polymers is more limited when compared with LCST polymers because most of them have UCST outside the range of 0-100°C. Thus, UCST polymers can be mainly

divided into two: The ones which exhibit UCST outside the range of 0-100°C like poly (ethylene oxide) (PEO), poly (vinyl methyl ether) (PVME), hydrophobically modified poly (vinyl alcohol) (PVA), poly (hydroxyethylmethacrylate) (PHEMA) and the ones which exhibit UCST within the range of 0-100°C [42]. Polymers which have UCST within the range of0-100°C in aqueous solutions are either based on hydrogen bonding or ionic interactions. For UCST polymers based on ionic interactions, mainly zwitterionic polymers or polyelectrolytes are in this class. Zwitterionic polymers are polymers that carry both positive and negative charges, and poly(sulfobetaine)s are the most popular UCST polymers in this group [37]. Other UCST polymers based on ionic interactions are some polyelectrolytes in the presence of multivalent cations such as block copolymers of PEO and poly(2-vinylpyridine) (P2VP) with addition of peroxodisulfate and carboxylic polymers such as PAA in low pH or high ionic strength [42]. Polymers which have both H-donor and H-acceptor groups can exhibit UCST behaviour due to intramolecular extensive H-bonding so that in order to solubilize these kind of polymers, heat is necessary [37]. The most studied UCST polymer based on thermally reversible H-bonding is poly(*N*-acryloyl glycinamide) (PNAGA)[42], [45]. Ureido based polymers due to resonance stabilized extensive H-bonding sties and pi-pi interactions and copolymers based on acrylamides are also among H-bonding based UCST polymers [43]. The common property of all H-bonding based UCST polymers is that they all have primary amine groups [42].

Addition of hydrophobic moieties, copolymerization, molecular weight are important internal factors that can influence the UCST behaviour of the polymers. Introducing a hydrophobic moiety or copolymerization with hydrophobic monomers is crucial because of the nature of thermo-responsive behaviour in aqueous solutions. Water is a structured solvent due to the intramolecular hydrogen bonding of water molecules and in polymer dissolution process, polar groups of the polymer and water interact [43]. In polymer dissolution process, non-polar groups or hydrophobic moieties of the polymer are surrounded by a cage of organized water molecules which results in the restriction of translational / rotational movement of water molecules and entropy loss [37]. In order to overcome this entropic loss, hydrophobic moieties interact with each other and release water molecules around them which increase the T_{cp}. Copolymerization depends on the hydrophilicity or hydrophobicity of the copolymer. In case of a more hydrophilic copolymer, the polymer can be better hydrated and T_{cp} can be lowered. Zwitterionic polymers tolerate better to copolymerization because their electrostatic interactions between ionic groups

are long range interactions [37]. Topological defects like cross-linking, branching, chain entanglements limit intramolecular interactions of UCST polymers, result in less positive ΔH_{mix} and increase T_{cp}. Influence of molecular weight stems from the fact that increasing molecular weight result in less positive ΔS_{mix} so generally T_{cp} is elevated and polymer solubilisation becomes sensitive to other interactions with water [43].

Stimuli such as pH or ionic strength also affect UCST behaviour of polymers. Especially, salt plays an important behaviour for zwitterionic UCST polymers since salt ions create a "screening" effect between ionic groups of the polymer. With this screening effect, intramolecular ionic interactions are disturbed since the Debye length in which opposite charges sense each other are affected so T_{cp} is lowered [37], [42], [43]. pH effect on UCST is significant for both zwitterionic and H-bonding polymers. For example, zwiterionic polymers show poorest solubility around their isoelectric point so when pH of the environment is far from this point, polymer is better hydrated and UCST behaviour becomes less prominent [37]. pH also influences the protonation state of the functional groups of H-bonding polymers, thus UCST behaviour directly. Higashi *et al* prepared poly (N-acrloyl amino acid)s from various amino acids and show that thermo-responsive property for these polymers is exhibited only under pH3 [46]. Understanding and manipulating UCST behaviour of such various stimuli can be very useful for various biomedical applications so anticipating these influences are important.

2.1.3.2 Polymers exhibiting LCST behavior in water

Polymers which exhibit LCST behaviour in aqueous solutions are polymers which phase separate from water upon heating accompanied with a decreased solubility and a conformational change from hydrated coil to collapsed globular for diluted solutions [35], [47]. If simply explained, polymer is soluble in water under LCST due to the hydrogen bonds and restricted interactions between polymer and water, but upon heating the interactions between water and polymer are disturbed, polymer intramolecular interactions dominate and polymer (Figure 2.4) curve and polymer phase separates from water [41].

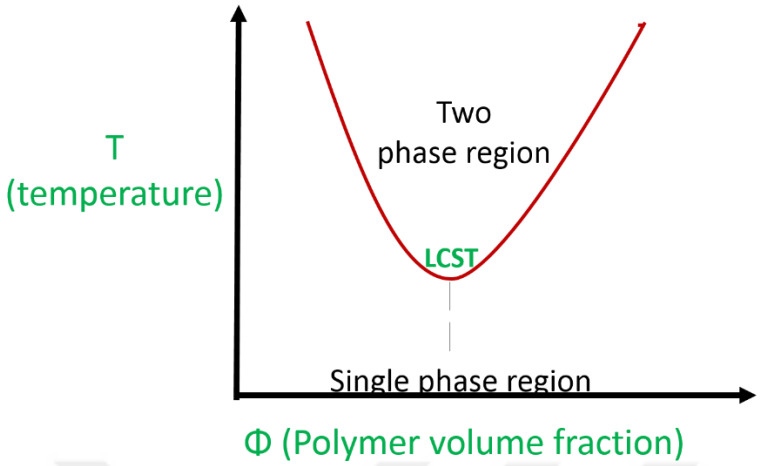

Figure 2.4: A sample phase diagram of a polymer which exhibits LCST behavior

LCST polymers show rapid, sharp and reversible phase transition and this phase transition is an entropy driven process, related with the configuration number of water molecules [36], [37]. During polymer dissolution process, enthalpic contribution to the negative ΔG_{mix} comes from the favorable interactions between polymer and water, and the entropic contribution comes from the mixing of polymer chains and water molecules [35]. Above LCST, hydrophobic aggregation and dehydration of polymer chains leads to a decrease in entropy and weakened interactions between water and polymer chains do not balance this entropic loss. Polymers that exhibit LCST behavior have both negative ΔH_{mix} and ΔS_{mix}.

T_{cp}, other phase-separation temperature for any polymer composition on the binodial curve, can be determined by a variety of methods. One method is based on the determination of the size of the polymer chain which requires the use of dynamic light scattering (DLS). Below T_c, polymers are individual coils and as the temperature approaches to T_c, these individual chains form large aggregates called mesoglobules [47]. During coil to globule transition, sharp increase in the light intensity is detected and differential refractive index between two phases indicates T_{cp}. Calorimetric methods is based on the differences between heat capacities of the sample and reference cell, and LCST transition is represented as endothermic process due to the breakage of H-bonds between polymer and water [47]. Measurements based on turbidity are usually done by UV (Ultra Violet) Visible Spectroscopy and Zhang *et al.* recommended optimal conditions to do that [47].

Most famous and the first investigated LCST polymer is PNIPAM which has LCST temperature around ~32°C in water. Poly (N-vinyl caprolactam) (PVCL) is also a popular LCST polymer due to having LCST transition around ~32°C [34], [36]. Poly (oxazoline)s (POX) polymers are also used in many applications in which LCST behavior is required and their LCST depends on generally the length of the alkyl side chains. Poly (N,N-diethylacrylamide) (PDEAAm) (~33°C) and PVME (~37°C) are also LCST polymers which have transition temperature close to body temperatures. Poly (ethylene glycol) (PEG) based amphiphilic polymers also exhibit a wide range of LCST (between 20-85°C) depending on the length of the ethylene oxide chains, size of the side chains and copolymerization partner [36]. Natural LCST polymers approved by Food Drug Administration (FDA) are derivatives of agarose and cellulose such as methyl cellulose (~40°C) or hydroxypropyl cellulose (~45°C) [36]. Gandhi *et al.* also commented that elastin like oligo- and polypeptides also exhibit LCST if their hydrophilic and hydrophobic units are balanced well due to hydrophobic folding and assembly [34]. Other LCST polymers can be poly(N-vinylalkylamide) based such as poly(N-vinylisobutyramide) (PNVIBA) (~39°C) which is a structural isomer of PNIPAM, or can be PDMAEMA based which has a T_{cp} around 14-50°C depending on molecular weight.

As a general rule for the factors that influence LCST, every factor that favours polymer-polymer interactions lowers LCST but every factor that favours polymer-water interactions or solubilisation of the polymer rises LCST [35]. In other words, LCST can be controlled via tuning polymer-polymer, polymer-water or water-water interactions in the solutions. Modification of the polymer structure via copolymerization [48], [49, 50], [51], addition of side groups or modification of the end groups [52] are some examples to tune the LCST of the selected polymer. The change in T_{cp} with above modifications depends on the hydrophilic or hydrophobic nature of the introduced moiety. If you copolymerize the polymer with a hydrophilic moiety, then the overall hydrogen bonding capacity of the polymer is increased with water and T_{cp} is increased, however, if the polymer is copolymerized with a hydrophobic moiety or the length alkyl side chain of the polymer is increased, T_{cp} is decreased [37], [41]. Introducing cross-links to the polymer increases T_{cp} since cross-links inhibit the hydrophobic aggregation of the polymer [37]. Increasing polymer molecular weight due to the entropic loss of water which stems from special organization of water molecules around the high molecular weight polymer [35].

Environmental conditions like pH, salt, ionic strength also have a great impact on the LCST behaviour of the polymers. Influence of Hofmeister salts on LCST behaviour is explained in the following sections. pH influences LCST in a great extent and the relation between pH and thermos-responsiveness can be exploited to produce multi stimuli responsive systems. For the pH and thermos-responsiveness, LCST polymers are generally copolymerized with acidic or basic moieties and pH affects the protonation/ deprotonation status. Zhang *et al*. synthesized random copolymers of N-isopropylacrylamide and 4-((2-carboxyallyl)oxy) benzoic acid P(NIPAM-co-CBA) and investigated how pH changes the LCST transition [53]. If the pH of the environment is smaller than the pKa of the acidic groups on the copolymer, copolymer becomes a more hydrophobic entity due to the protonation of the phenyl groups and LCST is decreased. On the other hand, if the pH is greater than pKa, the acidic groups are ionized, structure becomes more hydrophilic and LCST is increased. Gao *et al.* copolymerized N-isopropylacrylamide with acrylic acid units containing hydrophobic side groups and the synergic effect of the pH and thermo-sensitivity of these polymers and hydrogels was explored [54]. Same result was obtained: As pH increased, LCST of the polymer also increased due to the hydrophilicity of the acrylic acid units. Along with this result, swelling and release of protein were observed in the hydrogels of these synthesized polymers in small intestine environment where pH is 6-8, however, de-swelling and protection of the protein agent occur at the gastrointestinal track where pH is 1-3 [54]. Similar results were also obtained in the work of Weiss *et al.* [55], in which N-isopropylacrylamide is copolymeried with maleic acid, acid molecule bearing two –COOH groups and two pKa values. In this work, they concluded that the change in LCST behaviour is related to the deprotonation of the first –COOH group where swelling of the hydrogels is related with continued deprotonation of the second –COOH group. They concluded that LCST behaviour is largely controlled by the average chain length between the charges where volume transition is related with the ion concentration [55]. In conclusion, the interplay between pH and LCST behaviour of the polymer is critical especially in release applications, where a self-regulated release system can be obtained for the different parts of the body.

2.1.4 PNIPAM: a LCST polymer

PNIPAM was first reported to be a thermo-responsive polymer exhibiting LCST behaviour in 1968 [39] and the growing interest in this polymer in biomedical applications rises from the fact

that its LCST (~32°C) is close to the body temperature [35], [56], [57], [58], [59]. The presence of both hydrophilic and hydrophobic groups in PNIPAM is responsible from LCST transition and PNIPAM can be reversibly varied between hydrophilic and hydrophobic states by changing the temperature according to LCST [56], [60].

As indicated, the delicate balance between hydrophobic and hydrophilic groups determine the LCST behaviour. PNIPAM has a hydrophobic backbone and also a strong hydrophilic amide group ($O=C-NH_2$) substituted with a hydrophobic isopropyl group [60] (Figure 2.5). Amide groups interact favourably with water molecules through H-bonds while the hydrophobic isopropyl groups tend to escape from water and interact with each other via hydrophobic interactions. In terms of interactions, extensive hydrogen bonding between water and amide group of polymer is the dominant interaction below LCST while hydrophobic isopropyl groups lead to the ordering of water molecules and causing a decrease in ΔS_{mix} [60], [61]. On the other hand, above LCST, the interactions between amide group and water decreases, ΔH_{mix} becomes less negative and ΔS_{mix} drives PNIPAM to be in the collapsed state.

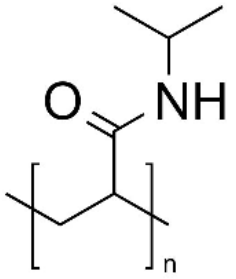

Figure 2.5: Chemical structure of PNIPAM

Wu *et al.* investigated for the first time the phase behaviour of single PNIPAM chain in water and discovered that upon heating, swelling and collapse of the polymer chain occurs in four states respectively: Coil, crumbled coil, molten globule and globule states [62], [63]. Bischofberger *et al.* showed that hydrophobic hydration was the main contributor governing the phase behavior of PNIPAM [64]. Thermal phase behavior of PNIPAM is type 2 behavior in which LCST transition is negligibly depends on the molecular weight of the polymer[57]. PNIPAM also shows broad hysteresis in cooling and heating cycles. The reason is that in the collapsed state, amide groups of PNIPAM form intramolecular hydrogen bonds and during cooling, rehydration

of PNIPAM chains are prevented with this additional interactions along with hydrophobic ones [35]. In fact, the property that mentioned above is not specific to PNIPAM but also valid for other macromolecules and polypeptides possessing both H-donor and H-acceptor groups.

Similar to phase behavior of PNIPAM in dilute solutions, for non-dilute solutions, aggregation and dissolution of PNIPAM chains follow multi-stage process: Disruption of additional hydrogen bonds formed in collapsed state and dissolution of PNIPAM chains [61]. Yan *et al.* studied different phase separated patterns of PNIPAM in non-dilute solutions above LCST which follow the colloidal particles, large precipitates and sponge-like solids respectively [61]. Below the LCST, depending on the polymer concentration, PNIPAM chains can exhibit as free chains and small clusters, large aggregates or gel-like networks.

For biomedical applications, PNIPAM can be used in different architectural forms. For example, PNIPAM hydrogels have soft architectural structure and large content of water with high solvent swelling which make these hydrogels ideal for cell encapsulation or drug delivery systems [56]. Other benefits of PNIPAM hydrogels are their straightforward and versatile synthesis, their ability to be combined with a large variety of materials from biological compounds to carbon nanotubes, thermo-sensitivity which expresses itself as volume phase transition (VPT) and biocompatibility [56], [60]. Surfaces that are either physically or chemically coated with PNIPAM can switch from hydrophilic / hydrophobic depending on the temperature due to its LCST behavior [65]. Above LCST, hydrophobic surface facilitates adsorption of extracellular proteins or agents so that cell adhesion is observed. On the other hand, below LCST, the hydrophilic surface and high content of water prevents adsorption of these agents and cell adhesion [65]. In addition to above examples, PNIPAM microgels in the form of dispersed particles are used in many biomedical applications such as drug / cell encapsulation, sensors etc. due to PNIPAM's flexibility, biocompatibility and hydrophilicity [58]. There are few drawbacks of PNIPAM such as limited biodegradability and toxicity of its monomer residues but when its advantages are considered, these drawbacks can be overlooked.

2.1.5 Poly (2-alkyl 2-oxazoline)s (PAOX): LCST polymers

PAOX polymers are a class of polyamides and they are homologues of *N*,*N*-dimethyl amides of carboxylic acids and at the same time, structural isomers of polyacrylamids (which have amide group in the side chain) and polypeptides (which have the amide group in the main chain) [66]. PAOX polymers are considered as pseudo-polypeptides, however, different from polypeptides they have tertiary amide groups in which nitrogen is located in the polymer backbone [66], [67], [68] and chiral center in the main chain is absent. They cannot form secondary structures like polypeptides because they are unable to form intramolecular hydrogen bonds. PAOX polymers exhibit side chain dependent properties since they contain both strong amide dipoles and alkyl group (R) at the same time [69]. The length and nature of the R group determine the physicochemical properties of these polymers.

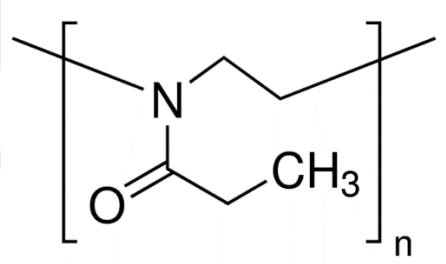

Figure 2.6: Chemical structure of poly (2-ethyl 2-oxazoline) (PEOX)

The length of the alkyl side chain also determines the LCST behavior and solubility properties of the PAOX polymers. PAOX polymer with methyl side chain, namely poly (2-methyl 2-oxazoline) (PMeOX), is soluble in all temperature range, hence do not exhibit LCST behavior. On the other hand, PAOX polymers with ethyl, isopropyl or n-propyl groups which are called poly (2-ethyl 2-oxazoline) (PEOX), poly (2-isopropyl 2-oxazoline) (PIPOX), poly (n-isopropyl 2-oxazoline) (PnPOX) exhibit LCST transition while PAOX polymers with higher alkyl groups are insoluble in water [66, 69]. In other words, LCST behavior and solubility of these polymers can be easily tuned via changing the alkyl side groups and as a general rule, alkyl side chains with intermediate hydrophobicity would provide LCST transition in water [67], [68]. Phase separation with increasing temperature observed in these polymers is a result of released water molecules which were previously interacting with the carbonyl oxygen of the amide group [70]. Lin et al. published the first study on the thermo-sensitivity of PEOX aqueous solutions in which LCST of PEOX was determined ~61-64°C depending on molecular weight [71]. Uyama and Kobayashi reported that PIPOX exhibits LCST transition in human body temperature, around ~36°C [72]. PnPOX also exhibits

LCST behavior but Tcp is very low (~15°C lower than PIPOX) due to the fact that linear n-propyl group reduces the area that is accessible for water molecules [70]. Copolymerization of EtOx, nPOX, iPOX monomers with each other or post-polymerization allow tuning LCST behavior [68], [70]. In general, copolymerization with more hydrophilic monomers rises T_{cp} while copolymerization with more hydrophobic monomers decreases T_{cp}. Architecture of the polymer also affects T_{cp}: For example, attachment of short PEOX fragments to the compact core drops T_{cp} and for the same reason, star polymers of PEOX have lower T_{cp} due to the enhanced polymer-polymer interactions with the increase in polymer concentration [68].

PAOX polymers obey to Type 1 LCST behavior, which means that increasing molecular weight reduce the LCST [67], [68], [70], [73]. Tunability of the LCST transition of PAOX polymers makes the transition reversible and no hysteresis can be observed during heating and cooling cycles [67], [70]. This property of PAOX polymers provides a great advantage over PNIPAM since large hysteresis is observed for PNIPAM in the cooling/ heating cycles. Due to the sensitivity of LCST to molecular weight, impact of the end groups on LCST is more prominent for low molecular weight PAOX than high molecular weight PAOX [70].

Although it was indicated that PAOX polymers show reversible LCST transition with heating/cooling cycles, it was previously shown that annealing of PIPOX above its T_{cp} resulted in the formation of irreversible nanofibers [74], [75]. In these studies, it was concluded that the formation of fibers was due to a slow crystallization process which was triggered by non-specific hydrophobic interactions between isopropyl groups and alignment of amide dipoles [74]. Demirel *et al.* observed fiber formation for PEOX molecules but in a much slower crystallization process [76]. Slower fiber formation and crystallization process are due to the shorter alkyl sides so that amide dipoles get closer and result in stronger interactions which require longer equilibration times. Demirel *et al.* also reported thermal properties of PAOX molecules with different chain lengths [69]. They concluded that T_g (glass transition temperature) decreases linearly with increasing alkyl side length since increased distance between the backbones of polymer chains decreases the average interaction strength between the amide dipoles. Weaker dipole-dipole interactions allow faster relaxation, however, shorter alkyl side chains prevent the relaxation of the polymer backbone to get the equilibrium structure. Mechanical properties of the polymer also depend on the length of the alkyl side chain so the crystal structure of the PAOX polymers. Chain mobility or chain length are also important in the surface properties: It was observed that surface energies of PAOX polymers decrease with increasing alkyl side chain [69], [77]. With longer and flexible alkyl side chains, these alkyl groups orient favorably towards the surface [69]. Amide group contributes to the high surface energy but longer alkyl groups shield the amide from the surface [77]. It can be concluded that thermal,mechanical

and surface properties of these PAOX polymers depend on the nature and length of the alkyl side chain.

PAOX polymers are highly desirable for biomedical applications since they are biocompatible and versatile due to the easy manipulation of side chains. These group of polymers are even considered as an alternative to PEG, which is widely used and approved polymer in biological applications. Hydrophilic PMeOX and PEOX enhance cell viability when grafted on surfaces, they have very limited interactions with human proteins to create "immune response", can be easily extracted from the body, possess very low toxicity and also exhibit antibacterial properties [67], [70], [78]. Their high biocompatibility and lack of toxic by-products are due to the absence of hydrogen donating groups in their structure, and are key advantages of PAOX polymers over PNIPAM [73]. In addition to those properties, resistance to oxidation, non-fouling properties and chemical versatility that result in many different self-assembled structures make this class of polymers highly attractive [78], [79]. Different bio-functionalities can be easily introduced to these polymers via R groups in the side chains or in their chain ends [66]. Easy access to hydrophilic or hydrophobic polymers by simply changing the side-chain of the monomer allows the preparation of a wide range of amphiphilic structures, which can self-assemble in water [67], [73], [80]. PAOX hydrogels can be also prepared for different applications; from controlled drug delivery to tissue engineering. For example, cell loaded and injectable hydrogels can be prepared via enzymatic processes to enable tunable mechanical properties, easy integration to body and longer cell viability [79].

It seems that in the future, PAOX polymers will be more widely used especially in the biomedical applications due to their incredible properties. Research is on-going to make these polymers easily available with low cost and investigate all these extraordinary properties to exploit them in different application areas, especially the biological ones.

2.2 The effect of Hofmeister salt series on the properties of stimuli-responsive polymers

In 1888, Franz Hofmeister reported and ranked the series of anions and cations based on their ability or potency to precipitate proteins from white egg [81]. This famous ranking of ions based on their ability to influence precipitation of proteins was given his name, called "Hofmeister" salt series and today it has been used to explain many biological phenomena.

2.2.1 Hofmeister salt series

Hofmeister salt series was originally based on the ions' ability to precipitate white egg proteins [81], however, today, it is used to explain physical, chemical or biological behavior of many aqueous processes [82], [83]. The influence of ions based on this ranking is more apparent for anions than cations. Therefore, for this reason, the scope of the discussion and previous literature work will be limited for the behavior of anions.

In Hofmeister series, the order of anions is like below:

$$CO_3^{2-} > SO_4^{2-} > S_2O_3^{2-} > H_2PO_4^- > F^- > Cl^- > Br^- \sim NO_3^- > I^- > ClO_4^- > SCN^-$$

The anions on the left side of Cl^-, including Cl^-, are called kosmotropic ions or kosmotropes; while the anions on the right side of Cl^- are called chaotropic ions or chaotropes. Originally, it was believed that this ranking was also related to ion's ability to alter hydrogen bonding network of water, whether the ion is a "water structure maker" or "water structure breaker" [82], [83]. If any solute is "structure maker", it means that the solute is increasing the less dense architecture at the expense of increasing the density of solute's hydration water [82], strengthening the hydrogen bonding network of water [83] . If any solute is "structure breaker", then it will have the opposite effect. Thus, kosmotropes are "water-structure makers", which means that they are strongly hydrated ions having stabilization and salting-out effect on proteins and macromolecules [82]. On the other hand, chaotropes are "water-structure breaker", which means that they are weakly hydrated ions having destabilization and salting-in effect on proteins and macromolecules. Properties of kosmotropic and chatropic anions are compared in Table 2.1.

Table 2.1: Properties of kosmotropic and chaotropic anions and their effects on proteins and macromolecules

Kosmotropes	**Chaotropes**
Strongly hydrated ions	Weakly hydrated ions
Enhances the hydrogen bonding network of water	Weakens the hydrogen bonding network of water
Increases surface tension	Decreases surface tension
Harder to make cavity	Easier to make cavity
Salting-out effect	Salting-in effect
Decreases solubility of proteins	Increases solubility of proteins
Decreases protein denaturation	Increases protein denaturation
Increases protein stability	Decreases protein stability
Prevents protein unfolding	Promotes protein unfolding

However, it was later understood that original hypothesis about "water-structure making" or "water-structure breaking" ability of ions do not sufficiently explain the ranking in Hofmeister series [82], [83]. Mainly, experiments and simulations show that physical properties of Langmuir monolayers obey to Hofmeister series, while the adjacent water structure doesn't [82], [83]. It was revealed that Hofmeister series reflect the ion's ability to penetrate the head group region of monolayer and to disturb the hydrocarbon packing [82]. Rather than affecting the bulk structure, Hofmeister salt series is related with direct interactions between anions and macromolecules. Anions' ability to polarize the first hydration shell of the macromolecule, -which is quantitatively expressed as hydration entropy (ΔS_{hydr})-, to affect hydrophobic hydration of macromolecule by increasing surface tension or to bind directly to the macromolecule better explains the ranking in Hofmeister series and the properties of these salts [83]. Kosmotropic and chaotropic anions have different working mechanism and they interact and influence the macromolecules in aqueous

systems in a distinct way. Their working mechanisms with macromolecules and proteins are discussed in a detailed way in below.

2.2.2 Hofmeister salt series and the stability of proteins and macromolecules in aqueous solution

Theory of Hofmeister salt series was originated from understanding the behavior and stability of proteins in the presence of different ions. For this reason, earlier literature works about their working mechanism were related to their effects on the stability of proteins. In those earlier works, it was generally discussed that Hofmeister ions exert their effects on the stability of proteins indirectly through changing the hydrogen bonding properties of water [84]. A cavity model was developed to explain the salting-out or salting-in effects of these ions, whereas cavity was defined as a work of a making spherical cavity in liquid, proportional to the surface area of the cavity and surface tension of the liquid. A Hofmeister salt can affect the size of this cavity through changing the thermodynamic activity and hydrogen bonding properties of the bulk water [84], [85]. Although this model can be used to interpret the salting-out of nonpolar groups of protein, the validity of this model at the molecular level was questioned: If Hofmeister ions affect the stability of the proteins by salting-out the nonpolar groups, then all Hofmeister series should be protein stabilizers, just like kosmotropes [84]. However, this is not the case for chaotropes since they salt in peptide groups by interacting via non-specific ion-dipole interactions more strongly with the unfolded form of protein than its native state [84]. Finally, Baldwin *et al.* concluded that the difference between protein stabilizers (kosmotropes) and protein denaturants (chaotropes) is a result of balance between two opposing interactions: salting-out nonpolar groups or salting-in the peptide groups of proteins [84]. Collins *et al.* considered salt ions as point charges and concluded that the effects of the salts are also related with the volume of the ion [86]. As the volume of the ion becomes larger, water molecules at the surface become more distant to the center of these point charges and water-ion interactions become weaker than the water-water interactions, which is the main effect of chaotropes.

Klement *et al.* investigated how the presence of different Hofmeister salt ions affect the potency of the aggregation of amyloid fibers, which are fibrillary polypeptide aggregates with

cross β-structure and considered as the main cause of Alzheimer's disease [85]. Although the formation of amyloid fibers is thermodynamically reversible, the type and concentration of Hofmeister salts in their physicochemical environment can trigger their aggregation with their structure and morphology. Three possible mechanisms were discussed for the salt effect on the aggregation of these protein fibrils: First mechanism was related to the "screening" effect of the ion which mainly depends on the ionic strength of the salt [85]. The other ones are specific ion-peptide interactions and changes to water structure induced by these ions as also suggested by the prior works [84], [85] [86].

More recent works in literature discuss that effects of Hofmeister salt series on the stability of proteins do not solely depend on changing the bulk water structure but also other mechanisms, such as direct ion-protein interactions, can be effective. Arosio *et al.* investigated the role of ions at various pH on the stability of a model protein, IgG2 immunoglobin [87]. Changes in pH and addition of salt trigger aggregation not only due to electrostatic interactions but also formation of an intermediate structure with an introduced hydrophobicity in a certain degree [87]. For the dimerization behavior of the protein, Cl^- and SO_4^{2-} . Dimerization constant was larger for SO_4^{2-} at low concentrations but after reaching a concentration value, this constant decreases. The larger dimerization constant was explained with the fact that divalent ions are more efficient screening and reducing repulsion, as also agreed with other authors [84], [87]. In this work, they also measured the binding potency of the ions to antibody which follow: $H_2PO_4^- < Cl^- < NO_3^- < ClO_4^- < SO_4^{2-}$, directly related with Hofmeister salt series with the exception of sulfate. The peculiar behavior of SO_4^{2-} was explained as its divalent character which promotes stabilizing effect due to the generated hydration forces although it is an ion with one of the largest salting-out activity. Also different from previous works about protein stability [84], [85]; this work pointed out that chaotropes not only bind to the polar regions of the protein but actually they interact more favorably with the nonpolar regions of the protein [87]. Okur *et al.* also reported the ion specific effects on proteins and concluded that chaotropic ions or weakly hydrated ions are attracted to the polymer backbone, especially the amide nitrogen and adjacent α-carbon [88]. Especially, Gibb *et al.* underlined that chaotropic anions especially bind to the hydrophobic concave surface of proteins and thermodynamics of hydrophobe binding mirrors the Hofmeister effect [89]. Molten globule state is generally favored in the presence of these anions because of its large and maximized hydrophobic surface area. Gibb *et al.* tested this hypothesis by using a water soluble

host (a amphiphilic molecule) and adamante carboxylic acid (ADC) as guest and determining binding constants and thermodynamic parameters through isothermal titration calorimetry (ITC) in the presence of different Hofmeister salts [89]. In the absence of any salt, largest contribution of binding comes from the enthalpy change; the entropic contribution is mainly derived from the release of ordered water molecules of solvation. In the presence of chaotropic anions, free energy of complexation decrease and hydrophobic effect is weakened since these ions compete for binding and interacting with these hydrophobic parts. Hydrophobic pocket of the host is hydrated with an entropic cost and enthalpy of binding of guest also decreased at the same time due to the binding of chaotrope anions [89]. Chaotrope anions shift the folding equilibrium of proteins by favoring molten globule state over fully folded state and they break the tertiary structure of proteins by solubilizing the hydrophobic parts of the proteins [89].

On the other hand, kosmotropes are preferentially excluded from the protein, protein surface energy increases and protein solubility decreases. These strongly hydrated ions are not preferentially partitioned to the interface [88]. Although increase in protein surface energy with the presence of kosmotropic ions favors more compact structure, at the same time, it would induce aggregation since the surface of dimer is smaller [87]. In the presence of kosmotropic anions, hydrophobic effect is strengthened and contribution of entropy favors the complexation process of proteins with a host [89]. The reason is that kosmotropes cannot lose their part of solvation shell to accommodate in the hydrophobic cavity so they don't prefer binding to protein surface [89]. These observations conclude that ions that are best at "stabilizing protein structures" are also the ones that promote the aggregation most.

Salt effects on macromolecule stability are also crucial in terms of modulating biological applications and further understanding the protein structure. As it was concluded before, working mechanism of Hofmeister salts is not related with the water making or breaking effect but with the direct interactions of salts and macromolecules and their adjacent hydration shell [82], [90]. Kosmotropic ions polarize the water molecules that are directly hydrogen bonded to amide moieties of polymer and dehydrate the polymer whereas chaotropic ions directly bind to the polymer and increase the solubility of it. For the PEO-PPO-PEO amphiphilic polymer, same mechanisms were also discussed [91]. Kosmotropic ions interact with polymer so that the entropy of water molecules around the hydrophilic portion of the polymer. The reason for dehydration by

these ions is that water molecules become less available to the polymer molecules. For the second mechanism exercised by chaotropic ions, these ions bind to the hydrophobic portions of the polymer, for PEO-PPO-PEO polymer, it was observed that these ions bind to PPO region [91]. In summary, the first mechanism is related with "salting-out" effect and the second mechanism related with "salting-in" effect. Third mechanism can be valid for both kosmotropic and chaotropic ions; since both of these types can increase the surface tension of water / polymer interface [82]. This surface tension in the water/polymer interface is due to the formation of cavity when a polymer is dissolved in water and hydrophobic hydration occurs with the dense structure of water around it [91]. If this interfacial energy rises, free energy of cavity formation also increases which causes "salting-out" effect of the protein. Especially, the influence of this ions to the interfacial energy is related with the polarizability of the ions [91]. Therefore, it is known that more polarizable species have a larger tendency to partition the hydrophobic phase and decrease the interfacial tension more.

Thormann also reported these three mechanisms of Hofmeister salt series and discussed the controversy of "water structuring" effect and ion-polymer interactions [90]. The suggested mechanism for the polymer-ion interaction was based on the overlap in the hydration zone of ion and polymer which leads to an effective force with a repulsive and an attractive component [90]. Balance of this attractive and repulsive components determines the relative "salting-in" or "salting-out" effect of the ion: If the attractive component is dominant, then a "salting-in" effect is expected. Salting-out effect that resulted from the repulsion of the kosmotropic ions from polymer-water interface. In summary, the effect of Hofmeister series is a combination of ion hydration, polymer hydration, their overlap in the hydration zone and direct polymer-ion interactions.

The effect of Hofmeister salts is not only limited to aqueous solutions of polymers or proteins but also properties of different polymer architectures are influenced. Li *et al.* studied the encapsulation stability and release properties of nanogel in which components are random copolymer of hydrophilic oligo (ethylene glycol) and a hydrophobic pyridyl di-sulfide functionalized co-monomer [92]. Size of nanogels increased in the presence of Na_2SO_4 and NaSCN compared to the nanogels prepared in pure water due to different reason. While Na_2SO_4 induced hydrophobic aggregation of the polymer; NaSCN made the nanogel more soluble in water; so water diffusion inside the gel caused it to be less stable. After these nanogels were prepared

either in Na_2SO_4 or NaSCN, they were put in the water again and encapsulation capacity of the nanogel prepared with Na_2SO_4 was observed to be high due to the restructuring caused by water and inner surface of the nanogel was turned to be more porous [92]. Naini *et al.* investigated the effect of Hofmeister salts on switching of swollen and deswollen states of PNIPAM brushes and concluded that sodium halides increase the both enthalpy and entropy of switching in the order of NaCl > NaBr > NaI- following Hofmeister series- due to the favorable interactions of the ion and amide group of PNIPAM except for the dilute concentrations of NaI [93].

2.2.3 Effect of Hofmeister salt series on the LCST of thermo-responsive polymers

Effect of a particular ion on T_{cp} of a thermo-responsive polymer depends on the chemical nature of the added ions and interaction between these ions and macromolecules. Freitag *et al.* investigated the effect of different salts at different concentrations on the thermo-responsive properties of PNIPAM oligomers [94]. T_{cp} of the pure polymer (1% w/w solution) was determined to be 32.7°C. In all cases, except polymers in lower concentrations (<0.5 M) of KI solutions, T_{cp} of the PNIPAM oligomer was decreased. SO_4^{2-} has the greatest salting out potential while low concentrations of I^- leads to salting-in effect. However, at higher concentrations of KI, a linear decrease of T_{cp} was also observed [94]. In this study, it was shown that viscosity B coefficient is linearly dependent on the transition temperature of the oligomer [94]. While negative B coefficient is related with salting-in effect, positive B coefficient is related with the salting-out effect. Thus, water making /breaking effects are not related with the changes of the T_{cp} of the polymer.

As also indicated in above, the effect of Hofmeister salts on the macromolecules were previously explained based on three mechanisms by Zhang *et al* [82], [95]. These mechanisms were polarization of adjacent water molecules bound to amide groups, hydrophobic hydration by increasing the surface tension of the cavity and direct binding. First two mechanisms depress LCST while the third mechanism increases LCST of thermos-sensitive polymers and this was confirmed through cloud point measurements of PNIPAM [95]. For kosmotropes, linear dependence of T_{cp} on salt concentrations was observed, however, beyond a certain salt concentration, two-step phase transition was stated for the first time [95]. While lower phase transition has a steeper slope, the slope of the higher phase transition is shallow. First two mechanisms result in linear dependence of T_{cp} on salt concentration, while the third mechanism result in a non-linear dependence on T_{cp},

which is explained with a saturation phenomenon. Lower temperature phase transition caused by kosmotropes is due to the ΔS_{hydr} of the anions, in other words, the first mechanism. On the other hand, higher temperature phase transition is correlated by surface tension increment caused by anions which is the second mechanism. Chaotropes bind to PNIPAM as explained by third mechanism, and the binding isotherm is Langmuir binding isotherm. The model which combines the effect of all three mechanisms on T_{cp} is given [95]:

$$T_{cp} = T_0 + c\,[M] + \frac{Bmax\,Ka\,[M]}{1+Ka\,[M]} \qquad (6)$$

T_0 is the LCST of PNIPAM in the absence of salt, [M] is the molar concentration, c has units of temperature/molarity which is directly related with ΔS_{hydr} for kosmotropes and surface tension increment of chaotropes. Ka is the binding constant of the anion and B_{max} is the increase in phase transition temperature due to direct ion binding. The distinct behavior between kosmotropes and chaotropes in this model is that the direct ion binding mechanism exercised by chaotropic anions [95]. Furthermore, Shecter *et al.* reported specific effects of a strong chaotropic salt, KSCN, on the phase transition of PNIPAM using microcalorimetric methods [96]. They added that strong binding of SCN^- is due to the resonance structure of the amide nitrogen with a partial positive charge and carbonyl oxygen with a negative partial charge in PNIPAM structure. Decreasing salting-in effect of these chaotropes, which is well-fitting with the above model and binding isotherm was also explained in this study: Number of sites accessible for SCN^- binding decreases due to the limited influence of bound ions on the hydration cages [96]. The increase in hysteresis during heating and cooling cycles also indicate that KSCN binds to PNIPAM chains since the hysteresis observed is decreased attraction between PNIPAM chains due to bound SCN^- ions so that re-hydration gets easier during cooling cycle [96].

Jhon *et al.* investigated how T_{cp} of grafted PNIPAM changes with varying salt concentration by using QCM-D (quartz crystal microbalance) [97]. In their study, they concluded that grafted PNIPAM chains lose more water of hydration than the PNIPAM chains in aqueous solutions. NaCl makes water molecules to form a rigid structure around the ions which reduces the hydration of hydrophobic groups and lowers T_{cp} [97]. This reduction in T_{cp} continues up to a salt

concentration of 0.25 M, but further increase in NaCl concentration produces a lower rate of decline in T_{cp} of the grafted polymer. In this study, they explained this effect as the lack of translational entropy and rather large density of the grafted PNIPAM chains [97].

In another work, Zhang et al. also investigated the effect of Hofmeister salts on the phase transition of PNIPAM as a function of molecular weight [98] . For high concentration of kosmotrope anions, where two transitions were observed before, the lower phase transition depends on molecular weight and concentration of PNIPAM while the upper phase transition doesn't. This is a reasonable result because tendency of the hydrophobic moieties of PNIPAM to remain hydrated is independent of molecular weight. In addition, only one phase transition was observed with the lowest molecular weight of PNIPAM in the presence of kosmotropic anions. Direct ion binding mechanism exerted by chaotropic anions also depend on the molecular weight of PNIPAM [98]. This is because B_{max} decreases with increasing molecular weight while Ka increases with increasing molecular weight due to more association of chain-chain interactions. Especially, highly chaotropic ions like SCN^- or ClO_4^- showed mot significance molecular weight dependence while weak chaotropic ions had a relatively weak dependence [98]. All of these results were interesting when evaluated that the effects of Hofmeister anions on the phase transition of PNIPAM is molecular weight dependent while LCST transition of PNIPAM in pure aqueous solutions is not influenced frommolecular weight of PNIPAM.

Other than PNIPAM, Cho *et al.* also studied effect of Hofmeister salts on the phase transition of elastin like polypeptides (ELP)s as a model polypeptide system [99]. Like in PNIPAM system, kosmotropic salts decrease T_{cp} of the ELPs which is directly related with the ΔS_{hydr} values of anions. Low concentrations of chaotropes cause increment in LCST of ELPs through binding, which is Langmuir isotherm, and at higher concentrations of chaotropes, LCST of ELPs is slightly increased due to the increased surface tension of polymer interface. In summary, the same mechanisms which are effective in the change of T_{cp} of the ELPs. The only distinct behavior of ELPs than PNIPAM is that ELPs always undergo a single phase transition while two phase transition is observed for PNIPAM in the presence of high concentrations of kosmotrope salts [99]. This difference stems from the location of amide groups in PNIPAM and ELPs: Amide groups are pendant in PNIPAM, on the other hand, they are part of the backbone for ELPs [99].

The effect of Hofmeister salt series on the LCST of PAOX polymers was also studied [100], [101]. Bloksma *et al.* investigated the effect of these salts on T_{cp} of PEOX, PIPOX, PnPOX and a comb polymer (poly) oligo 2-ethyl 2-oxazoline methacrylate (PEOXMA). Kosmotropes decrease T_{cp} linearly with increasing salt concentration while chaotropes increase it when their concentration is varied between 0-0.1 M. In contrast to PEOX and PEOXMa, T_{cp} of PIPOX and PnPROPX does not change due to their high hydrophobicity. The steep change in T_{cp} of PEOX and PEOXMA by addition of salt confirms that ionic response of more hydrophilic poly (oxazoline)s is larger [100]. This work concludes that architecture of the polymer has no effect on the response of polymer to the salt or its ionic strength [100]. Our group also studied the influence of Hofmeister anions on the T_{cp} of PEOX with different molecular weights. Two models describe the effects of kosmotropes and chaotropes on PEOX polymers.

$$T_{cp} = T_0 + c\,[M] \qquad (7)$$

Equation (7) only describes the linear dependency of T_{cp} of PEOX on salt concentrations, very similar to equation (6). This linear term arise from the dehydration of PEOX chains exerted by kosmotropic anions and from surface tension increment exerted by kosmotropic and chaotropic anions.

$$T_{cp} = \frac{Bmax\ Ka\ [M]}{1+Ka\ [M]} \qquad (8)$$

Equation 8 describes the effects of chaotropic ions: Like in PNIPAM case, chaotropic anions also bind to PEOX chains. When the effects of these salts on different molecular weight PEOX samples were compared, it was observed that surface tension mechanism contributes more to the lower molecular weight PEOX samples [101]. This is an expected result since smaller molecular weight PEOX molecules have a larger total area in the alkyl/water interface which results in larger interfacial energy. Although same mechanisms are valid for both PEOX and PNIPAM, PNIPAM showed a weaker dependence on ΔS_{hydr} due to the more hydrophilic structure of PEOX [101]. This means that dehydrated collapse state of PEOX would contain more bound water molecules than PNIPAM. Another reason is that PNIPAM is able to form intramolecular H-bonds so that more ions needed to dehydrate PNIPAM [101].

Since many biological systems contain mixtures of salt solutions, effects of salt mixtures on the thermal properties of LCST polymers was also reported [94], [102]. Mixture of one salting-

in and salting-out salt results in linear additive Hofmeister effect for both PPO and PNIPAM [94], [102]. In other words, phase transition temperature reflects both the effects of salting-in and salting-out species. When two salting-in or salting-out salts are mixed, their combined effects result in stronger salting-in effect (phase transition temperature increases more with a decreasing slope) or salting-out effect (phase transition temperature increases) [102]. Not only the effects of salt mixtures, but also effects of Hofmeister salts on the thermo-responsive behavior of macromolecules in the presence of crowding agents were investigated [103]. Song *et al.* used dextran and PEG to mimic the crowded environment of PNIPAM to study the effects of Hofmeister salts [103]. Three Hofmeister anions were selected: CH_3COO^- (kosmtrope), Cl^- (mid salt), SCN^- (chaotrope). T_{cp} of PNIPAM decreases with increasing concentrations of dextran no matter what the salt is. Continuous addition of dextran changes SCN^- from salting-in anion to salting-out anion for PNIPAM due to the competitive interaction of PNIPAM and dextran for SCN^- binding [103]. In addition to that mechanism, salting-out effects of kosmotropes are also weakened since dextran can interact with PNIPAM via H-bonding. PNIPAM also becomes less soluble in the presence of PEG since PEG competes for water molecules in the hydration shell of PNIPAM. This study shows that added crowding agents do not only exhibit volume exclusion effect, but also have actual interactions with Hofmeister anions [103].

Finally, it can be concluded that Hofmeister salt series alter the thermal properties of LCST polymers drastically. Comprehending these effects are crucial since these LCST polymers resemble the behavior of polypeptides and proteins in the body and these biological molecules function in a system which consists of different salt ions either with a salting-in or salting-out property.

2.2.4 Hofmeister Salt series and the biological processes

The major effect of Hofmeister salts or how they behave in the real biological systems have been realized in the literature. Hofmeister effects are important in the field of biology because these ions and their properties determine the structure or function of biological moieties which support life [104]. In the earlier works, it was previously shown that the mechanism of Hofmeister

salts and their effects are related to the enzyme activity, protein stability, protein-protein interactions, protein crystallization, bacterial growth etc… [85], [88], [104].

As an example to the Hofmeister effect on enzyme activity, Bauduin *et al.* showed that HIV-I protease enzyme showed different catalytic activity in the presence of KBr, KI and KCl due to the different mechanisms exercised by these salts following Hofmeister series [105]. These anions can affect the enzymatic activity by changing the bulk water structure, adsorbing specifically on to the enzyme or altering local conditions like hydrophobicity. Especially, ions that exhibit salting-out effect stabilize the native structure of the enzyme and enhance its catalytic activity.

The influence of Hofmeister effect on protein stability and protein interactions was also shown by Munishkina *et al.* by investigating structural changes and fibrillation of proteins in the presence of Hofmeister salts [106]. Aggregation and fibrillation of proteins induce neuro-generative diseases like Alzhemier's disease, Parkinson's disease... etc. For example, Parkinson's disease is caused by aggregation of the pre-synaptic protein, α-synuclein. The fibrillation of this protein was studied in the presence of 200 mM concentrations of Hofmeister anions and it was observed that all anions accelerated the fibrillation process. However, the improvement in fibrillation process followed the Hofmeister series: Kosmotropes are more effective than chaotropes in terms of inducing protein folding, aggregation and collapse of the structure [106]. Thus, the enhanced fibrillation in the presence of kosmotropes was related to the loss of uncompensated charge in the protein, screening effect, increase in preferential hydration with dehydration and hydrophobic effect [106]. The influence of Hofmeister salt series is also significant in protein crystallization because crystallization is directly related with the decrease in the solvent accessible area of the protein, so it is associated with the whether or not Hofmeister ions induce destabilization or suppress the aggregation [86].

The importance of Hofmeister salt series in the field of biology goes beyond from the concept of proteins, but its effects are also seen in biological processes like maintaining homeostasis or calcium signaling [88]. For example, the effect of Hofmeister salts on urinary stones was discovered: Kosmotropes inhibit the growth of calcium oxalate crystals and salting-out effect in responsible for promoting crystallization of calcium oxalate which is crucial in the development of pathogenesis in urinary stones [104], [107]. Hofmeister salt effects on bilayer

interactions are significant: Hofmeister ions can cause swelling, change in head group curvature and formation of stable vesicles in the cell [104]. Their effects are also highlighted in the biochemical processes in which interactions and structural changes are induced with light [104]. The effect of Hofmeister salt series must be further studied and the working principle of these salts must be better understood in order to realize and control different biological processes.

2.3 Self-Assembly of polymeric structures

Self-assembly is an autonomous and spontaneous process in which structures that are vital for life is formed. Interest in self-assembly arises from different reasons. First, self-assembly is a process in which ordered structures are formed from disordered parts. Second, the smallest unit of life, the cell, is formed with self-assembly process. Thus, by mimicking the self-assembly process from the nature, various polymeric structures can be formed and used for biomedical applications. In this section, self-assembly process is enlightened and especially self-assembled polymeric structures formed via hydrogen-bonding will be emphasized.

2.3.1 Polymeric self-assembled structures

Macromolecular self-assembly is a spontaneous process which is driven by non-covalent interactions between functional groups of molecules that ensemble and organize into supramolecular structures [108], [109]. There are two kinds of self-assembly, static self-assembly and dynamic self-assembly. In the static self-assembly, components are at equilibrium and do not dissipate energy, however, in the dynamic self-assembly, components dissipate energy [109]. Equilibration is required to obtain ordered self-assembled structures, components of the system must equilibrate between aggregated and non-aggregated states [109]. The main advantage of these self-assembled systems is the ability to tailor the properties of the bulk material during the ordering process and create a “synergic” effect by bringing together the materials with desired properties in a confined space [110].

Self-assembly is driven by non-covalent interactions that can involve hydrogen-bonding, π-π stacking, hydrophobic interactions, hydrogen bonding and electrostatic attractions [108], [109], [111]. Thus, the thermodynamic driving force for the self-assembly process is the de-solvation, collapse and hydrophobic interactions between non-polar regions of the components or attractive interactions such as hydrogen bonding or electrostatic interactions between the polar regions [112]. The equilibrium state and reversibility of the self-assembling systems is are due to the these weak non-covalent interactions [108]. In addition to that, environmental changes induce stimuli-responsiveness in the produced self-assembled structures, so self-assembly process itself is a dynamic process.

Among the non-covalent interactions that drive the self-assembly; hydrophobic interactions trigger the aggregation of nonpolar molecules into higher assemblies, reduction of the total interface area between water and solute molecules and decrease in the fraction of bound water molecules which create assemblies like micelles, polymersomes, liposomes, helices… [111]. Electrostatic interactions are based on attraction between two oppositely charged components. Nanoparticles or polyelectrolyte complexes can be formed by benefiting these electrostatic interactions. Especially, core-shell structure of nanoparticles can be formed by using one of the polyelectrolyte pairs in excess, electrostatically complexed polyelectrolytes accumulate in the core and excess polyelectrolyte pair forms the shell [111]. Self-assembled structures based on hydrogen bonding are explained in detail in the next section.

Properties of the polymeric self-assembled complexes depend on the several factors like molecular composition and structure, monomeric sequence arrangement and distribution along the macromolecular chain, macromolecular association type and stability etc… [113]. Polymeric self-assembled structures form due to the amphiphilic nature of the polymers [112], [113]. Among the self-assembled polymeric structures, polymeric nanoparticles in which their size changes from nanometers to few micrometers are largely synthesized and have a wide range of applications. One way to form these structures is to use coacervation, or simply liquid-liquid phase separation of polymer into polymer-rich phase and solvent-rich phase [114]. Different from precipitation, in coacervation, coagulated polymer chains are highly de-solvated. Another method to produce these polymeric nanoparticles is using adsorption. Polymer adsorbed on surface regulate interactions in the colloidal suspensions via electrostatic, bridging or steric effects [114]. Layer-by-layer method

(LbL) is another way to create core-shell structures in the polymeric nanoparticles. Solvent evaporation, nanoprecipitation and salting-out methods can be also used to form polymeric nanoparticles [113].

Another common self-assembled polymeric structure is micelle. In an aqueous environment, block copolymers in which each block differ in hydrophilicity from each other, self-assemble into micelles through weak interactions above a critical micellar concentration (CMT) or critical micellar temperature (CMT). In a micelle structure, a hydrophobic core is surrounded by a hydrophilic solvent exposed shell [112]. Packing parameter (p) is used to define the type of micellar aggregates formed.

$$p = v / a^* l_c \qquad (9)$$

In equation *(9)*, v is volume occupied by the packed copolymer block, a is the effective cross-sectional area per the amphiphilic block copolymer molecule at the interface and l_c is the statistical critical length of the polymer chain. When this p is smaller than 1/3, spherical micelles, when p is between 1/3 and ½, cylindrical micelles and when p is equal to 1, planar bilayer structures form like in the case of lipid bilayers [114]. Micelle like nanoparticles can be also prepared from an ionic complex from the self-assembly of block copolymers consist of oppositely charged polyelectrolytes [114].

Other polymeric self-assembled structures also include vesicles, tubules, hydrogeland fibers. Vesicles or polymersomes have hydrophilic core /outer shell with hydrophobic middle segment [112]. Hydrogels are 3D networks of fibers surrounded by a liquid aqueous phase [112]. Their main properties are encapsulation of large volume of water their porous structures and physical branch-point or fiber entanglement mechanical strength dependence [112]. All of these structures or polymeric complexes formed via non-covalent interactions can be manipulated through varying the strength of the interactions, or by selectively using one of the partners that form the self-assembled complex in excess [108]. Manipulating the interactions and tuning the hydrophilic / hydrophobic balance of the polymer segments are very common to vary the properties and morphologies of these self-assembled complexes.

2.3.2 Self-assembly via hydrogen bonding

By definition, hydrogen bonding is an attractive interaction between electron-deficient hydrogen and electron-rich electronegative element [115]. In other words, X-H…. Y interaction is a hydrogen bond when X and Y are both electronegative atoms, Y has at least one lone pair of electrons and X-H acts as proton donor to Y [116]. Thus, hydrogen bonding can be considered as a proton transfer reaction and it is related with the acidity/basicity of X and Y elements. Typical features of H-bonds include transfer of small electron density from proton acceptor to proton donor, stretching of X-H bond, shifting of infrared absorption band (which corresponds to X-H stretch) to lower frequency band [115], [116]. Strength of H-bonds depends on many factors like acidity of proton donor, basicity of proton acceptor, accessibility of acceptor and donor sites of the molecules, presence of bulky side groups or flexibility of polymer chains [115]. H-bonds involve electrostatic, covalent and dispersion contributions [116]. Strength of hydrogen bonds increase as the acidity/ basicity of the hydrogen-bonding partners or flexibility of chains increase. On the other hand, bulky side groups prevent accessibility to donor and acceptor groups and presence of these groups decrease the strength of H-bonds. In addition, polar solvents and dipolar repulsion decrease the strength of H-bonds between partners. In non-polar solvents, specific interactions remain intact more between H-bonding partners unless cooperative effects between partners prevail or steric hindrance is observed [117].

Self-assembling structures based on hydrogen bonding have many advantages due to the reversible, dynamic, directional, strong, oriented and specific nature [116], [117], [118], [119], [120], [121]. These properties of H-bonds provide phase segregating polymers properties like stimuli-responsiveness, self-healing capabilities, reversible ordering or reorganization, adaptation [117]. Complex self-assembled structures can be formed from simple building blocks by using the cooperativity and directionality of hydrogen bonds since these properties provide very specific complementarity to these building blocks. In addition to that, specific nature of H-bonds allow directed and sequential type of ordering of polymers into alternating sheets or 3D object [119], [121]. When used cooperatively, hydrogen bonds are strong. Thus, the strong nature of H-bonding also determines the chemical design of the self-assembled systems. For example, increasing number of H-bonds in a structure results in a “key-lock” type of binding between the self-assembling components [117]. In H-bonded polymer blends, relative strength of the bonds

determine the miscibility and properties like glass transition temperature (T_g) and crystallization state [115].

The simplest self-assembled structure achieved via H-bonding consists of double hydrogen bonds. In order to design this kind of a system, there are several design criteria which were explained by Sherrington *et al.* : Functional groups of the polymer which goes into polymerization should be close to the hydrogen bonding site and the complex formed should be also soluble in low polarity solvents in order to not the affect the strength and stability of the complex formed [118]. Furthermore, different self-assembled structures can be created by benefiting strong H-bonds via a phase separation process. In block copolymers, selective formation of H-bonds leads to the micro-phase separation in a controllable manner [120]. . Using hydrogen bonds, block copolymer PMMA-block-PVP is blended with PVPh poly (vinyl phenol) (both H-bonded to both blocks) and phase separation is controlled in nanometer scale, different micro-phase separated structures are obtained [122]. This is a good example showing that blending of block copolymers and associating them via H-bonds is a good method to produce hierarchical two-dimensional structures. Lee *et al*. studied pH-induced reversible complexation between PEO and PCL-block-PMMA poly (ε-caprolactone)-block-poly(methacrylic acid) and due to the formed H-bonds, the micelle structure is pH-responsive [123]. Shi and coworkers prepared complex micelles with tunable channels in which size / permeability of them are controlled via changing environmental conditions [124]. Hydrogen bonds can also be used inserting nanoparticles into polymer matrices. Nanoparticles can interact selectively to the functional block of the polymer which can be also used to create gel systems [121]. Mathias *et al.* used H-bonds to assemble pyroglutamic acids into gels in which first fiber structure, then gel structure is created via H-bonds [125]. The diversity of assemblies based on H-bonding is not limited with above examples. Self-assembled structures based on H-bonding include nanoparticles and complexes [126], polymersomes [127], capsules [128], [129] or layer-by-layer films [130], [131].

2.4 Layer-by-Layer (LbL) Self-Assembly of Stimuli-Responsive Polymers

LbL assembly of macromolecules, which is based on the sequential and alternate deposition of species through complementary molecular interactions, has been a simple and versatile method to prepare functional surfaces and thin films [132], [133], [134], [135]. Compared to other film preparation methods, such as Langmuir-Blodgett (LB) or self-assembled monolayers (SAM), LbL assembly has many advantages. For example, LB assembly requires expensive instruments and long processing time, is not applicable to non-amphiphilic material and requires pre-deposition of molecules on the substrate [133], [136], [137]. Furthermore, SAM method, is not useful to form multilayer structures [137].

LbL deposition is a versatile, simple and low-cost bottom-up fabrication technique to form multilayer assemblies. One of the most prominent advantages of this technique is the precise and nanometer scale control over the film thickness and physicochemical properties. The control over the film properties can be obtained during the assembly via adjusting parameters like pH, temperature, ionic strength [132]… In addition, a wide range of materials from polymers to colloidal particles and substrates, including the non-planar ones, can be used in this method [132-134, 136-140]. The availability and usability of wide range materials in LbL adsorption allow the multilayer assemblies to be stimuli responsive.

LbL deposition was first introduced by Decher and Hong by using synthetic polyelectrolytes as layers using electrostatic attraction [141]. Popularity of LbL films rose in 1997 with the work of Decher [142]. Then, LbL assembly has become a very common technique to create functional and versatile multilayer structures for a wide range of applications.

2.4.1 Properties and Methods of LbL Assembly

LbL deposition is the sequential and alternating adsorption of interacting species. In the LbL process, interacting species are adsorbed in a confined space and they are far away from equilibrium state [143], [144]. In such a dynamic and non-equilibrium state, adsorbing species try to relax and reach equilibrium through competitive inter-diffusional movements. These characteristics of LbL assembly gives rise to different functionalities that the multilayers can have so that the versatile properties that were mentioned are gained [144], [145], [146].

LbL assembly involves two steps of adsorption which is led by diffusion-driven kinetics. The first step involves initial anchoring of the coating material to the substrate and the second step is the slow relaxation of the adsorbed molecules so that interacting species form interpenetrating and densely packed structure on the surface [136]. First step of adsorption is fast and leaves unsaturated sites on the surface while the second step of adsorption is the slower and diffusion-controlled process in which deposited species re-arrange and interactions between them restructure the film [132], [136].

Dynamic properties of LbL films include chain re-arrangement within the films, tunable swelling degree and gradual disintegration under conditions of equilibrium control [138]. Re-arrangement and re-structuring of the film is due to the non-covalent nature of interactions that drive the deposition. Swelling degree of the films can be tailored by applying external stimuli so that films swell or shrink as a response to stimuli. Dubas and Schlenoff showed that films swell with increasing NaCl concentration due to the shift in equilibrium [147]. Another dynamic property of LbL assembled multilayers is that they gradually disintegrate under conditions of equilibrium control [138]. These dynamic properties can be exploited in various applications like surface patterning to create porous structures, drug release or bio-sensing.

Different species can be deposited through LbL process in five ways and assembly method is crucial in terms of determining the properties of the assembled films. The first method is called dip coating or immersive assembly and it is shown in Fig 2.7. Dip coating involves immersing substrates into solutions of the coating material with intermediate rinsing or washing steps. The rinsing or washing step is necessary to remove weakly bound molecules to the substrate and to prevent cross-contamination during the assembly [134], [136], [140], [148]. At the end of each cycle, drying can be applied to the coated substrate. With the drying, thicker and rougher films can be produced since successive dipping of the substrate into solutions provide a moist environment and improves chain mobility [134], [137], [140], [148]. Dip coating is the most commonmethod for LbL deposition, easy to handle, result in inter-penetrated structure, can be applied to non-flat substrates or substrates with various geometries. The only drawback of the dip coating is its time-consuming process but this drawback can be overcame by developing automated systems [140], [148].

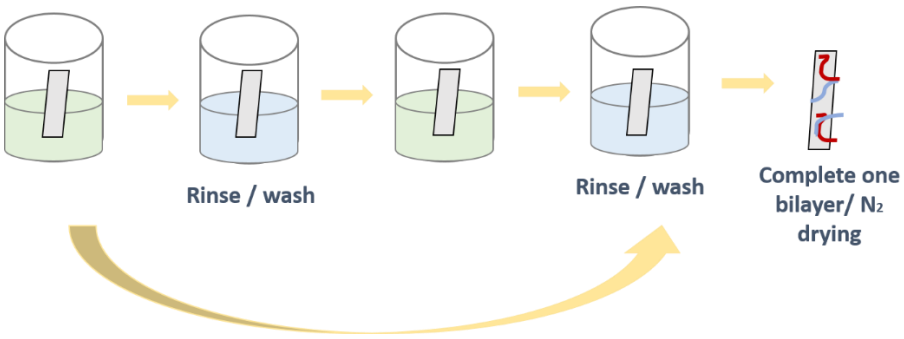

Figure 2.7: Illustrated scheme of LbL dip coating (immersive assembly) method

Spin and spray assembly for LbL deposition were also used commonly. Spin assembly results in more homogeneous, thinner and stratified films when compared with the films obtained by dip coating [134], [140], [148]. This is because spin coating involves not only molecular interactions but also viscous, shear and centrifugal forces [133], [140], [148]. Advantages of spin assembly compared to immersive assembly are being a time-efficient process, homogeneous and ordered film structure due to the suppression of the interpenetration of the adjacent layers and dense packing coverage [132], [133], [134]. Disadvantage of this method is mainly being not applicable to non-flat substrates and thickness differences on the surface between the parts where solution was cast and edges. Spray coating depends on the usage of aerosol polymer solutions and sequentially spraying them on the substrate. Film properties such as morphology, chemical structure depend on the on polymer concentration, spray duration, flow rate, resting duration, whether the solution is sprayed vertically or horizontally, whether or not the substrate is washed and these properties can be tailored like dip assembly [133], [148].

Film properties are affected from both the assembly method and conditions like pH, temperature, solvent, ionic strength during the assembly. For example, depending on the conditions, film growth can be linear or exponential. Linear growth means that polymers dissolved in solution which would be adsorbing interact well with the outer layer [136]. In case of linear growth, adsorbed species diffuse with constant distance in a limited manner within the layers. Exponential growth was first reported in 1999 [149], and the exponential growth mechanism was “in” and “out” diffusion. It was reported that as the number of bilayers increase, the growth trend

alters from exponential to linear due to the restructuring of the bottom of the film which hinders further diffusion. Another reason the exponential growth is the increasing surface roughness as the amount of adsorbing species increases at each consequent bilayer [132]. Film properties can also be modified via post-treatment or annealing of the LbL films. Tailoring structural properties either during the assembly or via post-treatment allow LbL multilayers to be used in a variety of application areas such as release and delivery of functional molecules, bio-protective coatings, sensors, bio-reactors, self-healing materials and platform for tissue-engineering and cell encapsulation [134], [137], [138]. Kozloskaya *et al.* mentioned that hydrogels can be built in LbL fashion and these ultrathin hydrogels can serve as a soft platform for the deposition of biological tissue and high capacity encapsulation platform for functional molecules [139]. When the properties and wide application areas of LbL assembly are considered, it seems like the popularity of this deposition method will likely increase in near future.

2.4.2 Molecular Interactions Driving LbL Assembly

Molecular interactions that drive LbL assembly vary from covalent bonding like metal-ligand interactions to non-covalent interactions like electrostatics, hydrogen bonding or hydrophobic interactions. In this section, mostly non-covalent interactions that drive LbL assembly will be discussed.

2.4.2.1 Electrostatically Bonded LbL Assembly

Electrostatic assembly is the first mechanism that was used in the deposition of LbL films as shown in the pioneering work of Decher *et al* [141]. Electrostatic interactions provide multilayers to have tunable properties. It is based on sequential adsorption of polyanions which carry negative charge and polycations which carry positive charge and the film growth will continue until a neutral charge on the substrate is obtained [135], [150]. Electrostatic interactions that drive the assembly have both attractive and repulsive components. Attractive component of electrostatics controls the polyelectrolyte binding whereas repulsive component controls the adsorbed amount [150].

Thermodynamic driving force in electrostatically bonded polyelectrolyte multilayers (PEM) is entropic due to the release of counter-ions during adsorption [150]. Besides, the loss in the degree of freedom during adsorption onto a 2D substrate is another factor that contributes to free Gibbs energy [150]. Mainly, there are two steps in the formation of PEMs: The first step is the fast adsorption step which is driven by electrostatic attraction and the second step is the slow re-arrangement step in which adsorbed polyelectrolytes move and change their conformation.

Among electrostatically bound multilayers, the most studied one is PSS / PAH (polyallylamine hydrochloride) films [151]. Especially, for the biological applications, these films are studied since sulfonate groups provide good cell adhesion and proliferation on them. Another popular assembly is PAA/PAH films, first shown by Mendelshon *et al* [152]. Different polyelectrolytes can be used as long as enough charge density on the polyelectrolytes are provided for the electrostatic attraction.

PEM growth can be also linear or exponential depending on the mobility of polyelectrolytes and "in" and "out" diffusion mechanism occurs as discussed above. Linear growth is observed for strong polyelectrolytes carrying high charge density like PSS and PAH [135]. For weak polyelectrolytes, inter-diffusion occurs due to formation of weak ionic cross-links. Schaaf *et al.* described that in an exponentially growing PEM, at least one of the polyelectrolytes diffuse throughout the film and an energetic barrier prevents the complete diffusion of the adsorbed molecule outward the film [153]. On the other hand, in a linearly growing film, none of the polyelectrolytes diffuse. Switching from linear to exponential growth or vice versa is possible depending on the factors involved in the assembly process. Michel *et al.* observed transitions in PEM films and concluded that this type of transition from one growth regime to another is due to the restructuring of the multilayer that hindered the diffusion of multilayers [154]. Both growth regimes have their own advantages. With linearly growing PEM films, more control on the morphology, for example, smooth films which are suitable for loading of small molecules, can be obtained [150]. In an exponentially grown LbL films, permeable and porous films can be obtained which are ideal for the encapsulation of big molecules.

Internal structure of electrostatically bound LbL films also depends on the nature of the polyelectrolytes used, so whether the growth regime is exponential or linear. For LbL films which grow linearly, the internal structure is glassy since the polyelectrolytes adsorbed are immobile

[150]. On the other hand, in an exponentially growing LbL, gel-like structure is observed. The architecture of PEMs includes three zones. Zone 1 is the region closest to the substrate, so the diffusion rate is very low [150]. In zone 2, diffusion rate is higher but constant. In zone 3, which is the region closest to the surface, diffusion rate increases with thickness. Polyelectrolytes are loosely bound and less interpenetrated.

Parameters influencing electrostatically bound LbL films are mainly pH, ionic strength, temperature, molecular weight, polyelectrolyte charge density and polyelectrolyte chain architecture. pH is an important factor since it affects the degree of the ionization of the polyelectrolytes used in the assembly. Studies show that especially in PEMs consisting weak polyelectrolytes pH variation results in changes in the film thickness, growth mechanism, interpenetration level or surface wettability [135], [155], [156], [157]. Yoo *et al.* indicated that two critical parameters are affected by assembly pH which are linear density of the polyelectrolyte and surface charge density [156]. Assembly pH not only determines the properties of LbL films but also post-assembly behavior like swelling.

Annealing or post-treatment of PEMs with solutions having different pH is also a way to modify the properties of these films. This is because variation in pH determines the degree of disassociation or the number of electrostatic bonds remained [150]. Most apparent change induced by pH is the swelling of the PEMs due to the repulsion of the charges of polyelectrolytes on the surface and increased osmotic pressure [150]. More radical changes like stability decrease or disassembly in PEMs can be also observed with pH treatment. Mauser *et al.* investigated the pH stability and morphology of LbL hollow capsules made of PMAA and PAH [158]. Due to the ionization of the weak polyelectolytes, the capsules first swelled, then dissolved when they were treated with solutions having pH smaller than 2.3 or higher than 11.

Salt is an important factor that affects the properties and morphology of PEMs. Presence of salt during deposition induces screening effect which results in repulsion between adsorbed polyelectrolytes. This “screening” effect has important consequences. Multilayers deposited at the low ionic strength, have lower porosity and higher swelling ratio since polyelectrolytes can still adopt an extended conformation in the solution. In addition, depending on ionic strength, between 0.001 M to 0.01 M, presence of salt results in rougher and thicker films [150]. However, when the salt concentration exceeds 0.1 M, thickness and roughness of the film decrease. In the study of

Dubas *et al.,* PEM film growth was dependent on NaCl concentration used during the assembly [147]. Film growth and thickness increase continued until a critical salt concentration, which is 0.3 M. When salt concentration exceeded 0.6 M, the film starts to dissolve. Fery *et al.* also showed that presence of salt can be used to produce nano-sized pores in the PEM structure; thus it can be an important parameter to tune the permeability of the PAA/PAH films [159]. Zhang *et al.* also formed porous LbL films and controlled the size of pores by tuning NaCl concentration [160]. Salomaki *et al.* illustrated that not only the ionic strength of the salt but also the nature and the location of the salt in Hofmeister series are critical for the properties of PEMs [161]. In this study, thicker films were obtained when chaotropes are used since the interaction between the chaotropes and polyelectrolytes was stronger.

Salt annealing of PEMs was used to trigger different diffusional responses between the layers so that swelling and smoothening of multilayers were observed [162]. In another work, quartz crystal microbalance (QCM-D) was used to investigate the swelling behavior of the electrostatically bound LbL films when they were exposed to four different salt solutions with variable monovalent anions. The type of the anion and salt concentration categorized to four different regimes were associated with the swelling behavior of the films [163]. Mjahed *et al.* showed that as the ionic strength of the post-treatment solution increases, swelling degree of the films increases accompanied with the spherical hole formation [164]. Formation of holes was due to the increased osmotic pressure inside the film with polyelectrolyte dissolution. Understanding the effect of the post-treatment of PEMs is also crucial to investigate their potential to be used in drug release applications when they are exposed to body conditions. Anandhakumar *et al.* used electrostatically bound PMMA/PAH films as a drug encapsulation and release platform [165]. When these films were treated with solutions having different pH and ionic strength, the speed of the drug release changed. For PMMA/PAH films, non-porous morphology of the films were retained at neutral pH and low ionic strength. At different pH values, pore formation was observed due to the repulsion of charges between PMMA carboxylate groups at basic pH and PHA amine groups at acidic pH. At the same time, as the salt concentration increases, with the screening effect polymer-polymer and polymer-surface interactions were reduced. As a result, drug release rates were enhanced. This work is also useful to show the potential of PEMs to be used in site-specific drug release.

Temperature is also a factor to be used during the assembly or post-treatment to tune the properties of the multilayers. Tan *et al.* formed PDDA/PSS films via electrostatic interaction at different temperatures and observed that films were thicker when the assembly temperature was higher due to swelling and increased interpenetration [166]. Similarly, Salomaki *et al.* reported that with increasing temperature, thickness of PAH/PSS films increased and the growth trend changed from linear to exponential [167]. The effect of temperature becomes more prominent when thermo-responsive species are used. In another work by Tan *et al.*, electrostatically bound LbL films composed of temperature-responsive triblock copolymer and either PSS or PAA as a polyanion exhibited temperature dependent behavior [168]. Temperature-dependence was due to the PPO block of the triblock copolymer , since PPO block changes from hydrophilic coil to hydrophobic globule with increasing temperature. For example, temperature induced swelling depends on whether H-bond forms between PPO and polyanion (PSS or PAA) or between PPO and retained water molecules in the multilayers. In this case, pH also affects temperature-induced swelling since it determines the degree of ionization of the polyanion.

Other factors are molecular weight, solvent type or polyelectrolyte charge density. Generally, as the molecular weight of the polyelectrolyte increases, stability of the multilayer structures increases due to the entropic effects and higher number of possible electrostatic bonds [150]. Kujawa *et al.* investigated the influence of molecular weight on the morphology of multilayers composed of chitosan and hyaluronan [169]. Increase in molecular weight results in thicker films as expected. On the contrary, Sun *et al.* observed that when lower molecular weight PAA is used in PAH/PAA films, thicker films formed since lower molecular weight PAA is more prone to diffuse over large distances [170]. Solvent type influences the properties of PEMs according to the polyelectrolytes used in the assembly and the quality of the solvent. For example, Poptoshev *et al.* changed the amount of ethanol in the polyelectrolyte solutions during the assembly and concluded that increased ratio of ethanol in solutions led to the increase in film thickness as the solvent quality worsens for the polyelectrolytes [171]. Finally, polyelectrolyte charge density is crucial because it will determine how electrostatically assembled multilayers form and grow. Below a critical charge density, formation of PEMs is impossible since the electrostatic driving force would not be strong enough.

Electrostatically bound LbL films are robust, firm and stable. As long as polyelectrolytes have enough charge density, PEMs quickly form and assembly or environmental conditions like pH, temperature, ionic strength can be adjusted to tune the properties of them for the desired applications.

2.4.2.2 Hydrogen-Bonded (H-bonded) LbL Assembly

After first studies show that PEMs were fabricated using electrostatic interactions, LbL films were assembled via H-bonds. First studies of H-bonded LbL assembly were shown by using non-ionic and neutral polymers by Stockton and Rubner / Wang *et al.* at the same time simultaneously [130], [172] . Stockton and Rubner suggested the use of poly(aniline) (PAni) with different water-soluble polymers such as poly(N-vinylpyrrolidone) (PVPON), PEO or PVA and assembled them into LbL multilayers via H-bonds [130]. In the second study by Wang *et al.,* H-bonded multilayers were formed between PAA and poly (4-vinylpyridine) (P4VP) [172]. H-bonds formed between the pyridine rings of P4VP and carboxylic acid groups of PAA. These studies show that H-bonded multilayers can be constructed by the self-assembly of neutral polymers and weak polyacids. Basically, H-bonded multilayers can be constructed if the components of the film have complementary H-accepting and H-donating groups. The importance of these first studies is not only because of being primary studies that show LbL films can be formed via H-bonding but also these studies show that biocompatible and neutral polymers which are ideal for biomedical applications can be used in these films [173] so toxicity issues with charged molecules can be overcame.

Advantage of H-bonded LbL films over electrostatic ones is not limited with the use of water-soluble, biocompatible and neutral polymers which gives rise to biomedical applications. Possibility of using wide range of polymers in H-bonded multilayers also allows the usage of polymers with low glass transition temperature (such as PEO) give the possibility of building free standing films [131]. The control of H-bonding in LbL deposition has offered responsivity to environmental stimuli such as pH or temperature at mild values [131] which are the interest of controlled release applications. Since H-bonds are disturbed usually at neutral pH values which

are relevant to physiological conditions, they have improved pH stability when compared to electrostatic ones.

Sensitivity to environmental stimuli of H-bonded multilayers enables tuning of them for the desired applications. Especially, understanding how these factors like pH, temperature, molecular mass and ionic strength affect the film properties is crucial. Each of these factors will be discussed separately.

2.4.2.2.1 Factors Affecting H-Bonded LbL Assembly

Important factors affect the H-bonded LbL assembly are mainly pH, temperature, molecular weight and ionic strength. These factors can be used to tailor the properties of LbL films during the assembly or as a post-assembly condition. Among these factors, chemical nature of the polymers is the primary factor that should be considered in H-bonded LbL assembly so that environmental conditions can be arranged accordingly. For example, bilayer thickness is highly affected from hydrophilic / hydrophobic nature of the polymer since it is correlated with the number of intermolecular contacts [174]. As the hydrophilicity of the polyacid increases, for instance changing polyacid from PMAA to PAA, film thickness increases and film growth transits from linear to exponential. In addition to that, films that contain polymers like PVPON exhibit linear growth while films that contain polymers like PEO grow exponentially due to weaker interactions and increasing surface roughness leading to increased surface area for the growth [173]. Kharlampieva *et al.* showed that PMAA/PEO multilayers showed higher permeability compared to PMAA/PVCL multilayers [175]. More hydrophobic nature of PVCL gives rise to additional interactions so that interpenetration between the layers is more and films are less permeable. The influence of different alkyl side of the PAOX polymers, in other words, the influence of water solubility and hydrophobicity on the thermodynamics of the LbL deposition with TA was investigated by Hoogenboom's group [176]. They concluded that the film formation between PMeOx and TA was enthalpy driven while film formation between PEOX and TA, as well as PnPOX and TA, were entropy driven [176]. Thermodynamics of the film formation was also reflected in different film morphologies. Films formed with PMeOx at room temperature were non-continuous and islands, which is a result of the drying process since the polymer contains

large amount of water, were observed. On the other hand, films containing PnPOX had cracks due to the adsorption of PnPOX as dehydrated / collapsed globules [176].

All these studies show that chemical nature of the polymers is important. After proper polymers are selected for the construction of H-bonded multilayers, other factors that were listed above should be considered carefully. The influence of these factors are described in below both as a factor during the assembly and as a post-assembly parameter.

Using H-bonding interactions in LbL assembly has offered pH responsivity to deposited multilayers [130], [131]. H-bonded multilayers of aqueous polymers and weak polyelectrolytes are generally prepared at acidic pH range due to the protonated state of polyelectrolytes in this range [177], [178]. After a critical pH value is reached, hydrogen bonds are disturbed due to the ionization of the weak polyacid and films start to dissolve. This pH value in which H-bonded multilayers starts to dissolve is called critical disintegration pH. At this critical pH value, dissolution starts because the number of remaining hydrogen bonds is not sufficient to keep the film integrated. Thus, this critical disintegration pH or the pH range in which the multilayers are stable depends on the pKa and ionization of the polyacid, and the strength of the hydrogen bonding [173], [174], [179]. When the interaction between adsorbed molecules are relatively weak, critical disintegration pH decreases since there are lesser number of hydrogen bonds to dissolve.

In this sense, chemical nature of the components is important for the pH stability of the multilayers. Kharlampieva *et al.* showed that PMrMA/PVCL multilayers have enhanced pH stability when compared with PMMA/PVME multilayers [175]. This is due to the more hydrophobic nature with two extra methyl groups in the caprolactam ring of PVCL gives rise to additional and stronger interactions. Our group, Demirel and coworkers showed that different molecular arrangements in structurally isomer polymers and different end groups also affect the pH stability of H-bonded multilayers [180]. PIPOX and TA formed thinner but more stable films compared to PNIPAM / TA films. This is due to the different conformation of PIPOX than PNIPAM; carbonyl groups of PIPOX is more accessible to hydroxyl groups of TA; giving rise to stronger H-bonding [180]. Enhancement in pH stability was also provided by functionalizing the end group of the polymer. Introduction of amino group resulted in enhanced pH stability and rather a gradual dissolution profile rather than a sharp profile due to the additional electrostatic groups between positively charged ammonium groups and negatively charged phenolate anions of TA

[180]. As seen from previous examples, there is a strong relationship between the structure of the polymers used in LbL assembly and the stability of the films.

Assembly pH affects the properties of multilayers like film thickness or morphology. Yang *et al.* illustrated that thickness and morphology of PVPON/PAA films can be controlled via assembly pH since pH changes the conformational state and ionization degree of PAA [181]. PVPON/ PAA films can be easily prepared below pH4 where the ionization of PAA is suppressed and dissolution of the multilayers occurs at pH5.5. In general, bilayer thickness decreases as the assembly pH approaches to critical disintegration value. Erel *et al.* fabricated hybrid H-bonded multilayers of PVCL / poly (l-aspartic acid) (PLAA) / TA [182]. Presence of TA shifted critical disintegration pH of multilayers to higher values, in the basic range, due to the high pKa of TA. Dissolution and release of the films were controlled by pH variations. In another work suggested by Erel *et al.,* H-bonded films of TA with several neutral polymers such as PVCL, PEO, PNIPAM or PVPON were constructed only at acidic conditions while electrostatically assembled TA containing films could not be formed [183]. High pH stability of the films was due to the presence of TA and pH stability was even further improved in TA/ copolymers of N-vinylpyrollidone multilayers with the presence of extra electrostatic interactions.

Exposing H-bonded multilayers to solutions at different pH values is a useful method to tune the properties. Our group illustrated that "pH annealing" of PVPON / TA multilayers, pH treatment of spin coated multilayers just below the critical disintegration pH, improved the pH stability of multilayers via relaxing the kinetically trapped molecules and increasing the number of H-bonds between PVPON and TA [144]. The effect of pH treatment was evaluated in terms of both varying the pH of the buffer solutions and pH- treatment time. As the pH of the treatment solutions approach to the critical disintegration pH, stability of the multilayers increase as a result of dynamic nature of H-bonds [144]. Erel *et al.* incorporated block copolymer micelle (BCM) of poly (2-diethylamino) ethyl methacrylate)-*block*-poly (N-isopropyl acrylamide) (PDEA-*b*-PNIPAM) with polybasic PDEA cores into H-bonded multilayers at a physiologically relevant pH [184]. The use of H-bonding in this study has offered the advantage of preserving pH response and micellar morphology since micellar corona (PNIPAM) is not in competition with their binding to ionizable polymers. When exposed to acidic pH, micellar dissolution or restructuring was inhibited

through conformational restrictions induced by H-bonding between micellar corona and the polyacid used in LbL deposition [184].

Assembly pH mainly influences the growth behavior and thickness of multilayers. On the other hand, post-treatment or "pH annealing" of H-bonded multilayers is a tool to tune the stability of the films.

H-bonding in LbL multilayers allows the incorporation of neutral and aqueous polymers, including the thermo-responsive ones. With the incorporation of these polymers, exhibiting either LCST or UCST, temperature has become an important parameter to influence the properties of these films.

The effect of assembly temperature on the H-bonded LbL films was first shown by Quinn and Caruso [185]. They showed that at 30°C, PNIPAM / PAA films are thicker and rougher than the films prepared at 20°C or 10°C. The reason is that 30°C is very close to the LCST of PNIPAM so PNIPAM molecules were adsorbed as globules on the surface [185]. Kharlampieva *et al.* incorporated polymers like PVCL or PVME into H-bonded LbL multilayers which also exhibit LCST behavior in aqueous solutions. In this study, as the temperature increases and approaches to LCST of the polymers, permeability of the film increases due to the phase transition of polymers and loosening of the film structure as a result of it [175]. Zhuk *et al.* used thermo-responsive polymers in the formation of H-bonded multilayers and observed that temperature affects the pH stability of the deposited films [186]. The pH scale in which the films are stable can be adjusted by temperature. As the temperature increases, for the films which are composed of LCST polymers, pH stability increases while films compromise of UCST polymers, pH stability decreases [186]. Ma *et al.* investigated the temperature effect on PVPON/PAA films, specifically how the temperature affects the film cloudiness and thickness of the film in defined intervals [187]. They found out that there was a critical temperature which the film transits to cloudy region due to the interface association caused by decreased number of H-bonding. In summary, temperature effect on PVPON / PAA multilayers was explained as a result of interfacial association and chain rearrangement that stem from the balance between hydrophobic interactions and H-bonding [187]. For poly (2-(n-propyl)-2-oxazoline)/TA multilayers, different growth mechanisms were also reported depending on the critical temperature of the polymer [188]. Above T_{cp}, polymer molecules are adsorbed as collapsed globules and deposited multilayers were thicker suggesting

that hydrophobic interactions play an important role with the adsorption of polymer molecules as collapsed globules [188]. In addition, the morphologies of the films were also different. While below $T_{cp,}$ films are smooth and flat, above T_{cp}, poly (2-(n-propyl)-2-oxazoline) globules form discrete islands on the surface resulting in a granular and rather rough morphology [188]. In addition, it was reported that thermo-responsiveness of the polymer was lost after deposition of poly (2-(n-propyl)-2-oxazoline)/TA multilayers above T_{cp} [188].

Post-assembly temperature can be also used to tune the properties of H-bonded films. For example, PVPON/PAA films were heated to 120°C and due to the dehydration, film surface became flat and smooth [189]. Quinn and Caruso also illustrated that dye release was enhanced with increasing post-assembly temperature from PNIPAM/ PAA multilayers [185]. The influence of temperature on the release rate indicates that temperature can be also exploited as a factor to be used in the controlled release applications.

Another important factor is the molecular weight of the polymers used in the film assembly. Influence of the molecular weight on H-bonded LbL films is related with the chemical nature of the polymer, whether the polymer possesses strong or weak hydrogen acceptor / donor groups [131], [174]. If the polymer attaches strongly to the components of the film, which is a property of polymer that has strong hydrogen acceptor groups, then the film thickness doesn't vary with molecular weight [131], [174]. Independence of molecular weight from the film growth in these systems is due to the high density of hydrogen bonds which results in chain flattening during the adsorption [131]. In addition, critical disintegration pH values of H-bonded films is independent from molecular weight of the polymers. The effect of the polymer molecular weight is limited to the kinetics of film disintegration, as the molecular weight of the polymer increases, the film endures longer at the basic range or pH values close to critical disintegration pH [131], [174].

Lee *et al.* prepared multilayer assemblies of PVA and weak polyacids such as PAA or PMMA based on H-bonding [190]. Influence of both the degree of hydrolysis and molecular weight of PVA on the film growth or pH stability was investigated. As the molecular weight of PVA increases, bilayer thickness of the films increases but the critical disintegration pH for the films remains at the same value [190]. Guan *et al.* also showed that the effect of molecular weight of polymers on the thickness of PVPON/ PAA multilayers and observed that the impact of the molecular weight was only below 40 kDa [191]. DeLongChamp and Hammond studied the effect

of molecular weight of PEO on PEO/PAA multilayers [192]. When PEO molecular weight was increased from 1.5 to 20 kDa, film thickness increases significantly. Furthermore, using PEO with very low molecular weight results in very rough and poor quality films [192]. All of these studies in the literature correlate well with the relation between molecular weight and film properties as explained above.

In the literature, salt effect in electrostatically assembled multilayers has been studied extensively. For H-bonded multilayers, ion type and its concentration is very crucial both as a factor in the assembly and in the annealing process because it affects the delicate balance between the hydrogen bonding between adsorbed molecules and induced hydrophobic interactions.

Ions screen the electrostatic charges within the multilayers and increase the degree of ionization of weak polyelectrolytes / polyacids [131], [174]. However, unlike electrostatically assembled multilayers, the effect of ions or salt is not limited with the screening effect, both the ion type and its concentration are important. Ion type affects the solubility of the polymers in aqueous solutions so it is a direct factor that can be manipulated during the assembly. The effect of the salt on the H-bonded LbL films also include dehydration effects and induced ion-dipole interactions [174].

Quinn and Caruso formed H-bonded multilayers which contain a hydrophobic-hydrophilic copolymer, poly (styrene-*alt*-maleic acid) (PSMA). Inclusion of this copolymer induced thermo-responsiveness and the effect of the salt was large. Films that were assembled in the presence of 0.2 M NaCl were much thicker than the films were assembled in the 0.02 M NaCl because of the solubility and adopted conformation difference of the polymers in two different salt concentration regime [193]. Addition of salts containing monovalent or divalent ions also affected the growth of H-bonded PAA/PEO films. First, with the addition of salts film growth was improved but after the concentration of lithium triflate exceeds 0.5 M, film growth was inhibited [192]. In the same study, pH stability of PAA / PEO films was also enhanced when exposed to lithium triflate solution [192].

Salt effect on the stability of H-bonded films is controversial. Sukhishvili and Granick concluded that exposure of PEO/PMMA films to 0.4 M NaCl solution resulted in enhanced pH stability [178]. On the other hand, same authors also reported that critical dissolution pH was

decreased in the presence of 0.5 M NaCl [174]. Annealing of H-bonded LbL films with salt solutions may also induce different morphologies in the film. Lin *et al.* showed that post-treatment of H-bonded PVPON/PAA multilayers with NaCl solutions resulted in micro-phase separation followed by a de-wetting process [194]. Erosion of the films was further enhanced with the increasing NaCl solution due to the increased ionization and dissociation of PAA [194], as SEM images of the films suggest, holes form in the film as a result of this erosion. De-wetting of the film is related to the diffusion ability of the polymers in the film [194]. Thus, even at low concentrations of salt solutions, these morphological changes could be easily observed in hydrogen bonded films since components of are relatively weakly associated compared to electrostatic ones, allowing diffusion within multilayers. In the same study, it was also shown that after the introduction of holes through salt annealing of PVPON/PAA films, it was possible to encapsulate ibuprofen and regulate the release of it was monitored [194].

Although there are few works in the literature reporting the effect of ionic strength on H-bonded multilayers, there is no inclusive work discussing the salt effect, especially considering the ion specificity, on hydrogen bonded multilayers in detail. Ion specificity and concentration are especially crucial in terms of modulating the stability and morphology of H-bonded multilayers so that salt-responsive multilayers can be formed to be used in controlled release applications.

2.4.2.2.2 Biomedical Applications of Hydrogen Bonded LbL Assembly

Main applications of H-bonded LbL multilayers are encapsulation / loading of functional molecules, controlled release and delivery of functional molecules or drugs, cell isolation, functional surfaces which control the protein and cell adhesion or self-healing materials.

A wide range of molecules, from drugs to proteins, can be loaded into LbL H-bonded assemblies. Unlike electrostatically assembled multilayers, H-bonded multilayers is a great platform to load a functional cargo since the loaded molecule is not required to be charged. There are three approaches for encapsulation: Functional molecule can be loaded during the assembly, post-loading or pre-loading [179]. Model proteins are generally loaded into H-bonded multilayers during the assembly. Mehrotra *et al.* showed that Bovine Serum Albumin (BSA) and lysozyme are assembled with PEG into H-bonded multilayers which grow on agarose gel as a substrate [195].

Hammond and coworkers encapsulated a hydrophobic drug into polymeric micelles composed of PCL/PEG and then drug containing micelles were associated with PAA through H-bonding into LbL multilayers [196]. A positively charged dye was also encapsulated into H-bonded films during the assembly [197]. Dye was added to the polycarboxylic acid solution at a pH value in which polyacid was slightly ionized so that the dye and the acid can interact through electrostatic interactions. Post-loading of the functional cargo relies on using an external stimuli to cause a morphological change within the deposited film so that the cargo can be encapsulated and retained within the film. For example, Rhodamine 6G was loaded into PEO/PMMA multilayers by treating the multilayers with a solution that has a high pH value so that ionization of PMMA groups can bound to positively charged dye [197]. In pre-loading, generally the cargo is loaded onto particle templates before the film deposition [179]. Advantages of the pre-loading over other encapsulation methods include increased efficiency of the encapsulation and prevention of the using external factors which can disturb the film integrity. Kharlampieva *et al.* showed that a hydrophobic anti-cancer drug, Doxorubicin (DOX) was encapsulated into H-bonded TA/PVPON capsules efficiently [198]. Drug was first loaded into porous silica particles and then loaded particles were coated layer-by-layer with TA/PVPON. Pre-loading of the drug ensured the high efficiency and prevention of the aggregation of the capsule suspension due to the usage of the hydrophobic solvents [198].

After encapsulation of the functional cargo, H-bonded assemblies are used for the release of the cargo. In general, there are three approaches for the release of the functional cargo: disassembly of the LbL films or capsules, integrating stimuli-responsive components into LbL films and using degradable cross-linkers [179]. General mechanisms for the first approach involves change in the ionization state or charge of the components, shielding of charges or competitive binding of a chemical moiety [199]. When the first method is used, generally H-bonded films are post-treated with solutions which have higher pH than the critical disintegration pH so that the film disassembles and functional cargo is released. Competitive binding that leads to destruction of the film is generally useful in glucose-responsive systems. For example, Ding *et al.* showed that multilayer films of PVA and phenyl boronic acid (PBA) functionalized polyacrylamide (PAAD) degrade very fast in the presence of glucose at the physiological pH [200]. However, a drawback of this approach is that release of the functional cargo in an uncontrollable manner, usually resulting in “burst release”. In the second method, components that are responsive

to specific environmental stimuli are incorporated into LbL films and release of the cargo is achieved without the disassembly of the film [179]. An alternative approach is using degradable cross-linkers which can be cleaved e; for example enzymatically induced degradation of the films. The scope of this work is based on the second method, in which specific components that are responsive to pH or temperature are incorporated into LbL multilayers and release of the functional molecule is provided in a controlled manner.

In order to isolate the cells, Rubner *et al.* used responsive ability of H-bonded multilayers to attach polymer patches to individual cells [201]. Multilayers are composed of 3 stratified layers: Release region which is composed of PMMA/PNIPAM layers, payload region and cell adhesion region. H-bonded LbL multilayers can be also used as functional surfaces which control or prevent protein or cell adhesion. He *et al.* prepared H-bonded multilayers of partially hydrolyzed PEOX and PAA so that cell/ bacteria attachment onto the coatings can be controlled [202]. Ethylene imine groups of partially hydrolyzed PEOX can form covalent links with carboxy groups of PAA at elevated pH so that pH-induced disintegration of the multilayer assembly was prevented. A recent work by our group introduced Ag nanoparticle-loaded PEOX / TA films as antibacterial coatings [203]. H-bonded multilayers of Ag NP loaded PEOX / TA can function as antibacterial coatings both below the critical pH and above the critical pH with the disintegration of the film.

Some examples of the biomedical applications of H-bonded LbL films were listed above. As these examples illustrate, H-bonded multilayers have a great potential in terms of these applications. The next section focuses controlled release applications of H-bonded LbL films.

2.4.2.3 Role of Hydrophobic Interactions in LbL Assembly

Hydrophobic interaction refers to the clustering of non-polar groups of molecules and their interaction in an aqueous environment so that these non-polar groups hinder their exposure to water. Hydrophobic interactions alone are not sole driving force for the LbL film formation but these interactions are crucial in terms of affecting the film properties and stability [204]. Kotov underlined the importance of the hydrophobic interactions in PEM multilayers and analyzed how

hydrophobic interactions contribute to the formation of PEM multilayers thermodynamically [204]. Kotov's study listed the independent contributions to the Gibbs free energy of the formation of the electrostatically bound LbL multilayers. These contributions include transformation of the ionic atmosphere of the charged PEs in solution, in other words ion-ion interactions between charged polyelectrolytes, transformation of the hydration shell around PEs, in other words ion-dipole interactions with water, electrostatic attraction between oppositely charged PEs which is the main driving force for LbL assembly and finally, hydrophobic interaction of the organic parts of PE molecules [204]. Gibbs free energy of the hydrophobic interaction is composed of mainly entropic contribution since when non-polar parts of the PEs on adsorbed surfaces make a contact, water molecules are released. Thus, total entropy change in the formation of LbL multilayers have contributions from release of ions from solvation shell, reorientation of water molecules of PEs, destruction of the shell of water molecules around hydrophobic parts of PEs, and loss of the mobility of PE shell which actually contributes negatively to the entropy of PEM formation [204]. While entropy change of release of ions and reorientation of water molecules contribute to the electrostatic interactions, entropy change resulted from the destruction of the shell of water molecules contribute to the hydrophobic interactions. Kotov's analysis shows that strong hydrophobic forces make LbL multilayers stable.

Clark and Hammond reported that in electrostatic multilayer deposition, secondary interactions including hydrogen bonding and hydrophobic interactions have a significant role for selective adsorption on functionalized surfaces [205]. Hydrophilic or hydrophobic nature of the polymer affects the region of the surface that the deposition will take place so by exploiting these interactions, one can have control over preferential adsorption on pattern surfaces to create 3D structures [205]. For example, as the hydrophobicity of the polyamine increases at a moderate pH level, polyamine preferably adsorbs onto ethylene oxide functionalized surface rather than -COOH surface. On the other hand, at high pH level, in which the -COOH surface is highly ionized, hydrophobic interactions become less important because almost all of the protonated amine group of polyamines bind to the ionized surface. This shows that pH also determines the relative strength of hydrophobic interactions over electrostatic ones.

Growth behavior of LbL multilayers can be also controlled by introducing hydrophobic interactions. Li *et al.* showed that growth trend of LbL multilayers can be tuned from exponential

increase to logarithmic slow-down by regulating hydrophobic interactions [206]. In this study, electrostatically bound LbL multilayers were composed of chitosan-graft-phenyl and poly(aspartic-graft-octadecyl) and growth of multilayers was obtained via regulating the relative strength of hydrophobic interactions to electrostatic interactions by adjusting the concentration of NaCl solution [205]. It is known that salt ions cause screening effect so in the presence of NaCl solution with high concentration, electrostatic interactions are reduced. Hence, Cl^- ions contribute to hydrophobic interactions so in the presence of NaCl solution with high concentration, adsorbed polymer chains with limited mobility interact more and become tightly packed [206]. Fastest growth was obtained in the absence of salt, in which hydrophobic interactions and electrostatic interactions are maximized.

Hydrophobic interactions are also important when adsorbed molecules are uncharged. For example, hydrophobic interactions play a crucial role in the fabrication of stable ultrathin films of PVA onto a gold substrate [207]. Guyomard *et al.* investigated how hydrophobicity of polysaccharide derivatives influenced the deposition and growth of the multilayers [208]. The presence of hydrophobic interactions stabilizes the fabricated multilayers and ensures the multilayer growth. The correlation between the increase in multilayer thickness and molar mass of the components indicates the conformation and aggregation of macromolecules are preserved, especially in the presence of hydrophobic interactions. In addition, hydrophobic micro domains are also observed in these films [208]. Zhao *et al.* produced LbL multilayer membranes of gelatin and TA onto polyacrylonitrile (PAN) ultrafiltration membrane via hydrophobic interactions and then reinforced hydrogen bonds [209]. The role of hydrophobic interactions in this study include enabling LbL self-assembly via binding of TA to the hydrophobic pocket of the side chains of the amino acids of gelatin, decreasing the number of hydrophobic groups exposed on the surface so pronouncing the hydrophilicity of the separation membrane, and finally supporting the interaction strength so that increasing the free volume characteristics and stability of the membrane [209]. In conclusion, separation performance of gelatin / TA LbL membrane is improved. Tirilly *et al.* showed that elastic modulus of the PVP/ PAA or PVP/ PMAA multilayers can be varied significantly by the interplay between hydrogen bonding and hydrophobic interactions [210]. Between PMMA and PVP molecules interact through hydrophobic interactions and H-bonding while PAA and PVP molecules interact through weak hydrogen bonds. As a result, PMMA/PVP

and PAA/PVP multilayers exhibit similar static properties but different mechanical properties due to the differences in number of interactions and relative strengths of them [210].

Hydrophobic interactions also play an important role for the incorporation of hydrophobic molecules into deposited multilayers. Wang et al. fabricated biomaterial coatings via short-range hydrophobic interactions and observed that films were stable in physiological conditions and supported cell proliferation [211]. Shchepelina *et al.* designed hollow microcapsules to incorporate silk protein via hydrophobic interactions [212].

All above studies illustrate that hydrophobic interactions are crucial in terms of enabling the self-assembly, modulating the properties of LbL films and incorporating the functional molecules into them. This is the reason that understanding the role of hydrophobic interactions in LbL study is important; both in terms of tuning the properties of multilayers and incorporating functional molecules between the multilayers.

2.5 Controlled Release Applications of Self-Assembled Systems Based on Hydrogen Bonding

Controlled release application of a functional molecule is the most fundamental application of polymer self-assembled systems. Through intermolecular interactions between the drug and the polymer assembly, drug is first encapsulated in the polymeric structure. Then, drug is released in the presence of various stimuli to the target site. In this section, controlled release applications will be introduced with a special emphasis on release kinetics and applications of release will be discussed from several polymeric self-assembled structures.

2.5.1 Objectives of Controlled Drug Release

The main objective of the controlled drug release is to increase the effectiveness of drug therapy, which means the maintaining the drug concentration in the blood or target tissue in the desired concentration within the therapeutic window, between the minimum effective

concentration (MEC) and minimum toxic concentration (MTC) [213], [214], [215], [216] . In other words, with the controlled release system, the rate of drug release matches with the rate of drug elimination from the metabolism [213], [214]. In this sense, the administered drug produces beneficial effects without harmful side effects. Without applying a controlled drug release, multiple dosing of the drug can be applied to limit the fluctuations in the blood plasma [216]. However, multiple dosing can produce harmful effects to patients. Other advantages of a controlled release system include but not limited to improved efficacy, reduced toxicity, improved patient compliance and convenience, being site specific and reducing the dose and administration frequency [213], [214], [215].

There are two types of control when drugs are released in a sustained manner. The first is temporal control, which is beneficial for the drugs that are rapidly metabolized so that the drug is delivered over an extended period or at a specific time [213], [214]. Furthermore, in temporal control, drug molecules are protected from aqueous environment in the body. This protection involves delaying dissolution of drugs, inhibiting or slowing down the diffusion of the drug or controlling the flow of drug solutions [213]. Delaying drug dissolution is simply slowing the rate which drugs are exposed to water. Slowing down the diffusion of the drug is obtained by a polymer matrix so that drug molecules travel through torturous pathways to diffuse out from polymer matrix [213]. Finally, devices that control the flow of drug solutions utilize the osmotic potential gradients across semipermeable polymer barriers [213]. Water molecules pass this barrier due to osmotic pressure difference and then, drug molecules dissolve in water and flow through a pore with a controlled rate.

The second type of control is called distribution control. In distribution control, the objective is to release the drug in a site-specific manner, in other words, released drug targets the specific site of the body [213], [214], [215]. Distribution control is especially needed in two situations: The first one is when drug molecules enter to normal tissues and cause major side effects [213], [214]. The second situation occurs when drug molecules are distributed naturally within the body and they don’t reach to the diseased cells or tissues. For example, when drug molecules cannot pass blood-brain barrier, a controlled release system that applies distribution control is needed. Another application of distribution control is targeting cancer cells by taking advantage of

the abnormal vascular structure of tumors, known as the enhanced permeability and retention (EPR) effect [215].

To achieve the objectives of controlled release of the drugs, polymeric self-assembled systems are designed through physical interactions and drugs are encapsulated into them. As a result, the effectiveness of the drug therapy can be increased and side effects can be reduced significantly

2.5.2 Drug Release Mechanisms

Drug release mechanisms are categorized into several groups like diffusion based release, degradation controlled release, solvent-controlled release, stimuli-controlled release… [215], [217]. Diffusion based release is usually observed in polymeric systems and drug diffusion occurs with the random movement of drug molecules and the driving force for the release is that the concentration or chemical potential gradient [215], [217]. Diffusion based release is usually characterized by the short release time and especially seen in the release of low molecular compounds [218]. When drug diffusion occurs through water-filled pores, drug release rate is controlled via diffusion through a network of pores [217]. In a polymer-matrix system, especially when the polymer is a non-degradable one, the release rate is controlled via diffusion of the drug molecule out of the matrix. In these type of the systems, not only the concentration gradient but also the membrane properties like thickness or permeability affect the diffusion rate [217]. The release profile in these type of systems is first rapid release and then release with decreasing rate since diffusion distance that drug molecule travels becomes longer as drug molecules located in the interior part of the matrix starts to diffuse out [215]. On the other hand, in capsule type systems, drug first dissolves in the core and then diffuses out [215].

Diffusion controlled release is generally based on Fick's Law which relates diffusive flux to concentration with assuming steady-state condition [215]. In addition, Fick's second law relates the concentration variation with time. Fickian diffusion occurs when polymer relaxation time (t_r) is greater than the solvent diffusion time (t_d) [217]. Diffusion controlled release can result in zero order release kinetics, in which released drug concentration is independent from the initial concentration of the loaded drug but only depends on a dissociation constant, K [219]. However,

zero-order release kinetics is observed rarely in diffusion based systems, especially if drug molecules encapsulated in the polymeric structure is far away from the surface. Then, although zero order release kinetics is the ideal state for a controlled release application for ensuring steady-state plasma concentration, most of the controlled release systems follows a triphasic profile [217]. As the name suggests, triphasic profile has three phases: At the first stage, "burst release effect" is observed so that drug molecules release very rapidly due to the detachment of the surface-bound molecules [217]. Although burst- release can be beneficial in situations when rapid treatment is needed, however, most of the time, it can result in local or systematic toxicity with the uncontrollable released dosage in the body [217]. Second phase of the triphasic release is the rate-determining step since slow diffusion of the drug molecules occurs in this phase. In the final phase, release profile gets faster if diffusion is accompanied with the erosion.

Degradation controlled release can be surface degradation or bulk degradation. In surface degradation, degradation starts at the matrix / scaffold surface and degradation goes from exterior to interior part. Surface degradation occurs is observed when the rate of erosion of the polymeric structure is greater than the rate of water penetration [217]. Bulk degradation is a homogeneous degradation since water penetrates to the bulk of polymer [215]. In this case, water penetration rate is greater than the rate of erosion so that polymers in the matrix are hydrolysed [217]. Solvent controlled release includes osmosis controlled release and swelling controlled release. Osmosis controlled release is observed when the carrier system includes a semi-permeable polymeric membrane [217]. Then, water flows from outside of the carrier to the core where drug concentration is high. In swelling controlled release, release rate depends on the penetration rate of the water and chain relaxation rate of the polymer used [215]. Stimuli-controlled is the most preferable type of release in which target-specific release is required, this type of release is especially useful in cancer treatment. When different types of release are compared, the key to achieve "zero order release rate" is a surface erosion mechanism where diffusion based release and degradation based release are combined [220].

Korsmeyer-Peppas model can be used to describe the drug release from a polymeric system [216]. General equation for this model is shown in the below, as equation *(10):*

$$M_t / M_i = K\, t^{\,n} \qquad (10)$$

In this equation, M_t / M_i is the fraction of the drug released at time t, K is the release rate constant and n is the release exponent. If the release exponent (n) is around ~0.5, then drug transport mechanism becomes Fickian diffusion. If n is greater than 0.89, then the release mechanism is zero-order mechanism.

In summary, an ideal controlled drug release system should have characteristics of both stimuli responsive release and zero order release. Properties of polymeric self-assembled structures that are used in controlled release are tailored to achieve a zero order release kinetics. In this sense, understanding the drug release mechanisms is crucial.

2.5.3 Controlled Drug Release from Hydrogen Bonded LbL Assembly

Drug release from LbL based assembly are generally based on two strategies: In the first strategy, drugs are encapsulated into LbL assembled capsules so that they act as diffusion barriers to the encapsulated drug [221]. Permeability of the capsule can be regulated via changing pH, temperature, ionic strength or even with the number of bilayers. In the second strategy, drugs are incorporated into planar LbL films so that release can occur via diffusion of the drug or controlled degradation of the film [221]. In this sense, LbL based assemblies are surface-mediated drug release systems. They function as a both reservoir for the encapsulated functional cargo and a coating that can be tuned via exploiting the interfacial properties [221].

LbL films based on H-bonding are excellent platforms to achieve controlled release of a functional molecule. Their susceptibility and sensitivity to stimuli like pH, temperature, and being a non-toxic platform due to usage of neutral and uncharged molecules in the assembly make them very attractive in controlled release applications. In this part, pH and temperature triggered release from H-bonded LbL films are discussed. pH induced release is especially crucial for the targeted treatment of cancer cellssince the pH of tumor cells is slightly more acidic than the normal cells in the body. In addition, temperature triggered release can be also beneficial for the on time and targeted delivery of the drugs.

2.5.3.1 pH Triggered Release from Hydrogen Bonded LbL Films

pH triggered release is especially used in H-bonded multilayers since assembly or disassembly conditions strongly depend on pH. Especially, pH can be used as a triggering factor for site-specific delivery since internal pH of diseased cells, tissues or organs can be different than the physiological pH of the body. There are many studies in literature based on pH-controlled release from H-bonded multilayers. One of the earliest work belongs to Kharlampieva *et al.*, in this work, adsorption and release of Rhodamine 6G, a positively charged molecule, from H-bonded multilayers is studied [197]. H-bonded multilayers of PMMA and PEO were deposited at pH 2 in which both molecules are neutral and adsorption of the dye molecule occurred at pH 4.2 in which PMMA was partially ionized. Release of the dye was realized by immersing the film in PMMA solution at pH 4.2 so that PMMA chains in the solution were adsorbed on the surface, these adsorbed molecules reduced the charge of other PMMA molecules which were embedded in the film and finally, complexed with dye molecules in the film through long charge screening effect. Tomita *et al.* also pH-triggered studied release of model dyes like Rose Bengal (RB) or 5,10,15,20-tetraphenyl-21H,23H-porphinetetrasulfonate (TPPS) from H-bonded multilayers of carboxyl terminated poly(amidoamine) (PAMAM-COOH) and PMMA [222]. At pH 7, due to film disintegration, dye molecules were rapidly released. Although film was stable at pH 4 and 5, release of dye molecules was observed, having significantly lower release rate at pH 4. This difference in release rate between pH 4 and pH 5, is due to the different structures and swelling degrees that the films have [222]. Another work by Yuan *et al.* also showed the loading and pH or temperature controlled release behavior of model dye, Rhodamine B (Rb) from H-bonded films composed of PVPON/ PAA [223]. RB was loaded PVPON/PAA film in the pH region from 0.5 to 5.5. In this region, Rb has two forms: Zwitterion form and one-positive-charge form. Zwitterion form transits to one-positive charge form when pH changes from pH 4 to pH 2 [223]. Thus, as pH increases, loading rate becomes high but release becomes slow due to the transition of the dye molecules and involvement of electrostatic interactions together with H-bonds [223]. Bağ *et al.* incorporated transition metals into H-bonded multilayers of PVPON / TA-Zr (4) or PNIPAM/ TA-Zr (4) [224]. Films can encapsulate the positively charged model dye, methylene blue, at moderately acidic pH in which TA molecules are ionized and release it at strongly acidic

conditions. Release was due to the insufficient amount of negative charges provided by TA molecules in the film due to the protonated state of hydroxyl groups at these pH values [224].

Most of the drugs are poorly soluble in water. Usually, hydrophobic drugs are incorporated into H-bonded multilayers using amphiphilic copolymer micelles. Kim *et al.* demonstrated the first example of polymeric micelles incorporated into H-bonded multilayers without the use of a charged polyelectrolyte [196]. H-bonded multilayers are constructed from PAA as H-donor and biodegradable block copolymer poly(ethylene oxide)-block-poly(ε-caprolactone) as H-acceptor at pH 2.5 [196]. Films can be disturbed at physiological conditions to release the drug due to the sensitivity of H-bonds. In order to determine the efficacy of encapsulation and release of a hydrophobic drug, an anti-bacterial drug, triclosan, was selected, encapsulated into micelles, then the release test was applied via a common antibiotic susceptibility test against a gram positive bacteria. Test results showed that encapsulated drug diffuses out of the micelles and inhibits the growth of bacteria, leaving a circular area called zone of inhibition (ZOI) [196]. Especially at physiological conditions, whole film was degraded and all of the encapsulated drug diffused out from the H-bonded multilayers for 90 minutes. Release duration can last longer if films are cross-linked. Another work in which hydrophobic drugs are encapsulated and released from H-bonded multilayers belong to our group [225]. In this work, for the first time, micelles of diblock copolymer made of two cationic blocks with a hydrophobic molecule are incorporated into H-bonded multilayers [225]. At slightly or above acidic conditions, BCM has a polybasic core and H-accepting coronas. Then, H-bonded multilayers were constructed by using TA and BCM and control of film dissolution was obtained at opposite pH ranges so that pH-controlled delivery of functional molecules can be realized [225]. In diblock copolymer structure, pH response of both blocks arises from tertiary amino groups of poly (2-(*N*-morpholino) ethyl methacrylate (PMEMA) and 2-(diisopropylamino) ethyl methacrylae (PDPA). At basic pH values, multilayers disintegrate due to breakage of H-bonds between TA and micelles. At acidic pH values, both PDPA and PMEMA blocks are protonated. Between pH 4.5-5.5, slightly acid conditions, a restructuring occurs between micelles and TA due to slight ionization of TA so electrostatic interactions between amino groups of PMEMA and hydroxyl groups of TA also play a role together with H-bonds [225]. Thus, pH-induced release of hydrophobic molecule, pyrene, reflects the multilayer behavior related with pH. Fastest release of pyrene from multilayers occurs at pH 5 since micellar cores completely dissolve. At all pH values, release of pyrene was based on diffusion and at some

point release leveled off [225]. Above studies show that pH-induced release of hydrophobic drugs can be easily regulated by using micelles and incorporating these micelles into H-bonded multilayers.

Haktanıyan *et al.* fabricated a hydrophobic, anti-cancer drug DOX containing H-bonded multilayers of PIPOX and TA without using block copolymer micelles [226]. The key point in this study is release occurs at moderately acidic conditions while minimal release is obtained at physiological conditions. Films were constructed just below physiological pH, at pH 6.5. First, TA-DOX complexes were produced via electrostatic interaction between phenolate groups of TA and DOX, and H-bonding between ether oxygens, carbonyl or hydroxyl groups of DOX and hydroxyl groups of TA [226]. pH stability of TA-DOX complex containing films were also more stable and showed a more gradual decomposition under basic conditions due to the screening of negative charges of TA by DOX. DOX release from multilayers were conducted at pH 5.5, pH 6.5 and pH 7.5. In all temperature ranges, lowest amount of release was obtained at pH 7.5 due to the enhanced association between DOX and TA with increasing pH [226]. On the other hand, at pH 6.5, DOX release from multilayers via a self-diffusion mechanism while at pH 5.5, stimuli controlled release of DOX was observed due to the protonation of TA and loss of electrostatic interactions between TA and DOX [226]. Release kinetics were also different at these pH values. At pH 7.5, burst release followed by a slow but continuous release up to 8 hours while at pH 5.5, a significant amount of DOX released in the first couple of hours followed by a release of free DOX molecules in the multilayers in a slow manner [226].

All of these studies above show that drug release occurs either via diffusion or degradation. However, by exploiting the dynamic nature of H-bonds, zero order kinetics can be obtained so that incorporated drugs can be released into targeted area in a controllable manner. Zhou *et al.* showed that release from H-bonded PVPON / TA multilayers can occur via gradual disassembly of the film [221]. In this work, sustained and slow release of TA occurs due to the shift of the equilibrium with the reversible nature of H-bonds [221]. As pH increases, film disassembly and release occur more rapidly due to the ionization of hydroxyl groups of TA. In addition, electrostatic repulsion among charged TA molecules also accelerates film disassembly. Long term release profiles of TA are obtained at pH 5, 6 and 7.5. At pH 7.5, all TA is released into the media in 1 month while at pH>9, burst release effect is observed [221]. Same authors also showed that zero order release

profile can be obtained from H-bonded films by using monodispersed PEG as H-acceptors and TA as H-donors [227]. Due to the narrow weight distribution of PEG, H-bonded films disintegrate at constant rate. In addition, zero order release rate was also due to the unique feature of the H-bonded film; release mechanism occurs via film disintegration instead of diffusion or degradation [227]. Dissociation of film material (PEG/TA complex) releases free TA and PEG into the media while free TA and PEG may deposit back to LbL film. Zero order release kinetics was observed in all pH range; release of TA was accelerated as the pH of the release medium increases [227]. As a result, by regulating the disintegration of multilayers via pH, zero order release kinetics of functional molecules can be obtained.

2.5.3.2 Temperature Triggered Release from Hydrogen Bonded LbL Films

Temperature can be used as an external factor for controlled delivery applications, especially in site-specific treatments where hyperthermia is used. Due to the sensitivity and dynamic nature of hydrogen bonding, H-bonded LbL multilayers are good systems that can be used in temperature triggered release of functional cargo. In general, as temperature increases, the release rate of the functional molecule from H-bonded multilayers also increase due to enhanced dissociation of H-bonds with increasing temperature. Release rate of Rhodamine B from PVPON/PAA multilayers increase with increasing temperature due to the weakening of H-bonds between PVPON and PAA [223]. TA release was also enhanced when temperature was increased from PVPON/TA multilayers [221]. Zhao *et al.* also showed that zero order release profile of TA was obtained at all temperature ranges, although increasing temperature speeds up the release of TA from well-defined PEG/TA multilayers [227].

Using a temperature-sensitive polymer in H-bonded multilayers is a common way to regulate temperature triggered release of functional molecules. Caruso's group deposited H-bonded PNIPAM / PAA multilayers and during the deposition, assembly temperature was changed from 10 to 30°C [185]. As temperature increases, it gets closer to LCST of PNIPAM so conformational change of PNIPAM caused thicker and smoother films. Loading and release behavior of Rhodamine B was also affected from temperature; as temperature increases and gets closer to critical temperature of PNIPAM; loading and release of the dye becomes more [185].

This shows that loading and release behaviors for PNIPAM/PAA films are reversible [185]. Sukhisvili *et al.* prepared temperature responsive H-bonded LbL films of PMMA and poly (N-vinylpyrrolidone)-b-poly(N-isopropylacrylamide) (PVPON-b-PNIPAM) block copolymer micelles and controlled the swelling of the films and release properties via temperature [228]. PNIPAM core of BCM controlled the loading and release rate of small hydrophobic molecule from multilayers. Loading of the molecule was realized via hydrophobic interactions when assembly temperature is increased above T_C of PNIPAM [228]. When temperature was decreased below T_C, release of the encapsulated molecule was accomplished. Most importantly, all temperature induced changes made in BCM containing LbL films are reversible [228]. Zhu *et al.* also demonstrated that on-demand release can be achieved by using H-bonded BCM containing micelles that encapsulate DOX [229]. This study's difference from other studies that have BCM embedded films is that temperature responsive micelles enable films with temperature controlled swelling / de-swelling transitions and usage of TA as H-donor provides stability in physiological conditions so that micelles can be bridged [229]. DOX encapsulated in BCM (PNIPAM cores) are released when temperature is lowered to 20°C with the collapse of PNIPAM core, as evidenced from killing of breast cancer cells (MCF-7). In addition, cyclic release test was applied to the films, in this test, films immersed in phosphate buffer saline (PBS) for 30 minutes for 3 days. This test shows the possibility of re-using these films for temperature triggered release [229], as reproducible release profiles are obtained after re-loading films with drugs, drug loaded cores preserve their capacity after swelling / de-swelling cycles and use of TA provides strong binding and efficient stabilization of BCMs. As shown by above examples, release of hydrophobic drugs is usually done by using BCMs and incorporating them into H-bonded multilayers. Haktaniyan's work showed that without using a BCM, encapsulation and release of a hydrophobic molecule is possible into PIPOX/TA multilayers [226]. Amount of DOX released in 37.5°C is higher than at 25°C in all pH values. This result stems from the thermo-responsive behavior of PIPOX, since 37.5°C is higher than T_{cp} of PIPOX so that conformational change of PIPOX triggers void like structures in the multilayers [226].

Paramasivam *et al.* designed H-bonded TA / PnPOX based capsules and show their potential as drug release agents as temperature is elevated to the body temperature [230]. The main question in this work was whether t. he temperature induced collapse of PnPOX may trigger morphological changes on the capsules which were prepared at 10°C, well below T_{cp} of the

polymer [230]. Potential collapse of the polymer can lead to changes in shell stability and permeability so that release of different fluorescent molecules can be triggered. Among different model molecules, release of TRITC-Dextran, a cationic model molecule, was tested. Loading of molecule occurred via H-bonding and electrostatic interactions and 95% of the loaded dye was released within 3 hours. Thus, this work illustrates the encapsulation and release at physiological temperature of cationic drug is possible from H-bonded capsules [230].

In general, when temperature-triggered release is desired, polymers exhibiting LCST are used in the construction of multilayers. In these cases, application of a lower temperature as a stimuli to release cargo has limited practical applicability [231]. Instead, triggered systems with heating is desired and polymers exhibiting UCST are good choices to achieve that. Palanisamy *et al.* demonstrated on-demand release capability of UCST type micellar films for the first time [231]. At temperature below UCST of the BCM, hydrophobic model molecule pyrene was loaded into the multilayers and above UCST, release was triggered due to the hydration and expansion of micellar cores [231]. Release rate of pyrene increases with temperature. Furthermore, on-demand release capability of multilayers was also tested by switching temperatures between 5°C and 38°C, and pyrene release was observed in a step-like fashion [231].

In conclusion, temperature is an external factor to induce on-demand and site-specific controlled release. Properties of H-bonded LbL assemblies composed of temperature-sensitive polymers can be exploited in this application area.

2.5.4 Controlled Drug Release from Electrospun Fibers

In this section, examples from literature work about controlled release applications of electrospinning fibers were examined. Fibers are solid structures that have diameters from nano to micro scale. Advantages of nanofibers are their ability to be designed for a wide range of drug release profile by altering morphology, composition or porosity and routes for administration, protection of the drug from decomposition before they arrive to target site and availability for site

specific delivery [232], [233].Disadvantage of nanofibers is usually requirement of surgery to implant these materials, however, these materials can be very useful in cases where the surgery is already realized [233].

Electrospinning is the mostly used method to produce such fibers. In electrospinning process, strong electric field is applied to a polymer solution which is held at the end of capillary. Polymer solution from the capillary outlet is deformed into a cone. When the voltage reaches a critical value, then the charge overcomes the surface tension of the polymer droplet at the tip of capillary and a jet is ejected from the tip of the cone. Acceleration through the electric field causes elongation, thinning of the polymer jet and evaporation of the solvent that produce fibers [233].

Nanofibers that are used in sustained and prolonged release applications are generally prepared from biodegradable or swelling polymers. Drug release generally occurs via diffusion hen or degradation. For hydrophilic nanofiber matrices, first polymer matrix swells and then slowly dissolves, so as soon as dissolution medium penetrates into the matrix, drug diffuses out [232]. On the other hand, degradation based on surface erosion occurs when water penetration into the nanofiber matrix is slower than the matrix breakdown [232]. Controlled drug release from nanofibers are achieved by enzymatic degradation or controlled hydrolysis.

Fibers are grouped into four classes based on their structure [232]. Matrix-type nanofibers contain drug and polymer blends. The second class is core-shell nanofibers which are multi-matrix systems that contain multiple layers that were loaded with drug. In reservoir type systems, outer layer serves as a barrier to the drug release. Finally, sandwich type nanofiber meshes are prepared by sequential electrospinning of different polymer solutions or melts.

Matrix type fibers have two groups: Monolithic fibers are composed of a single polymer and blended fibers are composed of polymer blend [232]. Luong-Van *et al.* prepared fiber mats which were electrospun from PCL solutions containing different heparin concentrations [234]. Effect of heparin incorporation on fiber morphology, heparin distribution and release rates was studied. Due to the short half-life of heparin, continuous administration to the site of injury is required. Release from heparin /PCL fibers lasted for 14 days in PBS at 37°C. In this work, first burst release was observed, then via Fickian diffusion drug release was continuous [234]. Burst release was due to the incorporation of heparin into the amorphous regions of semi-crystalline PCL

so drug release occurs from these regions initially [234]. Zeng *et al.* showed drugs can be encapsulated directly into electrospun fibers of poly (L-lactic acid) (PLLA) by controlling fiber diameter and zero order release profile of the drug was observed from these fibers [235]. Drug release rate was constant in the presence of enzyme so zero order release rate was obtained due to the degradation of PLLA. Fibers derived from polymer blends would contain properties of both components so release profiles can be finely tuned. For example, Kim *et al*. used two base materials for fiber scaffolds: poly(lactide-co-glycolide) (PLGA) which controls the degradation rate of the fibers and high molecular weight poly(lactic acid) (PLA) which provides mechanical integrity and strength [233]. To control the drug release profile and encapsulate the hydrophilic drug, amphiphilic poly (ethylene glycol)-b-poly (lactide) (PEG-b-PLA) copolymer solutions were added into the fiber solutions. Thus, in this work, encapsulation and release of a hydrophilic antibiotic, cefoxitin sodium was demonstrated [233]. From these fibers, after an initial burst release, PLGA-PLA-PEG-b-PLA (80:5:15) scaffold showed a sustained release profile (27% of the drug was released over a week) which is very different from mediated PLGA scaffolds [233]. The reason for the burst release from PLGA fibers is the limited physical interaction between the drug molecules and PLGA, majority of the drug molecules was localized on the surface so in the aqueous environment, drug molecules on surfaces can be washed out easily [233]. In the work of Kenawy *et al.,* electrospun fibers are prepared from poly (ethylene-co-vinyl acetate) (PEVA), PLA and their blends [236]. Tetracycline hydrochloride was chosen a model drug. In release experiments, it was revealed that electrospun PEVA fibers show highest release rate than the fibers composed of 50/50 blends or fibers of PLA. This is because partial crystallinity of PLA which limits the water molecules into the polymer inner layers and limits the diffusion of the drug to the aqueous environment [236]. Blended structures give more sustained release: 5% amount of the drug was released with a smooth and regulated release profile afterwards [236].

Core-shell fibers contain drug loaded layers or an outer polymer layer that functions as a rate-controlling barrier [232]. To obtain core-shell structure, generally co-axial electrospinning is used. In core-shell reservoir systems, drug release rate is affected by both the drug concentration gradient and degradation rate of the shell layer [232]. Other nanofiber based approaches for prolonged drug release include preparation of sandwich type nanofiber meshes by sequential electrospinning of different polymer solutions or melts [232]. In these systems, control of bead diameter in the fiber structure also regulates the prolonged drug release.

Stimuli activated drug released fibers include thermo-responsive and pH-responsive ones. Tran *et al.* prepared poly (N-isopropylacrylamide-co-methacrylic acid) (PNIPAM-co-MAA) that are loaded with hydrophobic ibuprofen and studied the release of ibuprofen from these fibers at different temperature and pH conditions [237]. Release from electrospun PCL fibers were also studied for comparison. Diffusion rates of ibuprofen from two rates of fibers were investigated at 22°C and 40°C, at pH 1.7 and 7.4. 0.85 μmol of ibuprofen was quickly released from PNIPAM-co-MAA fibers in the first one hour at 22°C and pH 7.4, then the rest was released at a slower rate. At 22°C and pH 1.7, drug diffusion was much slower due to the hydrophilic structure of the polymer so water can easily permeate into matrix and resulted in much faster diffusion rate. At 40°C and pH 1.7, drug release was at the slowest rate and no burst release was observed. This is because pH 1.7 was lower than pKa of the carboxylic acid, so carboxyl groups were protonated making the polymer more hydrophobic. In summary, release of ibuprofen was mainly via passive diffusion triggered by temperature or pH. On the other hand, ibuprofen release from PCL fibers was insensitive to pH or temperature and serious burst release effect was observed from these fibers indicating that usage of temperature or pH sensitive polymers in the production of fibers can be useful.

Finally, biphasic drug release from fibers combine both immediate burst and sustained release [232]. These systems are especially desired to obtain maximum therapeutic benefits. Thakur *et al.* fabricated fibers which delivered an antibiotic, mupirocin, over at least 3 days against bacterial infections and immediate delivery of an anesthetic, lidocaine, for wound pains [238]. In summary, dual release from fibers were obtained. To achieve this aim, electrospinning from dual spinnerets was used. A single scaffold with two polymer fibers containing two different drugs were obtained [238]. Both dual spinneret and single spinneret fibers release the anesthetic in burst release fashion while dual spinneret fibers released the antibiotic in a sustained manner, 5% of the drug was diffused out in first hour and cumulative release was 12% over 72 hours [238]. When both drugs were electrospun by the traditional apparatus, it is possible that polymer matrix didn't have the capacity to hold both drugs homogeneously [238]. On the other hand, anesthetic drug was released in a burst release manner from both fibers due to the crystallization of the fibers with the phase separation triggered by chloride salts on the drug [238].

In conclusion, fibers can be also good choices for the sustained release of the drugs into the target site. They are generally produced from electrospinning, which in my studies, fiber formation was achieved via solely physical interactions in aqueous solutions and drug release from these fibers was shown.

Chapter 3: Materials and Methods

3.1 Chemicals

For the construction of LbL films of PEOX and TA, PEOX-200K (molar mass ~200000 g/mol) was purchased from Alfa Aesar and PEOX-500K (molar mass ~500000 g/mol) was purchased from Sigma. TA (molar mass = 1701.2 g/mol), sodium dihydrogen phosphate ($NaH_2PO_4.2H_2O$), hydrochloric acid (HCl) and sodium hydroxide (NaOH) were purchased from Merck. Polished Silicon (100) wafers were purchased from Ultrasil Corporation (USA). For the investigation of salt effect on H-bonded LbL multilayers, analytical sodium salts and nitric acid (HNO_3) were purchased from Merck. Controlled release experiments from H-bonded LbL films were conducted by using Rhodamine 6G which was purchased from Fluka. PNIPAM (~ 25.000 g/mol) was purchased from Sigma Aldrich.

For the formation of PEOX / Malonic acid (MA) fibers through self-assembly in aqueous solutions, MA (molar mass = 104.06 g/mol) was purchased from Sigma Aldrich. For the release experiments from the fibers, Ciprofloxacin (molar mass = 331.346 g/mol) was selected as drug and purchased from Murli Krishna Exports.

All chemicals were used without further purification. Deionized water (DI) (18 MΩ-cm resistivity) was purified through a Milli-Q system (Millipore).

3.2 Characterization Methods

3.2.1 Ellipsometer

In all studies, ellipsometer (Microphotonics ELX-01R) was used to measure the dry film thickness of PEOX/TA multilayers after each bilayer. The principle of working depends on the changes in polarization of the light when the light from the material is reflected or transmitted. Incident and reflected beams form a plane, called plane of incidence.

In the measurements, 632.8 nm laser light at 70° angle was used. To determine the film thickness, at least three measurements were made with the instrument and mean thickness and standard deviation were determined from these measurements. Furthermore, in pH stability tests, after immersing the films in buffer solutions at defined pH, thickness of the films was also measured by ellipsometer.

3.2.2 Optical Microscope (OM)

Optical microscope is a type of microscope that uses visible light for the magnification and visualization of samples. In the instrument, there is a system of lenses so that images can be magnified easily. The morphology of deposited PEOX/ TA multilayers was checked by optical microscopy (Leica LM DM). In addition, restructuring of LbL sheets of PEOX/TA were observed over a week by using OM. In the second part, morphology of PEOX / Mal.A. fibers were also examined by using OM.

3.2.3 Atomic Force Microscopy (AFM)

AFM is a type of scanning tunnel microscopy (STM) that has ha high resolution and can be used to image any kind of surface topology including polymer, ceramic, biological samples. Like in STM, a sharp tip is scanned over the surface, this diamond tip contacts the surface through interatomic Van der Waals forces. Vertical movement of cantilever is detected by the second tip.

AFM (Bruker Dimension) was used to determine the surface roughness of PEOX/TA LbL films in tapping mode using silicon cantilevers. The height and horizontal distance of PEOX/ MA fibers formed in aqueous solutions were also determined by AFM (Bruker Dimension) in tapping mode using silicon cantilevers.

3.2.4 Field Emission Scanning Electron Microscopy (FESEM)

Field emission scanning microscopy gives information about the material's morphology, topography and elemental content with limitless depth of field. The images obtained from FESEM are very high- resolution images and these images can be obtained at low accelerating voltages and working distances.

Working principle of FESEM is like below: Electrons are released from a field emission source and accelerated in electrical field. In the high vacuum column, these released electrons are deflected by lenses and bombards the material's surface. Then, these electrons called secondary electrons are emitted from material's surface. The detector catches the secondary electrons and forms an electronic signal. This signal is transformed to high resolution image.

The morphology of fabricated PEOX / TA multilayers was checked with FESEM (Zeiss EVO LS-15). Then, the morphology of fibers after restructuring of PEOX/TA multilayers are visualized by FESEM again. The fibers which were imaged were deposited on conducting carbon tape and images were formed by using secondary electrons. To determine the salt effect on the morphology of PEOX/TA multilayers, deposited multilayers assembled at different salt solutions at different concentrations were examined using FESEM (Zeiss Ultra Plus SEM). In addition, morphological changes before loading of Rhodamine 6G after releasing it from PEOX/TA multilayers and PNIPAM/TA multilayers were examined via FESEM (Zeiss Ultra Plus SEM). The morphology of PEOX/ MA fibers was characterized by FESEM (Zeiss Ultra Plus SEM) and characterization was done via transferring fibers from silicon wafer to carbon tape. In addition, analysis with FESEM by secondary electrons was done without any prior sputtering of conductive layer. Morphology of PEOX/ MA fibers after ciprofloxacin loading was also investigated by FESEM and morphological changes were compared before and after loading of the drug.

3.2.5 Thermogravimetric Analysis (TGA)

In this gravimetric analysis, the mass of substance is tracked as a function of temperature or time. TGA has a simple pan and this pan is supported by a precision balance. That pan is in the furnace so the sample is heated or cooled in a controllable fashion. This control is provided by purging an inert or reactive gas.

Thermal stability of fibers after restructuring of PEOX/TA multilayers in phosphate buffers was investigated by thermogravimetric analyzer (TA Q500, TA instruments). In addition, the composition and thermal stability of PEOX/MA fibers were also determined by using TGA. TGA of fibers were done using nitrogen as the purge gas.

3.2.6 X-ray Photoelectron Spectroscopy (XPS)

XPS is a surface analysis technique that gives information about chemical composition, chemical state and elemental information about the sample that is under investigation. XPS analysis is done by exciting the sample surface with Al K-α x-rays. After sample surface is excited with the X-ray beams, photoelectrons are emitted from sample surface. The energy of the emitted photoelectrons is measured by electron energy analyzer. From the binding energy and intensity of a photoelectron peak, the elemental identity, its chemical state and quantity of the detected element are determined. In summary, the basic working principle of XPS relies on photoelectric effect:

$$KE = h\nu - BE - \Phi \qquad (11)$$

In equation (11), KE is the kinetic energy of the emitted photoelectron, $h\nu$ is the energy of the incoming x-rays, BE is the binding energy of the photoelectron to the surface and Φ is the photoelectric work function, typically 4-6 eV.

XPS characterization of the fibers formed after restructuring of PEOX/TA multilayers was done by a Thermo Scientific K-Alpha instrument using monochromatized Al-Kα radiation. Charge compensation during the measurement was provided by a flood gun at $2x10^{-7}$ mbar pressure. The beam size was ~400 nm. With XPS analysis, elemental content of the fibers was determined.

3.2.7 Fourier Transform Infrared Spectroscopy (FTIR)

FTIR is a technique that is used to obtain infrared spectrum of absorption or emission, and this information can be used to identify materials. When exposed to infrared radiation, molecules absorb this radiation at specific wavelengths and causes the change of dipole moments of them. Then, vibrational energy levels are transferred from ground to excited state. The intensity of the absorption peaks is related to these energy levels and change of dipole moments. As a result, one can obtain information about molecular structure of the sample by analyzing the spectrum.

In general, FTIR is used to determine hydrogen bonding in the samples that are analyzed. Formation of hydrogen results in significant charge transfer from proton donor (X-H) to proton acceptor (Y) [115]. This weakens the X-H bond and results in decrease in vibration frequency. The shift to lower frequencies is called a red shift and usually an indicator of H-bond in species in FTIR characterization. Further discussion about FTIR characterization is given in the related sections.

FTIR characterization of deposited PEOX / TA multilayers and fibers formed after restructuring of multilayers was performed by Thermo Scientific Nicolet IS50 ATR-FTIR. In addition to that, in order to quantify PEOX to TA ratio in the fiber samples, dried PEOX/TA aggregates formed in aqueous solutions was investigated by FTIR (Thermo Scientific Nicolet IS50 ATR-FTIR) when PEOX was added to the aqueous TA solution at a constant concentration. PEOX / MA fibers formed in aqueous solutions were also dried and characterized by FTIR (Thermo Scientific iS10 ATR-FTIR) to show evidence of H-bond formation between PEOX and MA as a driving force for fiber formation.

3.2.8 Ultra-Violet Visible (UV-Vis) Spectroscopy

As the name suggests, UV-Vis spectroscopy consists the spectrum in the visible and UV region. When the sample is exposed to monochromatic light that has an energy which is enough to excite the electrons in the sample, these electrons transfer to a higher energy orbital. In this case, optical spectrometer records the amount of absorption and absorption wavelength.

Working principle of UV-Vis Spectroscopy relies on Beer-Lambert law, which relates the absorbance of the sample and concentration of it linearly. Beer-Lambert law is given in below:

$$A = \varepsilon \, l \, c \qquad (12)$$

A is absorbance, ε is the molar absorptivity (L mol^{-1} cm^{-1}), l is the length of solution that the light passes through (cm) and c is the concentration of the solution (mol L^{-1}). A is unitless and defined as:

$$A = \log (I_0 / I) \qquad (13)$$

I_0 is the intensity of the light passing through the reference cell and I is the transmitted intensity of the light.

To prove the fibers formed after restructuring of PEOX / TA multilayers consist of TA, fibers were dissolved in pH 10 solution. The presence of dissolved TA in the pH10 solution was determined by UV-Vis Spectroscopy (PG T80). In addition, Rhodamine 6G release experiments from PEOX / TA multilayers were conducted by using UV-Vis spectrometry. First, calibration curve of Rhodamine 6G was determined by measuring the absorbance at 525 nm of aqueous solutions containing Rhodamine 6G at different concentrations. After loading dye to 5 bilayer (BL), 10 BL and 15 BL PEOX / TA films formed on quartz substrate, absorbance at 525 nm of these films were measured by UV-Vis spectroscopy. Then, release of Rhodamine 6G from 10 BL PEOX / TA multilayers and PNIPAM / TA multilayers to aqueous solutions at different pH or different temperature were conducted and remaining amount of dye on the films was measured every 20 minutes during 3 hours using UV-Vis Spectroscopy. For release of Ciprofloxacin (Cipro) from PEOX / MA fibers, calibration curve of Cipro was prepared using UV-Vis Spectroscopy (PG T80). Released amount of the anti-biotic from PEOX / MA fibers into aqueous solutions was also determined by taking UV-Vis spectrum of the aqueous solution and the drug amount was calculated using the calibration curve for Cipro.

3.2.9 Contact Angle Measurements

Contact angle (Θ) is the measured angle that is formed by a liquid, where solid, liquid and gas intersect at three phase boundary. Contact angle measurements provide information about the surface wettability or whether the surface is hydrophilic or hydrophobic. Low contact angle demonstrates that water spreads on the surface and hydrophilic surface whereas high contact angle shows that surface repels the water molecules and surface is hydrophobic. It is based on Young's equation, which is given in below as equation *(14)*:

$$\cos\Theta = (\Upsilon_{SV} - \Upsilon_{SL}) / \Upsilon_{L} \qquad (14)$$

In equation *(14)*, Θ is the contact angle, Υ_{SV} and Υ_{SL} is the solid-vapor and solid-liquid interfacial tensions and Υ_{L} is surface tension of the liquid. An illustration is shown in Figure 3.1:

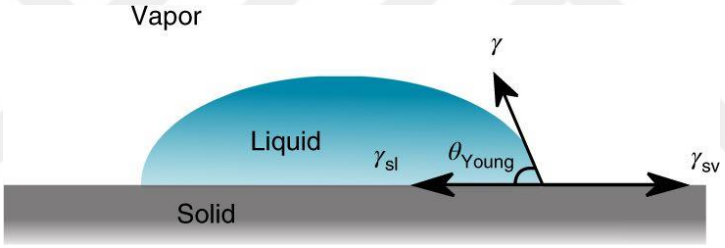

Figure 3.1: A drop of water on a solid substrate and contact angle (Θ) is shown geometrically with Υ_{SV}, Υ_{SL}, Υ_{L} [239].

In the contact angle measurements, two reproducibly measured angles are advancing contact angle (ACA) and receding contact angle (RCA). As the drop volume increases, contact angle of the drop increases and contact line reaches to ACA [239]. On the other hand, when drop volume decreases, contact line of the drop remains static and shape of the drop changes until RCA is reached [239]. Contact angle hysteresis, which is an indicator of the mobility of the drop on the surface, is defined as Θ_A (ACA) – Θ_R (RCA). Larger hysteresis values indicate drops are less mobile.

In this work, water contact angle measurements of PEOX / TA multilayers consist of different bilayers were performed by using DataPhysics OCA20 instrument. With contact angle

measurements, relative surface hydrophilicity / hydrophobicity of PEOX / TA films consist of different number of bilayers was determined.

3.2.10 Differential Scanning Calorimetry (Nano-DSC)

DSC was used to determine the T_{cp} of polymers in aqueous solutions. In DSC, thermal properties of different materials are determined, together with energetics of phase transition and conformational changes of macromolecules.

In the working principle of DSC, specific heat capacity is measured as a function of temperature [240]. Equation *(15)* shows the calculation of specific heat of solute(C_2):

$$C_2 = C_1 + 1 / m_2 (C_{sol} – C_1) \quad (15)$$

In equation *(15)*, C_1 is the specific heat of solvent, m_2 is the mass fraction of solute and C_{sol} is the specific heat of solution. $C_{sol} – C_1$ is also called excess apparent specific heat (C_{ex}). In a buffer solution, C_1 can be calculated as:

$$C_1 = M_b . C_b \quad \text{and} \quad C_{sol} = M_s .C°_{sol} \quad (16)$$

In equation (16), M_b and M_s are mass of the buffer and solution while C_b and C_{sol} are heat capacity of buffer and solution. Differential heat flow from the calorimeter is temperature dependent and as the scan rate is constant, time integral of the measured differential heat flow gives the enthalpy of the sample [240]. Specifically, integration of excess specific heat capacity over the temperature gives the specific calorimetric enthalpy (Δh).

DSC instruments contain a sample and a reference cell. Sample and reference are degassed before starting the experiment to avoid bubble formation. Temperature is scanned at a constant rate either in heating or cooling mode. If a phase transition is observed, temperature difference and deflection is seen to maintain temperature constant depending whether the process is exothermic or endothermic.

Van't Hoff equation gives the enthalpy of the process when differential heat flow is integrated, as shown in equation *(17):*

$$d (\ln K) / d (T) = \Delta h / RT^2 \quad (17)$$

Phase transition is represented as the maximum point of the peak. ΔH is the area under the peak. After calculation of ΔH, other thermodynamic parameters can be also calculated.

T_{cp} of PEOX in respective sodium salt solutions were determined and thermograms were obtained by using differential scanning calorimetry (Nano DSC, TA Instruments). Salt solutions were prepared in deionized water in various concentrations and the concentration of PEOX in these solutions was kept constant at 1.25 mg mL^{-1}. To avoid bubble formation during heating and cooling, all solutions were degassed for 10 minutes before the measurements. All measurements were made with a constant heat rate of 1°C min^{-1} and under a pressure of 3 atm. Heat rate of PEOX solutions in the cell of Nano-DSC was measured relative to the reference solution in the reference cell which has the same salt concentration as the polymer solution.

For PEOX/TA solutions, PEOX solutions were prepared in either distilled water or respective 0.1 M sodium salt solutions. In all solutions, the final concentration of PEOX was kept constant at 1.25 mg mL^{-1}. To determine the influence of TA on the T_{cp} of PEOX, TA solutions were prepared in distilled water in various concentrations so that the relative number of PEOX carbonyl group to the TA phenol group is varied from 10 to 100. Then, equal volume of TA solution with PEOX solution is added dropwise to PEOX solution through continuous mixing for 3 hours. To investigate the effect of pH on T_{cp} of PEOX/TA solutions, PEOX and TA solutions were separately prepared in respective 0.1 M sodium salt solutions at a specific pH and final concentrations of PEOX and TA were held constant at 1.25 mg mL^{-1} and 0.17 mg mL^{-1} respectively. Equal volume of TA solutions was added to PEOX solutions dropwise and mixed. T_{cp} of the PEOX/TA solutions was checked by Nano-DSC relative to the reference solution which is either water or 0.1 M salt solutions at specific pH.

3.2.11 Isothermal Titration Calorimetry (ITC)

ITC is a calorimetric technique that measures the heat absorbed or released upon mixing of two solutions at constant temperature. ITC measurement is based on the repetitive addition of a solution of one of the interacting molecules (generally called ligand) into a cell containing a solution of the second molecule (generally macromolecule) at constant temperature [241]. During the injection of the ligand into the cell containing the macromolecule, ITC detects the heat released or absorbed due to the f interaction between the ligand and macromolecule. The detection of the heat absorbed or released is done by measuring the changes in the power to maintain the isothermal condition. As the injections proceed, the peak size becomes smaller and constant indicating that macromolecule in the cell is saturated with the ligand molecules. After titration is completed, the integration of the peaks is done and heat (enthalpy) of interaction is determined.

The titration results are presented in Wiseman plot and a proper binding model should be chosen to determine the binding constant (K_a). Determination of the binding constant (K_a) yields Gibbs free energy (ΔG) according to the equation (18):

$$\Delta G = -RT \ln K \qquad (18)$$

In equation (18), R is the gas constant, T is the temperature that the experiment is conducted.

Then, since ΔG is calculated and ΔH of interaction is already known, entropy of the interaction (ΔS) can be determined with equation (19):

$$\Delta G = \Delta H - T\,\Delta S \qquad (19)$$

After determination of ΔS of interaction, the nature of interactions can be understood by comparing ΔH and ΔS values. Non-polar interactions like hydrogen bonding, electrostatic interactions contribute to ΔH of the interaction while hydrophobic interactions contribute to ΔS interaction. By comparing these two values (ΔH and ΔS), the nature of the interaction (whether the process is enthalpy or entropy driven) between the macromolecule and ligand can be easily understood.

In this research, ITC was used to determine the nature of interaction in self-assembly processes. First, the binding between PEOX and TA was determined by ITC (TA Instruments Affinity ITC) at 25°C, preparing 0.05 mM PEOX and preparing TA at various concentrations (0.294 mM, 0.176 mM, 0.0587 mM) in DI water. pH of PEOX solution was adjusted to 4.5 in order to ensure H-bond formation between TA and PEOX. For the binding experiments that involve sodium salt solutions, PEOX (0.05 mM) and TA (0.0587 mM) solutions were prepared in 0.1 M sodium salt solutions and their pH was adjusted to ~4.5. To run ITC experiments, PEOX solutions were always placed in the sample cell (960 µL) and TA solutions were always placed in the syringe (250 µL). The titration was achieved by injection of TA solution in the syringe to the PEOX solution in the sample cell using 25 titrations, 10 µL aliquots in each titration. Between each injection, there were 10-minute intervals for equilibration and to ensure uniform mixing. Also, the sample cell was continuously stirred at 125 rpm. Each injection produced a characteristic peak due to the absorbed or released heat. In the analysis of the data, baseline was subtracted from the data since it corresponds to the signal between consecutive injections when no change in heat flow was detected. The raw heat data was integrated using the instrument software. After integration, to determine the thermodynamic parameters (ΔH, ΔS, ΔG) and the binding constant (K_a), independent binding model from the software was used for fitting. The first three data that derived from the first three injections were always neglected since they represent the dilution effect. In addition, neglecting the first three data ensured proper fitting to the independent model.

In the self- assembly process of PEOX and MA, the interaction parameters between PEOX and MA were determined using ITC (TA Instruments Affinity ITC) at 25 °C. 0.05 mM PEOX aqueous solution was placed in sample cell (960 µL) and 2.4 mM aqueous MA solution was placed in syringe (250 µL). The titration was done by injection of MA solution in the syringe to the PEOX solution in the sample cell. In total, 25 titrations were done with 10- minute intervals and each titration is composed of of 10 µL aliquots. 10- minute intervals were to ensure uniform mixing. The sample cell was continuously stirred at 125 rpm. Each injection results in a characteristic peak due to the absorbed or released heat. In the analysis of the data, baseline was subtracted from the data, since it corresponds to the signal between consecutive injections when there was no change in heat flow. The integration of the raw data was done by using the instrument software. After integration, independent binding model was used for fitting the integrated data and thermodynamic

parameters (ΔH, ΔS, ΔG) and K_a were determined. The first data that derived from the first injection was neglected to ensure proper fitting to the model.

Chapter 4: Self Assembly and Restructuring of PEOX and TA into Layer-by-Layer Multilayers

4.1 Overview

H-bonded multilayers of PEOX and TA were deposited by LbL method. H-bonded PEOX/TA LbL films are expected to be both pH and temperature responsive as previously reported in the literature [203], [180], [188], [176], [230]. In the formation of H-bonded multilayers, PEOX is the H-acceptor and TA is the H-donor. The multilayers are stable in physiological conditions due to stability of TA in the protonated form up to pH~8.5. H-bonds are mainly formed between carbonyl groups of PEOX and hydroxyl groups of TA.

After formation and characterization of H-bonded multilayers, we illustrate for the first time that PEOX / TA multilayers restructure into fibers in acidic phosphate buffer solutions [242]. Free floating PEOX / TA multilayers restructure easier into H-bonded and pH-responsive fibers. The restructuring of the film is especially evident in the growth profile when number of bilayers of LbL film exceeds 15 bilayers and reaches a certain thickness. For this reason, film growth profiles consisting of different number of bilayers were analyzed.

Fibers were analyzed by different characterization methods. Characterization of fibers demonstrated that fibers are composed of PEOX and TA molecules, an indication of fiber formation with the restructuring of multilayers in the phosphate buffer. The results shown were especially important in contributing to our understanding of the stability of LbL films in different chemical conditions and ways to alter the morphology of self-assembled structures. In addition, pH-responsive fibrous structures are very useful in different biomedical application areas, such as controlled release applications or sensors [243].

4.2 Experimental Details

4.2.1 Preparation and Characterization of PEOX / TA Multilayers

0.2 mg mL^{-1} PEOX (200K) and 0.2 mg mL^{-1} TA solutions were prepared in 0.01 M NaH_2PO_4 solution at pH 3. PEOX-200K / TA LbL films with different thickness were deposited by dip coating method. Silicon (100) wafers were used as substrates and treated with UV-Ozone (Model 42-200, Jelight Company) for 15 minutes. After the treatment, substrates were rinsed with DI water and dried under the flow of nitrogen. By dip coating, Silicon (100) wafers as substrates were alternately immersed into PEOX and TA solutions for 13 minutes with intermediate rinsing steps for 5 minutes. Rinsing solutions were composed of 0.01 M NaH_2PO_4 solution at pH 3. After completing the deposition of each PEOX/TA bilayer, thickness of the film was measured with ellipsometer (Microphotonics ELX-01R) using 632.8 nm laser light at 70° angle.

pH stability of the films was tested by immersing the films into phosphate buffer solutions at specific pH for 20 minutes. After immersion, films were dried under the flow of nitrogen and thickness of the film was measured with ellipsometer. pH of immersing solution was incremented ~0.25 units at each immersion.

The morphology of deposited multilayers was checked by optical microscopy and scanning electron microscopy. Then, FTIR characterization of the film was completed. Finally, contact angle measurements of the LbL films with different number of bilayers were done.

PEOX-500K, higher molecular mass of PEOX, was used to build free floating films. Higher molecular mass of PEOX ensures easy lift-off of intact PEOX/TA multilayers from the substrate. First, 12 bilayers of PEOX (500K) / TA LbL films were prepared on Si wafer, then the films were immersed in a phosphate buffer solution at pH 7.4. Large areas of the film detached from the substrate spontaneously in phosphate buffer after ~3-4 weeks. Detached and freely floating sheets of PEOX/TA multilayers were transferred to a 0.01 M NaH_2PO_4 solution at pH 3. Then, free floating LbL sheets and their restructuring was observed using optical microscopy over a period of one week.

4.2.2 Preparation and Characterization of PEOX / TA Aqueous Complexes and Aggregates

In the preparation of aqueous PEOX / TA complexes, TA concentration was held constant at 0.2 mg mL^{-1} in 0.01 M phosphate buffer at pH 3. Then, PEOX solution prepared in 0.01 M phosphate buffer at pH 3 was added dropwise to TA solution. Prepared PEOX solutions had different concentrations so that in the formed complexes, different ratios of PEOX monomers to TA can be obtained. Formed PEOX / TA aggregates were dried and FTIR characterization was performed with Thermo Scientific Nicolet IS50 ATR-FTIR.

4.2.3 Characterization of Fibers Formed by Restructuring of PEOX / TA Multilayers

Fibers formed as a result of restructuring PEOX / TA multilayers in phosphate buffer were washed with DI water and dried. The morphology of the fibers was checked with optical microscopy and SEM. Then, XPS characterization of fibers were performed followed by thermal stability test provided by TGA.

To check whether the fibers were pH responsive or not, morphology of the fibers was checked with optical microscopy. Then, fibers were treated with pH 10 solution, and dissolved aggregates were checked with optical microscopy again. In addition, the presence of dissolved TA molecules in pH 10 solution was detected by UV-Vis Spectroscopy.

4.3 Results and Discussion

4.3.1 Restructuring of PEOX/ TA LbL Films into Fibers

LbL films of PEOX / TA with different number of bilayers (BL) of PEOX and TA were deposited at pH3 in a phosphate buffer. Figure 4.1 demonstrates the growth profile of deposited PEOX/TA films consisting of different number of bilayers. All the films with different number of

bilayers had similar growth profiles as seen in Figure 4.1. After an initial growth stage, linear growth profile was observed between 5 BL and 15 BL. The average thickness of 15 BL films was ~118 nm which means an average BL thickness of the multilayers is approximately ~8.8 nm. For films thicker than 15 BL, a continuous decrease in thickness was observed between 15 BL and 20 BL from ~118 nm to ~85 nm. After 20 BL, the thickness of the films increased again and linear growth trend was regained with negligible fluctuations.

On the other hand, when films were grown in the absence of NaH_2PO_4 at pH 3, the growth profile and BL thickness of the 30 BL PEOX / TA films were different. Figure 4.1 shows that the growth profile is almost perfectly linear and average BL thickness is ~6.7 nm. It was previously reported that when PEOX / TA LbL films prepared in 0.2 mg mL^{-1} TA solution (pH~4.5) without addition of NaH_2PO_4, average BL thickness was ~5 nm [203]. The thickness difference and larger BL thickness in the linear region, together with thickness fluctuations above 15 BL in our films prepared at pH 3 in phosphate buffer is due to the presence of additional hydrophobic interactions along with H-bonding [180]. Kosmotropic $H_2PO_4^-$ ions in the assembly solution decrease T_{cp} of PEOX [101], make PEOX chains more hydrophobic and the hydrophobic interactions trigger destabilization in the aqueous solution.

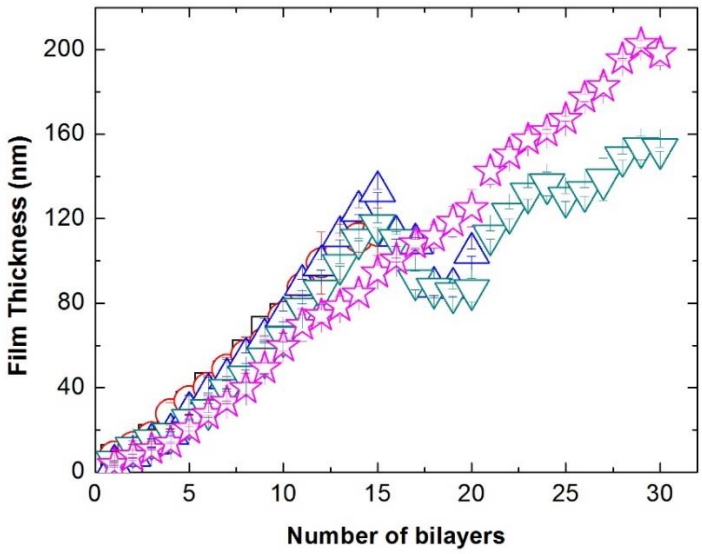

Figure 4.1: Thickness of PEOX/TA LbL films as a function of number of bilayers for four different films grown to a final thickness of 10 BL (squares), 15 BL (circles), 20 BL (up triangles) and 30 BL (down triangles) at pH 3 in the presence of NaH_2PO_4 solution, together with a 30 BL film grown at pH 3 without NaH_2PO_4 (stars)

Both 15 BL and 20 BL films appeared uniform to the naked eye. Both films were analyzed by optical microscopy. The detached patches were apparent in 20 BL LbL films in both OM and AFM images, as seen in Figure 4.2. These patches have irregular shapes and the sizes of patches varied between 10 μm to 150 μm.

Large area (5.48 mm x 4.11 mm) optical microscope image of the 20 BL film was generally uniform except small heterogeneities which is usual for dip coated LbL film (Figure 4.2 a). Figure 4.2 b illustrates the higher magnification OM image of the same film. In this figure, detached patches of the film can be clearly observed, as evident from color contrasts. Thinner regions on the substrate are blue and have irregular shapes. AFM height image of the same film and its height profile can be seen in Figure 4.2 c and d. Calculated patch width and depth were ~8 μm and ~40 nm respectively. In contrast, detached patches were not observed in 15 BL film and film had almost uniform morphology. It can be concluded that the thickness difference between 15 BL and 20 BL films was due to the detachment of film patches from the surface.

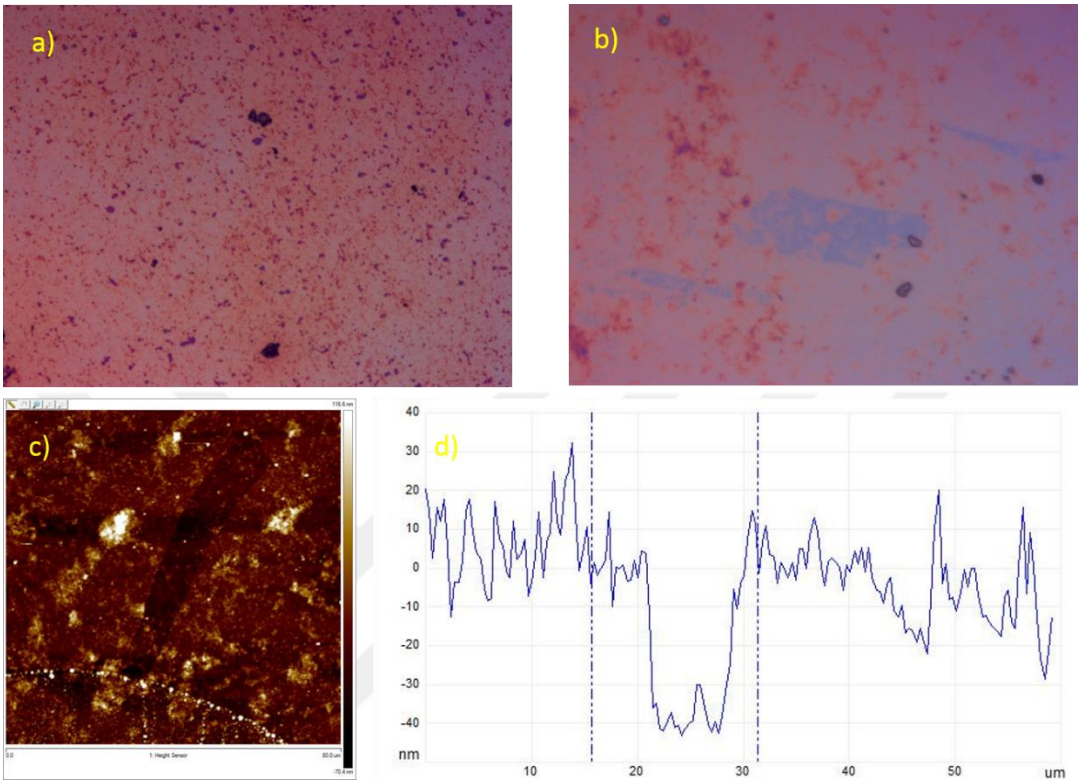

Figure 4.2: (a) Optical microscope image of the 20 BL PEOX/TA film (5480 mm x 4110 mm), (b) optical microscope image of the 20 BL PEOX/ TA film (548mm x411 mm), (c) atomic force microscope (AFM) height image of the 20 BL PEOX /TA film. Detached part of the film from the surface is shown (d) height profile of the detached part in (c)

Other than detached regions for the films thicker than 15 BL, rinse solutions of these films contained visible aggregates. In Figure 4.3, the aggregates that were collected from rinse solutions can be observed. Aggregates that were collected after PEOX adsorption and TA adsorption were demonstrated in Figure 4.3 (a) and Figure 4.3 (b), respectively, after 30 BL LbL films were grown. These aggregates are composed of long fibrous structures.

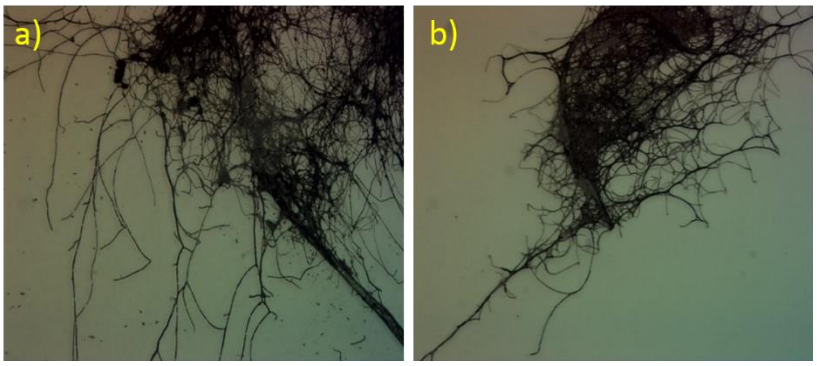

Figure 4.3: (a) Optical microscope image (5.48 mm x 4.11 mm) of the fibers that were collected from rinse solution (phosphate buffer at pH 3) after PEOX adsorption (b) Optical microscope image (5.48 mm x 4.11 mm) of the fibers that were collected from rinse solution (phosphate buffer at pH 3) after TA adsorption

To check whether films grown are porous or not, film morphologies of 30 BL PEOX/TA films prepared in the presence or absence of $H_2PO_4^-$ ions were checked with SEM. Figure 4.4 shows that both films were not porous and had uniform morphology.

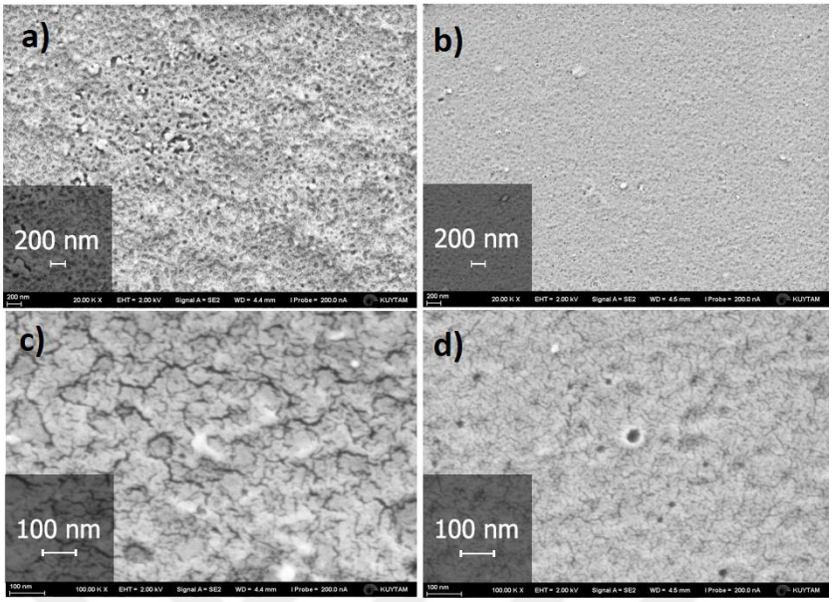

Figure 4.4: (a), (c) SEM images of 30 BL PEOX/TA film prepared in the presence of $H_2PO_4^-$ anions (b), (d) SEM images of 30 BL PEOX/TA film prepared in the absence of $H_2PO_4^-$ anions

Finally, it was concluded that decrease in film thickness and fluctuations in film growth in the presence of phosphate buffer, when the BL of the LbL films exceeded 15 BL, were due to the detachment of film patches from the substrate. Detached films restructure into well-defined fibers in pH 3 phosphate buffer, in the presence of $H_2PO_4^-$ ions. On the other hand, for films grown at pH 3 in the absence of phosphate buffers and $H_2PO_4^-$ ions, film growth profile was linear, and no fibers were seen in the rinse solutions of these films. Figure 4.5 compares the surface morphology of 30 BL PEOX /TA films prepared in the presence or absence of pH3 phosphate buffer and kept at various conditions for three days. Optical microscope images in Figure 4.5 confirmed the hypothesis that some parts of LbL film detach and restructure in pH 3 phosphate buffer, even some fibers were observed on the surface of the film when kept in pH 3 phosphate buffer. On the other hand, at pH 3, the films grown and kept in the absence of NaH_2PO_4 were very stable on the substrate and typically remained intact for several weeks. When the films were assembled in the presence $H_2PO_4^-$ ions, and kept at pH 3 in the absence of phosphate buffer (in the absence of $H_2PO_4^-$ ions), detached parts were observed locally on the top surface of the film, but no fibers were observed at pH 3 phosphate buffer solution. For the films assembled in the absence of NaH_2PO_4

and kept at pH 3 in the presence of $H_2PO_4^-$ ions, fibers formed in the presence of pH 3 phosphate buffer but no detached parts were observed on the surface of the film.

In addition to optical microscope images at Figure 4.5, Figure 4.6 also illustrates the optical microscope images of fibers restructure around the detached parts of PEOX / TA multilayers grown in the presence of $H_2PO_4^-$ ions. In Figure 4.6, fibers that were collected in and around the gaps can be clearly observed, further supporting the hypothesis that films grown in the presence of $H_2PO_4^-$ ions detach and restructure in phosphate buffer.

All these results show that thickness fluctuations when films were grown in the presence of NaH_2PO_4, are due to the detachment of film patches. Especially, between 15 BL and 20 BL, desorption or detachment of film patches dominated over LbL growth regime so that decrease in film thickness is observed in Figure 4.1. On the other hand, when detachment and desorption of film patches from the surface slowed down, film thickness started to increase again, recovering the growth rate. When film thickness exceeded 20 BL, film growth reached a dynamic steady state. Thus, it can be concluded that two competing mechanisms, film growth through adsorption of components vs. detachment of film patches through desorption of films are effective in film growth mechanism.

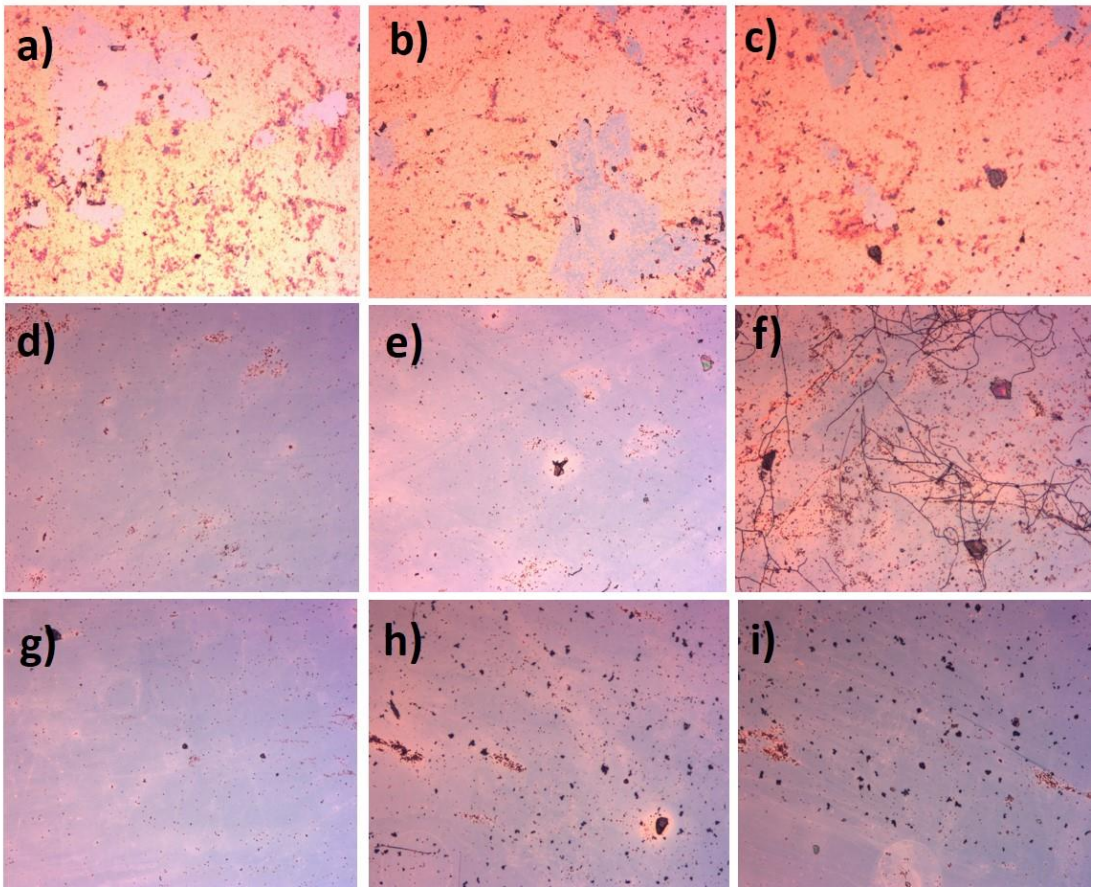

Figure 4.5: Optical microscopy images of 30 BL PEOX/TA films grown and kept at various conditions: a-c) 30 BL PEOX/TA film prepared at pH3 phosphate buffer and observed at pH3 in the absence of $H_2PO_4^-$ anions: a) after preparation, b) after 1 day at pH3, c) after 2 days at pH3; d-f) 30 BL PEOX/TA film prepared at pH3 in the absence of $H_2PO_4^-$ anions and observed at pH3 in the presence of H2PO4 - anions: d) after preparation, e) after 1 day at pH3, f) after 2 days at pH3; g-i) 30 BL PEOX/TA film prepared at pH3 in the absence of $H_2PO_4^-$ anions and observed at pH3 in the absence of $H_2PO_4^-$ anions: g) after preparation, h) after 1 day at pH3, i) after 2 days at pH3. All images are 2.74 mm x 2.05 mm.

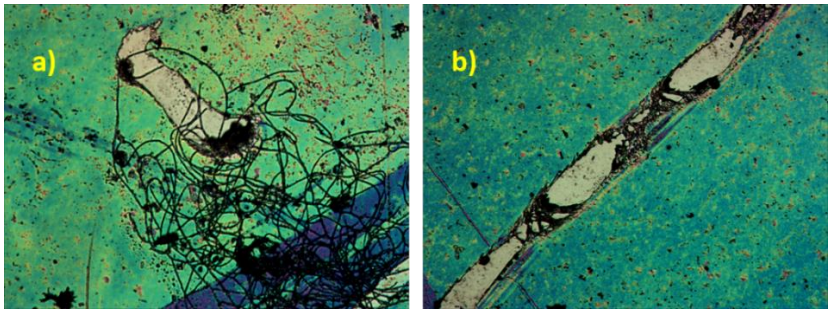

Figure 4.6: Optical microscope images of detached parts of PEOX/ TA LbL film and fibers restructured around these regions. (a) A flaked region of the film and the attached fibers around it (2740 mm x2055 mm). (b) Fibers that were restructured at the gap between the two parts of a uniform film (2740 mm x 2055 mm).

Figure 4.7 also shows the SEM images of detached parts of 30 BL PEOX / TA LbL films. As previously demonstrated, films are uniform and homogeneous, except the detached and flaking parts. In Figure 4.7 (a), around the detached regions, no fibers were observed, probably fibers formed had fallen into the phosphate buffer solution. In Figure 4.7 (b), a big patch that was delaminating from the surface can be observed. Furthermore, at the tip of the delaminated film patch started to restructure into fibers. In addition, Figure 4.7 (c) also illustrates how detached film parts on the surface formed plenty of fibers. SEM images in Figure 4.7 confirms that fiber formation started on the surface of the film. The fibers were collapsed ribbons and several μm long.

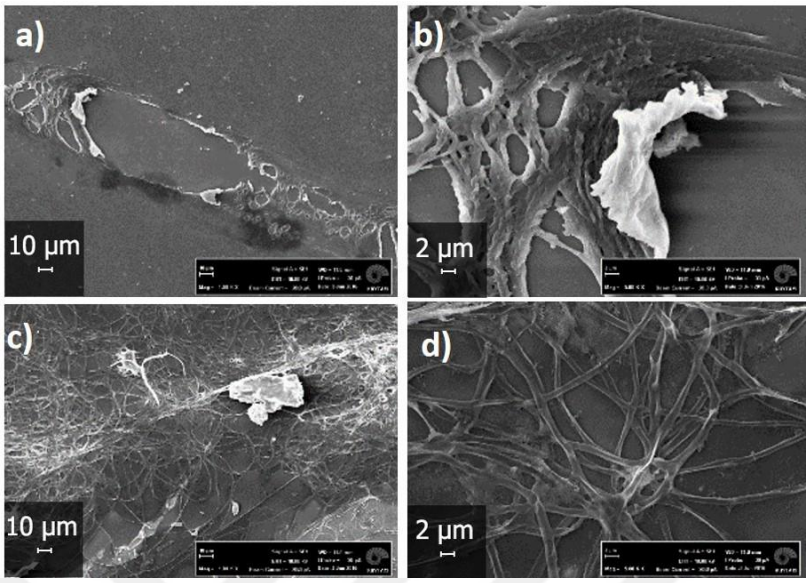

Figure 4.7: SEM images of 30 bilayer PEOX/TA LbL film and fiber formed. Scale bar for (a) and (c) are 10 µm. Scale bar for (b) and (d) are 2µm.

Figure 4.8 shows the pH stability of 30 BL PEOX / TA films in phosphate buffer having different pH conditions. Mainly, pH stability of the films grown either in the presence or absence of NaH_2PO_4 are compared. The critical disintegration pH for both films was ~8.5. At this critical pH, hydroxyl groups of TA start ionizing, so H-bonds between PEOX and TA are broken. However, stability behaviours of these two films below critical disintegration pH (pH ~8.5) were different. Thickness of the films grown in the absence of NaH_2PO_4 didn't change below pH 8.5. On the other hand, films prepared in the presence of NaH_2PO_4 showed continuous thickness decrease below pH 8.5 and at pH 8.5, only 70% of the film remained on the substrate.

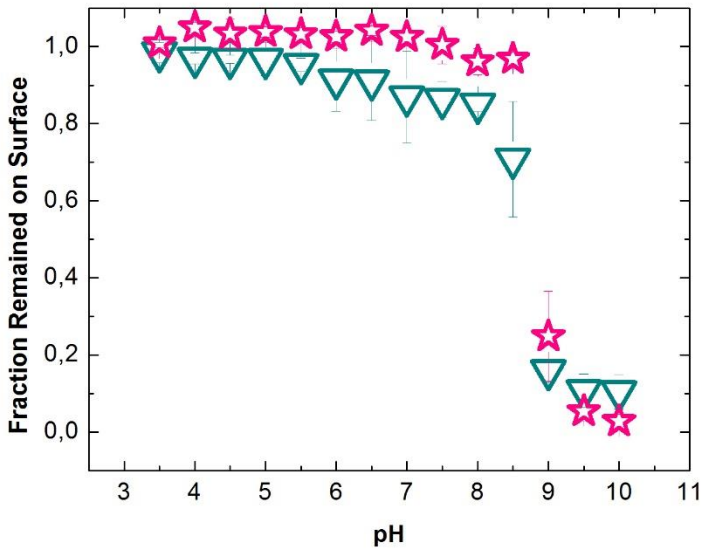

Figure 4.8: pH stability of 30 BL PEOX/TA LbL films grown at pH 3 in the presence (down triangles) and the absence (stars) of NaH_2PO_4. pH stability is shown and plotted as the fraction of the film remained on the substrate as a function of pH of the phosphate buffer.

All these results show that LbL films formed by PEOX and TA in phosphate buffer are not as stable as those prepared in the absence of phosphate ions on solid substrates. Especially when these films are post-treated with pH 3 phosphate buffer, detached film parts restructure into fibers. On the other hand, films grown in the absence of NaH_2PO_4 are very stable in acidic conditions. This difference in stabilities and fiber formation with the film detachment is attributed to the increasing hydrophobicity caused by $H_2PO_4^-$ ions. Other reasons for detachment and flaking of films parts are inhomogeneity in surface chemistry, local stress or scratches in the random parts of the film.

As a final confirmation of the proposed hypothesis, free standing PEOX / TA sheets were obtained by treating LbL films in pH 7.4 and lifting the film off the substrate. Then, lifted sheets were placed in a petri dish at pH 3 buffer solution and observed under optical microscope for a period of ~ 5 days. Figure 4.8a shows the LbL sheet just after placing it into pH 3 buffer. Figure 4.8b, the image taken after placing LbL sheet for one day, demonstrates that fiber formation started at the edges. Restructuring of LbL sheet continued and amount of fibers increased for the next two days. After four days, the sheet started to disappear. Finally at the fifth day, LbL sheet disappeared

completely and turned completely into aggregate of fibers. The hypothesis that PEOX / TA films are instable when grown in phosphate buffer and this instability causes restructuring of detached film parts into fibers was confirmed through optical microscopy images as shown in Figure 4.9. The reasons for the instability and restructuring of the films are further discussed below together with the characterization of the formed fibers.

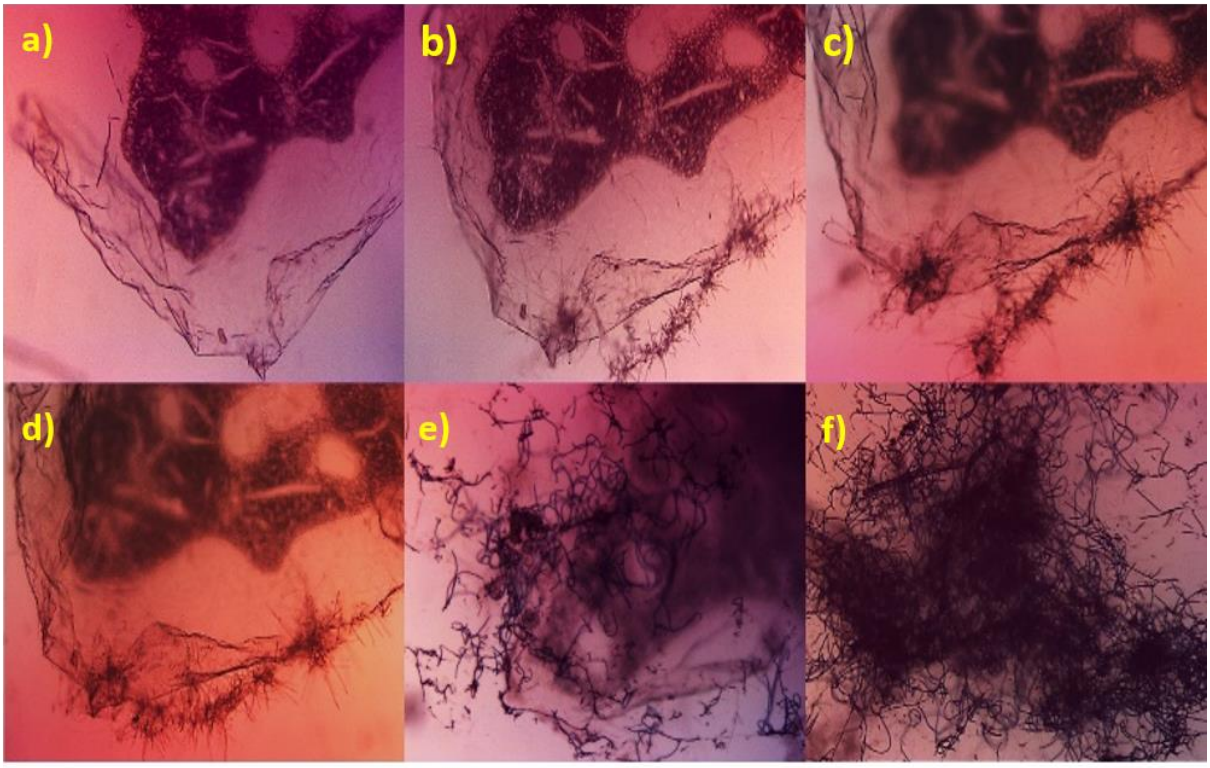

Figure 4.9: Optical microscopy images of restructuring of a PEOX/TA LbL sheet into fibers at pH3 buffer solution: (a) initial sheet, (b) after 1 day, (c) after 2 days, (d) after 3 days, (e) after 4 days, (f) after 5 days. All images are 5480 mm x 4110 m.

4.3.2 Characterization of Fibers

Fibers formed from restructuring of PEOX / TA multilayers were first washed, dried and characterized by different methods.

TGA data of the dried fibers of PEOX and TA is shown in Figure 4.10. TGA is performed under nitrogen gas. PEOX and TA decompose at a single decomposition temperature at 400°C and 250°C, respectively. Dried fibers decomposed at two different temperatures at 250°C and 400°C. Decomposition of fibers at these temperature values showed that fibers were actually composed of TA and PEOX. From TGA results, it was calculated that the amount of TA is ~88% by weight and the amount of PEOX is ~%12 by weight.

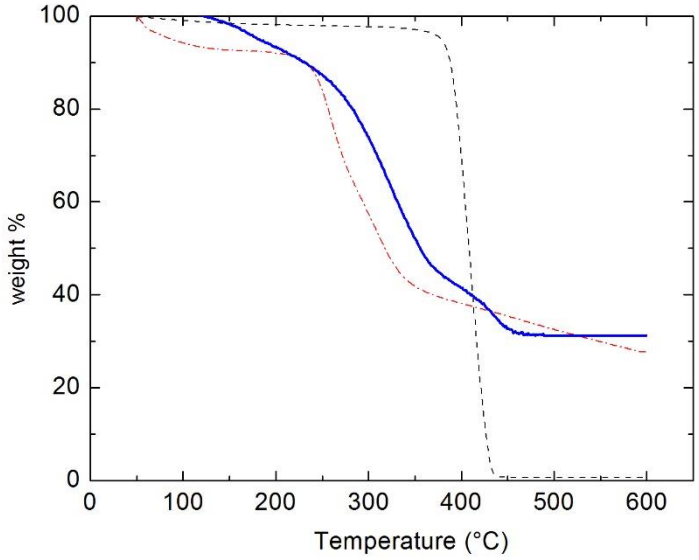

Figure 4.10: TGA of PEOX (dashed line), TA (dashed dotted line) and dried fibers (solid line)

XPS analysis gave more detailed information about the chemical composition of the fibers. Table 4.1 shows the atom % of the elements according to the peaks observed in XPS spectrum, Figure 4.11. N peak in the spectrum is an evidence for the presence of PEOX in the fibers. From XPS data, the number of PEOX monomers for each TA in the fibers can be also approximated. 2.58% N corresponds approximately to the presence of 4 PEOX monomers for each TA molecule in the dried fibers when total number of atoms in PEOX monomer and TA are considered.

Observed Na and P peaks in XPS data were due to the residual NaH_2PO_4 salt molecules on the fibers after rinsing.

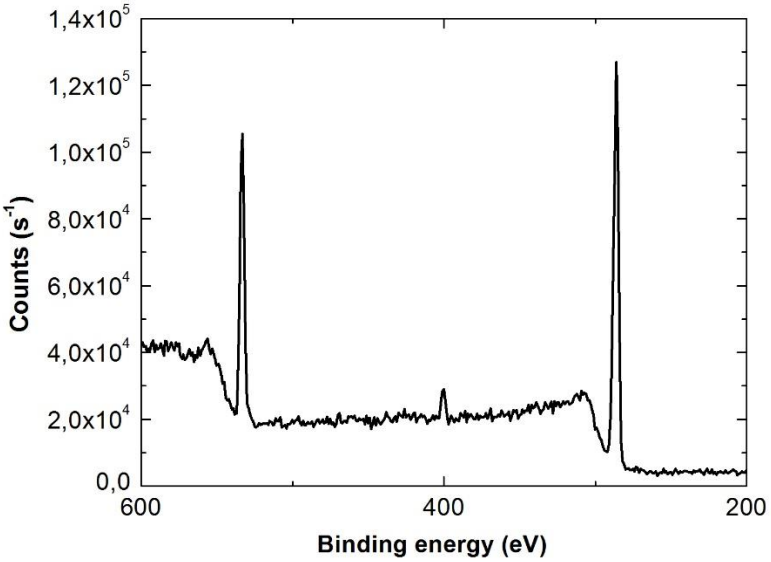

Figure 4.11: XPS spectrum of dried PEOX/TA fibers. The peaks correspond to C 1s at 286 eV, O 1s at 533 eV and N 1s at 400 eV.

Table 4.1: Elemental composition of the fibers as atomic weight % determined by XPS

Element Name	**Atom %**
C 1s	76.28%
O 1s	20.71%
N 1s	2.58%

TGA and XPS results show that the films have a high content of TA and it is probable that TA molecules bind weakly to PEOX molecules. Thus, we tried to increase the content of PEOX in the film and improve the stability of films by depositing at higher temperature. We prepared PEOX/TA LbL films at higher temperature of 50^{o}C (below the PEOX critical temperature of ~60 ^{o}C) both in the presence and absence of $H_2PO_4^-$ and investigated the film stability and the fiber formation. Results show that independent of the growth temperature, fiber formation was observed

in the presence of $H_2PO_4^-$, but not in the absence of $H_2PO_4^-$. In conclusion, no change in film stability was observed as a function of growth temperature.

FTIR characterization also verified that PEOX and TA molecules were present in the fibers and H-bonds exist between them. In Figure 4.12 (a) and (b), FTIR spectrum of 30 BL PEOX/TA LbL film and fibers obtained from restructuring of multilayers is demonstrated. Especially, carbonyl (-C=O) region of the film was shown, together with the spectra of PEOX and TA. Carbonyl peak of PEOX is a single peak at 1629 cm^{-1}. In the same region, TA also has two peaks: A peak at 1606 cm^{-1} due to –C-C- stretching and in-plane vibrations of benzene ring and carbonyl peak at 1698 cm^{-1}, due to -C=O groups H-bonded to -OH groups of TA at 1698 cm^{-1}. In 30 BL LbL films, a single peak at 1616 $cm^{-1,}$ between the individual peaks of PEOX and TA, can be clearly observed. Shift of –C=O groups to lower wavenumbers indicates presence of H-bonds. Upon hydrogen bonding, the resonance structure of the amide bond in PEOX molecules is stabilized which results in weakening of C=O bond character and increasing in the bond length [244]. At the same time, TA peak at 1698 cm^{-1} shifted to 1725 cm^{-1}, almost by 27 cm^{-1} change.

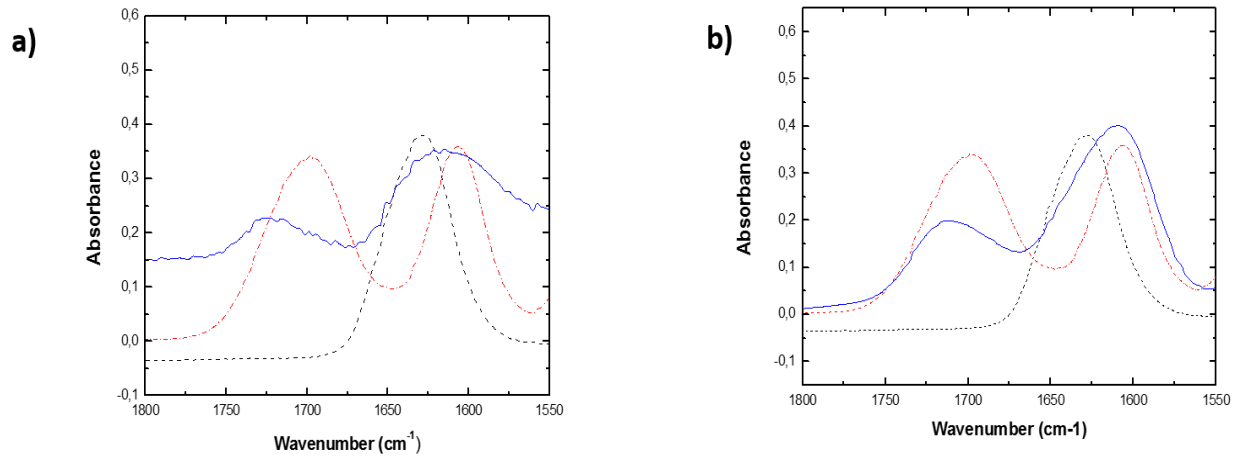

Figure 4.12: (a) FTIR data of 30 BL PEOX / TA LbL film (solid line), PEOX (dashed line) and TA (dashed dotted line). (b) FTIR data of dried fibers from restructuring of PEOX / TA multilayers (solid line) with PEOX (dashed line) and TA (dashed dotted line).

To confirm H-bonding and show the shift in TA peak at 1606 cm^{-1}, PEOX / TA aggregates were formed in aqueous solutions, then dried and characterized with FTIR. Complexes of PEOX and TA were formed by adding PEOX to the aqueous TA solution at constant concentration. As PEOX amounts were increased in the formed complexes, TA peak at 1606 cm^{-1} shifted to lower wavenumbers by 7 cm^{-1}. 7 cm^{-1} shift corresponds to a composition of 6 PEOX monomers for 1 TA molecule. At the same composition, TA peak at 1698 cm^{-1} shifted to 1718 cm^{-1}, almost 20 cm^{-1} shift. Figure 4.12 shows FTIR spectra of PEOX / TA complexes prepared in aqueous solutions.

At the same time, FTIR spectrum of the dried fibers at Figure 4.12 (b) is very similar to the spectrum of PEOX / TA complexes that have composition of 6 PEOX monomers to 1 TA molecule and 30 BL PEOX / TA LbL film. PEOX carbonyl peak shifted to 1609 cm^{-1}, between the individual peaks of PEOX and TA. Also, TA peak at 1698 cm^{-1} was shifted to 1712 cm^{-1}. Thus, it was shown that fibers contain H-bonds and these bonds exist between carbonyl groups of PEOX and hydroxyl groups of TA.

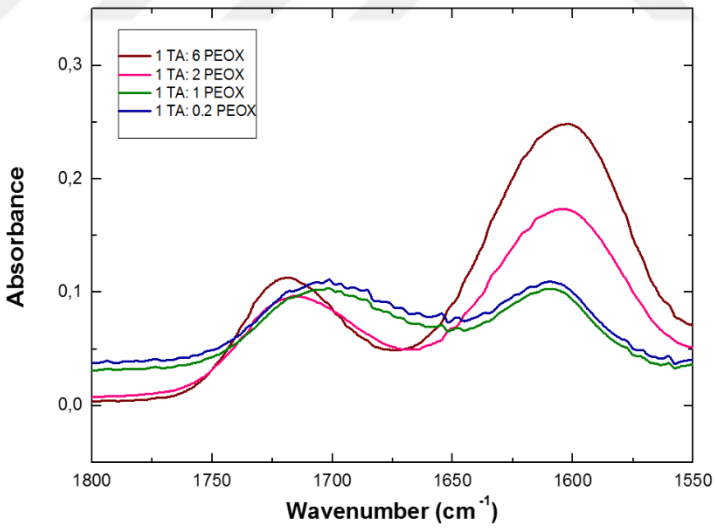

Figure 4.13: FTIR spectrum of PEOX/TA complexes with changing PEOX monomer ratio at a fixed concentration of TA showing the shifts in carbonyl (C=O) group of both PEOX and TA.

pH stability of dried fibers in aqueous solutions was also checked to further verify the presence of TA molecules and H-bonds in the fibers. For that, fibers formed via restructuring of PEOX / TA multilayers were observed at pH 3 solution. Fibers were stable at pH 3 solution for

several months. Fibers at pH 3 solution were then transferred to pH 10 solution and gently stirred for 24 hours. At the end of 1 day, fibers were dissolved significantly as observed in Figure 4.14.

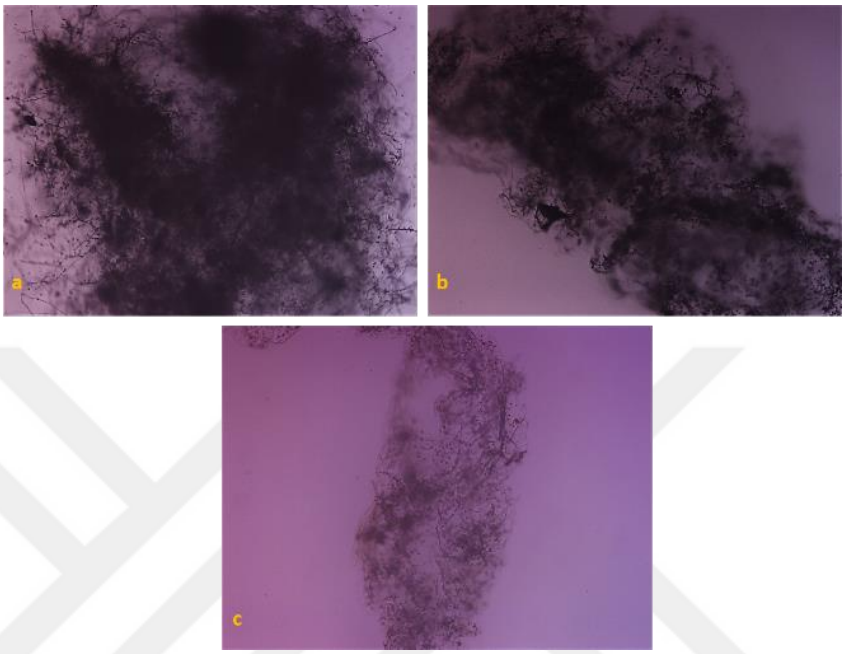

Figure 4.14: a) Optical microscope image of PEOX/TA fibers in pH3 phosphate buffer solution before transferring into pH10 solution (5480 µm x 4110 µm) b) Optical microscope image of PEOX/TA fibers in pH10 aqueous solution after several hours (5480 µm x 4110 µm) c) Optical microscope image of PEOX/TA fibers in pH10 aqueous solution after 24 hours (5480 µm x 4110 µm).

Dissolution of fibers were due to the breakage of H-bonds with the ionization of hydroxyl groups of TA since pH of solution is higher than pKa of TA (~pKa 8.5). This confirms the presence of H-bonds in the fibers. After fibers were dissolved, UV-Visible spectrum of the solution was obtained. The peaks at 244 nm and 276 nm indicate the presence of ionized TA molecules in the dissolving solution at pH 10. UV-Visible spectra of dissolved fibers and TA solution at pH 3 were given in Figure 4.15.

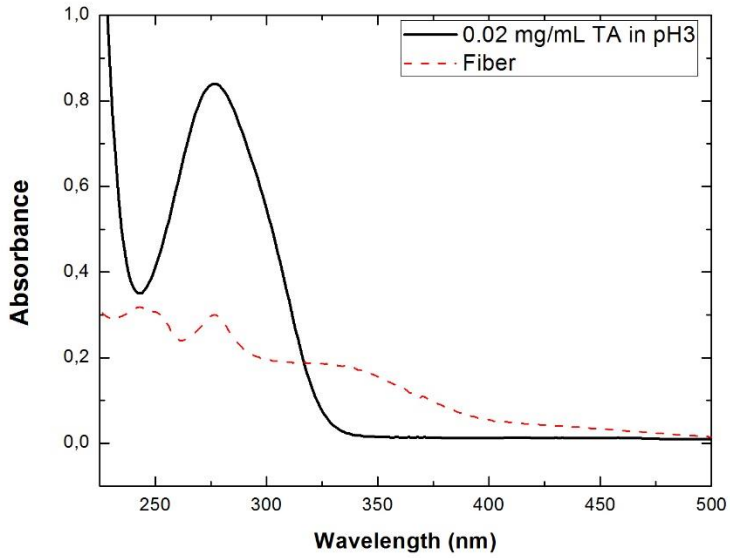

Figure 4.15: UV-Visible spectrum of dissolved PEOX/TA fibers at pH 10 (solid line) which confirms the presence of ionized TA in pH 10 solution. The dashed line is the UV Visible spectrum of TA at pH3 (non-ionized) showing a single peak at 276 nm.

In summary, TGA, XPS and FTIR investigations conclude that fibers were formed by restructuring of PEOX and TA multilayers and composed of H-bonded PEOX and TA molecules. Dissolution of fibers at pH 10 solution also showed that formed fibers were pH-responsive. Fibers were stable below pH 8.5, but when pH exceeded 8.5, fibers were unstable due to the deprotonation of TA molecules in the fibers.

The morphology of dried fibers was also investigated with SEM, as shown in Figure 4.16. Fibers are ribbon-like structures and they have a width of 1-2 μm. Fibers lay on top of each other and their morphology looks like collapsed hollow tubes. A possible explanation for this morphology is that formation of fibers was due to the curling of planar PEOX /TA LbL sheets, as shown in Figure 4.16 (b). Curling of detached PEOX/TA patches result in torsional stress exist in multilayers and a possible reason can be chemical anisotropy. Chemical anisotropy can be caused hydrophilicity difference that the top surface and bottom surface are exposed. Top side of the film could be exposed to pH 3 solution which is richer in TA and bottom side of the film can be richer with PEOX molecules and could be more hydrophobic. With this hydrophilicity difference, detached planar film patches curls onto itself when forming fiber. The inner part of the fiber is

more hydrophobic and richer with PEOX molecules. Chemical anisotropy and inhomogeneity in surface chemistry are among the reasons for the restructuring of PEOX / TA multilayers into fibers.

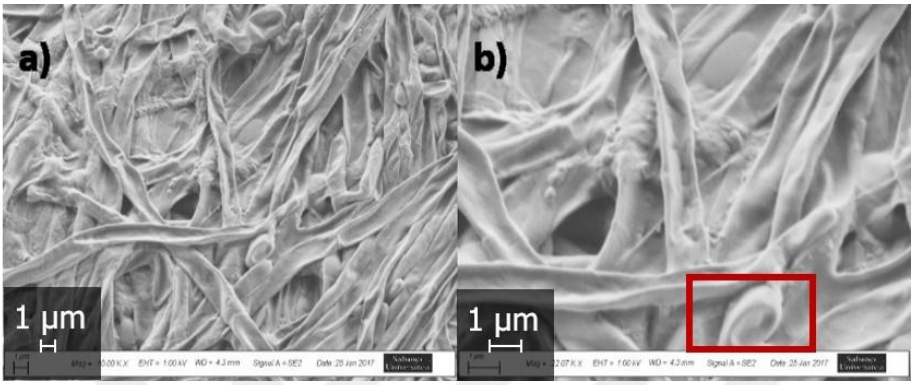

Figure 4.16: FESEM images of dried fibers from restructuring of PEOX / TA multilayers collected from the rinse solutions of 30 BL PEOX / TA LbL film.

Chemical anisotropy and less hydrophilic regions in LbL film are due to the presence of $H_2PO_4^-$ ions in the solution. $H_2PO_4^-$ is a kosmotropic ion and has a "salting-out" effect on polymers. In aqueous solutions, salting effect causes decrease in T_{cp} of the thermo-responsive polymers in aqueous solutions [101], [95]. In their working mechanisms, "salting-out" effect by these ions results in dehydration of the polymer chains by replacing H-bonded water molecules bound to polymer and increased surface tension between the polymer chains and aqueous solution [68], [183], [245].

$H_2PO_4^-$ ions penetrate to interior parts of the multilayers, especially loosely bounded regions, during the assembly of LbL film. Penetration of $H_2PO_4^-$ ions to these regions is possible since LbL film is deposited via dip coating so that uniform film cannot be built. With the penetration of $H_2PO_4^-$ ions and change in hydrophilicity locally on the film, hydrophobic domains were probably formed. These hydrophobic domains in aqueous solution are especially not stable since they are exposed and sit onto hydrophilic film parts. When treated with aqueous solutions, these instable hydrophobic domains lift off and detach as patches with the penetration of water driven by the minimization of interfacial energy. In the literature, it was previously reported that presence of hydrophobic interactions enhance the pH stability H-bonded LbL multilayers when distributed uniformly between the polymer chains [180], [182]. However, in this case, hydrophobic

interactions were not distributed uniformly throughout the film and mostly, it dominated at the interfaces. As a result, this causes instability of the film in aqueous solutions, detachment of the film patches and restructuring of the patches into fibers in aqueous solutions.

The possibility that the presence of residual water in the film can be the cause of restructuring was also tested. To test this, 30 BL PEOX/TA films prepared at pH 3 phosphate buffer were kept in vacuum oven at 50^{o}C for ~5 hours. The annealing temperature was kept below the critical temperature and the glass transition temperature of PEOX (~60 ^{o}C) not to disturb the morphology of the grown films. The films were then kept at pH 3 phosphate buffer as a function of time. To check fiber formation, samples were investigated under optical microscope. Figure 4.17 shows and compares the optical microscope images of the 30 BL PEOX / TA films before putting under vacuum at 50^{o}C and after placing under vacuum at 50°C. Similar to those films that were not annealed, fiber formation was observed on the films at the 2nd day. Based on these results, it was concluded that the presence of residual water in the LbL films is not the cause of restructuring.

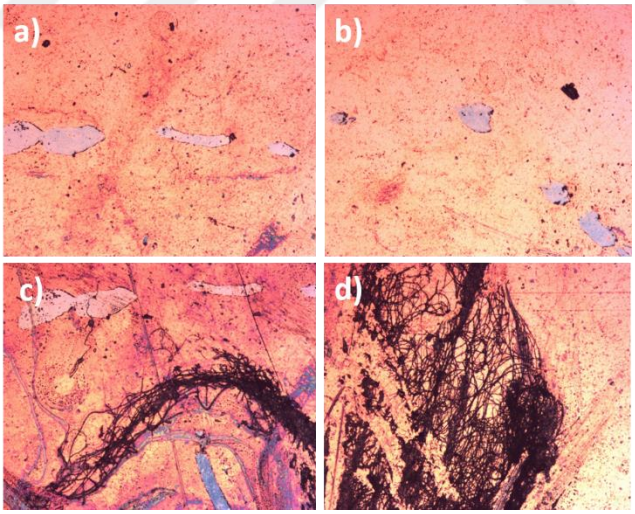

Figure 4.17: (a), (b) Optical microscopy images of 30 BL PEOX / TA LbL films before putting in under vacuum at 50°C (c), (d) Optical microscopy images of 30 BL PEOX / TA LbL films after putting in under vacuum at 50°C. All images are 5480 mm x 4110 m.

In order to support the hypothesis above, contact angle measurement were made to show increasing hydrophobicity of the growing PEOX / TA LbL films. Figure 4.18 illustrates the water contact angle on the surface of PEOX / TA LbL films. Contact angle of LbL films was measured

as a function of number of bilayers. Contact angle of 10 BL film and 30 BL film were recorded as 30° and 50°, respectively. As a result, with increasing number of bilayers, hydrophobicity of the surface also increases. AFM height images of PEOX / TA LbL films with different number of bilayers were also shown in Figure 4.18 b. The root mean square (rms) roughness (~23.7 nm) of the films remained almost same and didn't change for films having different number of bilayers. This shows that change in contact angle and hydrophilicity with number of bilayers is not related with the roughness of the films. A possible reason can be stronger interaction induced between $H_2PO_4^-$ ions and PEOX chains as number of bilayer increases. Salt induced changes in hydrophilicity and wettability of the nanocomposite thermo-responsive surfaces were previously reported [245]. Advancing contact angle of the nanocomposite surface changed from ~80° to ~140° for 1-1.2 M aqueous NaH_2PO_4 solution. Indeed, these obvious changes for PEOX / TA LbL films are not expected so quickly since the concentration of rinse solutions and post-treatment solutions are 0.01 M. Instead, gradual changes are more expected in larger time scales as restructuring of PEOX / TA multilayers took 5 days as shown in Figure 4.8. As a result, increased hydrophobicity on the top surface of PEOX / TA multilayers after ~18 hours of treatment of multilayers in 0.01 M NaH_2PO_4 solution is within our expectations. The detachment of film patches (~40 nm thick) from the top surface of the film (as shown in Figure 4.2) is also consistent with the results that were reported.

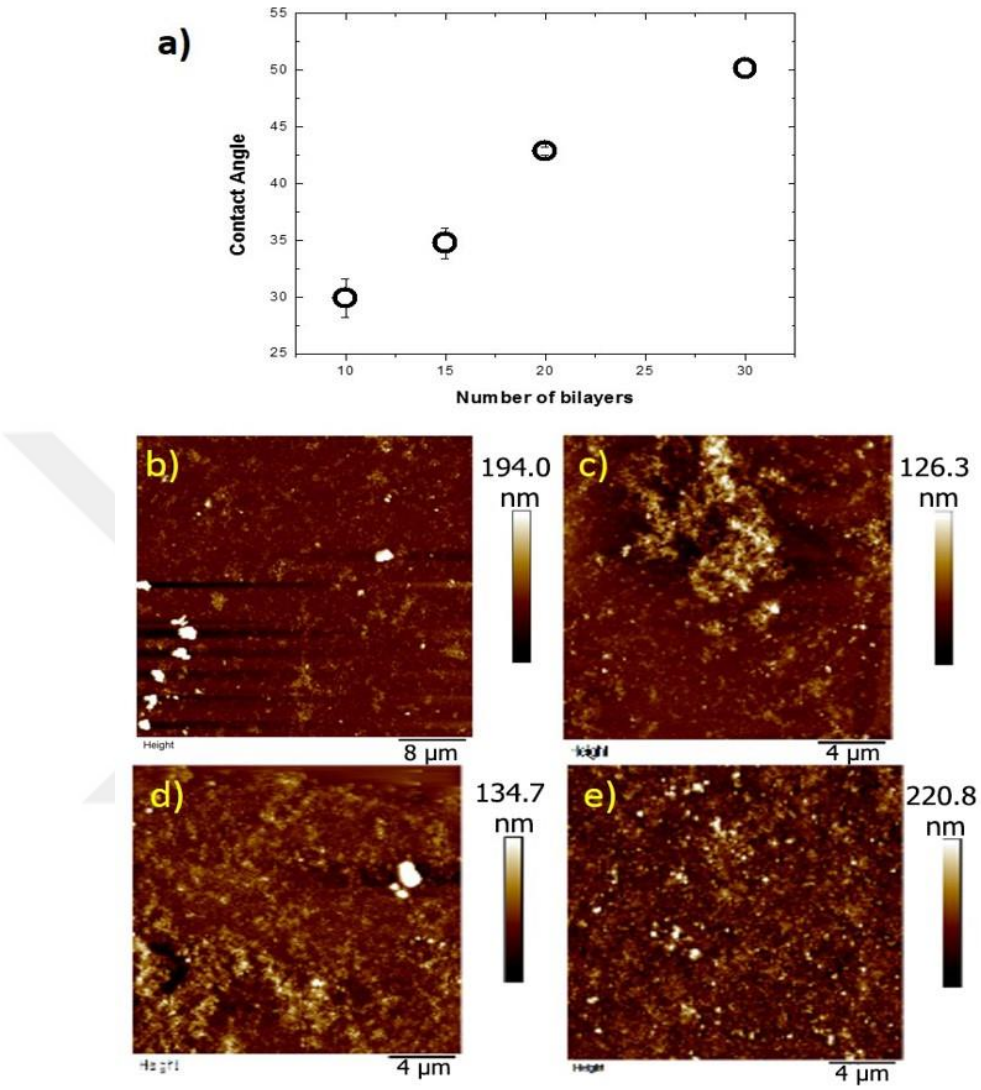

Figure 4.18: (a) Contact angle measurements of PEOX / TA LbL films as a function of number of bilayers (b) AFM height image of 10 BL PEOX / TA LbL film (c) AFM height image of 15 BL PEOX / TA LbL film (d) AFM height image of 20 BL PEOX / TA LbL film (e) AFM height image of 30 BL PEOX / TA LbL film

4.4 Conclusion

pH responsive LbL multilayers of PEOX and TA were prepared in pH 3 phosphate buffer via H-bonding between carbonyl groups of PEOX and hydroxyl groups of TA. Prepared multilayers restructure into fibers in phosphate buffer solutions at pH 3, the pH value in which H-bonds between PEOX and TA were still stable.

The restructuring process of multilayers into fibers was also evident during the growth of multilayers, especially for the films thicker than 15 BL. The growth profile of 30 BL film showed that fluctuations in thickness exist during the growth in phosphate buffer. A significant decrease in thickness was observed between 15 BL and 20 BL, then after 20 BL, films started to re-grow again with small fluctuations. The decrease in thickness was due to the detachment of film patches from the surface of the film. Fibers were also observed in the rinse solutions of the multilayers since detached multilayers restructure into fibers in the presence of $H_2PO_4^-$ ions. pH stability test also indicated that instability of the film was due to the presence of $H_2PO_4^-$ ions, since in the absence of NaH_2PO_4 solution, films didn't show a significant decrease up to pH 8.5, the pH in which TA molecules started to ionize and H-bonds broke. Decreased stability in the presence of $H_2PO_4^-$ ions is because of the domination of local hydrophobicity in the interfaces. This increased local hydrophobicity in the film with the presence of $H_2PO_4^-$ ions also resulted in detachment of film patches and restructuring of the film patches into fibers.

As observed from free floating multilayers, the restructuring process was rather slow since transformation of multilayers to fibers took 5 days. Fibers were characterized by various characterization methods. TGA and XPS results demonstrate that fibers were consisted of PEOX and TA molecules. In addition, fibers were pH responsive and disintegrated above pH 8.5. SEM images of fibers indicate how the fiber formation process evolved. A possible reason could be the curling of detached planar film patches. The curling of the detached sheets indicated torsional stress in the films due to the presence of chemical anisotropy in the films. Chemical anisotropy can be due to the hydrophilicity difference between top and bottom surface. The hydrophilicity difference is due to the exposure of the top surface to pH 3 solution which is richer in TA. On the other hand, bottom side is more hydrophobic and richer in PEOX chains. On solid substrates, dried fibers looked like collapsed hollow tubes in which inner side of the tube is more hydrophobic and

richer in PEOX. The hypothesis about the restructuring of detached film patches into fibers was also verified through contact angle measurements. Contact angle measurements and AFM indicated that increase in hydrophobicity with increasing number of bilayers is not related to the surface roughness. Gradual changes in larger time scales support the proposed hypothesis about restructuring.

The results that were shown about restructuring of PEOX / TA multilayers into well-defined fibers improved our understanding of the stability of LbL films in different chemical conditions. With this anticipation, various ways to change the morphology of self-assembled structures were also foreseen. By this way, modifying the LbL multilayers into fibrous structures under certain conditions, can be useful in various biomedical applications.

Chapter 5: Effect of Hofmeister Series of Salt on the Properties of Hydrogen Bonded PEOX / TA Multilayers

5.1 Overview

The mechanisms about how ions affect the protein or macromolecule stability were discussed by Hofmeister in the work published in 19th century[81]. Mainly, three different mechanisms are effective in thermo-responsive properties of aqueous solutions of LCST polymers as also discussed in detail in Chapter 2 : Dehydration mechanism and surface tension mechanism decrease T_{cp}; while direct binding mechanism of chaotropic salts increase T_{cp} of polymers that exhibit LCST behavior in aqueous solutions [95].

The effect of Hofmeister salts on the electrostatically bound PEMs have also been extensively studied in the literature. Salt annealing of PEMs was used to trigger different diffusional responses between the layers so that swelling and smoothening of multilayers were obtained [147, 162]. In another work, quartz crystal microbalance with dissipation (QCM-D) was used to investigate the swelling behavior of LbL electrostatic films upon exposure to different monovalent anions and four salt concentration regimes were associated with the swelling behavior [163]. Besides salt annealing of PEMs, the effect of Hofmeister salts used during the assembly of multilayers were also investigated. These studies indicate that when different salts and ionic strengths were used during the formation of multilayers, different growth regimes and multilayers with different thickness were obtained [161, 246-248]. Different morphologies in electrostatically bound LbL films can also be induced via preparing film assemblies with different salts with varying ionic strength[160], [249]. Zhang *et al.* formed porous LbL films and controlled the size of pores by tuning NaCl concentration while preparing films [8]. The salt effects on hydrogen bonded films were not investigated as much as those of electrostatically bound films. It was shown that post-treatment of H-bonded poly (vinyl pyrrolidone) (PVPON) and poly (acrylic acid) (PAA) in salt solutions caused phase-separation between components and de-wetting between multilayers [194]. Sukhisvili *et al.* studied the construction of hydrogen bonded multilayers of polycarboxybetaine (poly-N-ω-carboxypentyl-4-vinylpyridinium bromide (PCB_5) with poly(N-vinylcaprolactam) (PVCL) and observed that potassium halide salts are required to promote the

deposition of multilayers [250]. Binding of anions to PCB_5 chains followed Hofmeister series [250]. Zhao *et al.* showed that addition of NaCl into releasing medium slowed down the release of TA from hydrogen bonded PEG / TA multilayers [227].

In this thesis, the effect of Hofmeister series of salts at different ionic strengths on H-bonded PEOX/TA films was systematically investigated and it was shown for the first time that salt effects can be exploited to induce different film thickness, pH stabilities and morphologies in them. The nature of the interaction between PEOX and TA in the presence of different salts was investigated by isothermal titration calorimetry (ITC) measurements and calculated thermodynamic parameters were related to the structural properties and stabilities of PEOX/TA multilayers in different chemical conditions. Although, there are studies about how salt affects the properties of LbL films, these works are limited mostly to either electrostatically bound films or morphological changes of H-bonded multilayers via salt annealing. Thus, this study contributed to our understanding of how the interaction mechanism between different salt and PEOX/TA in aqueous solutions affected the properties of H-bonded LbL films. Insights from this study would be important for biomedical applications like encapsulation and controlled release of drugs [92] .

5.2 Experimental Details

5.2.1 Preparation and Characterization of PEOX / TA Multilayers

10 bilayer (BL) PEOX/TA multilayer films were prepared by dip-coating LbL deposition. 0.2 mg mL^{-1} PEOX (200K) and 0.2 mg mL^{-1} TA solutions were each prepared in respective sodium salt solutions (Na_2CO_3, Na_2SO_4, NaH_2PO_4, NaF, NaCl, $NaNO_3$, NaBr and NaSCN) with various concentrations at pH 3. pH adjustments were made using either HCl, H_2SO_4, HNO_3 or NaOH solution according to the character of the sodium salt in order to prevent counter ion effect For the salts that are strongly kosmotropes (Na_2CO_3, Na_2SO_4), H_2SO_4 is used and for the salts that are chaotropes ($NaNO_3$, NaBr and NaSCN) , HNO_3 is used. For the mid-Hofmeister salts (NaH_2PO_4, NaF, NaCl), HCl is used for pH adjustments. Type of acid solutions for pH adjustments are selected according to how close SO_4^{2-}, Cl^- or NO_3^- ions in acid solutions to the of the location of respective ions in Hofmeister salt series.

Multilayer film deposition was achieved by alternating dipping of the substrate into PEOX and TA solutions for 15 min each and rinsing in these respective salt solutions at various concentrations at pH 3 for 5 minutes between the adsorption cycles. Silicon (100) wafers were used as substrates, after pre-treatment in UV-ozone (Model 42-200, Jelight Company) for 15 minutes, rinsing with DI water and drying under the flow of nitrogen. After deposition of each bilayer of PEOX/TA, the thickness of the film was measured by an ellipsometer (Microphotonics ELX-01R) using 632.8 nm laser light at 70° angle. The morphology of deposited multilayers was checked by optical microscopy and field emission scanning electron microscopy. Surface roughness of the films were determined by atomic force microscopy in tapping-mode using silicon cantilevers. pH stability of LbL films was assessed by immersing the films in water t a specific pH for 20 minutes and measuring the thickness of dried films by ellipsometer afterwards. pH of the immersing solutions was incremented ~0.5 units at each immersion.

5.2.2 Cloud Point Measurements by Differential Scanning Calorimetry (Nano-DSC)

T_{cp} of PEOX in respective sodium salt solutions were determined and thermograms were obtained by using differential scanning calorimetry (Nano DSC). Salt solutions were prepared in deionized water in various concentrations and the concentration of PEOX solutions was kept constant at 1.25 mg mL^{-1}. To avoid bubble formation during heating and cooling, all solutions were de-gassed for 10 minutes before the measurements. All measurements were made with a constant heat rate of 1°C min^{-1} and under a pressure of 3 atm. Heat rate of PEOX solutions in the cell of Nano-DSC was measured relative to the reference solution which had the same salt concentration as the polymer solution.

For PEOX/TA solutions, PEOX solutions were prepared in either distilled water or respective 0.1 M sodium salt solutions. In all solutions, the final concentration of PEOX was kept constant at 1.25 mg mL^{-1}. To determine the influence of TA on the T_{cp} of PEOX, TA solutions were prepared in distilled water in various concentrations so that the relative number of PEOX carbonyl group to the TA phenol group is varied from 10 to 100. Then, equal volume of TA solution with PEOX solution is added dropwise to PEOX solution through continuous mixing for

3 hours. To investigate the effect of pH on T_{cp} of PEOX/TA solutions, PEOX and TA solutions were separately prepared in respective 0.1 M sodium salt solutions at a specific pH. pH adjustments were made using either HCl, H_2SO_4, HNO_3 or NaOH solution according to the character of the sodium salt. For the salts that are strongly kosmotropes, H_2SO_4 is used and for the salts that are kosmotropes, HNO_3 is used. For the mid-Hofmeister series, HCl is used for pH adjustments.

Final concentrations of PEOX and TA were held constant at 1.25 mg mL^{-1} and 0.17 mg mL^{1} respectively. Equal volume of TA solutions was added to PEOX solutions dropwise and then, obtained solution was stirred continuously. T_{cp} of the PEOX/TA solutions was checked at various pH below the pKa of TA by Nano-DSC relative to the reference solution which is either water or 0.1 M salt solutions at a specific pH.

5.2.3 Determination of Interaction Parameters between PEOX and TA by ITC

First, 0.05 mM PEOX and 0.294, 0.176, 0.0587 mM TA solutions were prepared in DI water. pH of PEOX solution was adjusted to 4.5 in order to ensure H-bond formation between TA and PEOX. The binding constant (K) between PEOX and TA was determined by ITC at 25°C, using aqueous solutions of PEOX and TA prepared in DI water.

To investigate the salt effect, binding experiments in ITC were conducted by using solutions of sodium salts at 0.1 M. PEOX and TA were dissolved in these 0.1 M sodium salt solutions. Final concentration of PEOX and TA was 0.05 mM and 0.0587 mM respectively. pH of these solutions was adjusted to ~4.5 using HCl, H_2SO_4, HNO_3 or NaOH according to the kosmotropic / chaotropic character of the sodium salt. For the salts that have strong kosmotropic character, H_2SO_4 is used and for the salts that have chaotropic character, HNO_3 is used. For the mid-Hofmeister series, HCl is used for pH adjustments.

To run ITC experiments, PEOX solutions were always placed in the sample cell (960 µL) and TA solutions were always placed in the syringe (250 µL). The titration was achieved by injection of TA solution in the syringe to the PEOX solution in the sample cell using 25 titrations, 10 µL aliquots in each titration. Between each injection, there was 10 min intervals for equilibration. To ensure uniform mixing, the sample cell was continuously stirred at 125 rpm. Each

injection produces a characteristic peak due to the absorbed or released heat. In the analysis of the data, baseline is subtracted from the data since it corresponds to the signal between consecutive injections when no change in heat flow was detected. The raw heat data was integrated using the instrument software. After integration, to determine the thermodynamic parameters (ΔH, ΔS, ΔG) and the binding constant (K_a), independent binding model from the software was used to fit the integrated data. The first three data that derived from the first three injections were always neglected since they represent the dilution effect. By this way, a proper fitting to the model was ensured.

5.3 Results and Discussion

5.3.1 Effect of Hofmeister Series of Salts on the Growth of PEOX / TA Multilayers

10 BL of LbL films of PEOX and TA were prepared in different sodium salt solutions at pH 3. To investigate the effect of different salts on LbL growth, we measured the thickness of each bilayer of the films that were grown in different salt solutions by ellipsometer and results of this experiment were shown in Figure 5.1. Figure 5.1a illustrates thickness of the films as a function of number of bilayer while in Figure 5.1b, final thickness (10 BL) of the films that were grown in different salt solutions was shown. As indicated in Figure 5.1a, films grown in the presence of different salts showed different growth profiles. In addition, final thickness of the films depended on the salt type that was used in the solutions. As the salt type used in the assembly exhibited more kosmotropic character according to the Hofmeister series, LbL films became thicker and the growth profile changed from linear to exponential. On the other hand, films prepared with the chaotropic salts were thinner and the growth profile was linear. This prominent difference is due to the different mechanisms induced by the kosmotropic or chaotropic salts. In the presence of kosmotropic salts, polymer chains are “dehydrated” which induce hydrophobic interactions between the adsorbing chains on the substrate. Dehydrated polymer chains have a more globular conformation rather than being in extended state. These additional hydrophobic interactions cause “locking” of the globular conformation of the polymer so that these chains become kinetically frozen on the substrate [144], [246]. On the other hand, chaotropic salts act by directly binding on

the polymer chains [95], [101] - in our case PEOX chains, so that polymer chains become more soluble in aqueous solution. They tend to "interact" more with water molecules rather than adsorbing on a surface. Thus, PEOX molecules adsorb less on the surface in the presence of chaotropic ions. In this case, LbL film growth between adsorbed PEOX and TA chains occur via solely by hydrogen bonds and the effect of hydrophobic interactions is neligible. Thus, the polymer chains of PEOX are extended coils which result in flattened conformation on the surface. The thickness difference between the films prepared in the presence of the most kosmotropic salt (Na_2CO_3) and prepared in the presence of the most chaotropic salt (NaSCN) is ~50 nm. This significant thickness difference between the films shows that different mechanisms induced by different Hofmeister salts are effective even in the low ionic strength (0.01 M) during the growth of the multilayers.

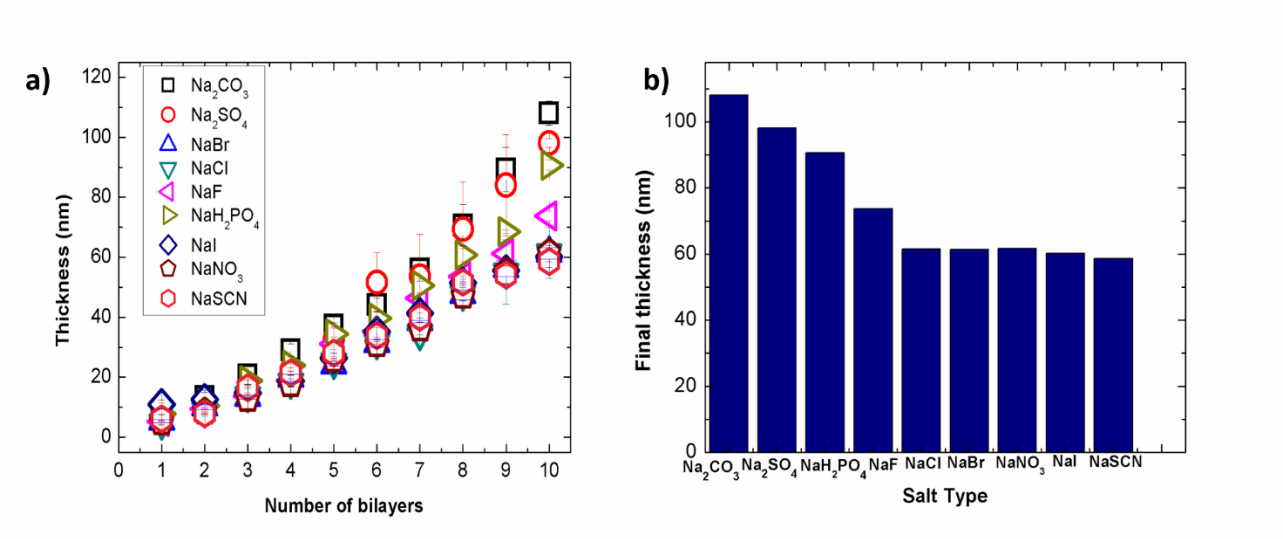

Figure 5.1: (a) Thickness of PEOX/TA LbL films as a function of number of bilayers for nine different films grown to a final thickness of 10 BL and prepared in the presence of 0.01 M different sodium salts (**b)** Final thickness of 10 BL PEOX/TA LbL films prepared in the presence of 0.01 M different sodium salts

To investigate the influence of ionic strength on the growth profile of PEOX/TA LbL films, five different sodium salts (Na_2CO_3, NaH_2PO_4, NaCl, $NaNO_3$, NaSCN) from Hofmeister series were selected. Then, PEOX/TA multilayers were deposited in the presence of aqueous solutions of these selected salts at nine different concentrations (0.01 M, 0.02 M, 0.05 M, 0.07 M, 0.1 M, 0.2 M, 0.5 M, 0.7 M and 1 M). Figure 5.2 shows the growth profile of PEOX/TA multilayers in

the presence of kosmotropic salt ions having different concentrations. Figure 5.2a demonstrates the growth profile of PEOX / TA films as a function of number of bilayers in the presence of Na_2CO_3 at different concentrations. Similarly, Figure 5.2b and c illustrate growth profile of PEOX / TA films in the presence of NaH_2PO_4 and NaCl at various concentrations, respectively. For the films which were prepared in the presence of highly kosmotropic salts (Na_2CO_3 and Na_2SO_4) Figure 5.2a and b, the growth profile of the films follows two different trends according to the different concentration regimes: For the films prepared in the presence of Na_2CO_3 and when the concentration of the aqueous solution of the salt is lower than 0.1 M, exponential growth was observed. Similarly, in Figure 5.2c, when NaCl concentration ranges between 0.1 M - 0.5 M, exponential increase in bilayer thickness was observed. This was an expected result due to the character of the kosmotropic salts. It is known that kosmotropic ions induce additional hydrophobic interactions between polymer chains along with hydrogen bonding. For the films prepared in higher concentration range (0.1 M-0.5 M) of Na_2CO_3, PEOX chains were partially dehydrated due to the induced hydrophobic interactions. Although, LbL assembly on the surface continues due to H-bonding between PEOX and TA, this partial dehydration of PEOX chains causes the formation of unstable domains in the film as explained in our previous work [242]. These unstable domains trigger desorption and detachment of the film from the surface as a result of which the film thickness decreases after reaching a certain thickness. For polyelectrolyte films, it had been also argued that after reaching a certain thickness, film growth may not be observed since the exposure time of the film with polymer solutions during the assembly may not be enough. This insufficient time prevents polymer chains to penetrate within the film and between the "kinetically frozen" layers [248]. However, for the films prepared at lower concentrations of Na_2CO_3 (<0.1 M), hydrophobic interactions were not strong enough to cause partial dehydration of the polymer chains and instability in the film. Continuous film growth was observed in the absence of unstable domains. This is because instead of two competing process, namely adsorption and desorption, only adsorption occurred. In the highly concentrated regime of Na_2CO_3 (~0.5 M), polymer chains were completely dehydrated rather than partial dehydration. During the growth of the film, adsorption rate exceeded the desorption rate so at each newly incoming layer, kinetically frozen and loopy polymer chains were adsorbed and stratified on top of each other. Without any desorption events taking place, very thick films were obtained when prepared in the presence of highly concentrated Na_2CO_3 solutions.

Same discussions are also valid for the films prepared in the presence of NaH_2PO_4 (Figure 5.2b) solutions, but in different concentration ranges. This is because $H_2PO_4^-$ ion is less kosmotropic than CO_3^{2-} ion. For the films prepared in the presence of NaH_2PO_4, partial dehydration of the films and desorption events take place between 0.1 M and 0.7 M, while continuous growth and significant thickness increase without desorption were observed for only 1 M NaH_2PO_4 solution.

Different from Figure 5.2 a and b, in Figure 5.2 c, linear growth profile was observed for the films prepared in the presence of 0.01- 0.05 M NaCl solution. Cl^- is an ion that is placed in the center of Hofmeister series so when compared with CO_3^{2-} or $H_2PO_4^-$, it is the ion that has least kosmotropic character among the ions that were shown in Figure 5.2. When films were prepared in the presence of low concentrations of NaCl solution, the contribution of additional hydrophobic interactions was less and the conformation of the polymer chains was less loopy. During the adsorption of polymer chains onto the substrate, the mobility of these on the surface also increased. As the concentration of NaCl solutions increased and moved towards mid-concentration range (0.1 M-0.5 M), the contribution of hydrophobic interactions was more. Finally, at the highest concentration of the NaCl (0.7 M-1.0 M), polymer chains are partially dehydrated and desorption events take place as it was explained for the films prepared in the presence of Na_2CO_3 and NaH_2PO_4. As a result, fluctuations in the thickness was observed during the growth of multilayers in the presence of NaCl in this concentration range.

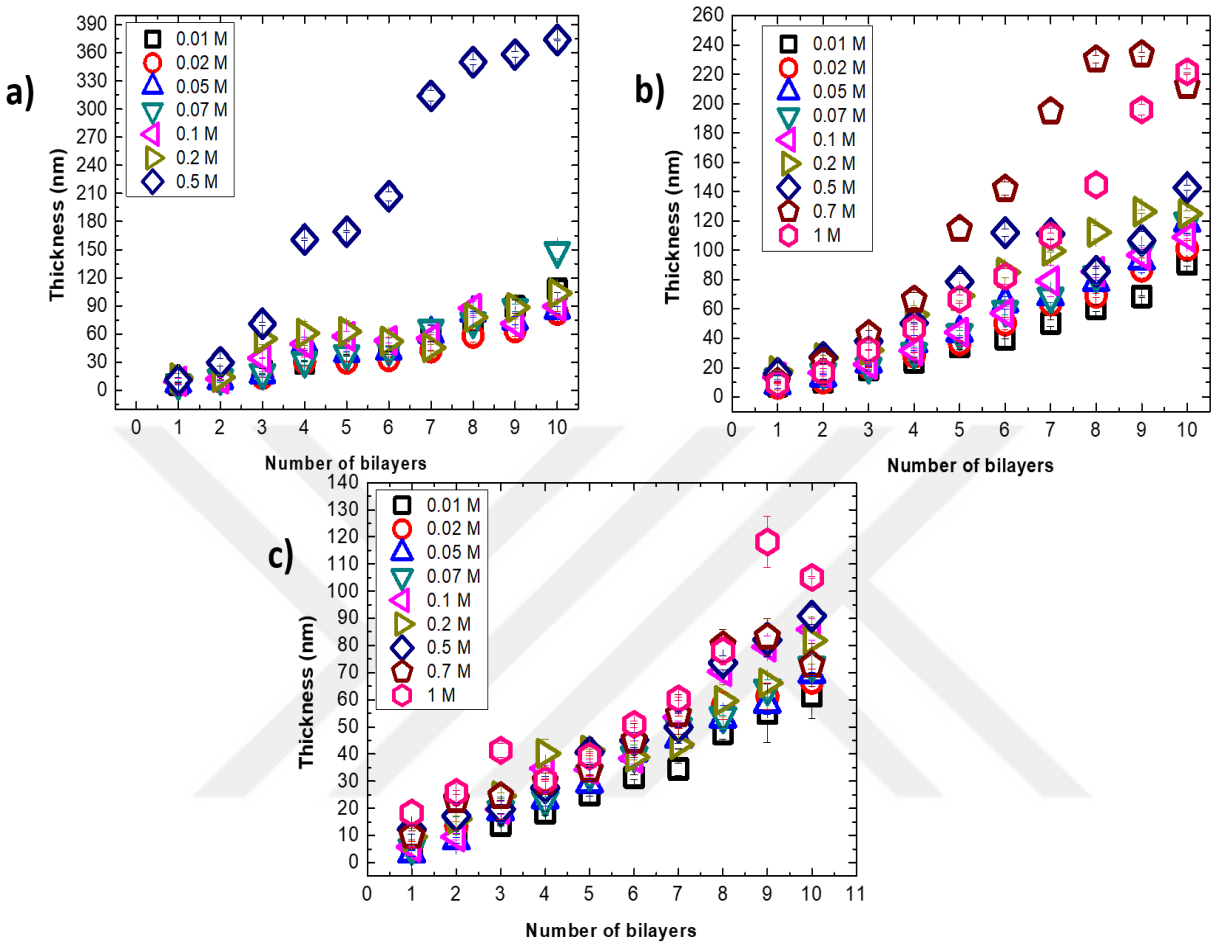

Figure 5.2: Thickness of PEOX/TA LbL films as a function of number of bilayers for nine different films grown to a final thickness of 10 BL. **(a)** Prepared in the presence of Na_2CO_3 at different concentrations **(b)** Prepared in the presence of NaH_2PO_4 at different concentrations **(c)** Prepared in the presence of NaCl at different concentrations

Figure 5.3 illustrates the growth profiles of H-bonded PEOX/TA LbL films prepared with chaotropic salts at different concentrations and average bilayer thickness as a function of concentration of the salt solution. Generally, both films have linear growth profile in almost all concentration range as shown in Figure 5.3 (a) and (b). Linear growth profile and slow growth rates are related with the nature of chaotropic ions. These ions bind to the polymer chains and

binding of the ions both decreases the strength of the interaction between PEOX and TA and cause water uptake by the polymer chains. As a result of them, diffusivity and mobility of the adsorbed polymer chains increase inside the film [251], [252]. As indicated before, this is also related with the polymer's flattened conformation in the presence of chaotropic salts when adsorbed on the surface. For the films prepared with $NaNO_3$, as shown in Figure 5.3 a and Table 5.1, the film with highest thickness (~67 nm) was obtained when films were prepared in the presence of 0.02 M $NaNO_3$ solution. When films were prepared in the presence of $NaNO_3$ solutions that have higher concentration than 0.05 M, final thickness of these films become almost same independent from the concentration of the salt solution. This is also related with the binding mechanism of the chaotropic ions: Hydration of the polymer with chaotropic ions reaches a plateau (as shown in Figure 5.3) after certain concentration threshold. Thus, the tendency of the polymer chains adsorbing onto a substrate in the presence of chaotropic ions decreases after exceeding this concentration threshold. Same discussions are also valid for the films prepared in the presence of NaSCN solutions (Figure 5.3 b and Table 5.1), however, the film with highest thickness (~53 nm) was obtained when films were prepared in the presence of 0.01 M NaSCN solution. The reason is that SCN^- is the most chaotropic ion in Hofmeister series so binding of SCN^- ions to PEOX chains is minimal at this concentration. When films were prepared with NaSCN solutions that have 0.7-1.0 M concentration, thickness of the films (average ~34 nm) remained constant after reaching to a certain thickness value (~ 30 nm). This can be explained with the binding mechanism of ions to polymer chains and saturation of these chains with ions. Chaotropic ions occupy PEOX functional groups. When these groups are saturated with ions, strength of the H-bonding interaction between

PEOX carbonyl groups and TA hydroxyl groups decreases so that film growth reaches steady state as a function of salt concentration.

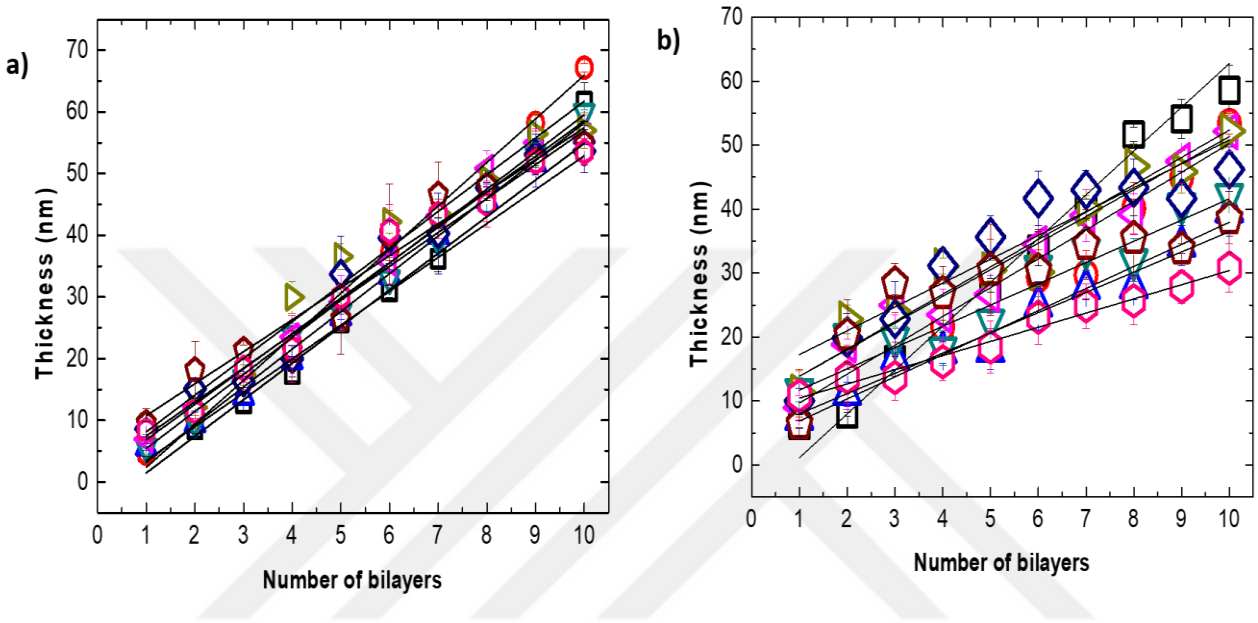

Figure 5.3: Thickness of PEOX/TA LbL films as a function of number of bilayers for nine different films grown to a final thickness of 10 BL. **(a)** Prepared in the presence of $NaNO_3$ at different concentrations **(b)** Prepared in the presence of NaSCN at different concentration.

Table 5.1: Average BL thickness of PEOX / TA films prepared in the presence of chaotrpic salt solutions as a function of concentration of the salt solutions

Salt Type	Concentration (M)	Average BL Thickness (nm)
$NaNO_3$	0.01	6.165
NaSCN	0.01	5.860
$NaNO_3$	0.02	6.719
NaSCN	0.02	5.334
$NaNO_3$	0.05	5.624
NaSCN	0.05	3.965
$NaNO_3$	0.07	5.994
NaSCN	0.07	4.222
$NaNO_3$	0.1	5.592
NaSCN	0.1	5.216
$NaNO_3$	0.2	5.699
NaSCN	0.2	5.221
$NaNO_3$	0.5	5.365
NaSCN	0.5	4.622
$NaNO_3$	0.7	5.488
NaSCN	0.7	3.852
$NaNO_3$	1	5.352
NaSCN	1	3.078

Differences in growth profile of PEOX / TA films in the presence of different salt solutions was also reflected in optical microscope images. Figure 5.4 shows OM images of PEOX /TA films prepared in salt solutions that have kosmotropic ions at different concentrations. Detached patches from the film and significant thickness differences in PEOX / TA multilayers prepared in the presence of Na_2CO_3 solution that has a concentration 0.05 M (Figure 5.4 a) can be clearly seen in optical microscope images. These detached patches and differences in film thickness are also evident in OM images for the films prepared in the presence of 1 M NaH_2PO_4 (Figure 5.4 f) or 0.5

M NaCl (Figure 5.4 (i)). Surface of the films prepared in the presence of NaCl solutions that have concentration lower than 0.5 M are rather smooth.

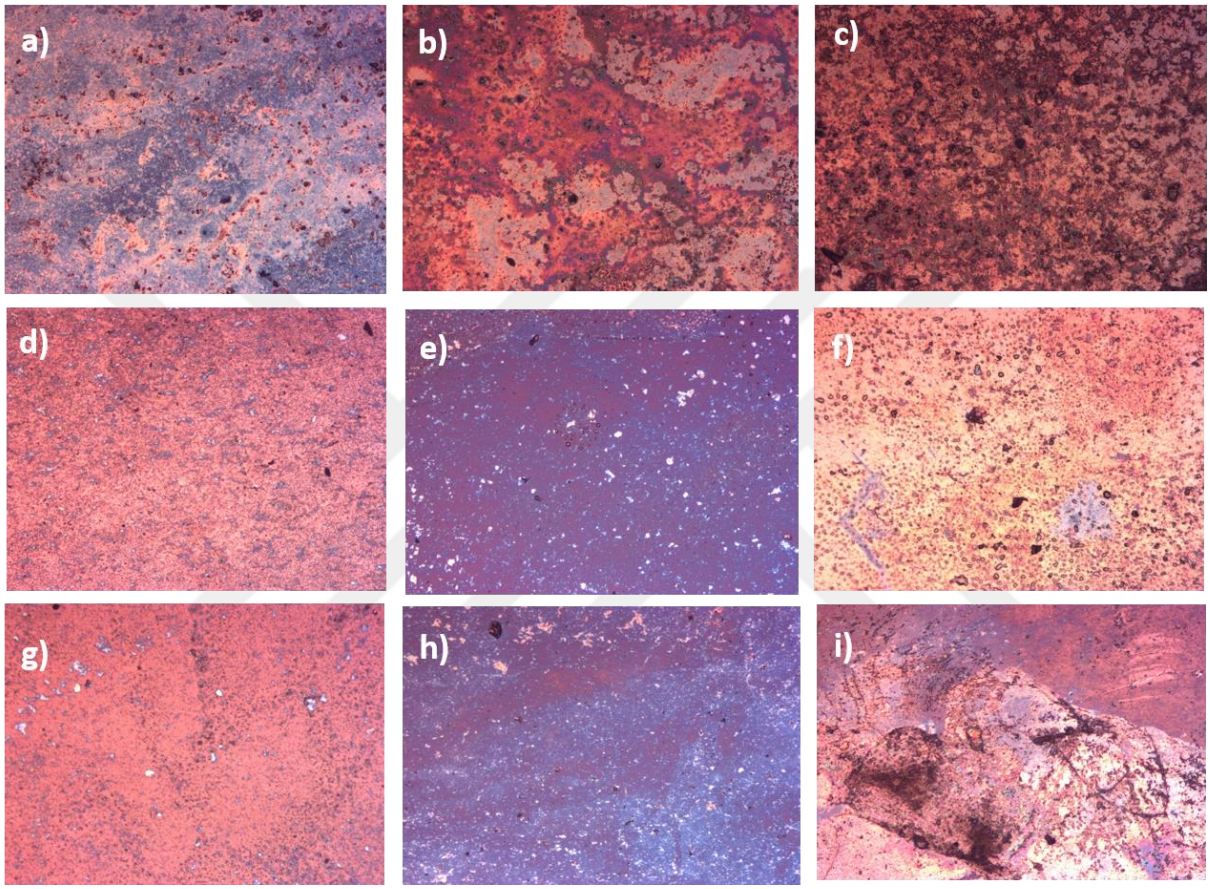

Figure 5.4: Optical microscope images of 10 BL PEOX / TA LbL films prepared in the presence of different salt solutions **(a)** prepared in the presence of 0.05 M Na_2CO_3 **(b)** prepared in the presence of 0.1 M Na_2CO_3 **(c)** prepared in the presence of 0.5 M Na_2CO_3 **(d)** prepared in the presence of 0.05 M NaH_2PO_4 **(e)** prepared in the presence of 0.1 M NaH_2PO_4 **(f)** prepared in the presence of 1 M NaH_2PO_4 **(g)** prepared in the presence of 0.05 M NaCl **(h)** prepared in the presence of 0.1 M NaCl **(i)** prepared in the presence of 0.5 M NaCl

Previously, the growth trend of PEOX / TA films in the presence of chaotropic solutions was explained with binding mechanism of chaotropic ions. Binding of these ions were especially evident in high concentrations, as shown in optical microscope images of Figure 5.5. In these images, binding of the ions are clearly evident, because the crystal parts are observed on the surface of the PEOX / TA films. PEOX / TA films prepared in the presence of chaotropic ions have smooth surface and thickness differences were not observed as in Figure 5.4.

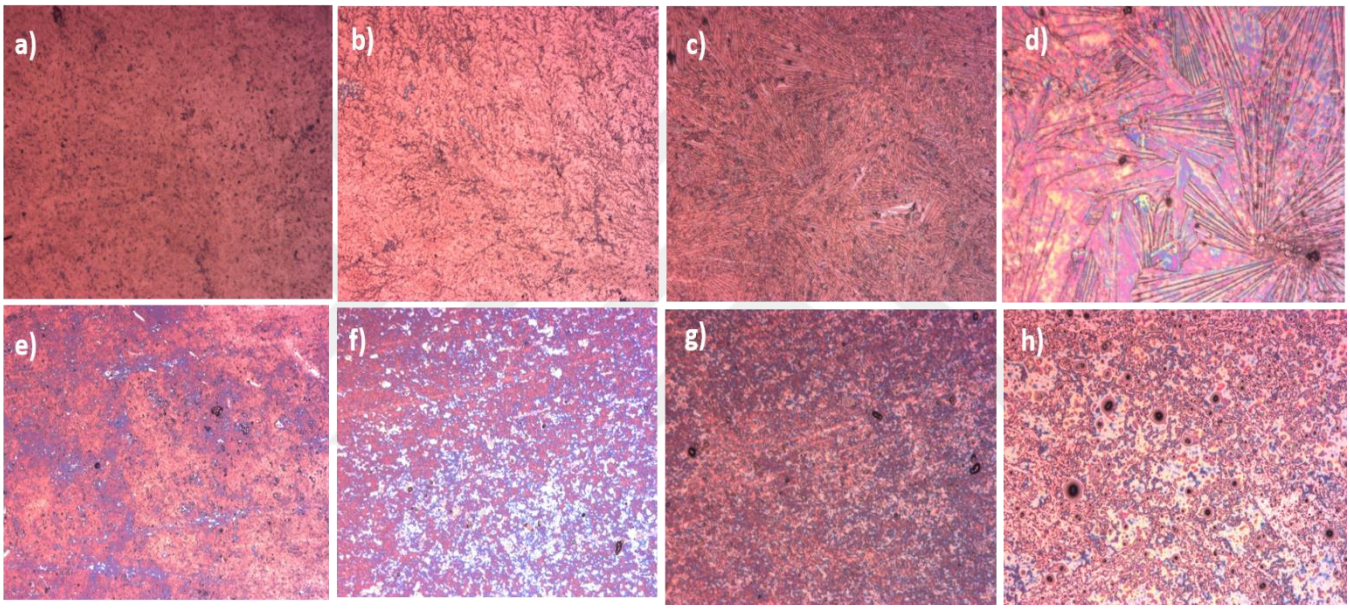

Figure 5.5: Optical microscope images of 10 BL PEOX / TA LbL films prepared in the presence of different salt solutions **(a)** prepared in the presence of 0.05 M $NaNO_3$ **(b)** prepared in the presence of 0.1 M $NaNO_3$ **(c)** prepared in the presence of 0.5 M $NaNO_3$ **(d)** prepared in the presence of 1 M $NaNO_3$ **(e)** prepared in the presence of 0.05 M NaSCN **(f)** prepared in the presence of 0.1 M NaSCN **(g)** prepared in the presence of 0.5 M NaCl **(h)** prepared in the presence of 1 M NaSCN

Figure 5.6 demonstrates the T_{cp} of PEOX prepared in the aqueous solutions of selected salts. The concentrations of aqueous solutions of the selected salts are same with the concentrations of the salt solutions that were used during the assembly of PEOX / TA multilayers. DSC thermograms provide information about phase separation by illustrating changes in the enthalpy and heat capacity. Salting-in and salting-out effects can be also clearly seen in DSC thermograms

since these are phase changes related with polymer hydration [90]. Due to the loss of the specific hydrogen bonds between water and polymer (dehydration of the polymer), LCST transition represents an endothermic process [47]. T_{cp} of PEOX was determined according to a second order transition towards endothermic direction as shown in Figure 5.6 a. T_{cp} of PEOX is determined as ~62.38°C when prepared in aqueous solution. In Figure 5.6 b, T_{cp} of PEOX in respective salt solutions was measured by Nano-DSC. Nano-DSC results represented in Figure 5.4 fit well with our group's previous work [101]. In that work, T_{cp} of PEOX solutions was determined in respective salt solutions by using dynamic light scattering (DLS) [101]. Kosmotropic ions have linear dependence on concentration: As the concentration of salt solutions increase, T_{cp} of PEOX decreases via dehydration and surface tension mechanisms. On the other hand, chaotropic ions directly bind to polymer chains through a Langmuir adsorption isotherm. These trends observed in PEOX aqueous solutions also reflect in the growth profile of PEOX/TA LbL films prepared in different salt solutions. For the films prepared with salt solutions that have kosmotropic ions, thickness of these films increases with the concentration of solutions. On the other hand, films prepared in the presence of salt solutions that have chaotropic ions, do not exhibit concentration dependence on thickness, especially for the mid / high concentration range.

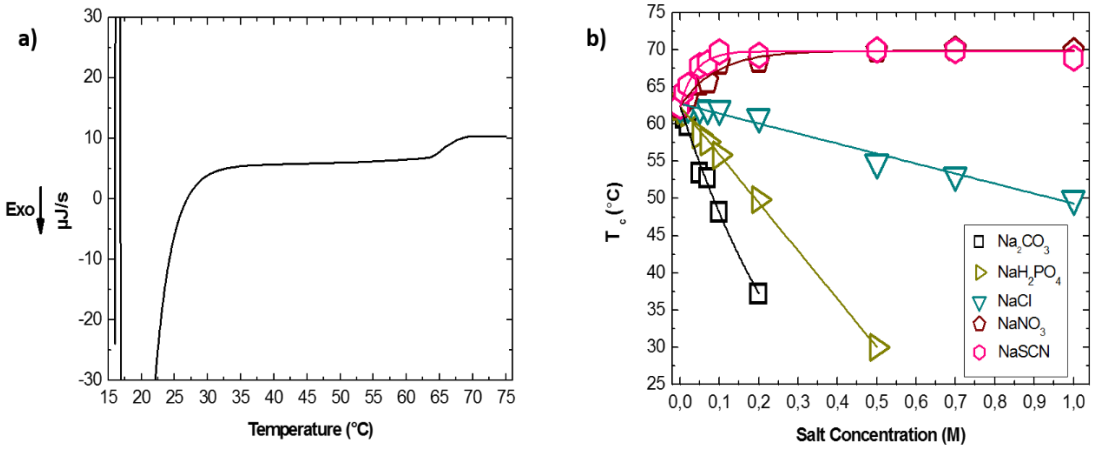

Figure 5.6: (a) DSC thermogram of PEOX aqueous solution showing LCST transition **(b)** T_{cp} of PEOX solutions as a function of concentration of salt solutions measured by NanoDSC

5.3.2 Effect of Hofmeister Series of Salts on the Morphology of PEOX / TA Multilayers

Different morphologies of PEOX/TA multilayers were obtained when these multilayers were prepared in different salt solutions. The main reason for different morphologies is that these salts alter the conformation of polymer chains in the solution and as a result on the surface as well. Figure 5.7 shows the FESEM images of these films prepared in the presence of different salts and at different concentrations.

PEOX / TA films, shown in Figure 5.7 a-c, were prepared in the presence of 0.05 M, 0.1 M and 0.5 M of Na_2CO_3 solutions. As observed, the structure of these films becomes rougher as the concentration of Na_2CO_3 solution increases. We had already reported that in the presence of highly kosmotropic ions, like CO_3^{2-}, the hydrogen bonds are destabilized between the amide groups of PEOX and water, in other words, the ions make these chains dehydrated. This was also observed on the surfaces in which PNIPAM was grafted. These aggregated domains form with the presence of kosmotropic salts due to the hydrophobic interactions and dehydration of the hydrocarbons in the PNIPAM chains by the ions [253]. With hydrophobic interactions, the repulsion and distance between polymer chains were reduced so aggregated domains were formed.

Figure 5.7 d-f illustrates the images of PEOX/TA multilayers prepared in the presence of NaH_2PO_4 solutions. As the concentration of the salt solution increases, especially the size of pore-like structures and aggregated domains on the films becomes more apparent. Similar to the films prepared in the presence of Na_2CO_3 solutions, kosmotropic salt ions cause dehydration of polymer chains. As a result, these ions reduce the repulsion between neighbouring adsorbed molecules and trigger aggregation on the surface. Films prepared with 0.05 M, 0.1 M and 0.5 M NaCl solutions (Figure 5.7 g-i) exhibit similar surface features but the size of these features is smaller due to the less kosmotropic character of the Cl^- ions.

In Figure 5.7 j –o, the morphology of films prepared salt solutions that have chaotropic ions can be examined. Morphological differences between the films prepared in the presence of kosmotropic ions and the films prepared in the presence of chaotropic ions are apparent: PEOX/TA multilayers prepared with chaotropic ions have much smoother surface when compared with

multilayers prepared with kosmotropic ions. Chaotropic ions bind to the chains of PEOX and hold the entrapped water inside the multilayers. Hydration of the adsorbed molecules by the entrapped water molecules triggers the smoothening of the film surface so that surface of the films becomes featureless. Since SCN^- is the most chaotropic ion in Hofmeister salt series, the surface of the films prepared with SCN^- ions is much smoother than the surface of the films prepared with NO_3^- ions, in all concentrations.

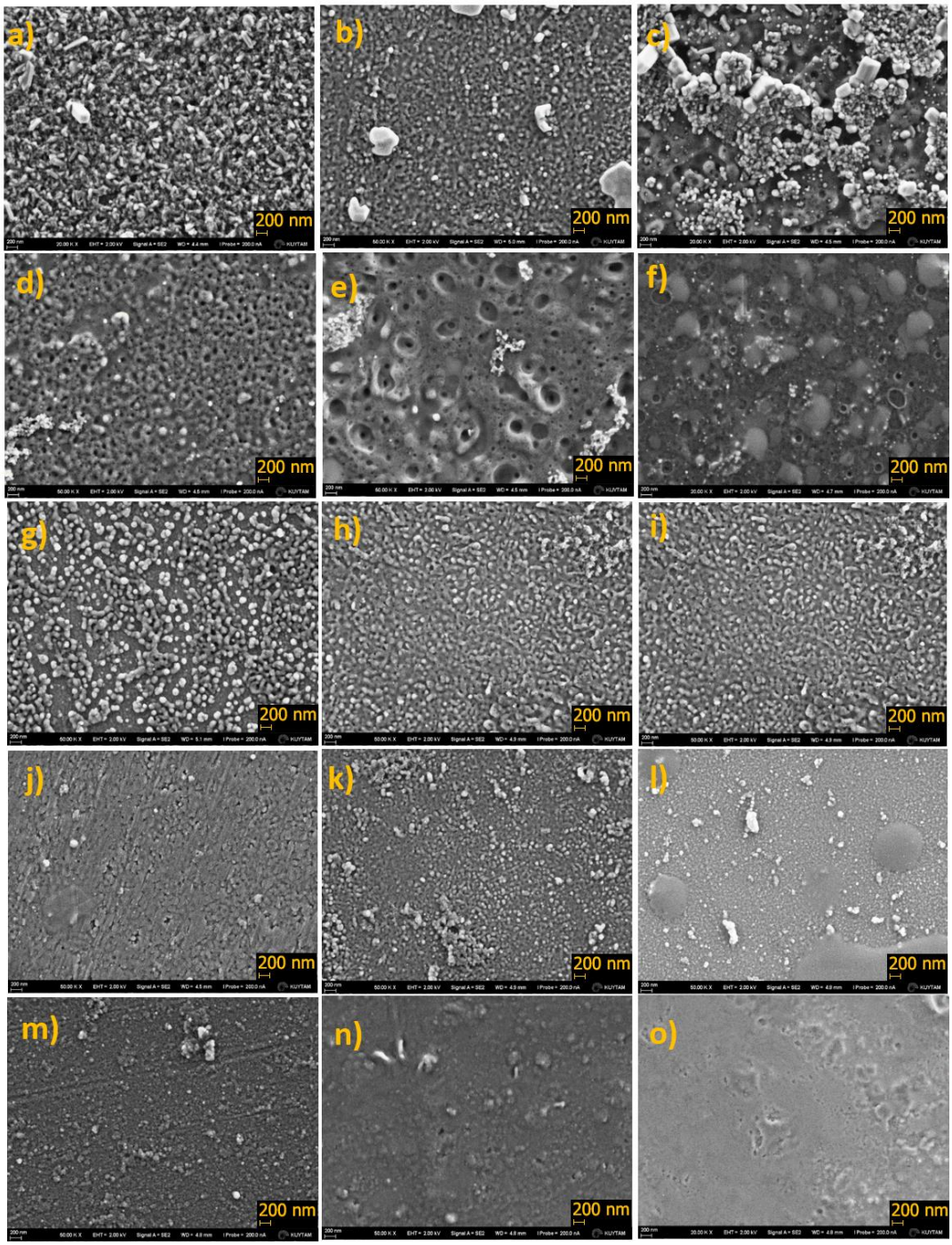

Figure 5.7: FESEM images of 10 BL PEOX/TA LbL films prepared in the presence of salt solutions with different concentrations **a)** 0.05 M Na_2CO_3 **b)** 0.1 M Na_2CO_3 **c)** 0.5 M Na_2CO_3 **d)** 0.05 M NaH_2PO_4 **e)** 0.1 M NaH_2PO_4 **f)** 0.5 M NaH_2PO_4 **g)** 0.05 M NaCl **h)** 0.1 M NaCl **i)** 0.5 M NaCl **j)** 0.05 M $NaNO_3$ **k)** 0.1 M $NaNO_3$ **l)** 0.5 M $NaNO_3$ **m)** 0.05 M NaSCN **n)** 0.1 M NaSCN **o)** 0.5 M NaSCN

AFM height images shown in Figure 5.8 also correlate well with FESEM images provided in Figure 5.7. The root mean square (rms) roughness of the films vary significantly with the type of salt solution that was used during the assembly of multilayers. The rms roughness of the film prepared in the presence of 0.5 M Na_2CO_3 solution is 125 nm, being the roughest film as shown in Figure 5.8 (a). The rms roughness values of the other film prepared in the presence of 0.5 M NaH_2PO_4, NaCl, $NaNO_3$ and NaSCN solutions are 94.5, 47.5, 106 and 31.6 nm respectively. It can be concluded that as the films prepared with ions that have more kosmotropic character, the roughness of the films increases due to the kosmotropic character of the salts increases, as also indicated in the study of Liao *et al.* [245]. The only exception is the film prepared with $NaNO_3$ solutions. This is because NO_3^- ions at this concentration significantly bind to PEOX chains and these salt crystals produce roughness on the surface. As previously shown, presence of salt crystals is also evident in Figure 5.5. For the films prepared with 0.5 M NaSCN solution, roughness due to presence of salt crystals is not observed because produced film is very thin.

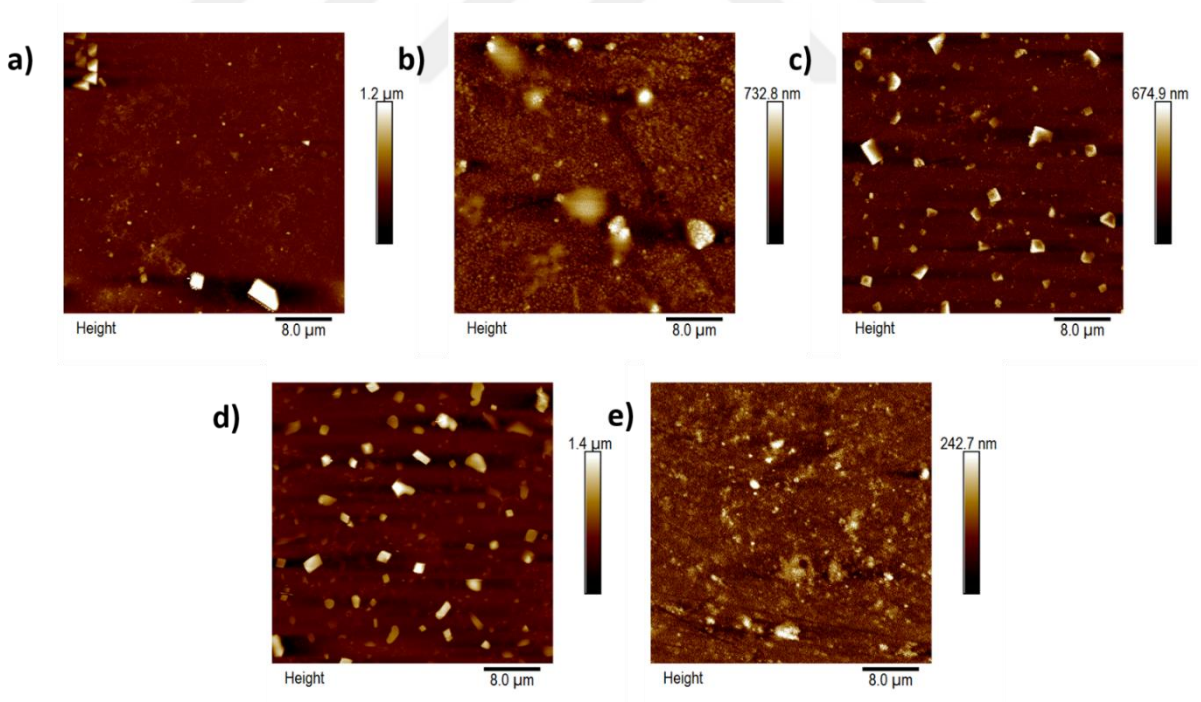

Figure 5.8: AFM height image of 10 BL PEOX/TA LbL film **(a)** prepared in the presence of 0.5 M Na_2CO_3 **(b)** prepared in the presence of 0.5 M NaH_2PO_4 **(c)** prepared in the presence of 0.5 M NaCl **(d)** prepared in the presence of 0.5 M $NaNO_3$ **(e)** prepared in 0.5 M NaSCN.

5.3.3 Nature of Interaction Between PEOX and TA in the Presence of Hofmeister Series of Salts

First, thermodynamic parameters of the interaction between PEOX and TA were determined with varying TA concentration in water without salt. The results were shown in Figure 5.9. The interaction between PEOX and TA is based on both hydrogen bonding between amide groups of PEOX and phenolic groups of TA and hydrophobic interactions between ethyl groups of PEOX and aromatic rings of TA [254]. Figure 5.9 illustrates that when TA concentration is higher than a threshold concentration, the entropy of binding of TA molecules to PEOX increases. At the lowest TA concentration (0.0587 mM), the binding of TA to PEOX occurs through H-bonding. Figure 5.9 (a) illustrates the raw ITC data of heat rate of TA binding to PEOX with injection time when TA concentration was 0.0587 mM. Up to a critical TA concentration, (in our case when TA concentration is 0.0587 mM), TA can interact freely with PEOX through intermolecular H-bonding. Hydroxyl groups (-OH) groups of TA is H-bonded to carbonyl (C=O) groups of PEOX. In this case, the process becomes enthalpy driven. When TA concentration is higher, extensive bridging of PEOX chains by TA molecules led the complex to be easily separated from the water molecules and in this formed entity, hydrophobic interactions are induced. It is known that the source of hydrophobic interactions is entropic due to the ordering of water molecules around the complex and as a result, the process becomes entropy driven. In addition, TA concentration should not be too high so that precipitation in the ITC system could be prevented.

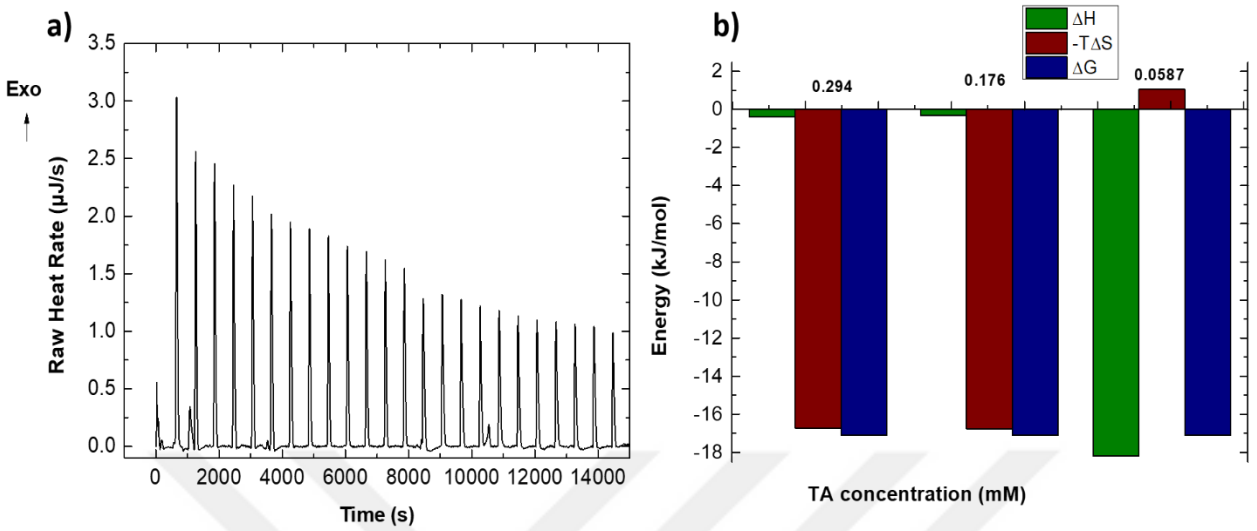

Figure 5.9: (a) ITC data of raw heat rate (µJ/s) with time (s) for the injection of TA (0.0587 mM) to PEOX (0.05 mM) in the absence of any salt **(b)** ITC thermodynamic data of binding of TA at various concentrations (0.294 mM, 0.176 mM and 0.0587 mM) to PEOX (0.05 mM) in the absence of salt.

After investigating the influence of TA concentration on the interaction between PEOX and TA, concentrations of PEOX and TA were kept constant and solutions were prepared separately at 0.1 M sodium salt solutions. Results of the ITC experiment were shown in Figure 5.10. In the presence of the most kosmotropic ion, CO_3^{2-}, the free energy of binding of TA to PEOX increased significantly in negative direction. This is due to the dehydration effect and induced hydrophobic interactions by these ions as expected. With the introduction of hydrophobic interactions and dehydration, conformation of PEOX chains change from extended coils to globular forms so that amide groups of PEOX is less accessible for stronger hydrogen bond formation with TA. However, especially, in the presence of CO_3^{2-} ions, this free energy increases in negative direction and stabilizes due to the entropic contribution with the dominancy of the hydrophobic effect. For the other highly kosmotropic ions, such as SO_4^{2-} and $H_2PO_4^-$, the process of TA binding to PEOX chains is also entropy driven due to the release of ordered water molecules from the hydration shell of PEOX molecules and dehydration of PEOX chains with the presence

of kosmotropic anions [89], [255]. At the presence of SO_4^{2-} and $H_2PO_4^-$ ions, even though the enthalpy of binding of TA to PEOX is exothermic, the contribution of enthalpy is very small when compared with entropic contribution. As indicated, the entropy driven binding process in the presence of kosmotropic ions are due to the acting mechanism of these ions: Dehydration of PEOX chains by kosmotropic ions is more dominant than the interaction between PEOX and TA which is based on hydrogen bond formation. In the presence of ions that are located at the centre of Hofmeister series, there is a significant increase in the enthalpy of exothermic binding of TA to PEOX. In other words, in the presence of F^- and Cl^- ions, the enthalpy of binding of TA to PEOX chains increases in the exothermic direction, while the entropic contribution significantly decreases. In the presence of these ions, the process is entirely enthalpy driven due to the less effective hydrophobic interactions and dehydration effect.

On the other hand, in the presence of chaotropic ions, as the chaotropic character of the ions increases, the enthalpy of binding of TA increases and becomes less negative. This means that TA binding to PEOX becomes weaker. While enthalpy decreases, the entropic contribution slightly increases, however, the binding process of TA to PEOX is mainly enthalpy driven. This is due to the nature of chaotropic ions: In the presence of chaotropic ions, the weak binding of TA to PEOX is due to the competition between TA and other chaotropic ions for binding to the chains of PEOX. Results that derived from ITC experiment were also confirmed by the work of Gibb *et al* [89]. In their work, they also studied the electrostatic binding of adamantane carboxylic acid (AC) to a water-soluble host in the presence of different ions through ITC and Nuclear Magnetic Resonance (NMR). They concluded that binding of chaotropic ions to hydrophobic concavity of the guest molecules is the central mechanism that explains the working principle of Hofmeister series of salts [89].

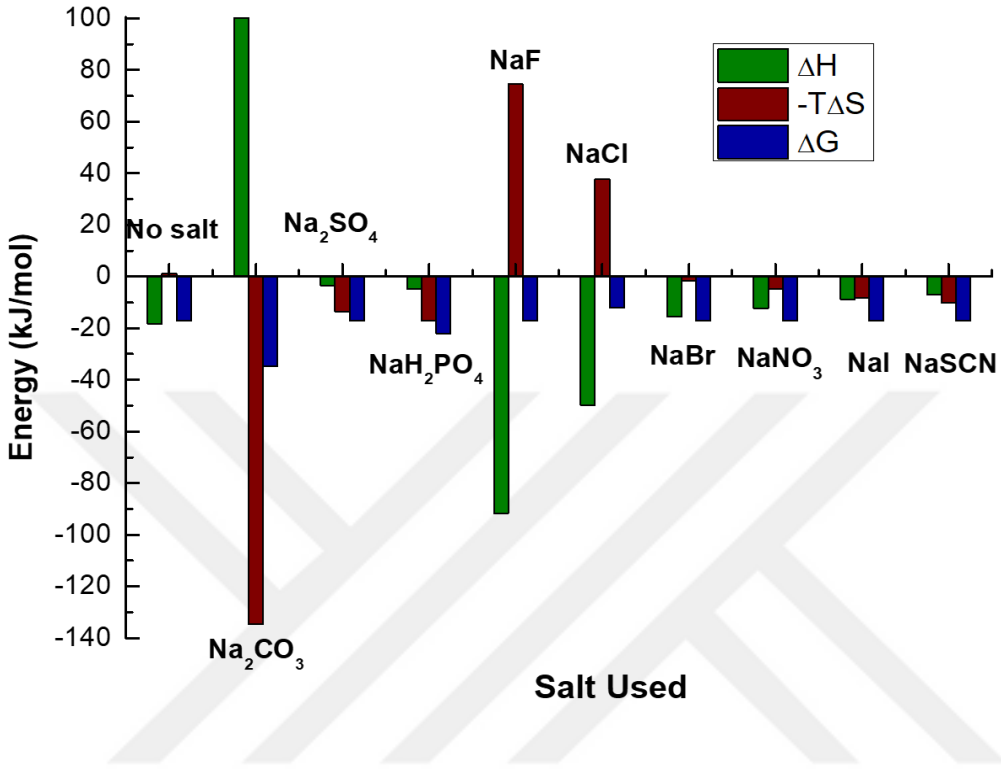

Figure 5.10: ITC thermodynamic data of binding of TA (0.0587 mM) to PEOX (0.05 mM) in the absence or presence of various salts (100 mM)

5.3.4 Effect of Hofmeister Series of Salts on the Stability of PEOX / TA Multilayers

Figure 5.11 demonstrates the pH stability of 10 BL PEOX/TA films grown in the presence of 0.01 M different salt concentrations. As observed in Figure 5.11 (b), there is ~1.5 unit difference in pH stability between the films prepared in the salt solution that contains the most kosmotropic ions (CO_3^{2-}) and the films prepared in salt solution that contains the most chaotropic ions (SCN^-). For the other films, which were prepared in the presence of solutions that contain other ions from Hofmeister series (SO_4^{2-}, $H_2PO_4^-$, F^-, Cl^-, Br^-, NO_3^- and I^-), critical disintegration pH is 8.5. The stabilities of the films prepared in the presence of different salt solutions are different. Below pH 8.5, films prepared with salt solutions that contain chaotropic ions remain more intact than the

films prepared with solutions that contain kosmotropic ions. As we have explained in our previous work [242], the penetration of kosmotropic ions during the LbL film growth alters the local hydrophobicity with time, especially at the loosely bound interfaces. This causes instability in the film when exposed to solutions that have different pH and change the behaviour of the films below disintegration pH. In addition, continuous wetting of the films due to the presence of chaotropic ions [245] cause films to be more stable below pH 8.5. .

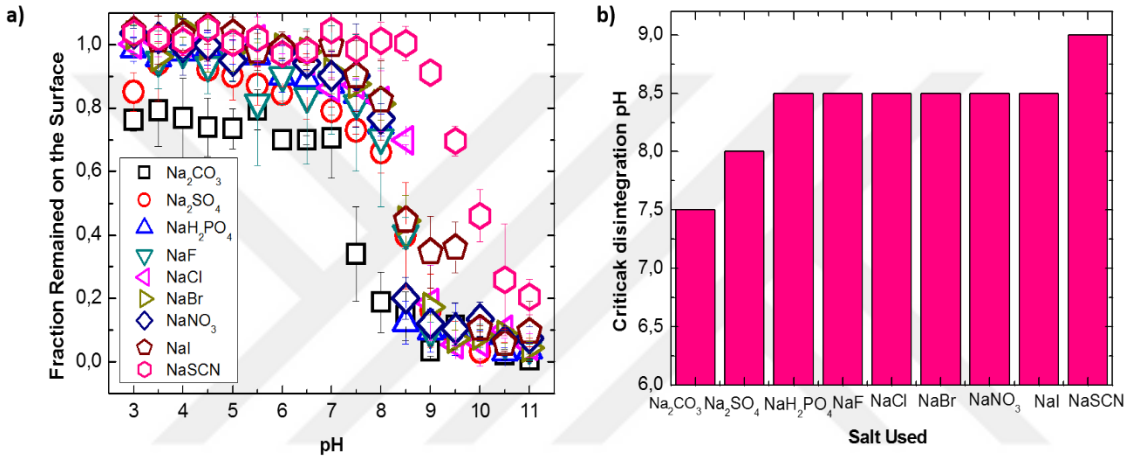

Figure 5.11: (a) pH stability of 10 BL PEOX/TA LbL films grown in the presence of 0.01 M sodium salt solutions that contain different ions from Hofmeister series of salts **(b)** Critical disintegration pH of the films prepared in the presence of 0.01 M sodium salt solutions that contain different ions from Hofmeister series

Figure 5.12 shows how the critical disintegration pH of PEOX/TA multilayers changes with the concentration of selected Hofmeister series of salts (Na_2CO_3, NaH_2PO_4, NaCl, $NaNO_3$ and NaSCN). Especially at the mid and high concentration range, the stability of the PEOX/TA films is significantly lower when grown in the presence of kosmotropic ions. The reason is that the presence of hydrophobic domains formed by kosmotropic ions create instability in the film since both TA and PEOX are hydrophilic components in the film structure [242]. Although it was known that additional hydrophobic interactions can lead to the increased stability when distributed uniformly [180], [183], but generally migration of kosmotropic ions to the interface of the films

lead to the instable domains and further decrease the stability of the film in aqueous concentration as the pH of the solution becomes closer to the pKa of TA. Details were given in Figure 5.13 as the fraction of the film remained on the surface with changing pH. For the films prepared in the presence of ions that have strong kosmotropic character, the dehydration effect and surface tension mechanisms are more apparent with increasing concentration [91]. As a result, the disintegration of the film occurs even at the slightly acidic conditions.

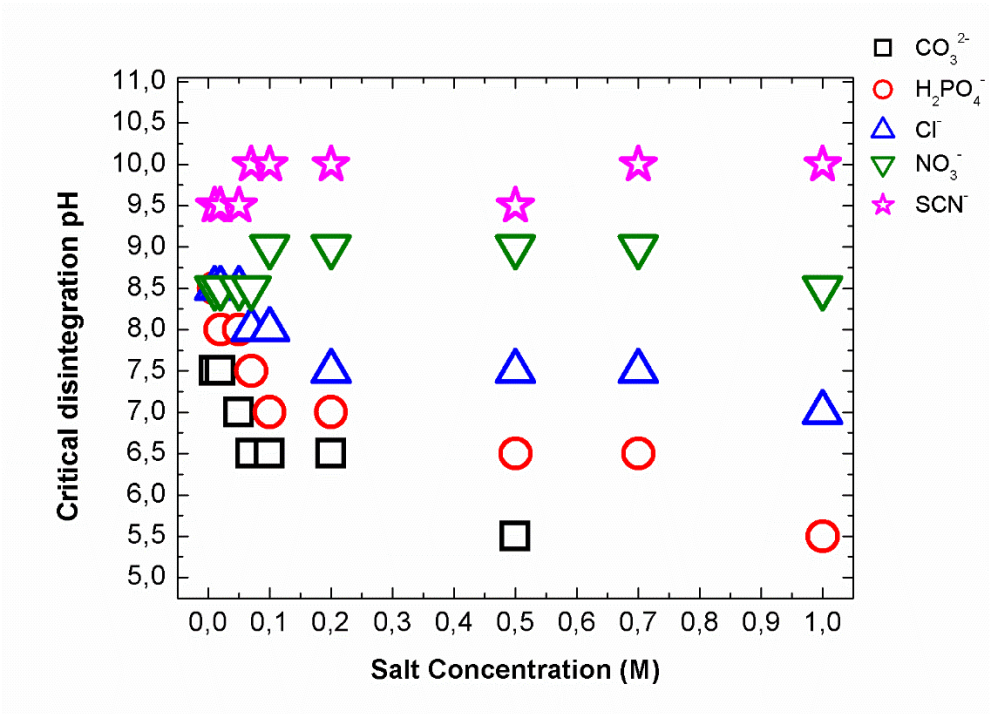

Figure 5.12: Critical disintegration pH of 10 BL PEOX/TA multilayers as a function of concentration of sodium salt solutions used during the preparation of films

For the films grown in the presence of chaotropic salts, the binding of chaotropic ions to the hydrophobic cavity of adsorbed PEOX chains [89] on the film triggers the release of ordered water molecules. Then, due to the binding of these ions, polymer chains reorganize and arrange themselves in a way that they adopt a flattened conformation on the surface. By this way, carbonyl groups of PEOX become more accessible to the hydroxyl group of incoming TA molecules during the LbL assembly [180]. This results in stronger H-bond formation between PEOX and TA so that stability of the film increases in a wider pH range. Especially, in the basic conditions when pH of the immersing solution exceeds the pKa of TA, the presence of bound chaotropic ions to PEOX

chains produce “screening effect” for the slightly ionized TA molecules and prevents the repulsion among aromatic TA rings [161].

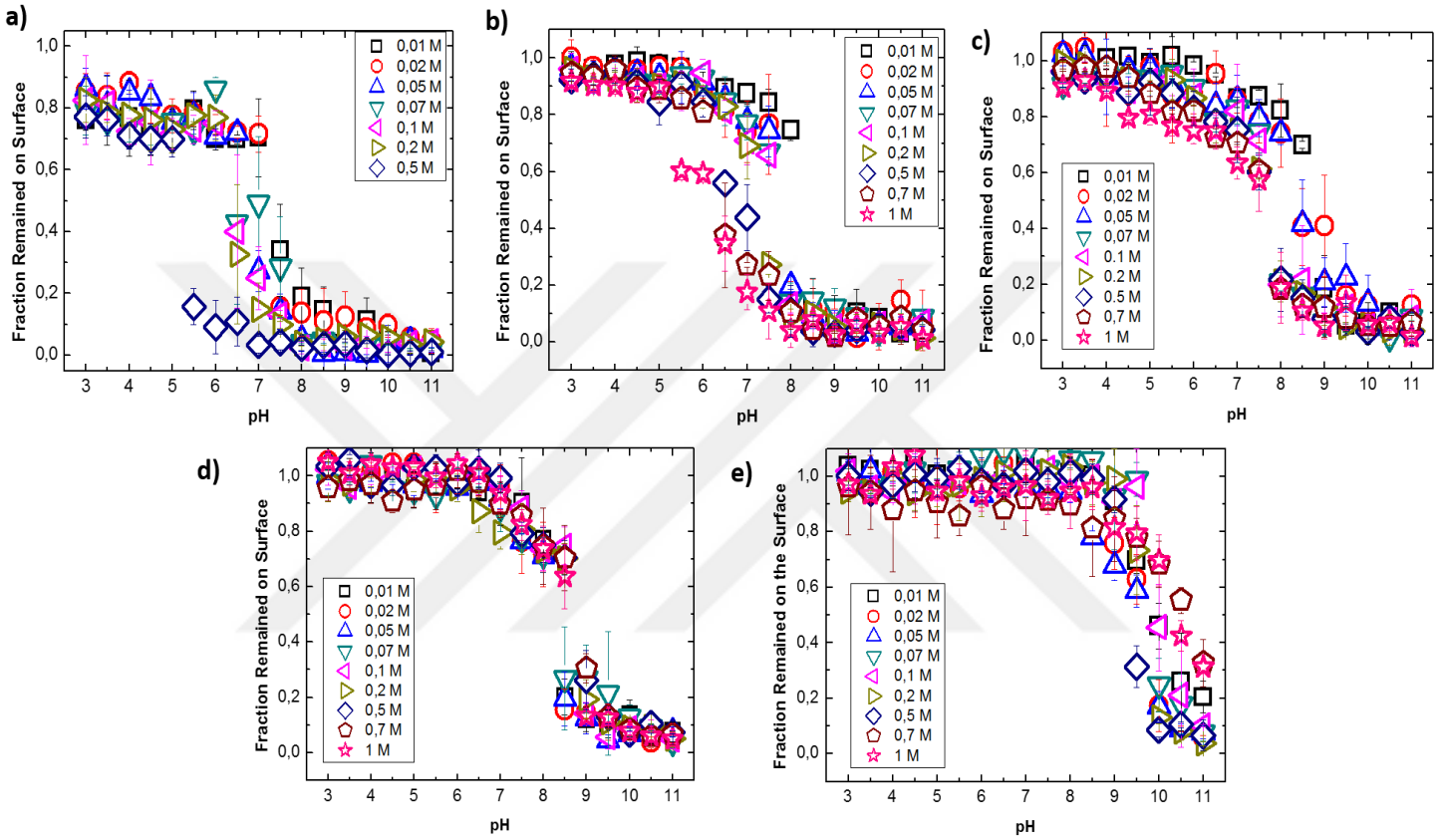

Figure 5.13: pH stability of 10 BL PEOX/TA LbL films grown in the presence of sodium salt solutions at various concentrations **(a)** in the presence of Na_2CO_3 solution at various concentrations **(b)** in the presence of NaH_2PO_4 solution at various concentrations **(c)** in the presence of NaCl solution at various concentrations **(d)** in the presence of $NaNO_3$ solution at various concentrations **(e)** in the presence of NaSCN solution at various concentrations.

To relate the critical disintegration pH of the films with the cloud point measurement, PEOX and TA solutions at various concentrations were prepared separately and then mixed with each other. Finally, colloidal mixtures of PEOX and TA were obtained. The objective is to observe the same trend in pH stability of PEOX/TA solutions prepared in the presence different salt solutions with PEOX/TA LbL films. By this way, film and solution properties can be related with each other. To start with, the effect of the concentration of TA on the T_{cp} of PEOX was investigated at pH 4.5. Table 5.1 illustrates the representative T_{cp} measured by NanoDSC at different TA concentrations. Different TA concentrations were determined according to the ratio of the amount of PEOX carbonyl groups to the amount of TA phenol groups.

Table 5.2: T_{cp} of PEOX/TA aqueous solutions with changing TA concentration according to the ratio of PEOX carbonyl groups to TA phenol groups.

PEOX carbonyl / TA phenol	**T_{cp} (°C)**
10	-
15	-
25	56.2
40	59.9
100	60.1

As observed in Table 5.2, when TA concentration is high and the ratio of PEOX carbonyl groups to TA phenol groups is low, T_{cp} could not be measured because immediate precipitation and phase separation in the mixture [256], [257], [254]. It was previously demonstrated that above a threshold concentration of TA, LCST of the poly (N-isopropylacrylamide) (PNIPAM), is suppressed by TA since TA physically cross-links the polymer with H-bonds[254]. Especially in the acidic pH range, suppression of LCST behaviour of PEOX occurred for lower TA content due to extensive H-bonding between PEOX and TA. In mixtures which have high to moderate TA concentrations and low PEOX carbonyl to TA phenol ratio, LCST behaviour was suppressed so T_{cp} could not be measured. In colloidal mixtures where TA concentration is low and the ratio of

PEOX carbonyl to TA phenol groups is high, T_{cp} of PEOX in the mixture was significantly reduced.

It is also known that T_{cp} of the polymers that contain pendant acid groups can be tuned via changing pH [53],[55],[258],[259]. This hypothesis is also true for the polymers exhibiting LCST and form complexes with molecules that have functional acidic groups. To test this hypothesis, T_{cp} of PEOX/TA colloidal solutions prepared at different 0.1 M salt solutions was measured with respect to pH. Results of the measurement were shown in Figure 5.14. Figure 5.14 illustrates that the type of salts that the mixtures were prepared in is more critical than the pH of the mixtures in determining T_{cp}. T_{cp} of the PEOX/TA solution is lower in the acidic pH range, no matter the type of sodium salt solution that were prepared in. This is due to the extensive H-bonding between PEOX and TA in the acidic range. The formation of H-bonds between PEOX and TA leads to the formation of PEOX-TA complexes and T_{cp} of the mixtures is lowered. Above pH 4, T_{cp} of the mixture solutions vary with the type of ions that the salt solution contains in which they were prepared in. After pH 4, T_{cp} of the solutions exhibit less dependence on pH of the mixture but more dependence on the type of salt solutions that the mixtures were prepared in. Almost same trend in T_{cp} change can be observed for PEOX / TA mixtures independent from pH. An apparent exception is PEOX / TA mixtures that were prepared in the presence of Na_2CO_3. PEOX/TA mixtures in 0.1 M Na_2CO_3 solution exhibit lowest T_{cp} at ~pH 5, which is also almost the same critical disintegration pH value of PEOX/TA LbL films when prepared in 0.1 M Na_2CO_3 solution. This is because equilibrium reaction and conversion of CO_3^{2-} ions to bicarbonate (HCO_3^-) ions in the presence of H^+ ions, in acidic ranges. For example, between pH 7 and pH 8, T_{cp} of the solutions increase as a result of decreased concentration of CO_3^{2-}. At pH~9, both TA molecules are ionized and bicarbonate (HCO_3^-) ions are converted almost fully to carbonate ions (CO_3^{2-}) As a result, both presence of ionized TA solutions and CO_3^{2-} ions decrease T_{cp} of PEOX / TA mixtures significantly. At higher pH values (~pH 10 and pH 11), this decrease in T_{cp} is even more apparent with the influence of CO_3^{2-} ions due to its kosmotropic character.

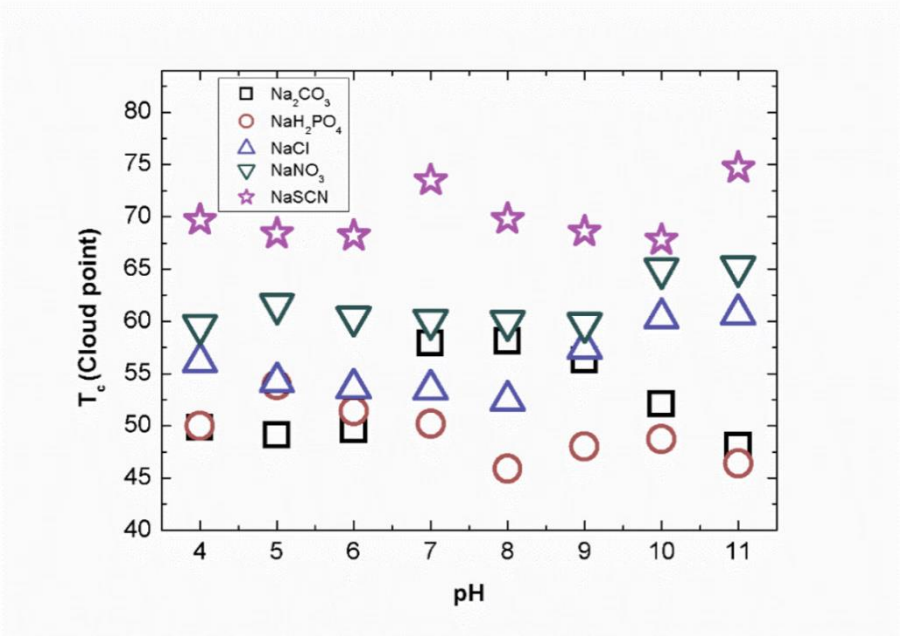

Figure 5.14: Measured T_{cp} of the PEOX/TA mixture solutions prepared in different 0.1 M salt solutions as a function of pH

For PEOX/TA colloidal mixtures prepared in the presence of other salt solutions that contain kosmotropic ions, the same trend can also be observed in different pH ranges. In the acidic range (pH~4-6) measured T_{cp} was lower for both PEOX/TA assembly in 0.1 M NaH_2PO_4 and NaCl, due to the extensive H-bonding between PEOX and TA and kosmotropic character of $H_2PO_4^-$ and Cl^- ions. The lowest T_{cp} observed for the PEOX/TA mixture system prepared in 0.1 M NaH_2PO_4 and in 0.1 M NaCl is at ~pH 8. When this pH value was exceeded, T_{cp} of the mixtures started to increase because hydroxyl groups of TA molecules were de-protonated and hydrophilic character of the mixture increased. Similarly, at pH 10-11, all TA molecules were almost completely ionized, no hydrogen bonds exist between PEOX and TA, so PEOX-salt interactions become dominant. T_{cp} of the PEOX / TA mixtures are same with the T_{cp} of the PEOX solutions prepared in the respective sodium salt solutions.

The lowest observed T_{cp} for PEOX/TA solutions prepared in 0.1 M $NaNO_3$ is at pH~9 and in 0.1 M NaSCN is at pH~10. This pH value in which the lowest T_{cp} was measured is same with the critical disintegration pH values of PEOX/TA LbL films prepared in the presence of 0.1 M

$NaNO_3$ and 0.1 M NaSCN. After pH 10, T_{cp} of the solutions started to increase with the effect of chaotropic salts. After TA molecules are ionized, instead of PEOX-TA interactions, PEOX-salt interactions are dominant and T_{cp} of the mixtures was determined according to the chaotropic characters of the salt ions. Chaotropic ions bind to PEOX molecules and increase T_{cp} of the mixture solutions which is apparent especially at basic conditions.

According to the above results, it can be concluded that solution properties of PEOX / TA assemblies correlate well with the film properties of PEOX / TA properties. Measured T_{cp} values reflected the stabilities of PEOX / TA films in different pH values and effect of kosmotropic or chaotropic of salt types to T_{cp} of mixtures. This correlation means that properties of PEOX / TA films can be predicted by examining the properties of mixtures of PEOX / TA.

5.4 Conclusions

Properties of PEOX/TA multilayers prepared in different salt solutions are influenced by the respective ion's location in Hofmeister series of salt and whether the salt used in the LbL assembly has a "salting-in" or "salting-out" effect. The growth profile and final thickness of PEOX/TA multilayers depend on the type of salt solution used during the preparation of the films. When PEOX / TA films were prepared in 0.01 M solutions that contain different ions, we observed that as the kosmotropic character of the ions that the salt solution contains increased, the thickness of the films also increased due to the additional hydrophobic interactions and dehydration effect. However, in the mid- and high concentration range, in the growth profile of the films prepared in the presence of kosmotropic ions, thickness decrease and fluctuations were observed due to the creation of instable hydrophobic domains and detachment of some parts of the film. Morphological differences between PEOX/TA multilayers prepared in the presence of kosmotropic and chaotropic ions are also apparent. While rough surfaces and even porous structures can be observed in the presence of kosmotropic ions, the morphology of the films prepared with chaotropic ions is smooth and regular. It is proposed that hydrophobic effect caused by the kosmotropic ions reduce the repulsion between assembled and adsorbed complexes and trigger aggregation of the complexes on the surface. On the other hand, in the presence of chaotropic salts, entrapped water molecules adsorbed on the film resulted in smooth PEOX/TA multilayers.

pH stabilities of PEOX / TA multilayers also differ when these films are prepared in the presence of different sodium salt solutions. Films that were prepared in the presence of chaotropic ions are much stable especially in the basic range due to the "screening" effect induced via direct binding mechanism. The influence of chaotropic ions on the conformation of PEOX chains on the surface also leads to stronger H-bond formation between PEOX and TA due to wider accessibility of carbonyl groups of PEOX. The film properties that were investigated also correlated well with the solution properties. ITC was used to determine interaction parameters quantitatively between PEOX and TA in the presence of different salts. Enthalpic and entropic components of the interaction between PEOX and TA were calculated. T_{cp} measurements at different pH values of PEOX/TA assemblies prepared in the various salt solutions also reflect the different pH stability behavior of these multilayers when grown in different conditions. The good correlation between

solution properties and PEOX/TA LbL films has contributed to our understanding of tailoring the properties of these films in various applications such as release of functional molecules or bio sensors.

Chapter 6: Controlled Release Applications of H-Bonded PEOX/TA and PNIPAM/TA Multilayers

6.1 Overview

The objective of forming controlled drug release systems is to improve the efficiency of drug therapy or administered conventional "free drugs" [213],[259]. In order to reach that objective, controlled drug release systems are designed to release and maintain the concentration of the drug in a therapeutic range, the concentration of the drug released should be higher than the therapeutic threshold but lower than its toxic level [227] , [260]. Most of the drug release systems follow "fast then slow" release trend. It is crucial that such release systems follow a zero-order release kinetics to achieve the objectives of controlled release systems. Zero-order release is the release of the drug independent of starting concentration and depending only on the dissociation constant K. The key to achieve a "zero order release" is to obtain surface erosion mechanism where diffusion based release and degradation based release are combined [220]. Another key success in controlled drug delivery systems should be stimuli-dependent release, which means that release systems will be "on" under specific conditions.

Among many polymeric controlled drug release systems, layer by layer assembly (LbL) has emerged as a powerful and versatile platform for this purpose [261-263]. Using LbL assembly as a drug release profile offers these advantages [220], [262], [264]: First of all, nanoscale film architecture allows precise control for the loading and releasing the target molecule. Other advantages include but not limited to the ability of coating structures which can have varying geometries, ability to adhere many surfaces that have different chemistries, easy and low cost of fabrication.

Most of LbL films that are used for controlled release systems are composed of polyelectrolyte multilayers which are formed through electrostatic interactions [220], [265]. Although exponentially grown PEMs have many benefits such as high order architecture and high thickness [266], the applications of PEM films are only limited to loading and release of charged molecules. On the other hand, hydrogen bonded LbL films have advantages like easier

manipulation of film stability and being a more biocompatible platform to load and release of drug molecules since drug release application is not limited to charged molecules, especially cationic ones [131],[133],[174]. Thus, H-bonded LbL films have recently become promising tools for controlled release platform.

In this study, the objective is to investigate a model system of H-bonded LbL films for drug release applications under different conditions. The components of the H-bonded films are chosen as PEOX or PNIPAM as hydrogen acceptor and TA as hydrogen donor molecules in order to take advantage of temperature-responsive property of PEOX and PNIPAM and pH-responsive property of TA. With this study, we were able to examine the release properties of PEOX / PNIPAM and TA multilayers and how these properties can be tailored to achieve zero order kinetics under different conditions. For this study, as a model molecule Rhodamine 6G was used. Rhodamine 6G is a small, neutral and hydrophilic dye molecule which can be used as a model molecule for many H-bonded LbL film applications [178]. Release study of a hydrophilic molecule is especially challenging because it is difficult to obtain a sustained release profile for a small hydrophilic molecule which usually has a fast diffusion rate from multilayers. Thus, this study can be important in terms of understanding the conditions that are required for H-bonded LbL multilayers to act as sustained and controlled release platforms of functional molecules.

6.2 Experimental Details

6.2.1 Preparation and Loading of Rhodamine 6G into PEOX/TA and PNIPAM/TA Multilayers

0.2 mg mL^{-1} PEOX (200K), 0.2 mg mL^{-1} PNIPAM (25K) and 0.2 mg mL^{-1} TA solutions were prepared in 0.01 M NaH_2PO_4 solution at pH 3. PEOX / TA and PNIPAM / TA LbL films with different thickness were deposited with dip coating method. Silicon (100) wafers and quartz were used as substrates and treated with UV-Ozone (Model 42-200, Jelight Company) for 15 minutes. After the treatment, substrates were rinsed with DI water and dried under the flow of nitrogen. With dip coating, Silicon (100) wafers and quartz as substrates were alternately immersed into PEOX / PNIPAM and TA solutions for 15 minutes with intermediate rinsing steps for 5

minutes. Rinsing solutions were composed of 0.01 M NaH_2PO_4 solution at pH 3. After completing the deposition PEOX/TA and PNIPAM / TA films on Silicon (100) wafers, thickness of the film was measured with ellipsometer (Microphotonics ELX-01R) using 632.8 nm laser light at 70° angle. To compare the pH stabilities of PEOX/TA and PNIPAM / TA multilayers, pH stability of the films was tested by immersing the films into phosphate buffer solutions at specific pH for 20 minutes. After immersion, films were dried under the flow of nitrogen and thickness of the film was measured with ellipsometer. pH of immersing solution was incremented ~0.5 units at each immersion.

For the calibration curve of Rhodamine 6G, aqueous solutions of Rhodamine 6G having different concentrations (0.0010, 0.0025, 0.0050, 0.01 mg mL^{-1}) were prepared and absorbance of the prepared solutions was measured with UV-Vis Spectroscopy (PG T80). To load dye molecules into PEOX / TA multilayers and PNIPAM / TA, 0.005 mg mL^{-1} R6G solution (pH~5) was prepared and PEOX/TA films were immersed into R6G solution for 3 hours. For PNIPAM / TA films, post-treatment duration was 4 hours. To test whether dye molecules were encapsulated into the multilayers or it was just a surface adsorption, absorbance at 530 nm of the films on the quartz as a function of number of bilayers were measured with UV-Vis Spectroscopy (Shimadzu UV-3600). Morphology of the films after dye loading was checked with FESEM.

6.2.2 Characterization of Release of Rhodamine 6G from PEOX / TA and PNIPAM /TA Multilayers

Release of Rhodamine 6G was tested at different pH and temperature conditions. For pH triggered release PBS solutions at different pH were prepared and pH arrangements were made to be used as releasing medium. pH of PBS solutions was adjusted to pH 6.5, 7, 7.4, 8.5 and 9. Films that were loaded with dye were immersed into PBS solutions having different pH values and UV-absorbance of the films at 530 nm was checked every 20 minutes for 200 minutes (Shimadzu UV-3600).

For temperature triggered release, dye loaded PEOX / TA films and PNIPAM / TA films were immersed into PBS solutions at 6.5, 7.4 and 8.5 having different temperatures. Selected temperature of the PBS solutions in which PEOX / TA films were immersed were 37°C, 42°C,

62°C and 75°C. For dye loaded PNIPAM / TA multilayers, selected temperature of PBS solutions for immersing the films were 15°C, 32°C and 37°C. To quantify the release amount, films that were loaded with dye were immersed into PBS solutions having different pH values and UV-absorbance of the films at 530 nm was checked every 20 minutes for 200 minutes (Shimadzu UV-3600). After release profile was obtained, morphology of the films was again checked with FESEM.

Finally, to investigate the effect of number of bilayers, 9 BL / 27 BL PNIPAM / TA films and 5 BL / 15 BL PEOX / TA films were immersed into releasing medium (PBS) at pH 7.4 and at room temperature. UV-absorbance of the films at 530 nm was checked every 20 minutes for 200 minutes (Shimadzu UV-3600) and release profile of the films was obtained for comparison.

6.3 Results and Discussion

6.3.1 Loading of Rhodamine 6G into PEOX / TA Multilayers

Rhodamine 6G is used as a model hydrophilic molecule for release studies. A UV-Vis calibration curve of Rhodamine 6G at 525 nm was obtained in order to establish the relation between concentration and absorbance. The maximum absorbance peak of the dye is placed around 525 nm. Figure 6.1 illustrates the calibration curve of Rhodamine G. The calibration curve establishes the linear relationship between the absorbance at 525 nm to the concentration of Rhodamine 6G aqueous solution (mg/mL) with a fit having R^2 is 0.999.

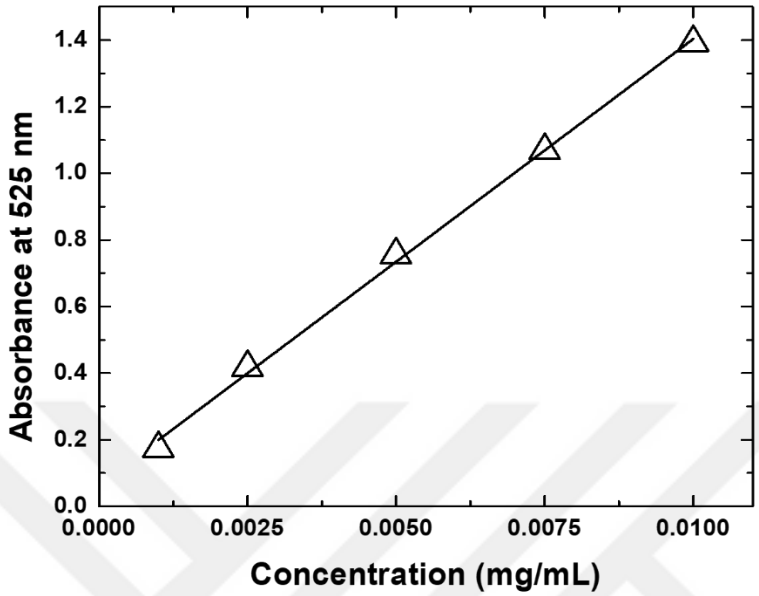

Figure 6.1: Calibration curve of aqueous Rhodamine 6G solution in terms of absorbance at 525 nm as a function of concentration as measured by UV-Vis Spectroscopy.

It is also important to show that loading of the dye into PEOX/TA multilayers and loading of the dye into multilayers was not limited to surface adsorption. For this purpose, three different PEOX/TA LbL films with changing number of bilayers were prepared. 5 BL, 10 BL and 15 BL PEOX/TA LbL films were formed on quartz substrate. Figure 6.2 (a) shows the UV absorbance spectrum of film while Figure 6.2 (b) illustrates the absorbance of PEOX/TA films at 525 nm versus number of bilayers formed.

In Figure 6.2 (a), maximum absorbance peak that belonged to Rhodamine 6G shifted almost 5 to 10 nm (from 525 nm to 530-535 nm). This type of shift in the wavelength is a sign of the aggregation behaviour of dye molecules when they adsorb on a surface. If this shift is towards to a higher wavelength, or a red shift, it is generally interpreted that dye molecules form J-type aggregates [267]. This means that Rhodamine molecules are arranged in one dimension to achieve a parallel orientation. This type of aggregation is favourable and generally seen as an indication of dye molecules forming H-bonds with the film while adsorbing. This is critical in terms of showing

that dye molecules do not adsorb to the film only by surface adsorption but are also loaded into PEOX/TA multilayers through different interactions.

In Figure 6.2 (b), the absorbance of dye at 530 nm increases with increasing number of bilayers. This means that loading amount of dye molecule into multilayers increases with increasing number of bilayers and that loading amount of dye into multilayers can be precisely controlled with changing film thickness due to the almost perfect linear relationship between absorbance and number of bilayers established. The amount of dye loaded per nm thickness of PEOX / TA multilayers is calculated as 0.013 ∓ 0.0018 µg/nm.

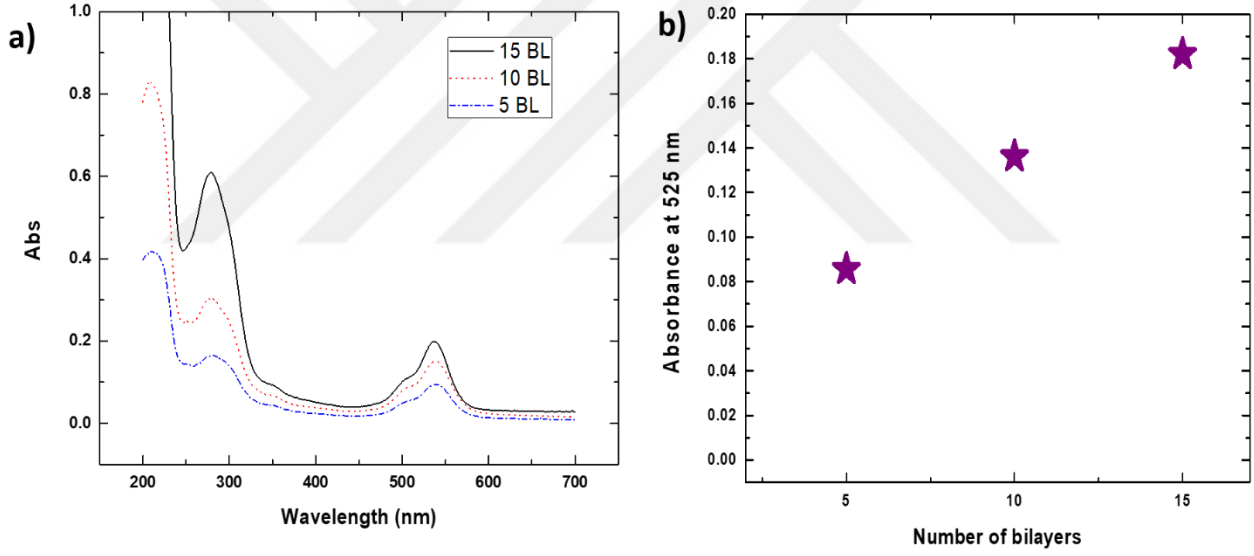

Figure 6.2: (a) UV -Vis spectra of Rhodamine 6G loaded PEOX/TA multilayers having different number of bilayers **(b)** Absorbance at 525 nm of PEOX/TA film on quartz substrate versus number of bilayers of PEOX/TA films

6.3.2 pH Triggered Release of Rhodamine 6G from PEOX/TA Multilayers

In order to test pH triggered release of Rhodamine 6G from PEOX/TA multilayers, 10 BL of PEOX and TA LbL films were prepared on quartz substrate. Dye molecules were loaded into films simply by post-treatment, dipping films into dye solution for three hours. After loading, pH adjustments were made to PBS solutions and release test was applied for 10 BL PEOX/TA films on quartz substrates at pH 6.5, 7, 7.4, 8.5 and 9. pH 6.5 and 7 are selected to mimic the pH environment of cancer cells, pH 7.4 of being physiological pH, pH 8.5 is the critical pH of TA in which TA hydroxyl groups are ionized and pH 9 is the pH value above the critical disintegration pH of PEOX / TA multilayers where more than 20% fraction of the film was dissolved.

For a sustained and controlled drug release to the target site, zero order release kinetics is favoured. Zero order release kinetics simply means that release rate is independent of initial concentration but only depends on a rate constant K. Ideally, if PEOX/TA multilayers release the dye molecules with zero order release rate, then we would expect that:

[Rhodamine 6G loaded PEOX / TA film] → [PEOX] + [TA] + [Rhodamine 6G]

In addition, zero order release kinetics would satisfy below equations

$$\frac{-\,d\,[concentration\ of\ remained\ dye\ on\ the\ film]}{dt} = \frac{d\,[concentration\ of\ released\ dye\ into\ PBS]}{dt} = Kdiss$$

or

$$\frac{d\,[fraction\ of\ cumulative\ release\ of\ dye]}{dt} = K\ diss \quad (1)$$

where K_{diss} is the dissociation constant or rate constant for the release system. Fraction of cumulative release can be calculated from:

Fraction of cumulative release = (initial concentration of dye – remained concentration of dye)/ (initial concentration of dye) *(2)*

Integration of the equation *(1)* would obtain a linear release profile. Linear release profile suggests that in each time interval, the released concentration of the drug is same.

Figure 6.3 (a) and (b) illustrate the release profiles of Rhodamine 6G from PEOX / TA multilayers in terms of concentration of dye remained in the multilayers versus time and fraction of cumulative release versus time respectively. For 3 hours, every 20 minutes, the absorbance at 530 nm of the dye loaded PEOX/ TA films on quartz substrate was measured and concentration of the dye was calculated from the calibration curve of Rhodamine 6G that was shown in Figure 6.1.

Release rate and released amounts of dye change with the pH of the releasing solution (PBS): At pH 6.5 only 50.2 % of the dye is released, at pH 7 the percentage of release increases to 70.8% and at pH 7.4, even more to 85.1%. On the other hand, at pH 8.5 or at pH 9, almost all dye is released in 40-100 minutes.

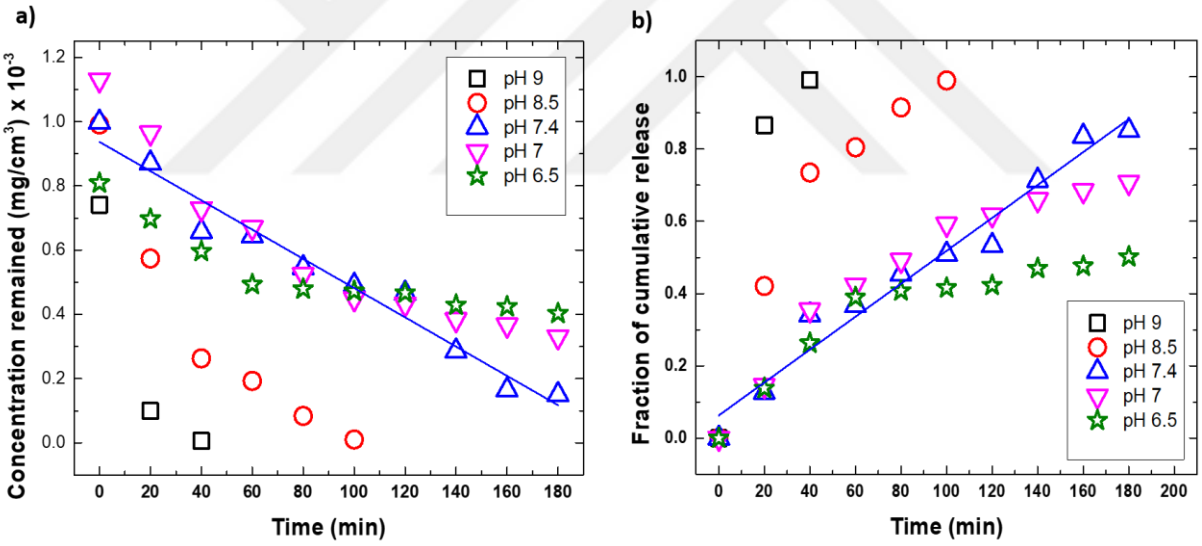

Figure 6.3: pH triggered release profile of Rhodamine 6G from PEOX/TA LbL films formed on quartz substrate at room temperature **(a)** Concentration of the dye (mg/cm^3) remained in the PEOX / TA multilayers versus time (min) **(b)** Fraction of cumulative release of the dye versus time (min).

When the pH of the releasing medium is 6.5 or 7, the release kinetics was not linear and consisted of two different regimes of release rate. This shows that at pH 6.5 or 7, kinetics of the release is not zero order. The release mechanism at these pH values is assumed to be diffusion-based release or diffusion limiting release. In this case, adsorbed polymer chains in the film swell due to the presence of ions at high ionic strength and having kosmotropic character. Another reason for polymer swelling in the multilayers is that pH 6.5 or pH 7 is close to the critical pH of TA in which hydroxyl groups start to ionize. At these pH values, hydrogen bonds between TA and PEOX are weakened. In the diffusion-based release mechanism, kinetics of release profile yields exponential fit. According to the Korsymeyer-Peppes model, Fickian diffusion fits to the release profile at pH 6.5 or pH 7 [259],[216, 268]. This means that polymer swelling advances faster than the drug diffusion from multilayers.

Just below the critical pH, at physiological pH (pH 7.4), the release mechanism fits to zero order release kinetics with linear fit (R^2= 0.96). This means that the release mechanism is assumed to be based on surface erosion mechanism. Thus, it can be concluded that for hydrogen bonded LbL films, the pH just below the critical pH or below the disintegration pH of the film may result in a zero order release because both swelling of the polymer chains and weak ionization of TA molecules in the film. This allows fast diffusion of the dye molecules out of the film. Previously, our group has previously showed that pH annealing of H-bonded multilayers just below the critical pH enhances pH stability of multilayers and slows down the release rate of the H-bonded molecules composing the film [144]. On the other hand, above the critical pH, neither an exponential nor linear fit can be made. This shows that when the pH is above the pKa of TA, the release mechanism is based on the burst release. This is due to the breakage of hydrogen bonds between PEOX and TA. When PEOX / TA multilayers disintegrate, burst release of dye molecule from PEOX/TA multilayers was observed. Table 6.1 summarizes the release mechanisms of dye molecule from PEOX / TA multilayers at different pH values with R^2 values for linear or exponential fit.

Table 6.1: Summary of the release mechanisms of dye molecules (Rhodamine 6G) from PEOX/ TA multilayers at different pH values

pH of release medium	**Release mechanism**	**R^2 for linear fit**	**R^2 for exponential fit**
6.5	Fickian Diffusion	0.73	0.94
7	Fickian Diffusion	0.85	0.99
7.4	Zero Order Release	0.96	-
8.5	Burst release	0.84	0.99

To further support the hypothesis about the suggested release mechanism, the morphology of the films was observed with FESEM and thickness measurements of the films before and after the release of Rhodamine were made with ellipsometry. FESEM images are given in Figure 6.4 and thickness measurements can be found in Table 6.2.

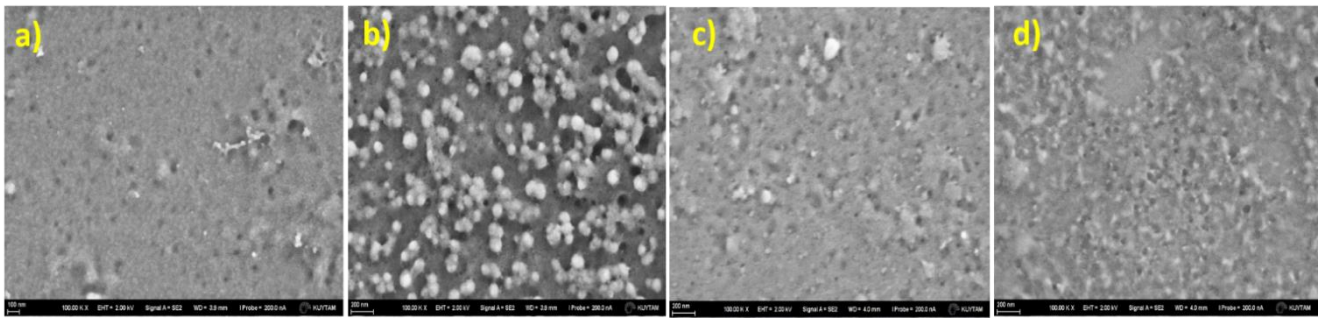

Figure 6.4: (a) FESEM image of the 10 BL PEOX / TA LbL film after Rhodamine 6G is loaded (**b)** FESEM image of the Rhodamine 6G loaded 10 BL PEOX / TA film after release of dye molecules is completed at pH 7 **(c)** FESEM image of the Rhodamine 6G loaded 10 BL PEOX / TA film after release of dye molecules is completed at pH 7.4 **(d)** FESEM image of the Rhodamine 6G loaded 10 BL PEOX / TA film after release of dye molecules is completed at pH 8.5

Table 6.2: Thickness (nm) data of Rhodamine 6G loaded PEOX/TA LbL films before and after release

pH of release environment	**Thickness before the release (nm)**	**Thickness after the release (nm)**
7	87.60	95.30
7.4	100.72	89.17
8.5	93.50	26.10
9	92.42	15.12

Rhodamine 6G loaded PEOX/TA films have smooth and regular surface as observed from Figure 6.4 (a). At pH 7, polymer chains swell and conformation of the adsorbed PEOX molecules change on the surface with the presence of kosmotropic ions that PBS solution contains. It is known that kosmotropic ions dehydrate polymer chains and induce hydrophobic interactions [95].With the dehydration of polymer chains and induced hydrophobic interactions, distance between polymer chains increased and also, slightly ionized adsorbed molecules repulse each other. Dehydration of the PEOX chains also reflected in the conformation change of the chains, PEOX chains adopt globular form As a result, aggregated domains were formed on the surface of the film.In the presence of kosmotropic ions due to dehydration effect along with the conformational change, the surface of the film becomes rougher with the aggregated domains, as indicted in Figure 6.4. A similar result was also obtained for the surfaces in which PNIPAM was grafted [253] as indicated in Figure 6.4 (b). The ionization of hydroxyl groups of TA starts weakly at pH 7.4. As surface erosion start at pH 7.4, the conformation of polymers on the surface became flattened with that erosion. As a result, in Figure 6.4 (c), the morphology of PEOX / TA films after release at pH 7.4 are flattened and smooth again. In Figure 6.4 (d), disintegration of the film that started from the surface can be observed. Thickness data in Table 6.2 also fits with the observations indicated for FESEM images. While at pH 7, swelling of the film was confirmed via thickness increase, above pH 8.5, sharp decrease in the film thickness indicates release of dye via film

disintegration. At pH 7.4, minor thickness decrease also suggests that film was eroded only from the top surface.

6.3.3 Temperature Triggered Release of Rhodamine 6G from PEOX/TA Multilayers

For temperature triggered release measurements, 10 BL PEOX/TA LbL films were put into the release medium at different temperatures: 37°C for being the physiological temperature, 42°C for being the temperature of heat treatment to cancerous tissues, 62°C (LCST temperature of PEOX) and 75°C (above LCST temperature) were selected.

Release profile of Rhodamine 6G from PEOX / TA multilayers at 37° is illustrated in Figure 6.5 and Table 6.3 illustrates the type of release kinetics at different pH values At pH 6.5, the release rate is higher than RT and release profile also changed. pH 6.5 release profile was linear for first 80 minutes and after that linear curve reaches to saturation. This means that after 80 minutes, release of dye becomes diffusion limited since concentration gradient outside and inside the film becomes less. pH 7.4 also exhibits a linear release profile at 37°C. Unlike at pH 6.5, release of dye at pH 7.4 doesn't reach to a saturation point. This is the reason at 37°C, pH 7.4, the release profile has two parts: First 80 minutes, it exhibits linear release while after 80 minutes, the release becomes closer to exponential.

The release at 37°C was faster compared to the release at room temperature, independent of the pH of the releasing medium. This indicates a higher rate constant (k) for the release with increasing temperature. As a result, diffusion rate of the encapsulated dye molecules out of the film is faster and swelling of the film is more. Increasing rate constant (k) with temperature is result of Arrhenius theory. As a result, release of the dye from LbL multilayers is favoured thermodynamically with increasing temperature.

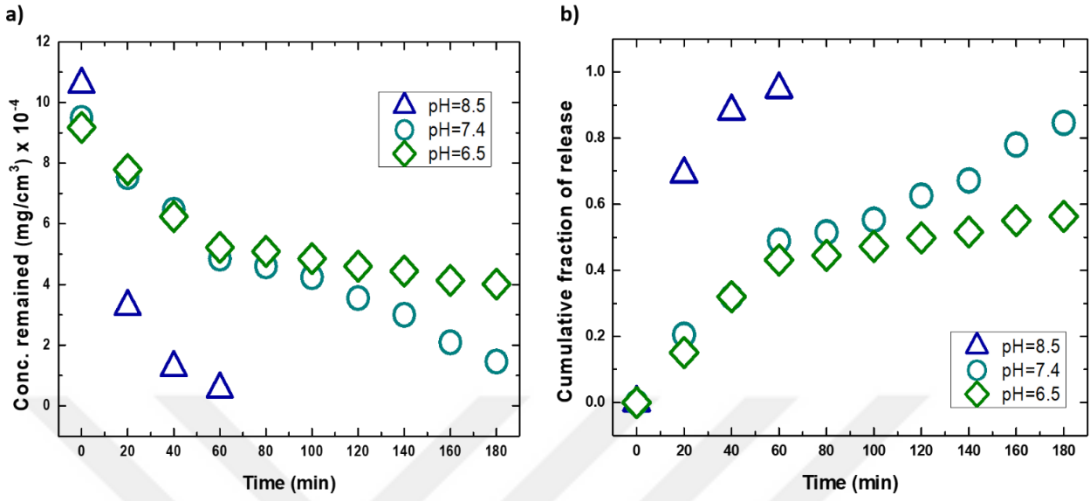

Figure 6.5: Release of Rhodamine 6G from 10 BL PEOX/TA LbL films at 37°C, at pH 6.5, 7.4 or 8.5 **(a)** Concentration remained (mg/cm^3) on film versus time **(b)** Fraction of cumulative release versus time.

Table 6.3: Summary of the release mechanisms of dye molecules (Rhodamine 6G) from PEOX/ TA multilayers at different pH values at 37°C

pH of the releasing medium	**Release mechanism**	**R^2 for linear fit**	**R^2 for exponential fit**
6.5	Fickian Diffusion	0.78	0.98
7.4	Zero Order	0.97	0.93
8.5	Burst Releasee	0.72	0.99

The release data at 42°C is demonstrated in Figure 6.6. Temperature of the release medium is higher, as a result, k (rate constant) of the release also increased more and the release rate was higher. Thus, higher release rate in all pH values at 42°C is related with the increasing rate of reaction with temperature and favouring of the release of film components and dye molecules due

to the shift of thermodynamic equilibrium constant. Weakening of H-bonds between PEOX and TA with increasing temperature is also a contributor for higher release rate below T_{cp} of PEOX. Weakening of hydrogen bonds changes the interpenetration between multilayers so the diffusion of the dye molecules from the film to the releasing environment is easier and faster.

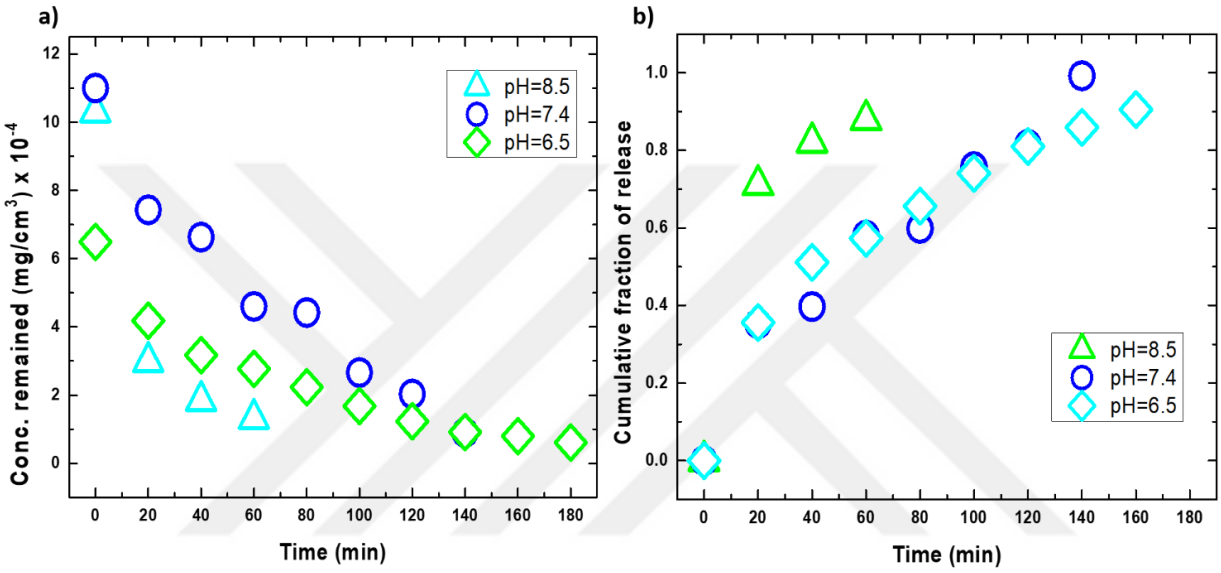

Figure 6.6: Release of Rhodamine 6G from 10 BL PEOX/TA LbL films at 42°C, at pH 6.5, 7.4 or 8.5 **(a)** Concentration remained (mg/cm^3) on film versus time **(b)** Fraction of cumulative release versus time.

62°C is the T_{cp} temperature of PEOX. At this temperature, PEOX chains are dehydrated and the conformation of the polymer chains change from hydrophilic coil to hydrophobic globule. Both incremented rate constant and weakening of hydrogen bonds within the film favors the release but specifically, conformation change of PEOXr chains at T_{cp}triggered accelerated release of dye molecules from LbL multilayers. With the conformational change of adsorbed PEOX chains, multilayers of PEOX and TA also contracted and hydrophobic interactions between adsorbed molecules became dominant. As a result, hydrophilic and small dye molecules cannot bind to the film anymore and preferably do not interact with the PEOX and TA that were adsorbed.

In addition, for this temperature range, the shift from diffusion limited release to zero order release is much more apparent with respect to different pH of the releasing medium. This is because conformation change of polymers allows faster diffusion of the dye. However, at pH 7.4, zero order release profile cannot be observed anymore but rather a burst release profile was obtained for the release of Rhodamine 6G. It is known that hydrophobic environment in the film and increased interdiffusions can manipulate the pH stability [144]. It is probable that critical disintegration pH of the film is lowered at this critical temperature and PEOX /TA multilayers became less stable. Thus, it is highly probable that, at 62°C, critical disintegration pH of the film could be lowered to close to pH 7.4, phyisological pH. Then, most of the binding points between PEOX and TA were broken and dye molecules were released in a fast manner, accompanying the film disintegration.

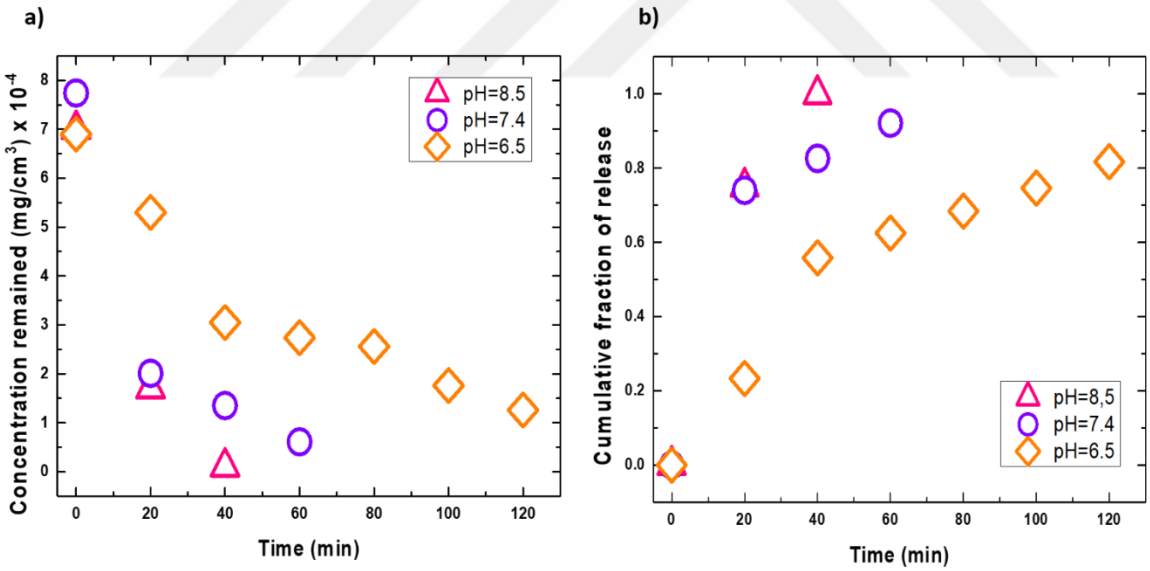

Figure 6.7: Release of Rhodamine 6G from 10 BL PEOX/TA LbL films at 62°C, pH 6.5, 7.4 or 8.5 **(a)** Concentration remained (mg/cm^3) on film versus time **(b)** Fraction of cumulative release versus time

Figure 6.8 shows the release profile at 75°C and pH 6.5. Since 75°C is above the T_{cp} temperature of PEOX, chains of PEOX were totally dehydrated. Hydrophobic interactions in PEOX/ TA multilayers were dominant and conformation of the adsorbed polymer chains was

changed to globular form. In this temperature range, stability of the film decreased significantly. For this reason, only at pH 6.5, a release profile for Rhodamine 6G from PEOX / TA multilayers could be obtained. When pH of the releasing medium was increased further, dye molecules were released in a burst release manner. As indicated, increased temperature even above the T_{cp} temperature of PEOX produces a very hydrophobic environment for the multilayers. Hydrophobic collapse of adsorbed PEOX chains decrease the interaction stability of the film and as a result, critical disintegration pH of the multilayers is lowered. When pH of the releasing medium is higher than pH 6.5, dye molecules release due to the diminishing interaction strength of H-bonded multilayers of PEOX and TA.

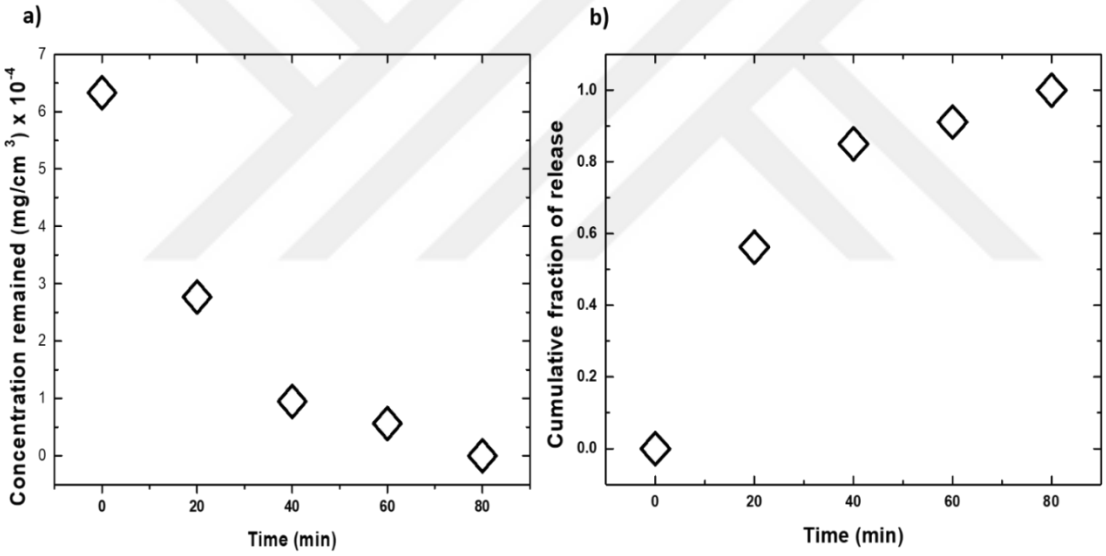

Figure 6.8: Release of Rhodamine 6G from 10 BL PEOX/TA LbL films at 75°C, pH 6.5 **(a)** Concentration remained (mg/cm^3) on film versus time **(b)** Fraction of cumulative release versus time

Figure 6.9 illustrates release profile of dye molecules from PEOX / TA multilayers at pH 6.5, at different temperature in terms of fraction of cumulative release. As the temperature increased, the fraction of the dye released from multilayers also increased. From Figure 6.8, it can be observed that the difference between the amount of released dye below and above T_{cp} (62°C)

is apparent. This can be explained with different behaviours of multilayers in release mediums having different temperature below and above T_{cp}. Below T_{cp}, the main reason for higher release rate is incremented rate constant with increasing temperature and weakening of H-bonds as indicated. Above T_{cp}, the main reason for higher release rate and burst release is hydrophobic collapse of adsorbed PEOX chains. This affects interaction stability between PEOX and TA so that dye molecules released in a burst release manner from the hydrophobic environment of the film.

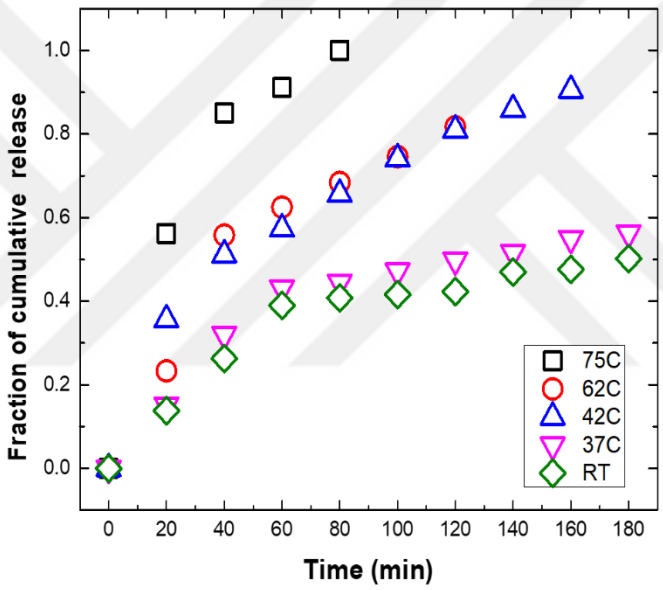

Figure 6.9: Release of Rhodamine 6G from 10 BL PEOX/TA LbL films at pH 6.5, different temperatures in terms of fraction of the cumulative release of the dye.

After obtaining release profiles at different temperature and pH values, morphology of the films after release was also examined. FESEM images of the films were shown in Figure 6.10.

In Figure 6.10 (a) and (b), the surface morphologies of the films after release at 37°C, pH 6.5 and 7.4 can be clearly seen. It was indicated that the release profile at body temperature (37°C), at pH6.5, the release profile slightly shifted from diffusion limited release to zero order release. Slight pore formation, which is a characteristic sign for zero order release kinetics, on the surface

can be observed in Figure 6.10 (a). On the other hand, at pH 7.4, the temperature increase didn't affect the release profile (still zero order release like in room temperature (RT) but the release rate of dye molecules was speeded up. After 180 minutes, surface erosion was more when the temperature was increased. In Figure 6.10 (b), this surface erosion is apparent with more flattened surface morphology compared to Figure 6.10 (a). Figure 6.10 (c) shows the surface morphology of the released film at 37°C, pH 8.5. Release mechanism at this condition is based on burst release, so after 80 minutes, almost all film together with loaded dye molecules was released. As a result, the surface is flat only with small portion of aggregates of PEOX / TA as observed in Figure 6.10 (c).

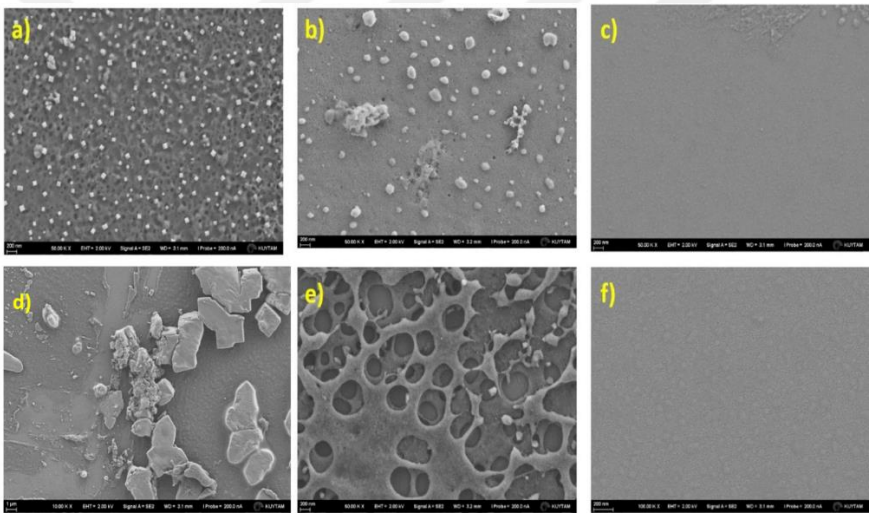

Figure 6.10: (a) FESEM image of the Rhodamine 6G loaded PEOX / TA film after 180 minutes of release at 37°C, pH 6.5 **(b)** FESEM image of the Rhodamine 6G loaded PEOX / TA film after 180 minutes of release at 37°C, pH 7.4 **(c)** FESEM image of the Rhodamine 6G loaded PEOX / TA film after 180 minutes of release at pH 8.5, 37°C **(d)** FESEM image of the film after 180 minutes of release at 42°C, pH 6.5 **(e)** FESEM image of the film after 180 minutes of release at 42°C, pH 7.4 **(f)** FESEM image of the film after 180 minutes of release at 42°C, pH 8.5. Scale bar is 200 nm for all images.

Figure 6.10 (d) and (e) illustrate the surface morphologies of dye loaded PEOX / TA films after release at 42°C at pH 6.5 and 7.4 respectively. In Figure 6.10 (e), large pores on the surface is observed. Figure 6.10 (f) shows the morphology of released film at 42°C, pH 8.5. In Figure 6.10

(f), the morphology of the PEOX / TA film after release is very similar to the morphology of the film shown in Figure 6.10 (c). In both films, very smooth and flat surface suggests that together with the dye release, film on the surface disintegrated and film was dissolved in release medium.

To sum up, release of Rhodamine 6G molecule from PEOX / TA multilayers was evaluated at different conditions in terms of temperature and pH. As the pH of the releasing medium approaches to pKa of TA, the strength of the interaction between PEOX and TA decreases. Weaker interaction between PEOX and TA causes the formation of loosely bound LbL multilayers. As a result, increase of pH in the release medium results in higher release rate and change in the release profile and kinetics. The influence of temperature was also investigated. Below T_{cp}, the major contribution to higher release rate is increasing rate constant which favors the release of film components and loaded dye molecules. Weakening of hydrogen bonds with increasing temperature is also a contributor to the higher release rates as the temperature of the releasing medium approaches to T_{cp}. When temperature of the releasing medium exceeds T_{cp} of PEOX, hydrophobic collapse of PEOX chains resulted in changes in the release profile and higher release rates. As the temperature of the medium increases, the release profile also changes at all pH values. Typically, as the temparute of the releasing medium increases, release profile changes from diffusion-based release to zero order release and eventually to a burst release in a gradual way.

6.3.4 Effect of Polymer Hydrophobicity on Release Mechanism for Hydrogen Bonded LbL Films

PNIPAM is another temperature-sensitive polymer which exhibits LCST at 32°C, close to physiological body temperature. [59],[269], [270]. PNIPAM is also a water-soluble and neutral polymer which is used in many biomedical applications including drug release and biosensors [58]. To investigate the effect of T_{cp} and chemical structure of the polymer, we have used PNIPAM instead of PEOX in dye encapsulted LbL multilayers and studied its effect in terms of release properties of LbL multilayers. PNIPAM is more hydrophobic than PEOX due to the chemical structure of its repeating unit. While one end of the amide groups resides in the backbone of PEOX,

the location of the amide groups is in the side chain of PNIPAM. This difference in the hydrophobicity between PEOX and PNIPAM is also reflected in the T_{cp} values of the polymers: T_{cp} of PNIPAM is ~32°C. Additionally, the accessibility to carbonyl groups (C=O) of PNIPAM to form H-bonds is much harder when compared with the carbonyl group of PEOX [180]. First, the LbL growth profile of PNIPAM and TA films was studied and the result was shown in Figure 6.11. 18 BL of PNIPAM/TA LbL films on Si wafer were grown in order to obtain LbL multilayers which have the same thickness with 10 BL PEOX/TA film. The films were grown with dip coating method. [203].

Figure 6.11 shows that PNIPAM / TA films also grow linearly with an avarage bilayer thickness of ~3.8 nm. Average BL thickness is smaller when compared with 10 BL PEOX / TA films since PNIPAM molecules adsorbed on the surface as tighter coils. The final thickness of 18 BL H-bonded PNIPAM / TA film is ~68 nm.

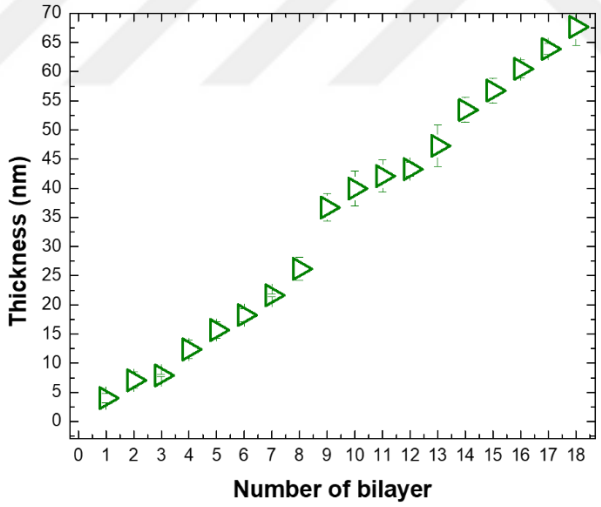

Figure 6.11: Thickness of PNIPAM/TA LbL film as a function of number of bilayers grown to a final thickness to 18 BL.

6.3.4.1 Loading of Rhodamine 6G into PNIPAM/TA Multilayers

As in PEOX/TA multilayers, Rhodamine 6G was incorporated into PNIPAM / TA multilayers by post-treatment, simply dipping the prepared films into Rhodamine 6G solution. First, 18 BL of PNIPAM/TA multilayers were fabricated on the quartz substrate for UV-spectroscopic measurements. In Figure 6.12, Rhodamine 6G loading to PNIPAM / TA multilayers as a function of post-treatment time was demonstrated. From Figure 6.12, it was concluded that the optimal loading or post-treatment time is 4 hours. After 4 hours, desorption rate of dye molecule is equal to the adsorption rate of dye molecules into film and the amount of dye in the film reaches steady state. Thus, post-treatment of PNIPAM/TA multilayers for the adsorption of Rhodamine 6G to PNIPAM / TA multilayers was limited to 4 hours for maximum and efficient loading of the dye molecules. UV-Vis spectra of loaded Rhodamine 6G into PNIPAM/TA multilayers shows that the maximum absorbance of the dye was shifted to ~10-15 nm to a higher wavelength, which is usually called as a red shift. This indicates that dye molecules form J-type aggregates when adsorbed [267], which means that they adopt one dimensional parallel orientation to favour H-bonding with multilayers of PNIPAM / TA.

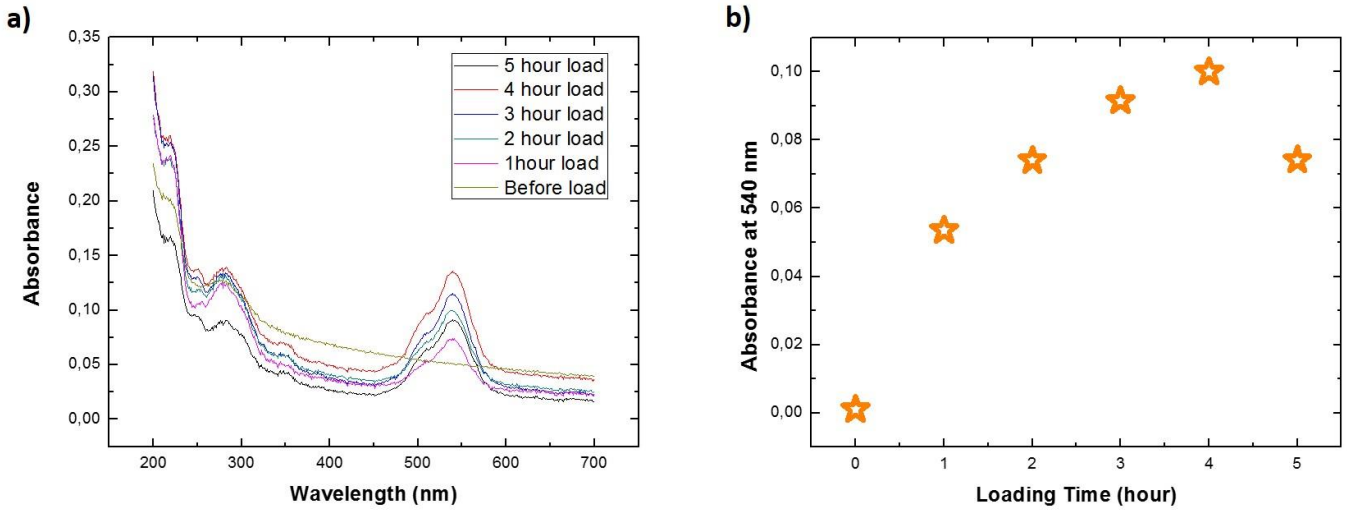

Figure 6.12: (a) UV-Visible spectra of Rhodamine 6G loaded 18BL PNIPAM/TA multilayers as a function of post-treatment time **(b)** Absorbance at 540 nm (maximum peak) of Rhodamine 6G in 18 BL PNIPAM/TA multilayers as a function of loading (post-treatment) time

Figure 6.13 shows that the loading amount of dye molecules can be controlled via film thickness. Figure 6.13 (a) indicates that not only surface adsorption but also interactions between dye molecules and PNIPAM or TA molecules are effective in loading of dye molecules into PNIPAM / TA multilayers. This is evident since as the number of bilayers (or film thickness) increase, the loading amount of dye also increases as illustrated in terms of absorbance. Figure 6.13 (b) compares the loading amount of Rhodamine 6G as a function of number of bilayers for PEOX/TA and PNIPAM/TA multilayers. According to Figure 6.13 (b), more dye molecules can be loaded into PEOX / TA multilayers when compared to PNIPAM / TA multilayers. This is due to the more hydrophilic nature and more accesible carbonyl groups of PEOX so that hydrophilic dye molecules can interact more with PEOX in the deposited multilayers via forming H-bonds.

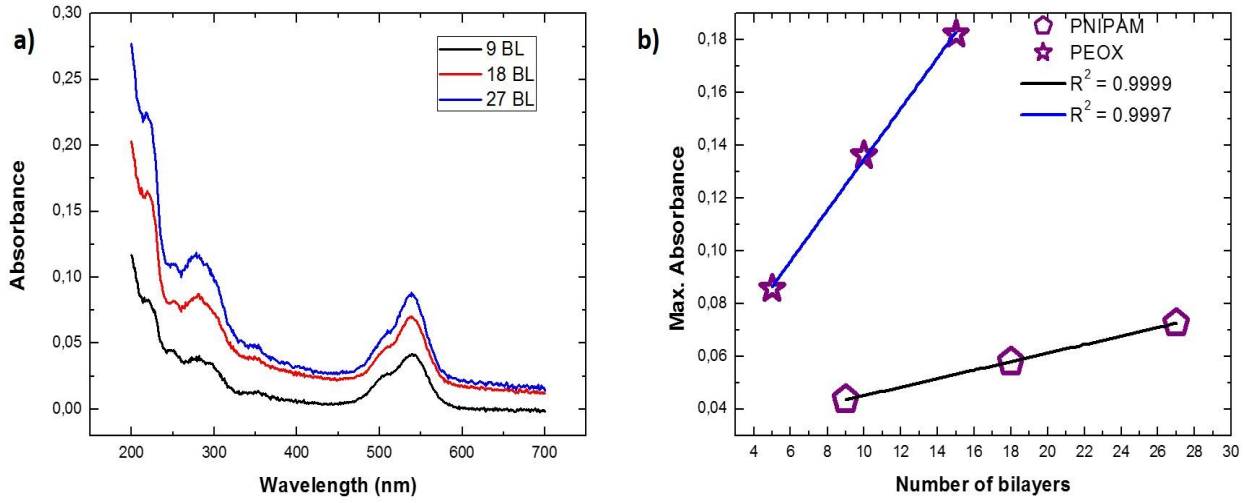

Figure 6.13: (a) UV -Vis spectra of Rhodamine 6G loaded PNIPAM/TA multilayers having different number of bilayers **(b)** Absorbance at 530 nm of PEOX/TA films and PNIPAM/TA films deposited on quartz substrate versus number of bilayers that the films have

6.3.4.2 pH and Temperature Triggered Release of Rhodamine 6G from PNIPAM / TA Multilayers

6.3.4.2.1 pH Triggered Release of Rhodamine 6G from PNIPAM / TA Multilayers

18 BL PNIPAM / TA multilayers were grown and loaded with Rhodamine 6G via post-treatment as described above. For the release medium, phosphate buffer saline (PBS) solutions were prepared to mimic the body conditions and necessary pH arrangements were made. PNIPAM / TA films loaded with dye on quartz samples were dipped into release medium and every 20 minutes, the absorbance of the samples was measured with UV-Vis Spectrometry for 140 minutes. Figure 6.14 shows the release profile of Rhodamine 6G from PNIPAM / TA multilayers into PBS solutions having different pH in terms of concentration of dye remained in the film and fraction of cumulative release.

At pH 6.5, 83.7% of loaded dye was released while at pH 7, 7.4 or 8.5, almost all of the dye loaded into multilayers were released effectively (cumulative released percentages are 95.7%, 100% and 100%, respectively). For PEOX / TA multilayers, it was reported that at pH 6..5, 7, 7.4 and 8.5, the cumulative released amount of dye was 50.2%, 70.8%, 85.1% and 99%, respectively. This data suggets that PNIPAM/TA multilayers are able to release the dye molecules in a much faster manner than PEOX/TA multilayers. This was due to the more hydrophilic nature of PEOX than PNIPAM which allows stronger interactions between dye molecules and adsorbed PEOX / TA molecules. So, the dye molecules were released in a slower manner compared to PNIPAM / TA multilayers for all pH values. Furthermore, above pH 7, dye molecules (Rhodamine 6G) are positively charged. It is true that as the pH of the releasing medium increases, positively charged dye molecules bind better to slightly ionized adsorbed TA molecules. However, stronger attractive ion-dipole interaction between carbonyl oxygen of PEOX and positively charged dye molecules existed due to the more accesible carbonyl oxygen of PEOX compared to carbonyl groups of PNIPAM.

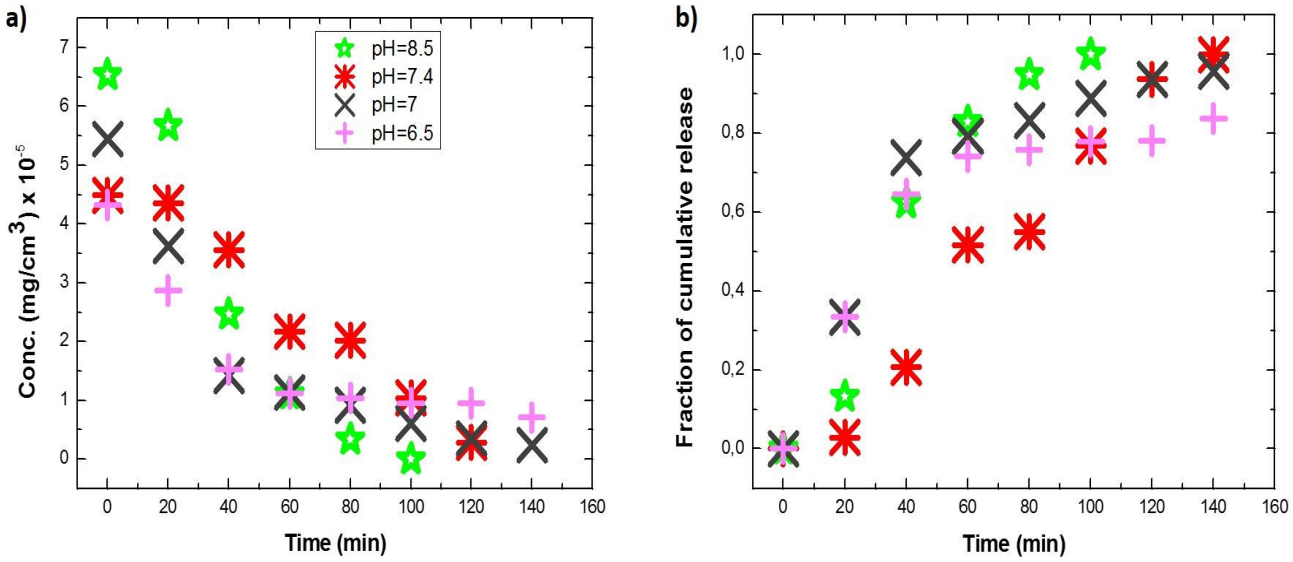

Figure 6.14: pH triggered release profile of Rhodamine 6G from PNIPAM / TA LbL films formed on quartz substrate at room temperature **(a)** Concentration of the dye (mg/cm^3) remained in the PNIPAM / TA multilayers versus time (min) **(b)** Fraction of cumulative release of the dye versus time (min)

Table 6.3 summarizes the release mechanisms of Rhodamine 6G from PNIPAM / TA multilayers at different pH values. When films were put in releasing mediums having pH 6.5 or 7, it was observed that the release mechanism was diffusion-based since release profiles at these pH values were almost perfectly exponential. Exponential release profile is expected in diffusion-based release mechanisms since they usually follow "initially fast but later slow" release rate. In PBS, multilayers of PNIPAM and TA swell due to the presence of kosmotropic phosphate ions. With the swelling of multilayers, dye molecules reside closer to the surface of the film initially and release into the medium easily. However, dye molecules which reside in deeper sites travel long distances to release into PBS medium. Similar to PEOX / TA multilayers, for PNIPAM / TA films, Fickian diffusion was assumed for the release profiles that fit to exponential decay according to the Korsymeyer-Peppes model [259],[216, 268].

Table 6.4: Summary of the release mechanisms of dye molecules (Rhodamine 6G) from PNIPAM/ TA multilayers at different pH values

pH of the release medium	**Release mechanism**	**R^2 for linear fit**	**R^2 for exponential fit**
6.5	Fickian Diffusion	0.67	0.98
7	Fickian Diffusion	0.73	0.97
7.4	Zero Order Release	0.97	-
8.5	Zero Order Release	0.90	-

At pH 7.4 and 8.5, the release mechanism obeys zero order release kinetics since the release profile of Rhodamine 6G from PEOX / TA multilayers is almost perfectly linear. This means that at these pH values, surface erosion takes place. From previous observations, it was concluded that zero order release mechanism usually takes place in pH values just below the critical disintegration pH. At pH 8.5, rather than burst-release profile that was observed in PEOX/TA LbL films, zero order release profile for the release of the dye was obtained for PNIPAM/TA multilayers. This is due to the more hydrophobic structure of PNIPAM: Contributions of additional hydrophobic interactions may result in the improvement of pH stability of PNIPAM/TA multilayers compared to PEOX / TA multilayers. To test this hypothesis, pH stability of PNIPAM/TA multilayers and PEOX/TA multilayers were illustrated in Figure 6.15.

From Figure 6.15, it can be concluded that PNIPAM/TA films are more stable than PEOX/TA films in all pH ranges even though both films disintegrate at pH 8.5. Disintegration of the film is due to the ionization of the hydroxyl groups of TA. This data shown in Figure 6.15 demonstrates that PNIPAM has a more hydrophobic structure reflected also in smaller T_{cp} value

and additional hydrophobic interactions result in more stable PNIPAM/TA films. It is also well accepted that additional hydrophobic interactions enhance the pH stability of H-bonded LbL multilayers [180], [183]. This increase in pH stability was evaluated in terms of H-bonded stabilized hydrophobicity. For this reason, at pH 8.5, a burst release profile for the release of dye was not observed for PNIPAM/TA films unlike PEOX/TA multilayers.

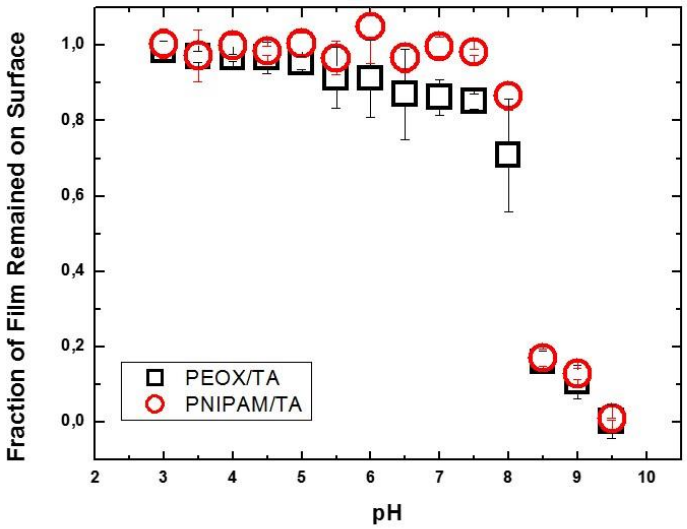

Figure 6.15: pH stability of 18 BL PNIPAM/TA films and 15 BL PEOX/TA films. The fraction of the film remained on the substrate is plotted as a function of pH of phosphate buffer.

Figure 6.16 shows the FESEM images of films before and after the release of 140 minutes at different pH conditions. Before putting into releasing medium, the surface of 16 BL PNIPAM/TA film was smooth with some aggregates. Figure 6.16 (b) shows the morphology of PNIPAM / TA film after the release of dye into the releasing medium at pH 6.5 was completed. In Figure 6.16 (b), it can be observed that the film was rougher than its initial condition, before the release. Increased roughness, after the release is an expected result for diffusion-based release mechanisms. In Figure 6.16 (c), the film's morphology after the release at pH 7.4 was very similar to the film's morphology before the release that was shown in Figure 6.16 (a). Zero-order kinetics does not result in swelling of the film, however, at least surface erosion was expected. To be more conclusive about the release mechanism of the dye from PNIPAM / TA multilayers at pH 7.4, the thickness of the films before and after the release was compared in Table 6.4.

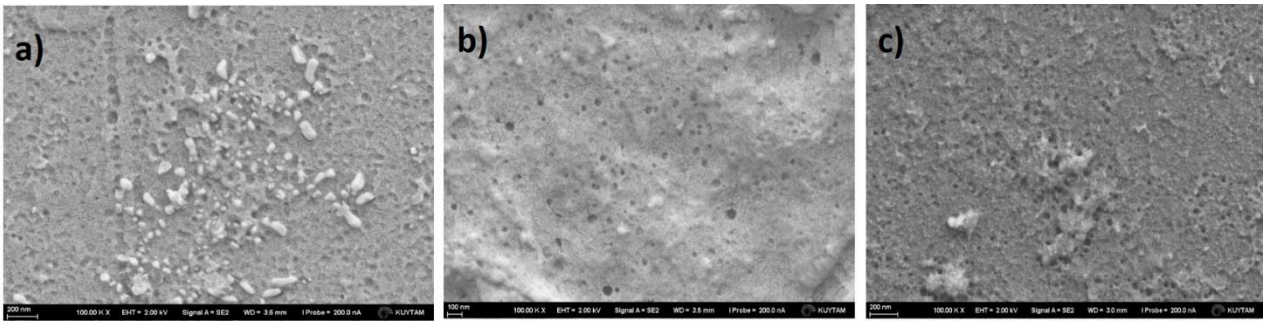

Figure 6.16: (**a)** FESEM image of the 18 BL PNIPAM / TA LbL film after Rhodamine 6G is loaded (**b)** FESEM image of the Rhodamine 6G loaded 18 BL PNIPAM / TA film after release of dye molecules is completed at pH 6.5 **(c)** FESEM image of the Rhodamine 6G loaded 18 BL PNIPAM / TA film after release of dye molecules is completed at pH 7.4

Thickness decrease of films after putting them into releasing mediums at pH 7.4 and at pH 8.5 was expected since release mechanism was zero order release kinetics. Surface erosion in zero order release can result in both diffusion of the dye and dissolution of the film from the surface. This is the reason for the decrease in film thickness after the release, as shown in Table 6.4.

Table 6.5: Thickness data of Rhodamine 6G loaded 18 BL PNIPAM/TA LbL films before and after release

pH of Release Medium	**Thickness before Rhodamine 6G loading (nm)**	**Thickness after Rhodamine 6G loading (nm)**	**Thickness after Rhodamine 6G released (nm)**
7.4	77.2341	86.5793	37.1901
8.5	70.0135	81.1531	25.4186

6.3.4.2.2 Temperature Triggered Release of Rhodamine 6G from PNIPAM / TA Multilayers

Figure 6.17 illustrates the release profile of Rhodamine 6G at 15°C in terms of concentration remained versus time (Figure 6.17 (a)) and fractional cumulative release versus time (Figure 6.17 (b)) at pH 6.5, 7.4 and 8.5. At 15°C, independent from pH of the releasing medium, release of dye molecules from the films follows diffusion-based release kinetics. As the temperature of release medium is lower than T_{cp} of PNIPAM, adsorbed polymer chains configure into multilayers as tight coils and loops. Thus, it is more difficult for dye molecules to escape into release medium from H-bonded multilayers. Another reason for diffusion-based release is that the rate constant k depends on temperature. As the temperature is lowered, rate constant k also decreases which results in slower release rate. It should be also noted that total release time of dye molecules is 60 minutes longer (total 200 minutes) at 15°C. Thus, at all pH values, lowering the temperature of release medium to 15°C provides longer and slower release rate of Rhodamine 6G from PNIPAM / TA multilayers.

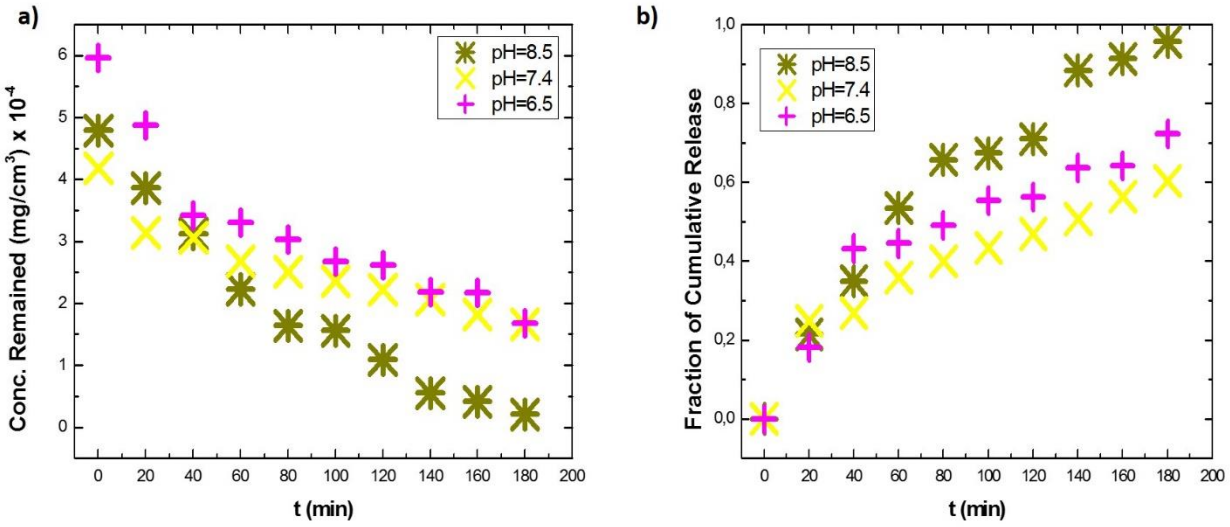

Figure 6.17: Release of Rhodamine 6G from 18 BL PNIPAM/TA LbL films at 15°C , pH 6.5, 7.4 or 8.5 **(a)** Concentration of the dye (mg/cm^3) remained in the PNIPAM / TA multilayers versus time (min) **(b)** Fraction of cumulative release of the dye versus time (min)

Figure 6.18 shows the FESEM images of films of Rhodamine 6G loaded PNIPAM/ TA multilayers on Si wafer that were put in release medium at 15°C. In all release mediums independent of pH, the release mechanism was diffusion-based and the morphologies in all three films were similar. However, at pH 6.5 and 7.4 (Figure 6.18 (a) and (b)), the PNIPAM / TA complexes have aggregated on the surface of the film. At pH 8.5, ionization of the hydroxyl groups in TA molecules can result in breakage of some H-bonds between PNIPAM and TA so that some part of the film may have been disintegrated. Even though, diffusion of dye molecules at pH 8.5, 15°C seems to be the dominant mechanism, aggregation of parts of the film was less as Figure 6.18 (c) suggests.

Figure 6.18: (**a)** FESEM image of the 18 BL PNIPAM / TA LbL film after release of Rhodamine 6G is completed at 15°C, pH 6.5 **(b)** FESEM image of the 18 BL PNIPAM / TA LbL film after release of Rhodamine 6G is completed at 15°C, pH 7.4 **(c)** FESEM image of the 18 BL PNIPAM / TA LbL film after release of Rhodamine 6G is completed at 15°C, pH 8.5. Scale bar is 200 nm for all images.

T_{cp} of PNIPAM is 32°C as previously stated. Similar to dye loaded PEOX/TA multilayers, with increasing temperature, there can be drastic changes in the release profile of films. For PNIPAM/TA multilayers, at pH 7.4 and 8.5, the release profile is not zero-order kinetics anymore. However, burst release of the dye with film components was observed at pH 7.4 and 8.5. Total release of the dye was completed in 60 minutes and 20 minutes respectively at these pH values. For this reason, the release profile of the dye at 32°C, pH 8.5 is not shown. As indicated before,

this is due to the dehydration of PNIPAM chains that leads to a conformational change of the adsorbed chains. In addition, this was accompanied with the swelling of the film which allows much faster diffusion of small hydrophilic dye molecules. It is also apparent that with increasing temperature, the hydrogen bonds between PNIPAM and TA weakens but release rate constant (k) increases.

Same disccusions are also valid for the release of dye from PNIPAM / TA multilayers at body temperature, 37°C. The release profile shifted from diffusion based release to zero order release at pH 6.5 at 37°C. While at pH 7.4, accelerated burst release mechanism was observed. Figure 6.19 and Figure 6.20 illustrate the release profiles of dye molecules from PNIPAM/TA at 32°C and at 37°C, respectively.

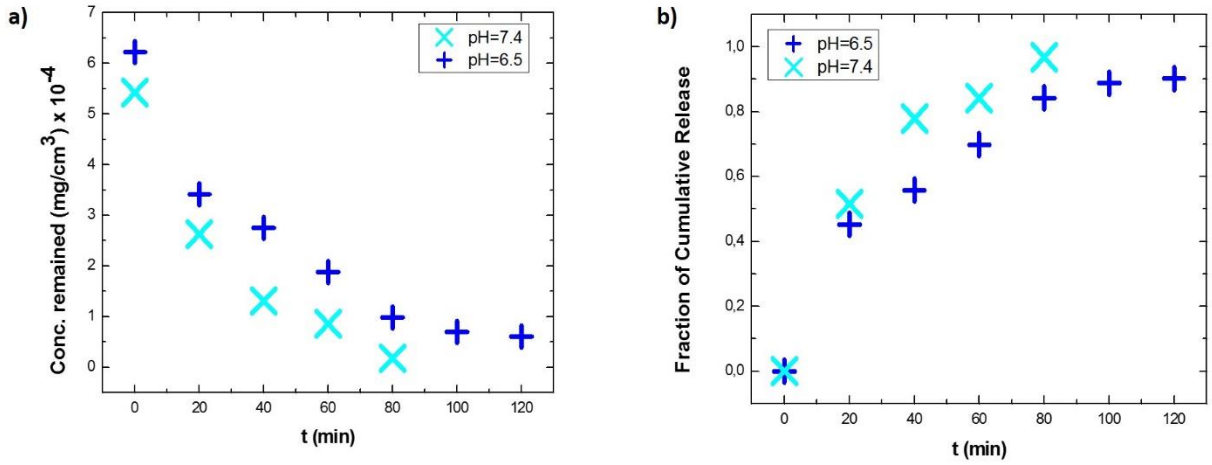

Figure 6.19: Release of Rhodamine 6G from 18 BL PNIPAM/TA LbL films at 32°C , pH 6.5 or 7.4 **(a)** Concentration of the dye (mg/cm^3) remained in the PNIPAM / TA multilayers versus time (min) **(b)** Fraction of cumulative release of the dye versus time (min)

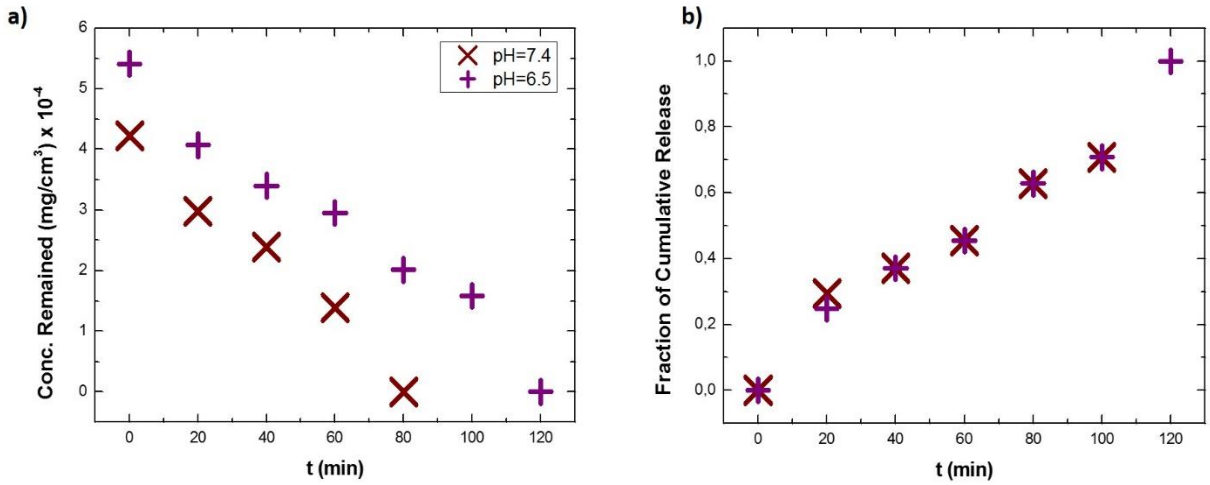

Figure 6.20: Release of Rhodamine 6G from 18 BL PNIPAM/TA LbL films at 37°C , pH 6.5 or 7.4 **(a)** Concentration of the dye (mg/cm^3) remained in the PNIPAM / TA multilayers versus time (min) **(b)** Fraction of cumulative release of the dye versus time (min)

Table 6.5 compares the thickness of PNIPAM / TA multilayers before and after release at different temperature and pH conditions. Thickness data in Table 6.5 confirms the release mechanism that was suggested in indicated conditions for PNIPAM / TA multilayers. In general, in cases where diffusion based release mechanism was suggested, thickness increase was observed whereas in burst release mechanisms, thickness of the film was decreased and most of the film was degraded.

Table 6.6: Thickness data of Rhodamine 6G loaded PNIPAM/TA LbL films before and after release at different conditions

Release Medium	**Thickness of the film after Rhodamine 6G loaded into multilayers (nm)**	**Thickness of the film after Rhodamine 6G is released(nm)**
pH 6.5, 15°C	60.1542	65.3066
pH 7.4, 15°C	63.9952	65.6939
pH 8.5, 15°C	59.2683	10.2653
pH 6.5, 32°C	70.3375	72.2810
pH 7.4, 32°C	66.5908	26.9900
pH 6.5, 37°C	62.3669	60.2696
pH 7.4, 37°C	65.5688	5.2636

In summary, the difference in the hydrophilicity of the polymer structure between PEOX and PNIPAM reflects to the release rate of Rhodamine 6G from PNIPAM / TA and PEOX / TA multilayers. In all conditions that have different pH and temperature, release rate of the dye from PNIPAM / TA multilayers is faster than PEOX / TA multilayers. The reason for the accelerated release for PNIPAM / TA films stems from the differences between chemical structure of PEOX and PNIPAM. Amide group reside in the backbone of PEOX while it is located in the side chain of PNIPAM. This makes carbonyl groups of PEOX more available for both H-bonding and ion-dipole interaction for dye molecules. As a result, the interaction between PEOX and dye molecules

is stronger and release is slower. In addition, more hydrophilic structure of PEOX provides, adsorbed PEOX molecules on the film interact better with the hydrophilic Rhodamine 6G molecules. As a result, release of the dye was expected to be harder for PEOX / TA multilayers.

6.3.5 Effect of Number of Bilayers (Film Thickness) on the Release Profile of Rhodamine 6G from PNIPAM / TA and PEOX / TA Multilayers

If a release system has zero-order release kinetics, it means that initial loading or initial concentration of the target molecules do not matter and in each determined time interval, multilayers would always release same amount of it. Since the initial concentration or loading amount of the dye can be controlled via film thickness (or number of bilayers of the film), this hypothesis was tested by investigating the effect of number of bilayers on release profile of PEOX/TA or PNIPAM/TA multilayers. It is expected that under certain conditions in which zero order release kinetics of dye was obtained, release profile shouldn't change with number of bilayers or film thickness. In other words, number of bilayers or thickness of multilayers shouldn't affect the release profile. PBS solution at pH 7.4, RT (25°C) was prepared as the release medium since in the indicated conditions, both PEOX/TA and PNIPAM/TA multilayers release dye molecules with zero order release kinetics.

Figure 6.21 shows the release profile of Rhodamine 6G from PEOX/TA or PNIPAM/TA multilayers which have different number of bilayers. It can be concluded that for all films that have different thickness, zero order release profile is for the release of the dye. Summary of R^2 values for the linear fit was provided in Table 6.6. It is also true that as the film thickness increases, the release profile fits more to linear fit, and as a result, zero order release profile. At the same time, as the number of bilayers increases, total release time of the dye molecule also increases. Thus, with changing film thickness one can tune both loading amount and total release time of the drug for PEOX / TA and PNIPAM / TA multilayers.

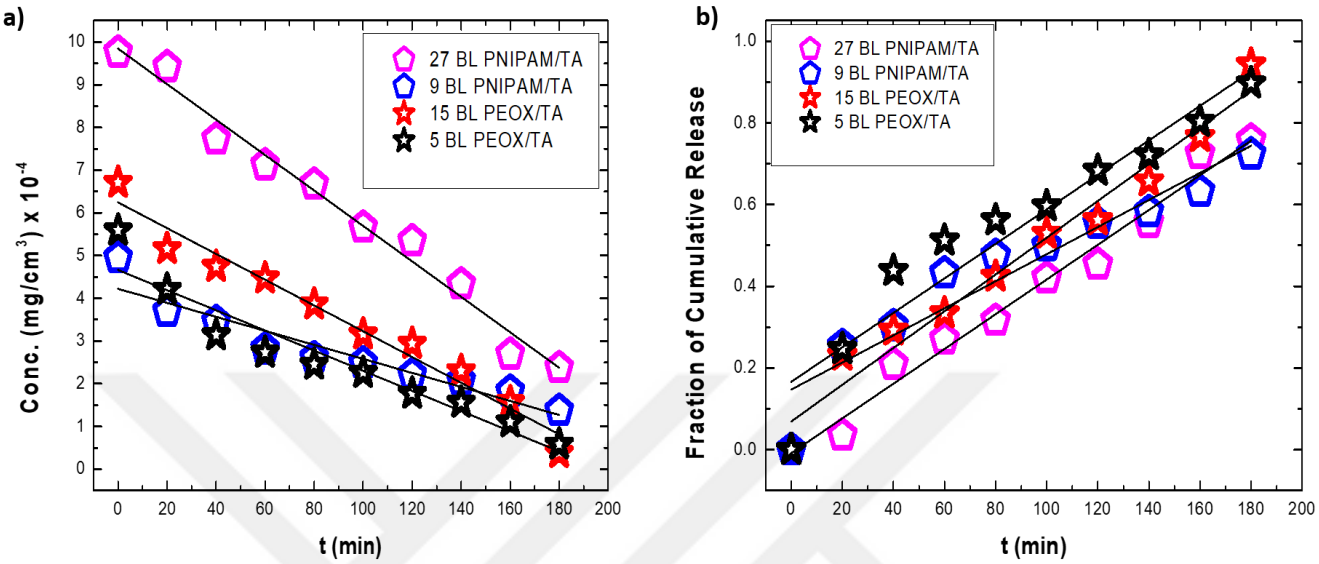

Figure 6.21: Release profile of Rhodamine 6G from PEOX/ TA or PNIPAM/TA LbL films having different number of bilayers formed on quartz substrate at RT, pH 7.4 **(a)** Concentration of dye remained on the film versus time **b)** Fraction of cumulative release versus time

Table 6.7: R^2 values for linear fit for the release profile of Rhodamine 6G from PEOX / TA or PNIPAM/TA multilayers having different number of bilayers

Sample	**Number of Bilayers**	**R^2 for linear fit**
PEOX/TA	5	0.91
PEOX/TA	10	0.96
PEOX/TA	15	0.97
PNIPAM/TA	9	0.89
PNIPAM/TA	18	0.97
PNIPAM/TA	27	0.98

6.4 Conclusions

Release properties of a small, hydrophilic molecule, Rhodamine 6G, from H-bonded LbL films were studied. The ultimate objective was to obtain zero order release profile for the release of small molecule since often release of small and hydrophilic drugs into usually occurs in a burst release manner and results in undesired side effects and low effectiveness.

As a model system, release from PEOX / TA multilayers and PNIPAM / TA multilayers were studied at different pH and temperature conditions. Rhodamine 6G was used as a model hydrophilic molecule. pH dependent release is mainly influenced from the ionization state of hydroxyl groups of TA. As the pH approaches to pKa of TA, release of the dye from multilayers changes from diffusion limited release to burst release. At physiological conditions (pH ~7.4), zero order release profile was obtained for both PNIPAM / TA and PEOX / TA multilayers which is very beneficial in terms of obtaining extended and sustainable release. Temperature dependent release is mainly influenced from PEOX or PNIPAM since these polymers exhibit LCST behavior and they are temperature sensitive polymers. As the temperature of the releasing medium approaches to the T_{cp} of the polymers, the release rate is higher and release profile approaches more to burst release. This is due to the conformational change of the adsorbed polymer chains: Their conformation changed from coils to globular forms so that diffusion of the dye from H-bonded multilayers was faster and release rate was higher. For PEOX / TA films, zero order release profile was obtained for the release of Rhodamine 6G at pH 6.5 and at 42°C. This is very advantageous for the cancer therapy, since pH of the releasing medium mimics the internal pH of the cancer cells and temperature of the releasing medium is the temperature that is used in the heat treatment of cancer cells.

Polymer structure and its effect on the release profile of Rhodamine 6G were also investigated in this study. It was concluded that in all conditions, PEOX / TA films provide longer and sustained release of the dye molecules. This is due to the hydrophilicity difference between PEOX and PNIPAM. Since PEOX is a more hydrophilic polymer, adsorbed PEOX chains on the film interacts more with the dye molecules via forming stronger H-bonds and release of Rhodamine 6G becomes harder. More accessible carbonyl groups of PEOX provides stronger interactions in terms of both H-bonding and ion-dipole interactions with dye molecules. Finally,

the effect of the number of bilayers was investigated. Both loading amount of the drug and total release time can be tailored via film thickness.

Finally, H-bonded LbL films are very good platforms to obtain zero order release profile for the release of hydrophilic drugs. Especially, when pH sensitive and temperature sensitive components were used as the components of multilayers, release kinetics of the drug can be tailored in a desired way. Release of the hydrophilic drugs in an extended time frame and in a sustainable manner is difficult so that this study can be beneficial in terms of being a model for the future applications.

Chapter 7: Self-Assembled PEOX and Malonic Acid Hollow Fibers in Aqueous Solutions

7.1 Overview

Polymer self-assembly can be used to obtain different structures and morphologies. Especially, using multiple H-bonds in these self-assembled structures provide reversibility and cooperativity [119], [118]. H-bonds are used in polymer blends to enhance miscibility [115].. One of the most important property of H-bonded interpolymer complexes of poly (carboxylic acid) s and non-ionic polymers in aqueous solutions is their pH responsivity, which makes them useful in pharmaceutical applications [271]. In these self-assembled complexes, PAA and PMMA were commonly used as hydrogen donors and poly(acrylate)s, poly(alcohol)s, poly(saccharides) and poly (amide)s were used as hydrogen acceptors [271], [272]. Complexation of PAAD and PNIPAM with PAA is stabilized by hydrogen bonding [273]. PAA molecular weight and weight fraction of PAA are main factors that influence the process of complexation of PVP and PAA in aqueous solutions. [274]. pH dependent properties of the H-bonded complexes of maleic acid-styrene copolymer and PVCL was evaluated also as a function of mixing ratio between two components [275]. Thus, stability and properties of H-bonded self-assembled complexes in aqueous solutions depend on various factors. In general, mixing two rather fast complexing components in aqueous solutions result in disordered aggregates.

In this study, PEOX was used as a proton accepting polymer. POX polymers are generally used in biomedical applications as microparticles, microspheres, microbeads, LbL capsules or films, micelles, polymersomes, or nanogels [276], [230, 256, 277]. In addition, fiber formation were also reported for PEOX and PIPOX above T_{cp} [74], [75], [278].

Malonic acid (MA), a type of dicarboxylic acid, was used as proton donating component. Dicarboxylic acids have an important place in biological and industrial processes [279]. Dicarboxylic acids have two pKa values ($pKa_1 < pKa_2$) and this is especially useful in constructing pH responsive highly ordered materials. In aqueous solutions, when pH of the solution is lower than both pKa values, both ends of the acid are protonated. On the other hand, when pH of the solution is higher than two pKa values of the dicarboxylic acid, both ends are ionized while in

between (pKa_1 < pH < pKa_2) only one end of the acid is protonated. Equilibrated structure of dicarboxylic acids in aqueous solutions was adopted according to the pH of the solution [280].

Self-assembly of PEOX and carboxylic acids has also been studied in the literature. For example, assembly of PEOX-b-PCL micelles with carboxylic acids, including malonic acid, via H-bonds was studied [281]. The effect of monocarboxylic acids on T_{cp} of PEOX was investigated [282]. T_{cp} change in the presence of monocarboxylic acid was determined according to the molar ratio of PEOX monomer as the repeating unit to functional acid groups. Interactions between PEOX and carboxylic acid molecules, including H-bonding and hydrophobic interactions, shift T_{cp} of PEOX molecules in aqueous solutions.

MA, as other dicarboxylic acids, have two pKa values (pKa_1=2.8 and pKa_2=5.7) in aqueous solutions. At pH 2, ~90% of MA molecules have protonated two ends which can make H-bonds with amide groups of PEOX groups. Through H-bonds between carboxylic acid groups and amide groups, MA molecules can bridge different PEOX chains, as illustrated in Figure 7.1. Multiple H-bonds with carboxylic acid groups of MA and carbonyl groups of the same PEOX chain is not expected since MA molecules are short compared to long PEOX chains. Thus, self-assembled structures of PEOX and MA can be formed via bridging effect.

The objective of this study is to show that complexation and assembly of PEOX and MA molecules induce the formation of well-defined fibers which have tubular and hollow morphology. Effect of pH, temperature and ionic strength on the self-assembly process was also emphasized and evaluated. The driving force for the self-assembly process and fiber formation was discussed in terms of molecular interactions taking place between MA and PEOX. Since formed hollow fibers of PEOX and MA are pH responsive, they can be used in biomedical applications such as drug delivery and release.

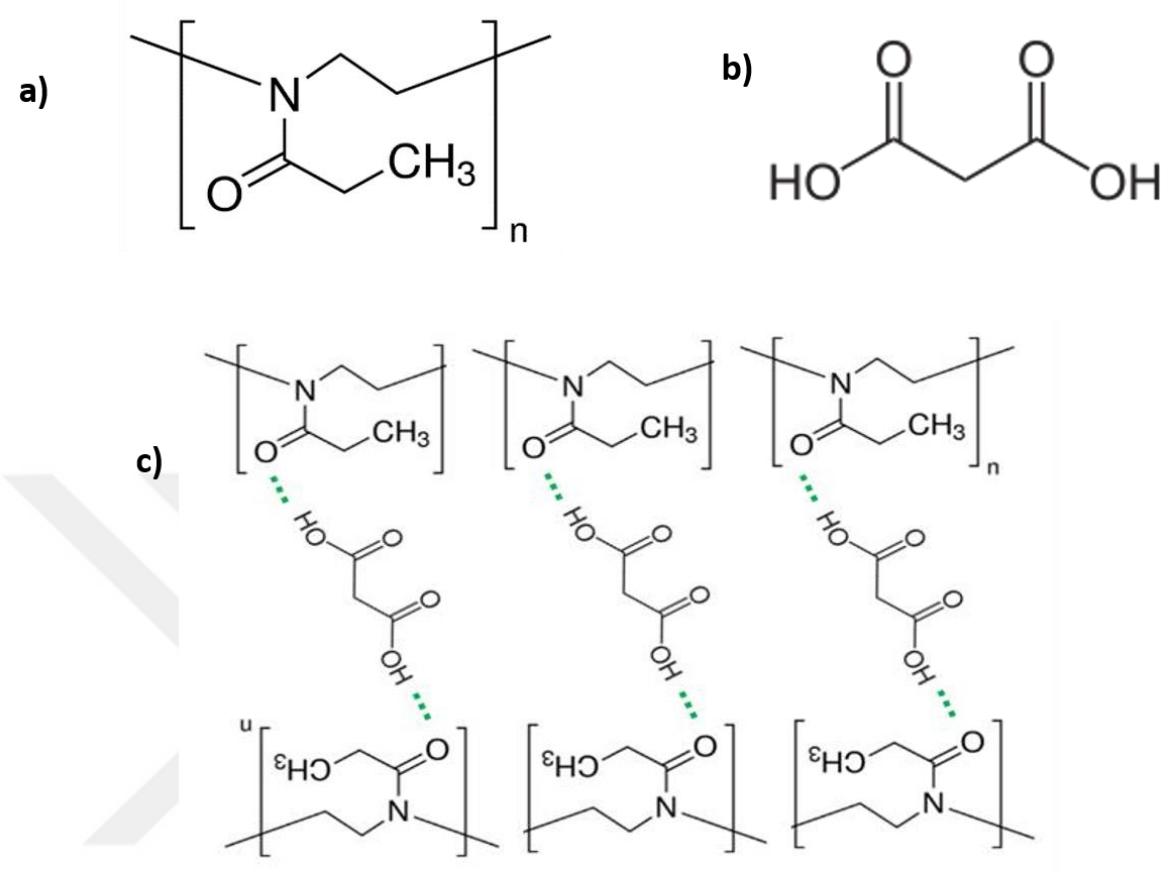

Figure 7.1: (a) Chemical structure of poly (2-ethyl 2-oxazoline) (PEOX) **(b)** Chemical structure of malonic acid (MA) **(c)** Schematic bridging of PEOX and MA via H-bonds

7.2 Experimental Details

7.2.1 Formation of Fibers through Self-Assembly of PEOX and Malonic Acid

0.8 mg mL^{-1} PEOX solution and 0.1 M MA solution were separately prepared in DI water. Then, equal volumes of PEOX and MA solutions were taken and mixed and pH of the mixed solution was adjusted to pH ~2. pH adjustments were done by using and adding necessary amounts of HCl or NaOH aqueous solutions. As a result, final concentrations of PEOX and MA became 0.4 mg mL^{-1} and 0.05M, respectively. PEOX / MA solutions were placed in an incubator at 25°C and observed daily. After ~7 days, tiny aggregates of ~0.5–1.0 μm scale were visible. Later, these

aggregates grew into larger aggregates. These aggregates were taken from the solution and characterized after ~15–20 days of incubation. Separate PEOX (0.4 mg mL^{-1}) and MA (0.05 M) aqueous solutions were also prepared as reference solutions. No fiber formation was observed in these solutions under the same conditions in 20 days for reference solutions.

To investigate the pH effect on fiber formation, three different pH values (pH 2, pH 4 and pH 7) were selected according to the two pKa (pKa_1 = 2.8 and pKa_2 = 5.7) values of MA. pH arrangements of mixed solutions were done by using HCl or NaOH solutions. All samples were preserved in an incubator at 25°C.

To investigate the effect of ionic strength on fiber formation, three salts from Hofmeister series were selected: Na_2CO_3, NaCl and NaSCN. First, 0.1 M salt solutions were prepared in DI water. Then, 5 mg mL^{-1} PEOX solutions and 0.05 M MA solutions were prepared separately in respective 0.1 M salt solutions. Equal volumes of PEOX and MA were taken and mixed. Final concentration of PEOX and MA was 2.5 mg mL^{-1} and 0.025 M respectively in mixed solutions. To study the effect of ionic strength, NaCl was chosen as being the central salt located in the middle of Hofmeister series. Concentration of NaCl solution was selected as 0.01 M, 0.1 M and 0.5 M. This time, 5 mg mL^{-1} PEOX solutions and 0.05 M MA solutions were prepared separately in NaCl solutions and then mixed. pH of all solutions was adjusted to either pH 2 or pH 4 with the addition of HCl or NaOH solutions.

Finally, for the temperature effect, 5 mg mL^{-1} PEOX solution and 0.05 M MA solutions were mixed at different temperature. Different temperatures of mixed solutions were selected according to the T_{cp} of PEOX: 70°C (above T_{cp}) and 4°C (below T_{cp}). All prepared solutions were adjusted to either pH 2 or pH 4. Fiber formation was observed at the indicated conditions for 45 days.

7.2.2 Characterization of Fibers

The fibers formed in the solutions were transferred to a 10 mL vial by Pasteur pipet and washed several times with DI water. The morphology of the fibers was analyzed by using optical microscopy (Leica LM DM) and field emission scanning electron microscopy (FESEM) (Zeiss Ultra Plus SEM). The fibers were transferred from the silicon wafer to carbon tape and analysis with FESEM by secondary electrons was done. For FESEM analysis, any prior sputtering of conductive layer was avoided. The height and horizontal distance of the fibers were determined by atomic force microscopy (AFM) (Bruker Dimension) in tapping mode using silicon cantilevers. FTIR characterization of washed and dried fibers was performed by using a Thermo Scientific iS10 ATR-FTIR. Renishaw Invia Raman Spectrometer was used for the Raman spectroscopy of wet fibers. The fibers were first washed in water to remove free or weakly bound MA molecules and then the wet fibers were placed under the objective. 100 acquisitions were collected with 50X objective using 633 nm laser light.

Interaction parameters between PEOX and MA were determined by ITC (TA Instruments Affinity). The temperature was set to 25°C. 0.05 mM PEOX aqueous solution was placed in sample cell (960µL) and 2.4 mM aqueous MA solution was placed in syringe (250µL). To investigate salt effect on the interaction parameters between PEOX and MA, 0.05 mM PEOX solution in 0.1 M Na_2CO_3 was placed in sample cell and 2.4 mM MA solution prepared in 0.1 M Na_2CO_3 was placed in syringe. The temperature was set to 25°C. Same procedure was repeated by preparing PEOX solution and MA solution with same concentration in 0.1 M NaCl or 0.1 M NaSCN and placing solutions to sample cell and syringe respectively. For the temperature effect, same ITC experiment was repeated by setting temperature to 4°C and 70°C. Thermal stability of the fibers was characterized by thermogravimetric analyser (TA Q500, TA instruments).

7.3 Results and Discussion

7.3.1 Hydrogen Bonded PEOX / Malonic Acid Fibers at pH <pKa_1 < pKa_2

Aqueous mixed solution of PEOX (0.4 mg mL^{-1}) / MA (0.05 M) at pH 2 was stored in incubator at 25°C. Small aggregates was observed in mixture solutions after ~7 days and micron sized fibrous structures were visible to eye in ~20 days. Figure 6.2 illustrates optical microscope images and FESEM images of such fibers that were observed in the mixed solution. From OM images, the diameter of fibers is seen to vary between ~1 to 2 µm.

In Figure 7.2 (c), SEM images of the fibers show that they have hollow morphology. Hollow morphology of PEOX / MA fibers indicates that the driving force for the formation of fibers is very different from the ribbon like PEOX fibers which were formed above T_{cp} of PEOX as a result of crystallization [283]. Smallest diameter range for the fibers were recorded in the range of 700-1000 nm and the wall thickness was ~40 ± 6 nm. Figure 7.2 (d) illustrates IR data of the dried fibers, PEOX and MA in the range of 1800–1525 cm^{-1}. Carbonyl (-C=O band) peak of PEOX was observed at 1629 cm^{-1} while carboxylic acid (-COOH) band peak was located at 1695 cm^{-1} of intermolecular H-bonded MA with a shoulder at 1721 cm^{-1} (residual water H-bonded to MA) [284]. IR spectra of fibers show two peaks at 1614 cm^{-1} and 1721 cm^{-1}. These two peaks of fibers are considered as the evidence for the presence of both PEOX and MA in fibers. The peak at 1614 cm^{-1} is observed with the downshift of the -C=O band that belongs to PEOX. This clearly shows the presence of H-bonding between PEOX and MA molecules in the fibers [244].

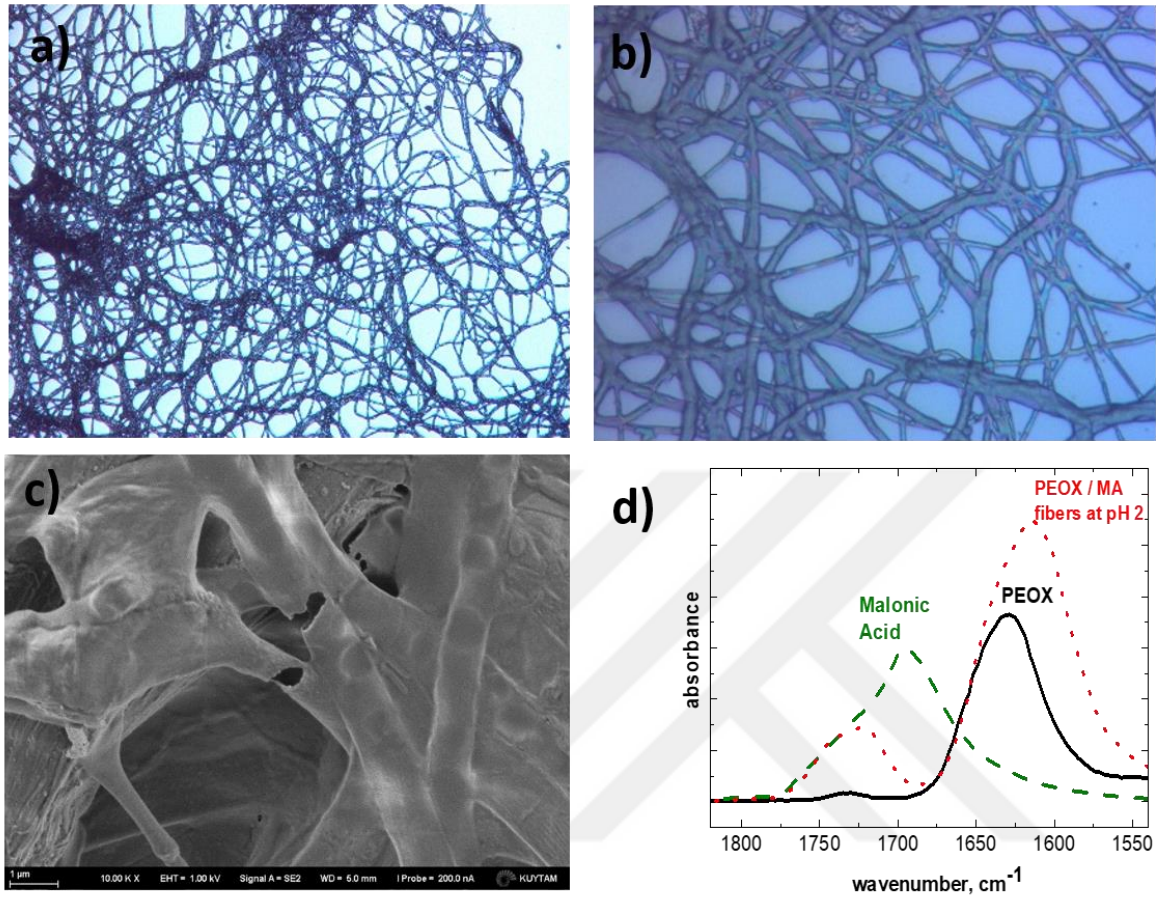

Figure 7.2: (a) and (b) Optical microscope images of PEOX / MA fibers formed at pH 2 after 21 days **(c)** SEM images of the fibers shown in (a) and (b) scale bar= 1 µm **(d)** IR data of PEOX, MA and dried fibers of PEOX / MA formed at pH 2.

IR data of PEOX / MA blends as a function of MA mole ratio was also investigated. The results are shown in Figure 7.3 (a). IR data in Figure 7.3 help us to clarify the IR data that was shown in Figure 7.2. Mole ratio of PEOX / MA was changed from 10 to 1 in these blends. As the amount of MA increases in the blends, observed shift in carbonyl group of PEOX increased. For example, carbonyl peak of PEOX was located at 1629 cm^{-1} while the carbonyl peak of blend that has PEOX/ MA mole ratio of 1 is at 1594 cm^{-1}. At the same time, peak of the carbonyl band of pure MA was at 1695 cm^{-1} while for the blend that has PEOX / MA mole ratio of 10, the carbonyl peak of MA was located at 1720 $cm^{-1.}$ These shifts with changing amount of MA indicates that as the amount of MA in the blends increased, number of H-bonds in the blends also increased.

According to the data in Figure 7.3 (a), fibers in which IR data was shown in Figure 7.2 (d) has a PEOX / MA mole ratio of 8.3. TGA data of the fibers formed at pH 2, PEOX and MA was shown in Figure 7.3 (b). Pure PEOX and MA exhibit single decomposition temperature at ~150°C and ~350°C, respectively. On the other hand, thermal degradation data of fibers formed at pH 2 demonstrate two distinct decomposition temperatures. First decomposition temperature was around ~150°C and the second one was around ~350-450°C. Two decomposition temperatures at these ranges are clear indications of the presence of both PEOX and MA in the fibers. The weight loss of fibers at 350°C was estimated as ~11.2 % which corresponds to the decomposition of MA molecules in the fibers together with the loss of water. TGA results were consistent with IR results which estimated PEOX / MA mole ratio of 8.3.

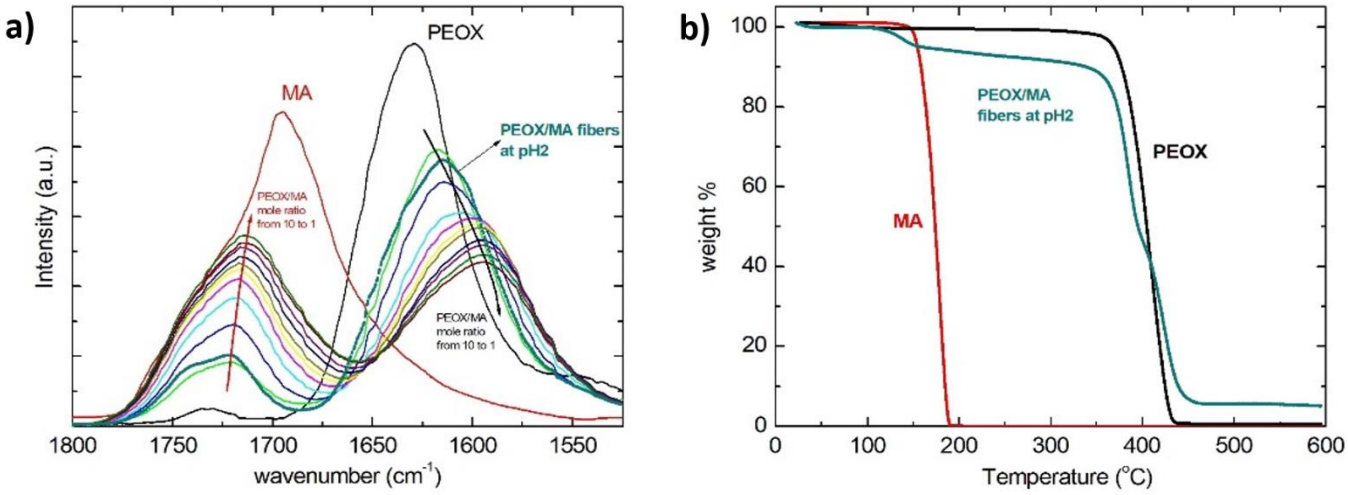

Figure 7.3: (a) IR data of PEOX/MA blends. PEOX/MA mole ratio was changed from 1:0.1 to 1:1 (the direction of the curved arrows). **(b)** TGA data of PEOX/MA fibers formed in aqueous solution at pH 2, PEOX and MA.

From the IR and TGA data, it is concluded that the driving force for the formation hollow PEOX / MA fibers is the hydrogen bonding between PEOX and MA. To check whether intramolecular H-bonding between MA molecules affects the formation of fibers, MA solutions prepared at different pH values were observed. It was concluded that MA molecules do not form

any self-assembled structures by itself via forming intramolecular H-bonds. On the other hand, crystalline PEOX fibers were formed when temperature was increased to above T_{cp} [283]. However, the morphology of crystalline PEOX fibers and PEOX / MA fibers are very different. While PEOX fibers have ribbon-like morphology, the morphology of PEOX / MA fibers formed at pH 2 is hollow. PVP was also able to form branched hollow fibers in aqueous solutions when the aqueous solution was preserved and aged for two weeks due to the hydrophobic interactions and intramolecular H-bonds [285]. Hydrophobic interactions resulted from the interaction between methylene groups while amide groups could be bridged with the solvent mediated H-bonding. Hydrophobic interactions between methylene groups that was proposed for PVP can be also observed for PEOX ethyl groups, however, fiber formation was not observed for PEOX in the absence of MA and at 25°C.

At the same time, thermodynamic parameters of the interaction between PEOX and TA were investigated by ITC. These thermodynamic parameters were calculated according to the independent model and the results of ITC data were presented in Figure 7.4. Enthalpy (ΔH), entropy (ΔS), and free energy (ΔG) of interaction are determined as -49.39 kJ/mol, -82.37 J/mol K and -24.83 kJ/mol respectively. It can be concluded that interaction between PEOX and MA is enthalpy driven (in an exothermic direction) since strong H-bonds form between two components. Enthalpy of interaction is large when compared with H-bonded interpolymer complexes [286] and TA / POX complexes [287]. ITC results showed that PEOX and MA form strong H-bonds and they interact immediately. However, fiber formation as a result of dynamic self-assembly between PEOX and MA occurred in a much slower rate.

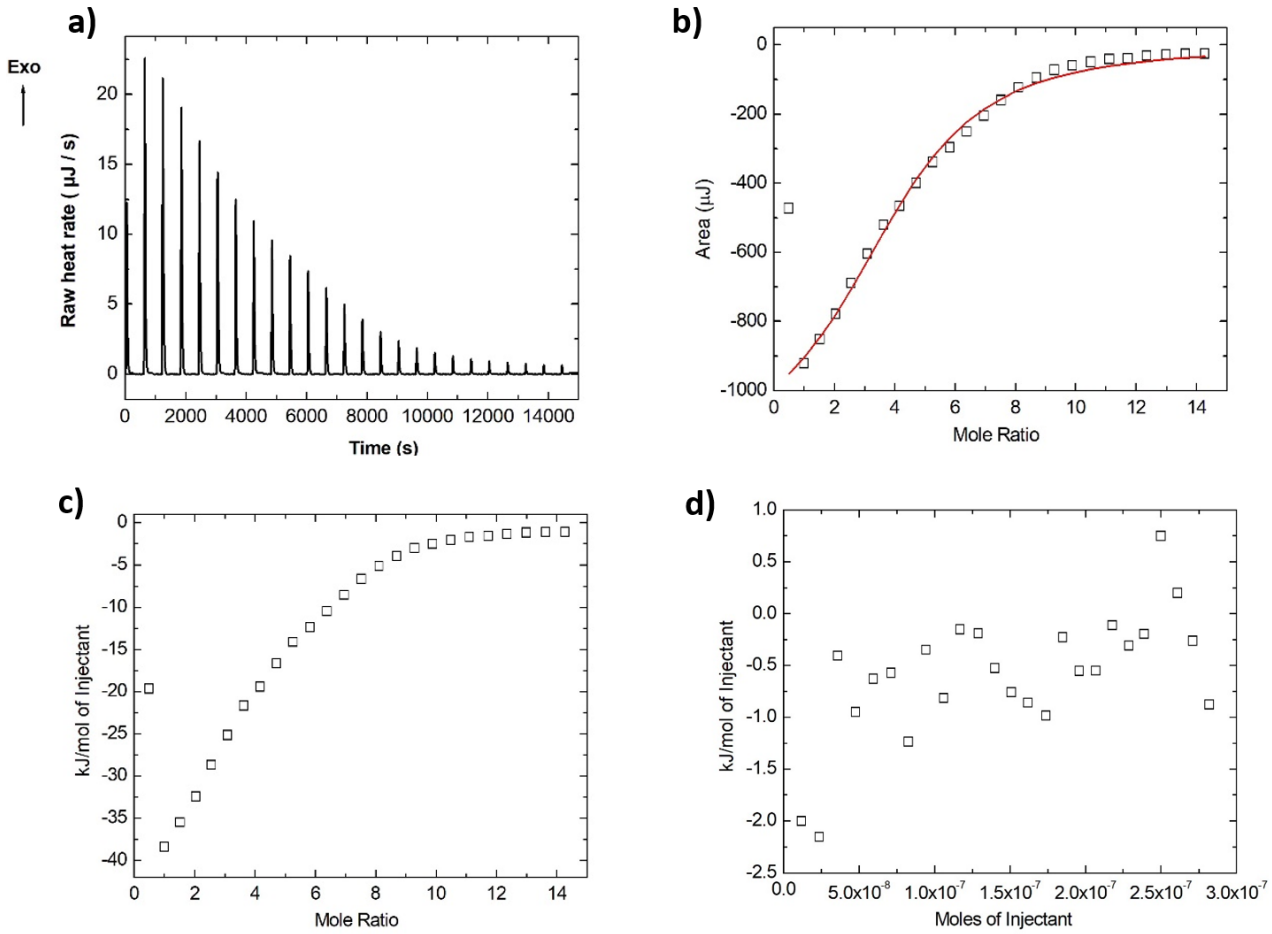

Figure 7.4: (a), (b), (c) ITC data of the interaction between MA (2.4 mM, pH2.5) to PEOX (0.05 mM, pH2.5) at 25°C. **(a)** Raw data **(b)** Independent Model fit (solid line) corresponding to n = 4.06; ΔH = -49.39 kJ/mol; ΔG = -24.83 kJ/mol; ΔS = -82.37 J/mol-K. **(c)** Heat in kJ/mol of injectant. **(d)** ITC data for addition of MA (2.4 mM, pH2.5) to pH 2.5 HCl (aq) at 25 °C

7.3.2 Effect of pH on the Formation of Hydrogen Bonded PEOX and Malonic Acid Fibers

Both ends of MA are deprotonated in aqueous solutions that have a pH > pKa_1 > pKa_2. Therefore, at pH 7, hydrogen bond formation between PEOX and MA is not expected since more than 95% of the carboxylic acid end groups of MA are ionized. At pH 7, some fibrous aggregates

were observed but the amount of fibers was less compared to pH 2 and morphology of the fibers was different than the fibers observed at pH 2. Figure 7.5 compares the morphologies of fibers that were formed at different pH. Figure 7.5 (c) illustrates PEOX / MA fibers formed at pH 7. Instead of hollow fibers, ribbon-like and flat fibers were observed at pH 7 which resembles PEOX fibers formed as a result of crystallization process above T_{cp} [283].

To check the driving force for the formation of solid and ribbon-like fibers, T_{cp} of PEOX solutions in the presence of MA molecules was checked. T_{cp} of PEOX solution having 0.4 mg/mL concentration has a T_{cp} at ~68°C and T_{cp} of PEOX solution didn't change significantly with changing pH. However, in the presence of MA (0.05 M), T_{cp} of PEOX solution varied significantly with pH. At pH 2, T_{cp} of PEOX decreased to 63°C, while at pH 7 T_{cp} of PEOX solution decreased to 60°C in the presence of MA. T_{cp} measurements showed that ribbon-like fibers observed at pH 7 were not formed as a result of slow crystallization process. A possible explanation for the fiber formation at pH 7 could be the complexation of small amount of carboxylic acid groups of protonated MA molecules with carbonyl groups of PEOX. Since the amount of protonated MA molecules is very small, amount of the fibers formed is also very small. Due to this, any thermal or spectral characterization of the fibers formed at pH 7 could not be done. This difference in the fiber amount between pH 2 and pH 7 indicates the significant role of H-bonding in the fiber formation. At pH 4 ($pKa_1 < pH < pKa_2$), in which MA molecules have one ionized and one protonated end and the concentration of $HOOC\text{-}CH2\text{-}COO^-$ is close to its maximum value of ~95%, fiber formation was also checked.

Figure 7.5 (b) and (e) shows the SEM and AFM images of PEOX / MA fibers formed at pH 4. Both the amount and the morphology of fibers formed at pH 4 is similar to the amount morphology of fibers formed at pH 2. Hollow PEOX / MA fibers formed at pH 4 can be observed from SEM images of fibers in Figure 7.5 (b). However, in the AFM height image of Figure 7.5 (e), fibers having flat and ribbon like morphology was also observed together with the hollow ones. The width and the height of the ribbon-like flat fibers are ~1.5 µm and ~70 nm respectively. While such flat fibers were not observed at pH 2, one possible explanation for the presence of this type of fiber is that they exist as precursor form of the hollow fibers.

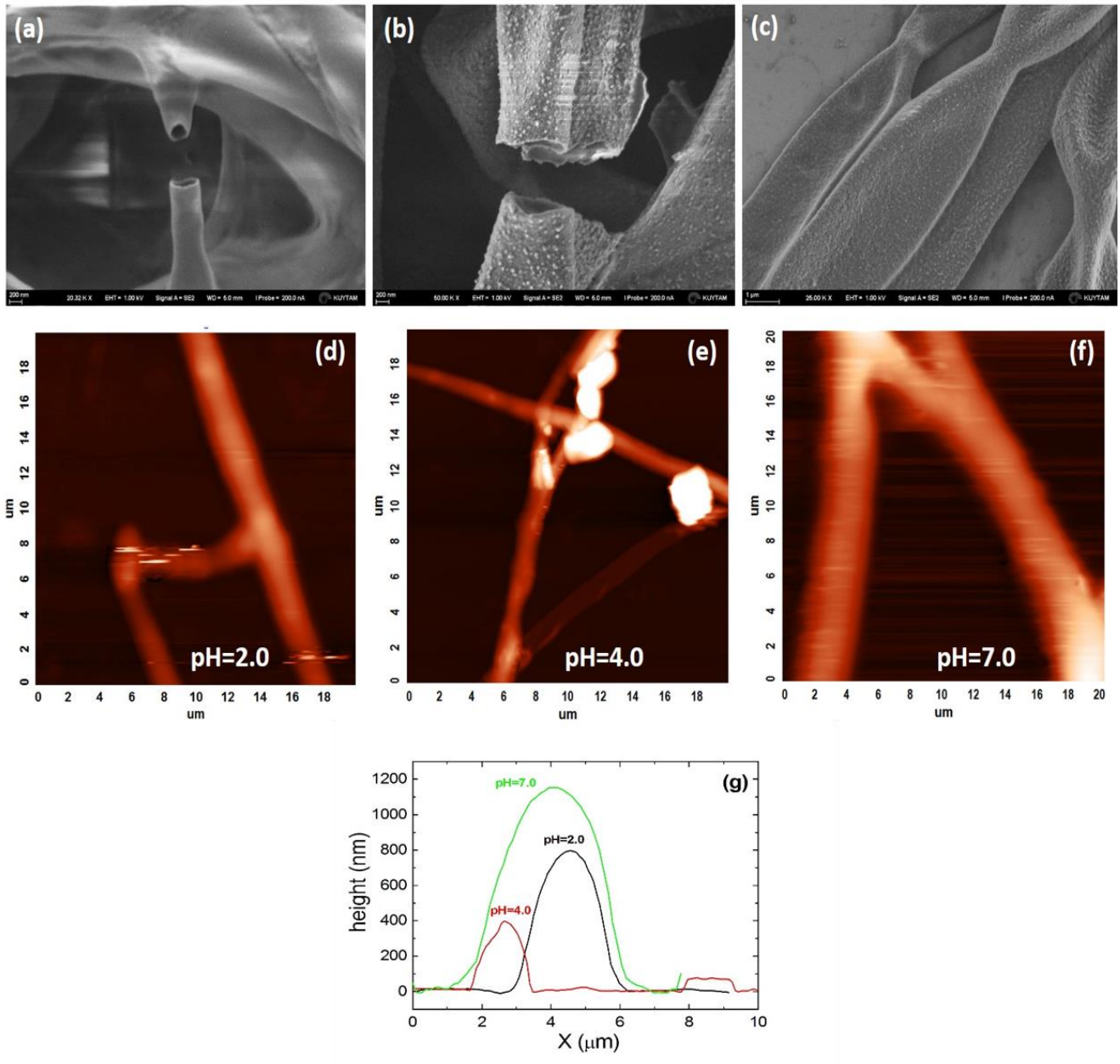

Figure 7.5: **(a)** SEM image of the PEOX/MA fibers at pH 2 (**b)** SEM image of the PEOX/MA fibers at pH 4 **(c)** SEM image of the PEOX/MA fibers at pH 7. Scale bar of (a) and (b) is 200 nm and (c) is 1 μm. **(d)** AFM height image of the PEOX/MA fibers at pH 2 **(e)** AFM height image of the PEOX/MA fibers at pH 4 **(f)** AFM height image of the PEOX/MA fibers at pH 7 **(g)** AFM height profiles of the fibers in (d), (e) and (f).

IR and TGA data of the fibers formed at pH 2 and pH 4 were presented and compared in Figure 7.6. IR and TGA data of two fibers clearly points out the differences in the formation of two fibers at pH 2 and pH 4. There are two peaks in the IR spectrum of fibers formed at pH 2 and these peaks correspond to carbonyl (-C=O) stretching of PEOX at 1614 cm^{-1} and -COOH stretching of MA at 1721 cm^{-1}. On the other hand, IR data of the fibers formed at pH 4 shows a peak at 1624 cm^{-1} which corresponds to PEOX carbonyl stretching and a shoulder at 1580 cm^{-1} corresponding to asymmetric stretching vibration of the carboxylate group of MA. In IR spectra of PEOX / MA fibers no shoulder at 1695 cm^{-1} is observed unlike IR spectra of MA. This is due to the absence of intermolecular H-bonds between MA molecules.

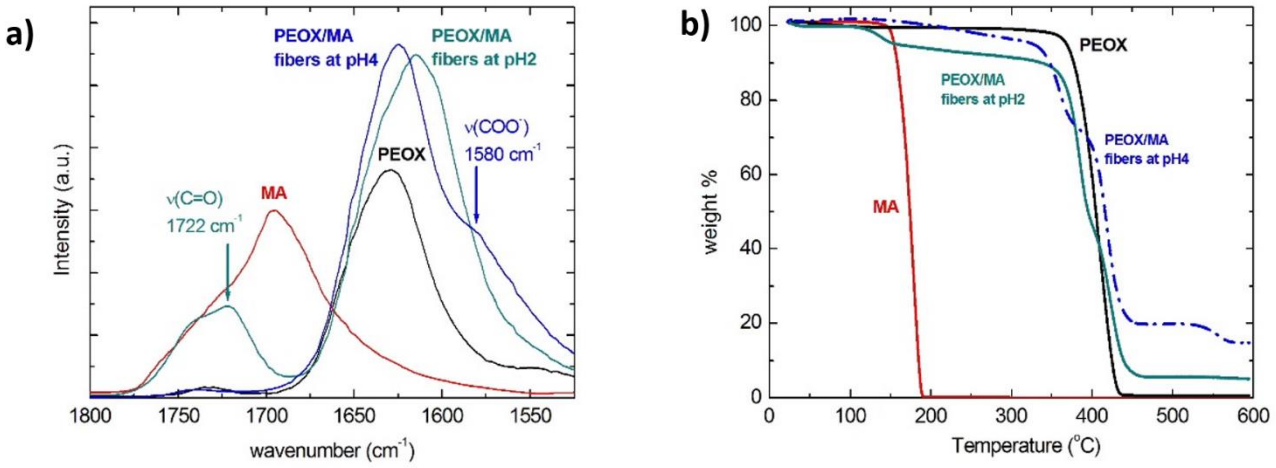

Figure 7.6: (a) IR data of dried PEOX/MA fibers formed at pH 2 and at pH 4 together with that of PEOX and MA **(b)** TGA data of dried PEOX/MA fibers formed at pH 2 and at pH 4 together with that of PEOX and MA.

The presence of carboxylate peak in the IR spectrum of fibers at pH 4 suggests that fibers consisted of carboxylate ($-COO^-$) groups. Thus, it was speculated that in the fibers at pH 4, electrostatic attraction between the negatively charged carboxylate and amide (-N-C=O) group of PEOX is present. On the other hand, no -COOH stretching vibration band could be observed in the IR spectrum of fibers formed at pH 4. This is due to the ionization of carboxylic acid groups to carboxylate ions. Then, complexation of carboxylate ions with the amide group of PEOX decreases the concentration of COO^- ions in the solution. As a result, there is not enough -COOH

concentration to observe -COOH stretching band in the IR spectrum. In a previous work, a similar result was also obtained from the complexation of poly (acrylamide) and PAA via H-bonds [273]. In this work, the shift was in favor of carboxylic acid groups. -COOH ionization leads to the increase of carboxylate concentration so that electrostatic interaction between carboxylate ions and amide groups of PEOX resulted in bridging of PEOX molecules through this complexation.

Similarly, TGA data of PEOX / MA fibers in Figure 7.6 (b) illustrates differences in the thermal properties of the fibers formed at pH 2 and pH 4. Both fibers that were formed at pH 2 and pH have two decomposition temperature. The first decomposition temperature in the range of 100-200°C corresponds to the presence of MA while the second one in the range of 330-450°C corresponds to the presence of PEOX. At 330°C, the weight loss of the fibers formed at pH 2 is ~9.5%, while the weight loss is ~5% for the fibers formed at pH 4. At 400°C, both fibers exhibit double transition with a shoulder unlike PEOX. First weight loss around 400°C is due to the complexation of PEOX with MA molecules. The first weight loss below 400°C was ~53.2% for the fibers formed at pH2 and ~32.3% for the fibers formed at pH 4 which are consistent with the weight loss of MA. The weight loss above 400°C is related with the loss of PEOX chains which are the parts that didn't interact with MA molecules. Above 450°C, some residue of the fibers remained as observed from TGA data. The presence of residue is due to the presence of sodium salts as a result of using NaOH to adjust pH. In addition, sodium carbonate remained as a residue at 700°C in the final phase as TGA measurements were done in air [288].

Hollow fibers formed as a result of bridging PEOX chains by MA molecules, either via H-bonds at pH 2 or via electrostatic interactions at pH 4. Through these interactions between PEOX and MA, first planar sheets form and then, these planar sheets curl into hollow fibers with time as observed in PEOX / TA LbL films [242]. Planar sheets curl into hollow fibers as a result of induced stress which derived from chemical anisotropy. This chemical anisotropy is due to the orientation of ethyl side chains of PEOX molecules so hydrophobic interactions were induced between these groups. Hydrophobic interactions in aqueous solution bring two opposite sides together so that interface between hydrophobic / aqueous side is minimized via bending the planar sheets. Then, curled fibers grow into hollow fibers with time in a dynamic attachment / detachment process. For this system, development of aggregates into hollow fibers happened after ~7 days.

In summary, when pH of the aqueous solutions is below or between the two pKa values of MA, hollow fibers of PEOX / MA form as a result of chemical anisotropy. The mechanism of fiber formation is different at pH 2 or pH 4. At pH 2, fibers form as a result of bridging of PEOX chains via H-bonding between carboxylic acid groups of MA and amide groups of PEOX while at pH 4, the dominant mechanism is the electrostatic interaction between carboxylate groups of MA and amide groups of PEOX.

7.3.3 Effect of Temperature on the Formation of Hydrogen Bonded PEOX and Malonic Acid Fibers

To investigate the temperature effect on the fiber formation of PEOX and MA, PEOX and MA aqueous solutions were prepared separately and mixed. Final concentrations of PEOX and MA were 0.4 mg/mL and 0.05 M respectively. Temperature selection was based on T_{cp} (~62°C) of PEOX: 70°C and 4°C were selected due to being higher and lower than LCST of PEOX polymer. Table 7.1 compares the fiber formation in PEOX / MA solutions at the indicated temperatures. To ensure whether fiber formation occurs at the indicated temperatures, fiber formation was observed for ~1 month. Aqueous solutions of PEOX and MA were kept at the incubator.

Table 7.1: Observation of fiber formation from PEOX and MA solutions prepared at different temperature based on LCST of PEOX (X= no fiber formation)

PEOX conc. (mg/mL)	**Mal.A. conc. (M)**	**pH**	**Temperature (°C)**	**Fiber Formation**
0.4	0.05	2	4	X
0.4	0.05	2	25 (RT)	✓
0.4	0.05	2	70	X
0.4	0.05	4	4	X
0.4	0.05	4	25 (RT)	✓
0.4	0.05	4	70	X

At 70°C, above T_{cp} of PEOX, fiber formation was not observed but the prepared solutions were cloudy and turbid. Above T_{cp}, the conformation of PEOX chains change from tight coils to globules and PEOX chains were dehydrated. This resulted in the dominance of hydrophobic interactions between PEOX molecules. At the same time, due to the globular conformation adopted by PEOX molecules, accessibility of carbonyl groups of PEOX by MA molecules were hindered. In this case, no fibers or any visible aggregates were formed since neither hydrogen bonding nor electrostatic interactions at pH 2 or pH 4 took place to trigger fiber formation mechanism.

At 4°C, below T_{cp} of PEOX, fiber formation was also not observed. This can be due to the enhanced solubility of PEOX in water as the temperature decreases. Enhanced solubility of PEOX was accompanied with increased number of H-bonds between PEOX and water molecules. In this case, PEOX chains preferably interact with water molecules rather than MA molecules. As a result, PEOX chains were surrounded by water molecules and accessibility of MA molecules to reach amide groups of PEOX was prevented.

In order to support the observations about the effect of temperature on the self -assembly of PEOX and MA, ITC experiments were conducted. 10 mg / mL PEOX and 0.25 mg / mL MA solutions were separately prepared in water and placed into cell and syringe, respectively. To investigate the temperature effect, ITC temperature was set to 70°C and 6°C respectively. ITC results were presented in Figure 7.7 and Table 7.2.

Raw data of the ITC experiment at 70°C was not shown in Figure 7.7 since no interaction between PEOX and MA was detected. This result supports our previous observations in aqueous solutions. No interaction was detected by the instrument above T_{cp} of PEOX. As presented in Table 7.2, free energy of complexation was driven by entropy. Conformation change of PEOX molecules led to dominancy of hydrophobic interactions and an entropy driven process. Interactions between PEOX and MA molecules were almost inhibited and PEOX chains interacted via hydrophobic interactions. When ITC experiment was conducted in 6°C, enthalpy of PEOX / MA interaction (-37.26 kJ/mol) is lower when compared with the experiment in which temperature was set to room temperature. This further supports the hypothesis about enhanced solubility with decreasing temperature. At 6°C, solubility of PEOX chains in water was more than at RT, so that PEOX

chains tend to interact more with water molecules instead of MA molecules. As observed from the mixed solution, weakly interacting PEOX chains and MA molecules would not result in a self-assembly process where the fiber formation could not be observed at 6°C. One possible reason is that the dynamic self-assembly process of PEOX and MA is so slow that due to kinetic limitations, fiber formation could not be observed in one month.

Table 7.2: Thermodynamic parameters (ΔH, ΔS and ΔG) of the interaction between PEOX and MA at different temperature

Temperature (°C)	**ΔH (kJ /mol)**	**ΔS (J / mol K)**	**ΔG (kJ / mol)**
6	-37.26	-39.42	-26.25
70	0	57.43	-19.71

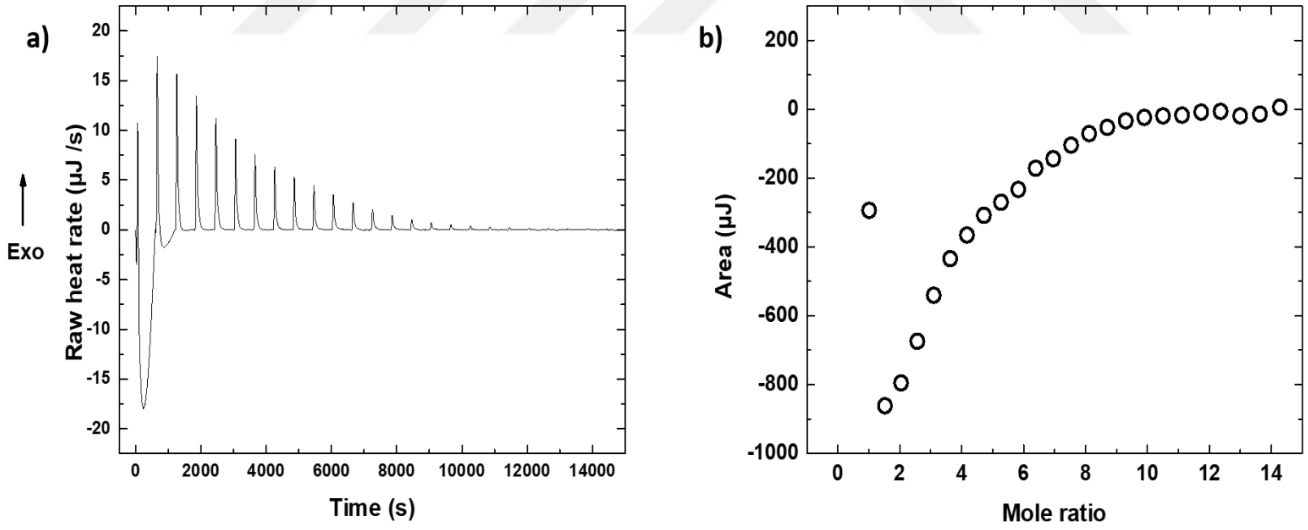

Figure 7.7: (a) Raw ITC data of the interaction between MA (2.4 mM, pH2.5) to PEOX (0.05 mM, pH2.5) at 6^{o}C. **(b)** Released heat versus mole ratio (MA / PEOX) of the interaction between MA (2.4 mM, pH2.5) and PEOX (0.05 mM, pH2.5) at 6^{o}C. Curve fitting is made according to independent binding model and ΔH, ΔS and ΔG values are -37.26 kJ/mole, -39.42 J / mole K and -26.25 kJ/ mole.

7.3.4 Effect of Salt Type on the Formation of Hydrogen Bonded PEOX and Malonic Acid Fibers

To investigate the effect of salt type on the fiber formation, first, aqueous solutions of PEOX (0.8 mg/mL) and MA (0.1 M) were prepared in either 0.1 M Na_2CO_3, 0.1 M NaCl or 0.1 M NaSCN solutions separately. Equal volumes of PEOX and MA which were prepared in salt solutions were taken and then, mixed. Final concentrations of PEOX and MA in the mixed solutions were 0.4 mg/mL and 0.05 M. Based on the visual observations during a period of one month, Table 7.3 compares the fiber formation of PEOX / MA solutions prepared in different sodium salt solutions.

Table 7.3: Observation of fiber formation from PEOX and MA mixed solutions prepared in different 0.1 M salt solutions

PEOX conc. (mg/mL)	**Malonic acid conc. (M)**	**pH**	**Salt type used**	**Fiber Formation**
0.4	0.05	2	0.1 M Na_2CO_3	**X**
0.4	0.05	2	0.1 M NaCl	**X**
0.4	0.05	2	0.1 M NaSCN	✓
0.4	0.05	4	0.1 M Na_2CO_3	✓
0.4	0.05	4	0.1 M NaCl	✓
0.4	0.05	4	0.1 M NaSCN	✓

From the mixed solutions, in which fiber formation was observed, fibers were collected and washed several times. After washing them, fibers were dried under open air and SEM analysis was done. Figure 7.8 illustrates SEM images of the fibers that were formed in the presence of different sodium salts.

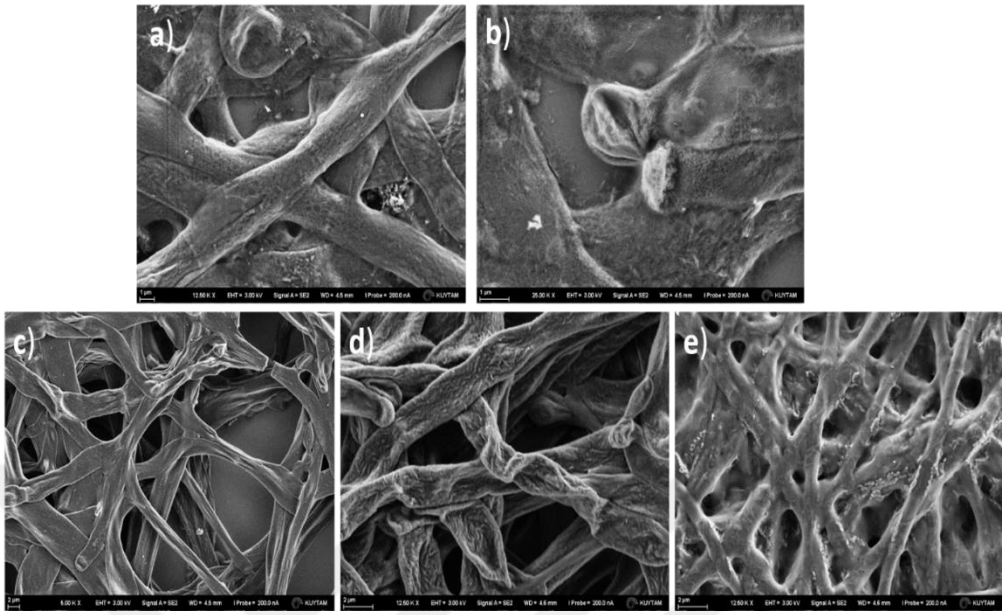

Figure 7.8: (a), (b) SEM images of the fibers formed in 0.1 M NaSCN solution at pH 2. Scale bar for (a) and (b) is 1 µm. **(c)** SEM images of the fibers formed in 0.1 M Na_2CO_3 solution at pH 4 **(d)** SEM images of the fibers formed in 0.1 M NaCl at pH4 **(e)** SEM images of the fibers formed in 0.1 M NaSCN at pH 4. Scale bar for (a) and (b) is 1 µm. Scale bar for (c), (d) and (e) is 2 µm.

At pH 2, only in the presence of NaSCN, PEOX/ MA fibers form as shown in Figure 7.8 (a) and (b). This is due to the different nature of NaSCN than NaCl or Na_2CO_3. SCN^- is the most chaotropic ion while Cl^- and CO_3^{2-} ions have kosmotropic nature according to Hofmeister series of salt. SCN^- ions bind to the hydrophobic cavity of PEOX molecules and make the polymer carbonyl groups more available and open for malonic acid [89]. As a result, in the presence of NaSCN solution, stronger H-bonds form between PEOX and MA in aqueous solutions. On the other hand, kosmotropic salts like Na_2CO_3 and NaCl dehydrate PEOX chains. At the same time, Cl^- and CO_3^{2-} ions tend to interact more with protonated MA molecules through electrostatic interactions. This would inhibit the formation of strong H-bonds between carbonyl groups of PEOX and carboxylic acid groups of malonic acid.

At pH 4, in the presence of all salt solutions, fiber formation is observed. However, in the presence of sodium salts, the morphology of the formed fibers was different. As shown in Figure 7.8 (c) – (e), formed fibers have flat morphology instead of being hollow when PEOX and MA interact in aqueous solution without any salt ions. This difference in morphology is due to the

"screening effect" of the added negatively charged ions. With this screening effect, repulsion between negatively charged carboxylate groups of MA molecules become less. This results in less stress and chemical anisotropy in the fiber structure so bending of them would not occur to result in a hollow structure. Another result of the screening effect is the aggregation of the self-assembled structures (fibers) due to the reduced repulsion. Unlike kosmotropic ions, SCN^- ions tend to bind to PEOX chains, making the carbonyl groups more available for MA molecules for the interaction. At pH 4, fibers were less in amount and thinner in the presence of NaSCN. This difference is in amount of fibers is due to the weaker H-bonds formed between MA and PEOX at pH 4 due to the ionization of the one carboxylic acid end of the MA molecules. In conclusion, difference in the amounts of fibers between pH 2 and pH 4 is due to the weaker H-bond formation between PEOX and MA with increasing pH and ionization of the one carboxylic acid group in MA.

To test our observations and to determine the thermodynamic parameters of interaction between PEOX and MA in the presence of salt, ITC experiments were conducted. Results of the ITC experiment were presented in Table 7.4 and Figure 7.9. In the presence of all ions, the complexation of PEOX and MA is enthalpy driven. When the enthalpy of the complexation of PEOX and MA were evaluated in the presence of Na_2CO_3, NaCl and NaSCN, highest enthalpy of interaction (ΔH) was obtained in the presence of SCN^- ions, even higher than the enthalpy value when PEOX and MA were complexed in aqueous solutions. This is related with the ability of SCN^- ions to make carbonyl groups of PEOX more available for MA molecules to bind it and interact because of chaotropic character of SCN^- ions. More favourable binding of MA molecules to PEOX chains in the presence of SCN^- ions is also evident from the increase of free energy of complexation of MA and PEOX. In the presence of CO_3^{2-} and Cl^-, saturation for the binding of MA to PEOX chains was reached more quickly. Enthalpic contribution to the free energy of complexation is relatively less and in the presence of kosmotropic ions, CO_3^{2-} and Cl^- ions compared to SCN^- ions. Triggered hydrophobic interactions with the dehydration of PEOX chains by the kosmotropic CO_3^{2-} and Cl^- ions decreases the relative contribution of enthalpy of the complexation between PEOX and MA via H-bonds.

Table 7.4: Thermodynamic parameters (ΔH, ΔS and ΔG) of the interaction between PEOX and MA in the presence of different sodium salts at 25°C

Salt Type (0.1 M)	ΔH (kJ /mol)	ΔS (J / mol K)	ΔG (kJ / mol)
Na_2CO_3	-52.07	-117.2	-17.12
NaCl	-65.83	-136.7	-25.08
NaSCN	-100	-250.3	-25.37

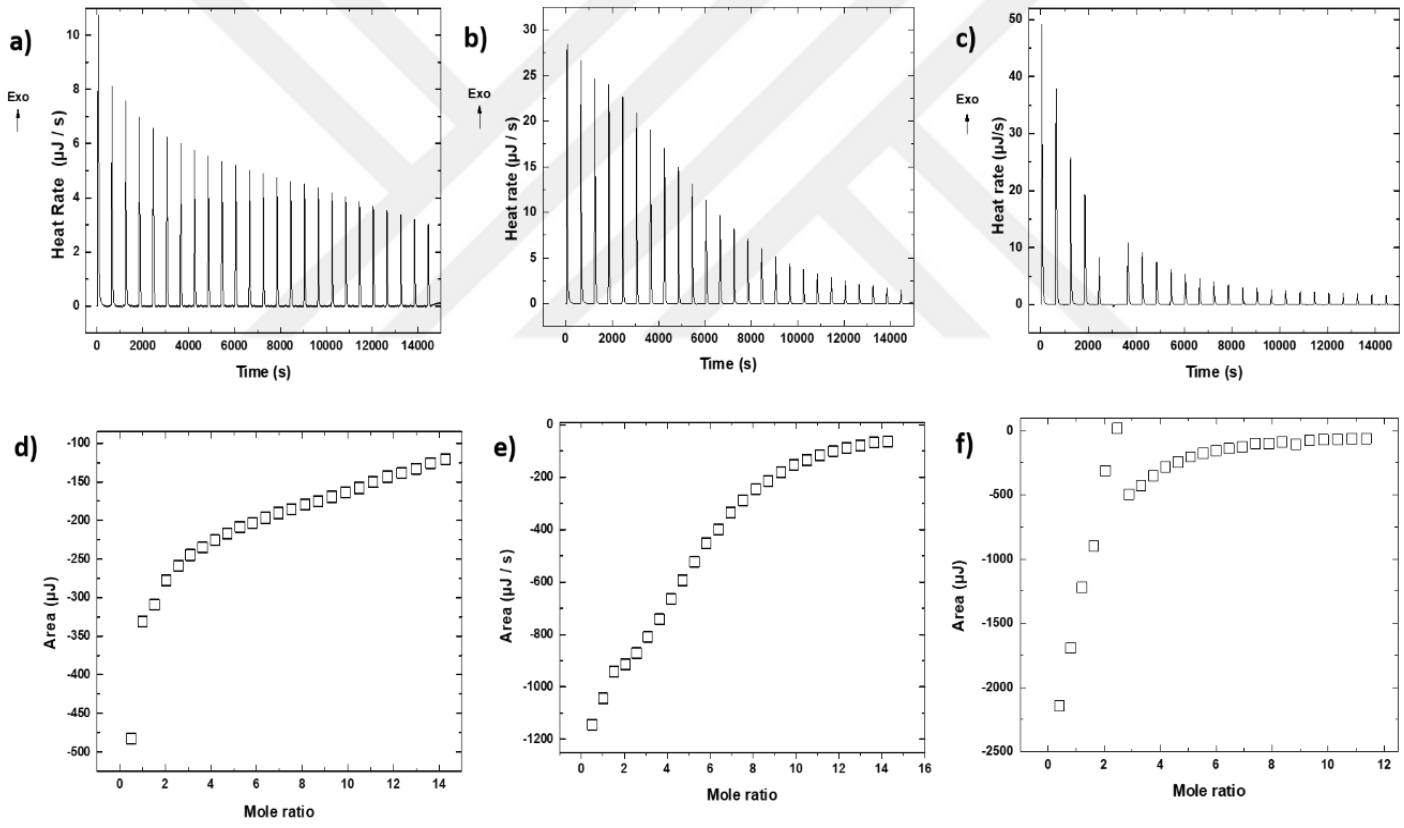

Figure 7.9: (a), (b) and (c) Raw ITC data of the interaction between MA (2.4 mM, pH2.5) to PEOX (0.05 mM, pH2.5) in the presence of Na_2CO_3 (a), NaCl (b) and NaSCN (c). **(d), (e) and (f)** Released heat versus mole ratio (MA / PEOX) of the interaction between MA (2.4 mM, pH2.5) and PEOX (0.05 mM, pH2.5) in the presence of Na_2CO_3 (a), NaCl (b) and NaSCN (c).

7.4 Conclusions

PEOX and MA hollow fibers were formed as a result of the assembly between PEOX and MA. pH has a pronounced effect on the formation of hollow fibers. At pH 2, the driving force for the fiber formation is H-bonding since both carboxylic acid ends of MA molecules are protonated and able to donate protons to form H-bonds with PEOX. The presence of H-bonds in the fibers were also evident from IR data as the downshift of -C=O stretching of PEOX is 15 cm^{-1} and -COOH stretching of MA. At the same time, from IR data, based on the data of PEOX / MA blends, the mole ratio of PEOX to MA was determined as 8.3. TGA data also confirmed the presence of both PEOX and MA in the fibers as two decomposition temperature was observed around 100-150°C and 350-450°C. The interaction of the complexation between PEOX and MA was determined by ITC and complexation was enthalpy driven. The enthalpy of the interaction was determined as -49.39 kJ/mol.

At pH 4, PEOX / MA hollow fibers were also formed. pH 4 is between the two pKa values of MA, so one end of MA is protonated while the other end is ionized. IR data of fibers formed at pH 4, -COOH peak was not observed while asymmetric stretching of carboxylate ($-COO^-$) group was dominant. This shows that the dominant mechanism for the fiber formation is the bridging of PEOX chains via electrostatic interactions. At pH 7, few fibers were formed with flat morphology and the possible mechanism is electrostatic interaction between carboxylate and amide groups of PEOX. However, fiber amount was not enough for further investigation and characterization. pH induced formation of PEOX / MA fibers with different morphologies show that fibers were pH responsive.

The effect of temperature on the fiber formation was also examined. Both below T_{cp} (6°C) and above T_{cp} (70°C), fiber formation between PEOX and MA was not observed. At 6°C, enhanced solubility of PEOX in water inhibits complexation of PEOX and MA. On the other hand, above LCST, conformational change of tight coils of PEOX to globular form induces hydrophobic interactions between them and hinders the accessibility of amide groups of PEOX to carboxylic acid groups of MA molecules. Interaction parameters of the complexation of PEOX and MA were also determined by using ITC and quantitative observations were confirmed by ITC results. While at 70°C, complexation of PEOX and MA was an entropy driven process, at 6°C, enthalpy of

complexation was rather small compared to the enthalpy of the complexation of PEOX and MA at RT.

To investigate the effect of the salt type, three sodium salts from Hofmeister series were selected: Na_2CO_3 (most kosmotropic salt), NaCl (located in the middle of Hofmeister series) and NaSCN (most chaotropic salt). At pH 2, fiber formation was only observed in the presence of NaSCN while at pH 4, fibers were formed in the presence of all salts. This is due to the different mechanisms involved due to the nature of salts. SCN^- is a chaotropic ion so that these ions bind to the hydrophobic cavity of PEOX molecules and make carbonyl groups more available for MA molecules to bind. At pH 4, non-hollow morphology and aggregated form of fibers are due to the screening effect induced by ions. With screening effect, repulsion between fibrous aggregates were reduced. Reduced repulsion between negatively charged carboxylate ends of MA also induces less chemical anisotropy and stress in the self-assembled structures which resulted in flat morphology of the fibers formed at pH 4. Salt effect on the self-assembly of PEOX and MA was also investigated by ITC. Highest enthalpy of the interaction between PEOX and MA were obtained in the presence of SCN^- ions as expected.

In conclusion, self-assembly of PEOX and a small dicarboxylic acid, MA resulted in the formation of pH and temperature responsive hollow fibers. Stimuli responsive hollow fibers can be used as templates for biomedical applications such as functional molecule loading, drug encapsulation and release of the functional cargo. Further studies could be done to uncover the mechanism of such fiber formation and study the potential applications of hollow PEOX / MA fibers.

Chapter 8: Encapsulation and Release of Ciprofloxacin from PEOX / Malonic Acid Fibers

8.1 Overview

In Chapter 7, pH responsive hollow PEOX / MA fibers formed through self-assembly of PEOX and MA in aqueous solutions via forming H-bonds were reported. Formation of hollow fibers are especially useful in biomedical applications such as functional cargo loading and release.

Nanofibers are frequently used as templates for drug encapsulation and drug release due to the advantages they offer. Main advantages of nanofibers are that the morphology, structure and composition of them can be easily tailored to obtain a sustained drug release kinetics, high surface area to volume ratio for loading high amount of drug and protection of the drug from decomposition before arriving the target site [232]. In the literature, generally fibers produced from electrospinning process are used for drug release applications.

In this work, for the first time, hollow fibers that were produced from self-assembly process in aqueous solutions were used as reservoirs for drug storage and release applications. The objective of this work is to show the potential of PEOX / MA fibers to be used in biomedical applications. These fibers can be used as reservoirs for the encapsulation and pH-responsive release of the drug to the body. Especially, insertion of the drug loaded fibers to the target side in the body can be very useful for wound healing applications.

To test the drug loading and release properties of PEOX / MA fibers for the wound healing application in the body, ciprofloxacin (Cipro) is selected as an antibiotic and anti-bacterial agent. Ciprofloxacin is a broad-spectrum antibiotic that is effective against most of both gram negative and gram positive bacteria [289], [290]. It is especially effective when orally and intravenously administered to the body. pKa of Cipro is 6.09, close to the physiological pH of the body, and has a UV absorption peak around 275 nm. It is a hydrophilic and water-soluble molecule and has both hydrogen donor and hydrogen acceptor groups. The chemical structure of Cipro is illustrated in Figure 8.1. Immediate and burst release of Cipro can result in harmful side effects in the body [291]. Thus, it is necessary to produce a release platform so that controlled and prolonged release

of the antibiotic to the target site in the body can be achieved. It is expected that PEOX / MA fibers can be great candidates to achieve this objective due to the simplicity of the method for the formation of fibers, high amount of loading of the target molecule and potential for the prolonged release of the hydrophilic antibiotic molecule.

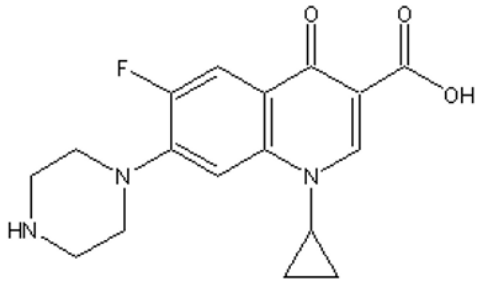

Figure 8.1: Chemical structure of Ciprofloxacin

8.2 Experimental Details

8.2.1 Preparation of PEOX / MA Fibers

For the formation of PEOX / MA fibers, PEOX solutions in water having two different concentrations (0.8 mg / mL and 10 mg/ mL) and 0.1 M MA solution were prepared separately. Then, equal volumes from PEOX and MA solutions were taken and mixed. pH of the mixed solution was adjusted to ~4. As a result, for the formation of fibers, two different sets of mixture solutions were prepared. In one set of the mixed solution, final concentration of PEOX and MA is 5 mg/mL and 0.05 M while in the second set of the mixed solution, final concentration of PEOX and MA is 0.4 mg/mL and 0.05 M. As a reference, PEOX solution at 10 mg/mL were prepared and PEOX fibers without MA were formed in room temperature. After ~7 days, tiny aggregates were formed both in MA containing PEOX solutions and PEOX solution. After ~21 days, tiny aggregates were grown into larger aggregates in fiber form. PEOX / MA fibers were collected

from the mixture solutions and washed with DI water several times. PEOX fibers were also washed with DI water.

8.2.2 Loading and Release of Cipro from PEOX / MA Fibers

First, calibration curve of Cipro was prepared using UV-Vis Spectrometry (PG T80). Aqueous solutions of Cipro having different concentrations (2, 4, 6, 8 and 10 µg/mL) were prepared and absorbance of the prepared solutions at 275 nm was measured. Before loading Cipro into fibers, dried PEOX / MA fibers having different PEOX concentrations were put in a petri dish and weighed with digital balance. Dried fibers were placed in 10 µg/mL Cipro solution for 5 hours. Every 1 hour, fibers were taken out with Pasteur pipettes from Cipro solution and absorbance of Cipro solution was measured with UV-Vis Spectrometry. Fibers were washed with DI water to get rid of loosely bound drug molecules and dried. Then, Cipro solution was refreshed after each measurement and fibers were put back into solution. After 5 hours, post-treatment of fibers with Cipro solution and loading of the fibers with the drug was completed as observed by the steady absorption at 275 nm of Cipro solution into which the fibers were immersed. After 5 hours, drug loaded fibers were dried and weighed again.

Thermodynamic interaction parameters between PEOX and Cipro was determined by ITC (TA Instruments Affinity). The temperature of ITC experiment was set to 25°C. Two different ITC experiments with Cipro solutions having different concentrations (0.1 and 0.2 mg/mL) were conducted. 0.05 mM PEOX aqueous solution was placed in sample cell (960µL) and 0.1 or 0.2 mg/mL aqueous MA solution was placed in syringe (250µL). The titration was achieved by injection of Cipro solution in the syringe to the PEOX solution in the sample cell using 25 titrations, 10 µL aliquots in each titration. Between each injection, there was 10 min intervals for equilibration. To ensure uniform mixing, the sample cell was continuously stirred at 125 rpm. Each injection produces a characteristic peak due to the absorbed or released heat.

To obtain pH induced release profile of Cipro from PEOX / MA fibers and PEOX fibers, PBS solution at pH~ 7.4 was prepared. Drug loaded fibers were immersed into PBS solutions. To quantify the released amount of drug, every hour, absorption of PBS solution at 275 nm were measured for 9 hours with UV-Vis Spectroscopy (PG T80). Morphology of the fibers was checked

both after the loading of the drug into fibers and after the release of the drug from fibers with FESEM (Zeiss Ultra Plus SEM).

8.3 Results and Discussion

8.3.1 Encapsulation of Ciprofloxacin into PEOX / MA Fibers

A calibration curve of Ciprofloxacin was obtained using UV-Vis Spectrometry to relate the concentration of the drug to the absorbance at 275 nm, at the maximum peak of the absorbance. The calibration curve of Cipro establishes the linear relationship between absorbance at 275 nm and concentration of the drug. The linear fit to the calibration curve of Cipro is almost perfect with R^2 equal to 0.999.

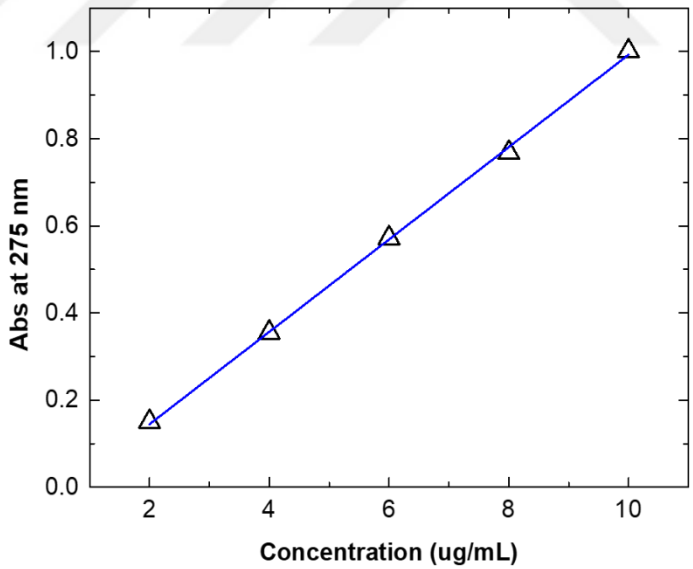

Figure 8.2: Calibration curve of aqueous Ciprofloxacin solution in terms of absorbance at 275 nm as a function of concentration measured by UV-Vis Spectroscopy

After the calibration curve of Cipro was prepared, PEOX / MA fibers formed at pH 4 were used as reservoirs to load the drug. Hollow structure of the fibers is an advantage for loading high

amount of drug and high storage capacity due to increased surface area [292], [293]. At pH 4, PEOX / MA fibers were formed as a result of electrostatic bridging of carboxylate groups of MA and amide groups of PEOX [278]. Hollow structure in the fibers was obtained as a result of chemical anisotropy and induced stress [278], [242]. Chemical structure of the fibers at pH 4 allows drug loading into fibers through H-bonding between PEOX / MA fibers and Ciprofloxacin. At pH 4, hydrogen donor groups of Cipro are protonated so this can provide possible H-bond formation between amide groups of PEOX and Cipro.

Dried PEOX / MA fibers having different PEOX contents and PEOX fibers were weighed. Two different sets of fibers were prepared for measurement and in these sets, PEOX/MA fibers having different PEOX contents and PEOX fibers have approximately same mass.

Figure 8.3 shows the concentration of Cipro loaded into fibers versus time. Concentration of the loaded Cipro into fibers was determined based on the calibration curve of the drug. After each measurement with UV-Vis spectrometry of the Cipro solution in which fibers were immersed was refreshed and fibers were washed several times to get rid of loosely bounded dye molecules. Total loading time of the drug was limited to 5 hours since after 5 hours, concentration of Cipro that was loaded in the fibers remained constant. As shown, Figure 8.3, concentration of the loaded drug reaches to a saturation point as the loading time approaches to 5 hours.

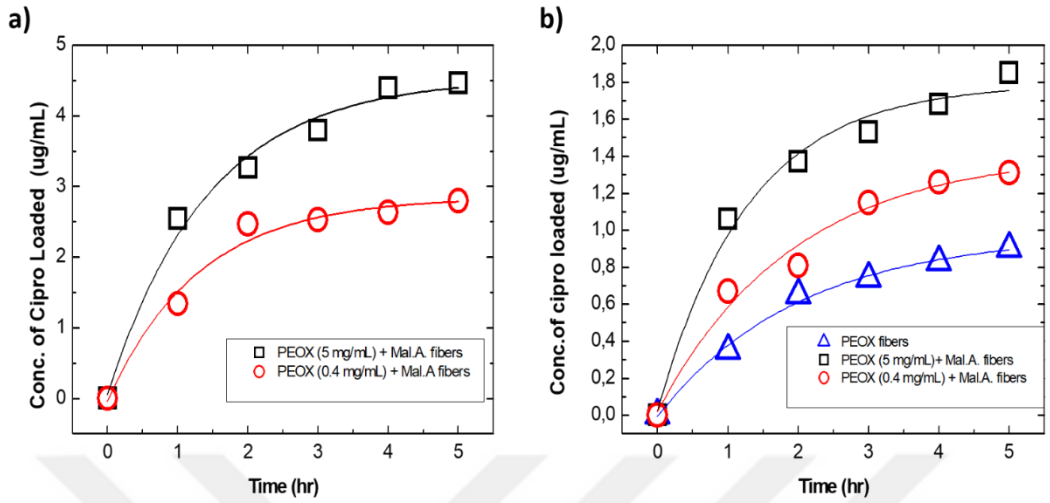

Figure 8.3: (a) Ciprofloxacin loading to sample set 1 in terms of concentration of cipro loaded (µg / mL) versus time (hours). Sample set 1 contains PEOX (5 mg/mL) / MA fibers (0.0220 g) and PEOX (0.4 mg/ mL) / MA fibers (0.0222 g). **(b)** Ciprofloxacin loading to sample set 2 in terms of concentration of cipro loaded (µg / mL) versus time (hours). Sample set 2 contains PEOX (5 mg/mL) / MA fibers (0.0118 g) and PEOX (0.4 mg/ mL) / MA fibers (0.0120 g) and PEOX fiber (0.0118 g)

From Figure 8.3, it can be concluded that Cipro was loaded successfully into three types of fibers. Loaded amount of drug into the fibers was calculated as 1.182 mg Cipro / gram of fiber, 2.793 mg Cipro / gram of fiber and 0.076 mg Cipro / gram of fiber for PEOX (0.4 mg/mL)/ MA, PEOX (5 mg/mL)/ MA and PEOX fibers respectively. Even though, Cipro was loaded into all three types of fibers, loading of the drug was more in PEOX / MA fibers compared to PEOX fibers. Higher loading of Cipro into PEOX / MA fibers is due to the two reasons. First, morphological difference between PEOX and PEOX / MA fibers resulted in higher loading into PEOX/ MA fibers. PEOX fibers were formed with the crystallization process and have a dense, flat ribbon-like morphology. On the other hand, PEOX / MA fibers are hollow so that surface area of the PEOX / MA fibers is higher compared to PEOX fibers. As a result, increased surface area results in more loading of the drug into the fibers. The second reason is that in PEOX fibers, carbonyl groups are not exposed and open along the outer surface so H-bonding between PEOX chains and drug

molecules cannot be formed easily. Less number of H-bonds between PEOX chains and drug molecules resulted in much less loading into PEOX fibers [283].

It was also shown that as the mass or amount of the fibers increases, loading amount of the drug also increased into the fibers when Figure 8.3 (a) and 8.3 (b) were compared. Encapsulation of drug molecules into the fibers can be a result of both the attachment of drug molecules on the walls of the fibers and the favorable interaction between Cipro and components of the fibers. For PEOX / MA fibers, as the PEOX content or concentration in the fibers increased, loading amount of the drug was more. It was assumed that Cipro interacts more favorably with PEOX, probably forming H-bonds with the amide groups of PEOX. This assumption is due to the fiber formation occurred at pH 4, in which one of the carboxylic acid groups of MA is ionized and the other protonated carboxylic acid group is bridged to the amide group of PEOX via H-bonds. To verify the favorable interaction between PEOX and Cipro, ITC experiment was conducted. Results of the ITC experiment were shown in Figure 8.4.

Figure 8.4 illustrates ITC data of the interaction between Cipro (0.3 mM and 0.6 mM) and PEOX (0.05 mM). When Cipro concentration was 0.3 mM, thermodynamic interaction parameters (ΔH, ΔS and ΔG) values are -100 kJ/mol, -248.3 J/mol K and -25.98 kJ/mol respectively. At Cipro concentration was 0.3 mM, thermodynamic interaction parameters (ΔH, ΔS and ΔG) values are -100 kJ/mol, -248.3 J/mol K and -25.98 kJ/mol respectively. At 0.6 mM Cipro, thermodynamic interaction parameters (ΔH, ΔS and ΔG) values are -39.66 kJ/mol -54.79 J/mol K and -23.32 kJ/mol, respectively. At both concentrations of Cipro, the interaction between PEOX and Cipro is enthalpy driven and the binding of drug molecules to PEOX is a favorable thermodynamic process. The decrease in the enthalpy and free energy with increasing Cipro concentration indicates that binding of drug molecules reaches to a saturation value. It was evident in these results that the interaction between PEOX and Ciprofloxacin was favorable. The favorable interaction was probably due to the formation of H-bonds between the amide groups of PEOX and hydroxyl or amine groups of Ciprofloxacin. H-bond formation between MA and Cipro is also possible in PEOX / MA fibers. At pH 4, since one end of MA molecule is ionized, H-bond formation between Cipro and MA would be less probable.

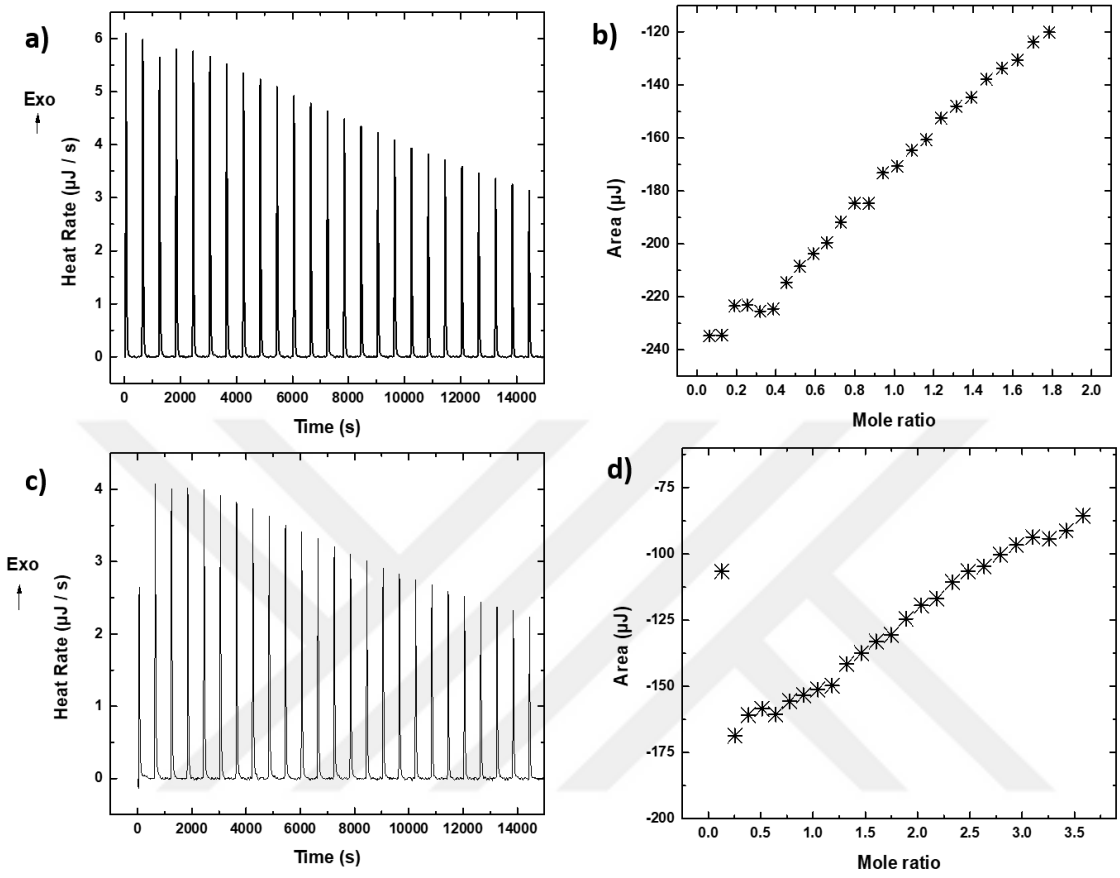

Figure 8.4: (a), (b) ITC data of the interaction between MA (0.3 mM, pH 4) to PEOX (0.05 mM, pH 4) at 25°C. **(a)** Raw data **(b)** Independent Model fit (solid line) corresponding to ΔH = -100 kJ/mol; ΔG = -25.98 kJ/mol; ΔS = -248.3 J/mol-K **(c), (d)** ITC data of the interaction between MA (0.6 mM, pH 4) to PEOX (0.05 mM, pH 4) at 25°C. **(a)** Raw data **(b)** Independent Model fit (solid line) corresponding to ΔH = -39.66 kJ/mol; ΔG = -23.32 kJ/mol; ΔS = -54.79 J/mol-K

Morphology of fibers before and after loading of Cipro was examined by SEM analysis. Analysis was done without any prior treatment. As observed from Figure 8.5 a-d, PEOX / MA fibers that contain two different concentrations of PEOX (0.4 mg / mL and 5 mg / mL) are hollow and inner side of the fibers are empty. After drug molecules are loaded, hollow fibers are partially filled. Some empty hollow fibers are also present (Figure 8.5 e-h). This indicates that Cipro molecules did not only adsorb on the walls of PEOX / MA fibers, but they also adsorbed inside

the fibers and filled them. FESEM images correlate well with the loading and ITC results that were presented above. Encapsulation of Ciprofloxacin into PEOX / MA fibers occurred due to the favorable interaction between the components of fibers and drug molecules. Some surface adsorption should also be present especially for empty hollow fibers in the FESEM images.

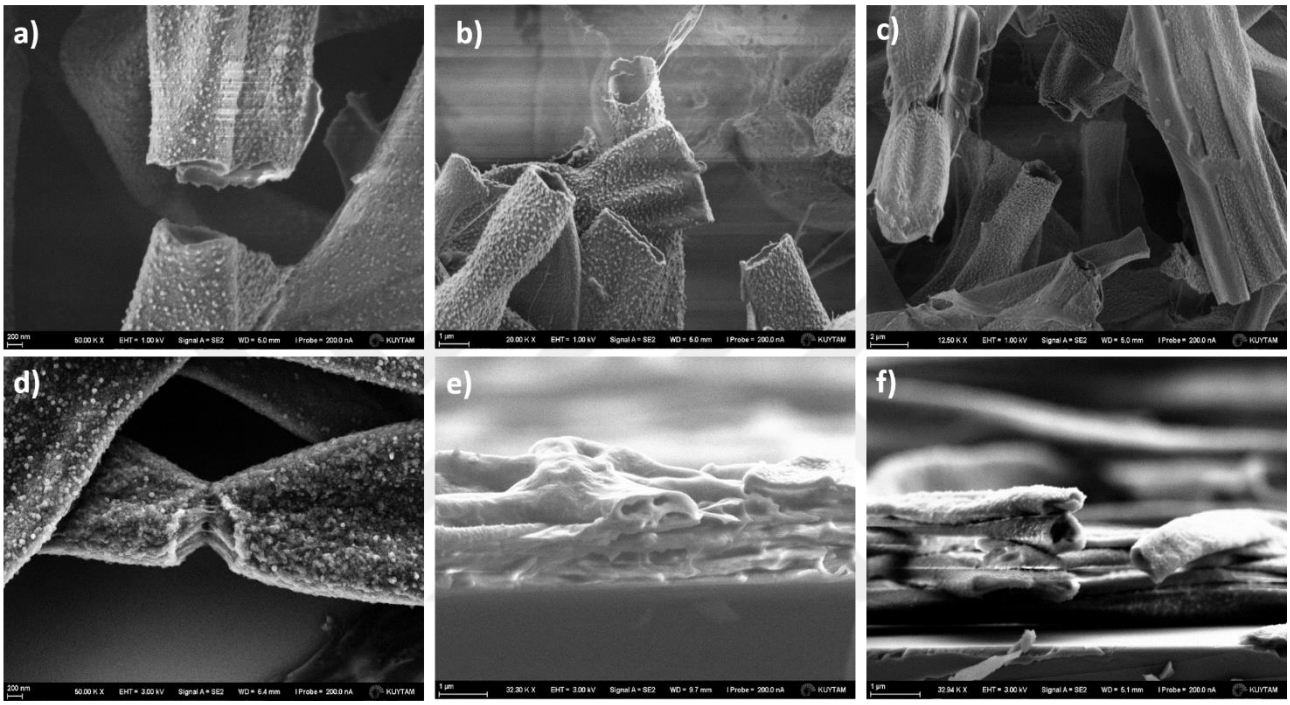

Figure 8.5: (a) SEM image of PEOX (0.4 mg/mL) / MA fibers before Ciprofloxacin loading. Scale bar is 200 nm. **(b)** SEM image of PEOX (0.4 mg/mL) / MA fibers before Ciprofloxacin loading. Scale bar is 1 µm. **(c)** SEM image of PEOX (5 mg/mL) / MA fibers before Ciprofloxacin loading. Scale bar is 2 µm. **(d)** SEM image of PEOX (0.4 mg/mL) / MA fibers after Ciprofloxacin loaded into them. Scale bar is 200 nm. **(e)** SEM image of PEOX (0.4 mg/mL) / MA fibers after Ciprofloxacin loaded into them. Scale bar is 1 µm. (**f)** SEM image of PEOX (5 mg/mL) / MA fibers after Ciprofloxacin loaded into them. Scale bar is 1 µm.

8.3.2 Release of Ciprofloxacin from PEOX / MA Fibers

To test the release of loaded Cipro from PEOX / MA fibers, PBS solutions were prepared to mimic the physiological conditions. PEOX / MA fibers that were prepared from two different

concentrations of PEOX and PEOX fibers were immersed in PBS solutions. Every hour, fibers loaded with drug molecules were taken out from PBS solutions and concentration of Ciprofloxacin was measured with UV-Vis Spectrometry by measuring the absorbance at 275 nm. Then, by using the calibration curve, concentration of the released drug molecules was determined. After the measurement with UV-Vis Spectroscopy, PBS solution was refresh and fibers were immersed again.

Figure 8.6 illustrates the release of Cipro from two different PEOX / MA fibers. Figure 8.6 (a) demonstrates the release of Cipro in terms of concentration of the drug versus time while in Figure 8.6 (b), release was shown as fraction of the drug released versus time. Release data of PEOX fibers was not shown since almost all drug molecules that were loaded into the fibers released almost in one hour. This means that when PEOX fibers were used as drug encapsulation templates, Cipro was released in a burst release manner. For PEOX / MA fibers, release of antibiotic molecules from these fibers occurred in a more controlled and prolonged way. Almost all Cipro molecules were released at the end of 8 hours from both of PEOX / MA fibers. However, for two fibers, the release profile was different. For PEOX (5 mg/mL) / MA fibers, zero order release kinetics was observed while for PEOX (0.4 mg/mL) / MA fibers, diffusion-limited release of the drug was observed. Differences in release kinetics would be explained in terms of structure-property relationship.

Burst release profile of Ciprofloxacin from PEOX fibers were related to the morphology that those fibers have. Since PEOX fibers have flat morphology, drug molecules could not be loaded into the interior parts of the fibers. Thus, loading of the drug molecules occur via simply physical adsorption on the walls of the fibers. The second reason is that C=O groups in PEOX fibers are along the long axis and not exposed much in outer surface. This decreases the possibility of H-bond formation between the Cipro molecules and PEOX chains. When PEOX fibers that were loaded with drug molecules are immersed into releasing medium, since drug molecules are weakly bound, diffusion of them into the releasing medium occurs in a fast manner.

Zero order release kinetics was observed in both PEOX / MA fibers. On the other hand, when PEOX concentration in the aqueous solution for the formation of fibers was 0.4 mg/mL, the release duration of the drug is shorter. This difference in the release profile was related to the difference in PEOX content in two type of fibers. Assuming higher PEOX content in PEOX (5

mg/mL) / MA fibers, number of hydrogen bonds between PEOX and Cipro molecules was more. As suggested in Figure 8.5, the diameter of PEOX (5 mg/mL) / MA fibers is smaller compared to PEOX (0.4 mg/mL) / MA fibers so higher release rate is not related with the surface area difference. At physiological pH, hydrogen bonds between PEOX and Cipro started to break so drug molecules release as a result of the degradation of H-bonds. When PEOX content in the fiber is low, dependence of the formation of H-bonds between PEOX and drug molecules for the encapsulation becomes less. Other than H-bond formation and physical adsorption, other mechanisms can also be effective and more prominent, such as physical interactions (electrostatic interactions) between Cipro and MA. As a result, the release of Cipro was limited to a concentration gradient between the releasing medium and inside the fibers but this would be a slower diffusion mechanism since the bonding of drug molecules to the fibers is not strong. This is related to the hollow structure of PEOX / MA fibers and their capacity to hold Cipro molecules inside the fibers. It can be concluded that differences in the release profile of Ciprofloxacin from fibrous structure was related to both morphology of the fibers and PEOX content in them.

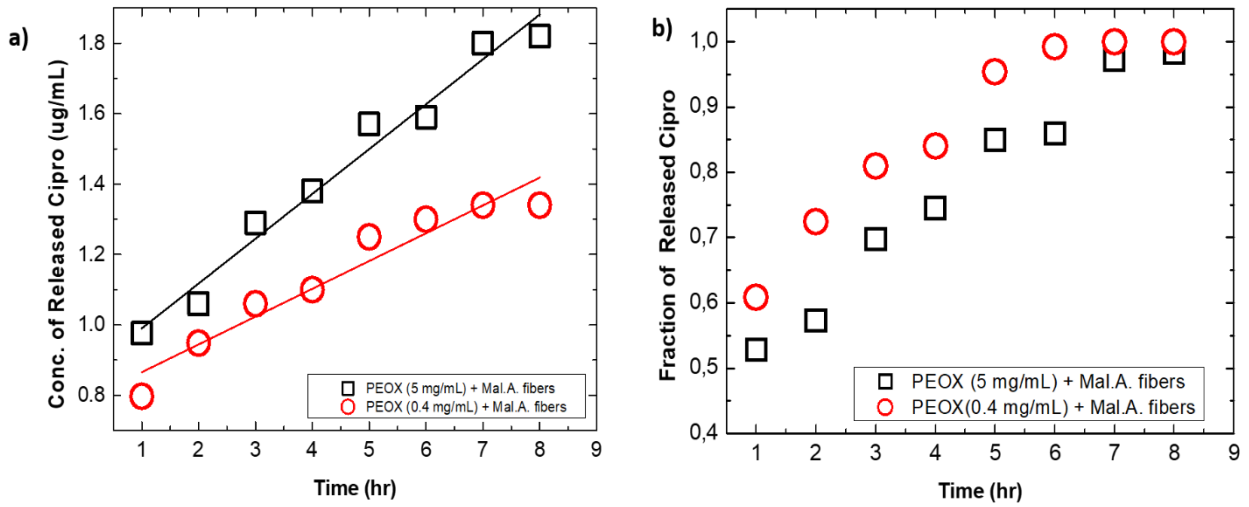

Figure 8.6: (a) Release profile of Ciprofloxacin from PEOX / MA fibers in PBS, at pH 7.4 in terms of concentration of released drug versus time **(b)** Release profile of Ciprofloxacin from PEOX / MA fibers in PBS, at pH 7.4 in terms of fraction of released drug versus time

8.4 Conclusions

The objective of this work was to show that hollow PEOX / MA fibers can be used as reservoirs for drug encapsulation and controlled release of them in biomedical applications. To reach this objective, a hydrophilic antibiotic drug, Ciprofloxacin was selected. Demonstration of the potential use of PEOX / MA fibers as templates for Ciprofloxacin loading and release would be especially beneficial for wound healing applications since Ciprofloxacin is a broad spectrum and frequently used antibiotic.

First, calibration curve of Ciprofloxacin was prepared to establish the relationship between the concentration and absorbance. Two different sets of PEOX / MA fibers were weighed and the mass of fibers in these sets was different. Loading curve of Ciprofloxacin showed that drug molecules were successfully encapsulated into three types of fibers. After 5 hours, concentration of the drug in the fibers reached to saturation. It was assumed that drug molecules do not bind to PEOX / MA fibers only through physical adsorption but also due to the H-bonding between fibers and drug molecules. In addition, the interaction between Ciprofloxacin and PEOX is more prominent in PEOX / MA fibers, since the amount of loaded drug into fibers increases with the PEOX content in them. To test this and verify that PEOX and Cipro interacts favorably, ITC experiments were conducted with different Cipro concentrations in the syringe. Binding of drug molecules to PEOX chains is an enthalpy- driven process, which indicates that the interaction between PEOX and Cipro was favorable. It was assumed that this favorable interaction is based on hydrogen bonding between the amide group of PEOX and hydroxyl / amine groups of Cipro. In addition to that, loading amount of Cipro was much more in PEOX / MA fibers than PEOX fibers. This is due to both morphological difference between PEOX / MA fibers and PEOX fibers and structure of PEOX fibers in which carbonyl groups are along the axis and not exposed to outer surface of the fibers. PEOX / MA fibers have hollow structure and high surface area which results in higher amount of loading of the drug. Encapsulation of the drug inside the fibers was also based on H-bonding so in PEOX fibers carbonyl groups are not accessible and the possibility for the formation of H-bonds between Cipro molecules and PEOX chains is low.

The release of loaded drug was also tested using UV-Vis Spectroscopy. Release of loaded Cipro from PEOX fibers resulted in burst-release and completed in one hour, this shows that

loading of the drug to fibers occur via physical adsorption through the walls. For PEOX fibers, drug molecules could not get into interior parts of the fibers and could not form H-bonds with the amide group of PEOX. Release of the drug from PEOX / MA fibers follows zero order release kinetics while the release duration from fibers prepared from 5 mg/mL PEOX solutions is longer. With assuming higher PEOX content in PEOX (5 mg/mL) / MA fibers, loading of the drug inside the fibers depends more on the formation of H-bonds. At physiological pH, H-bonds between PEOX and MA broke and degradation of H-bonds resulted in zero order release.

Finally, this study clearly shows the potential of hollow PEOX / MA fibers in biomedical applications such as drug release. Insights gained from this work would be beneficial to investigate the mechanism of loading / release of the functional molecules so that broader applications of these fibers could be investigated.

Chapter 9: Conclusion

The objective of this thesis work was to show that different forms of hydrogen-bonded self-assembled structures can be formed and these structures can be used for controlled release applications. Especially, self-assembly mechanism was investigated from molecular interactions perspective in terms of the role of hydrogen bonding and hydrophobic interactions, interplay between them and the thermodynamically driving force for the formation of them. For the characterization and analysis of self-assembled structures, both spectroscopic and calorimetric methods were used together with imaging methods.

In the first place, pH responsive LbL multilayers composed of PEOX and TA were fabricated via hydrogen bonding. PEOX / TA multilayers were restructured into fibers in phosphate buffer at pH 3. Restructuring of the films in phosphate buffer into fibers was obvious when the thickness of the films reached to a certain value, thicker than 15 BL. In addition, when PEOX / TA multilayers were grown in the presence of phosphate buffer and thickness of the films exceeded 15 BL, fluctuations in the film thickness were also observed. pH stability of PEOX / TA multilayers was also less in the presence of $H_2PO_4^-$ ions due to its kosmotropic nature. $H_2PO_4^-$ ions induce local hydrophobicity in the interfaces of the film and as the film grows due to this induced hydrophobicity, film patches were detached. Detached film patches restructured into fibers in rinse solutions as observed by optical microscopy images. Fibers collected from rinse solutions compose of phosphate buffer were characterized with various methods. These characterization methods confirmed that fibers were composed of PEOX and TA and formed with the restructuring of their LbL assembled multilayers. Morphology of the fibers indicated that detached film patches were curled up with the presence of torsional stress in the deposited films due to the chemical anisotropy induced with local hydrophobicity difference in the film. Fibers have hollow structures and interior part of the fibers was more hydrophilic and richer in PEOX. This part of the work shows that stability of hydrogen bonded LbL multilayers can be manipulated by growing or post-treating them into different salt solutions. For the first time, it was also demonstrated that LbL multilayers can be used to form pH responsive fibers, so converting from one self-assembled structure to another is possible by tuning the stability of the formed sheets. Biomedical applications of this work can be biosensors or controlled release of the drugs or functional molecules.

After observing that salt solutions were effective to modify the structure / morphology of hydrogen bonded LbL multilayers, effect of salts on the properties of hydrogen bonded multilayers were investigated. Thus, it was established that effect of salts on the properties were related to the location of the ion in Hofmeister's series and whether they have "salting-in" or "salting-out" effect. Hydrogen bonded PEOX / TA films that were prepared in the presence of kosmotropic ions are thicker, more stable in pH scale and rougher. Kosmotropic ions induce dehydration effect and hydrophobicity in the deposited multilayers. Additional hydrophobic interactions induced by kosmotropic ions increase the bilayer thickness of PEOX / TA films while in the presence of highly concentrated salt solutions, fluctuations in film thickness were observed with the creation of instable domains as in the previous part of the thesis work. Higher stability in PEOX / TA multilayers in the presence of chaotropic ions is related with their direct binding mechanism and formation of stronger hydrogen bonds between PEOX and TA due to the more accessible carbonyl groups of PEOX available for hydrogen bonding. In addition, morphological differences observed in the films that were grown in different salt solutions are also related with either smoothening effect of entrapped water by chaotropic ions or aggregation of PEOX / TA complexes on the film surface with reduced repulsion by kosmotropic ones. All these investigated properties of PEOX / TA multilayers were also confirmed by conducting parallel experiments with PEOX / TA complexes formed in different salt solutions. ITC experiments also enlightened the nature of interaction between PEOX / TA and salt solutions, whether the self-assembly process is entropy or enthalpy driven in the presence of salt solutions. This part of the work shows not only the ways to modify the properties of hydrogen bonded multilayers via using different salt solutions but also well-established correlation between film properties and solution properties.

Controlled release application of PEOX / TA multilayers in different conditions were studied and its release performance was compared with hydrogen bonded PNIPAM / TA multilayers. The main aim of this part of study is to obtain zero order release kinetics, with this way same amount of drug could be released into the target site in a given time interval so that burst release and undesired side effects could be avoided. Rhodamine 6G was used as a model molecule for releasing agent. pH induced release of Rhodamine 6G shows that as the pH of the releasing medium approaches to pKa of TA, the release profile is changed from diffusion-limited release to burst release (when pH of the releasing medium exceeds the pKa of TA). Zero order release profile

was obtained in physiological pH (pH ~7.4) for PEOX / TA multilayers. LCST behavior of PEOX or PNIPAM determines the temperature dependent release of Rhodamine 6G from LbL multilayers. As the temperature of the releasing medium increases, release of dye speeds up. When the temperature of the releasing medium exceeds LCST of the polymers, conformation of polymer chains changed to globular forms and hydrophobicity in the multilayers were induced. As a result, hydrophilic Rhodamine 6G was released in a very fast manner from this hydrophobic environment. Rhodamine 6G was released with zero-order release kinetics from PEOX / TA multilayers at pH 6.5 and 42°C, which is very beneficial for cancer therapy. Furthermore, polymer structure that was used as proton acceptor in LbL multilayers was critical. When release performance of PEOX / TA and PNIPAM / TA multilayers was compared, Rhodamine 6G was released from PEOX / TA in a slower manner due to the more hydrophilic structure of PEOX compared to PNIPAM. These conclusions indicated that hydrogen bonded LbL multilayers are perfect candidates to be functioned as a controlled release platform in terms of obtaining zero order release kinetics. Another advantage of LbL assembled multilayers is that both encapsulation amount and release duration of the cargo can be controlled via film thickness. For the first time, it was shown that PEOX / TA multilayers can be used for the controlled release of hydrophilic molecules in pH / temperature responsive way and in an extended time frame.

Another polymeric self-assembled structure, hydrogen bonded fibers were formed using PEOX and a dicarboxylic acid, MA. For the first time, without using any electrospinning process, hollow fibers were formed in aqueous solutions through hydrogen bonds. Another important part of the work is that hydrogen bonded hollow fibers were formed using small dicarboxylic acid, since most of the polymeric complexes formed in aqueous solutions were prepared by using poly (carboxylic) acid molecules. The effect of pH is determinant in terms of understanding the driving force and mechanism for the formation of hollow fibers. When pH of the aqueous solution is lower than the two pKa values of MA, the main driving force for the fiber formation is hydrogen bonding and the entire process is enthalpy driven. Hydrogen bond formation was confirmed through both gravimetric and spectroscopic methods. On the other hand, when pH of the aqueous solution is between two pKa values, the main mechanism for the formation of hollow fibers is the electrostatic bridging of PEOX chains. When pH of the aqueous solution exceeds two pKa values of MA, fibers with flat morphology are formed different from hollow fibrous structures. Since the amount of

fibers is less, enough characterization could not be done but a possible reason for the formation of such fibers can be electrostatic interaction of carboxylate groups of malonic acid and amide groups of PEOX. Fiber formation was also temperature dependent due to LCST behavior of PEOX. Below and above LCST, fiber formation was not observed for different reasons. Above T_{cp}, fiber formation was inhibited due to the hydrophobic aggregation of PEOX molecules with conformation change. Below T_{cp}, solubility of PEOX in aqueous solution was enhanced so instead of MA molecules, PEOX interacts with water molecules. In previous sections, the effect of Hofmeister series of salt on hydrogen bonded polymeric structures was demonstrated. For this reason, three sodium salts from Hofmeister series were selected and their effect on the process of fiber formation or fiber structure was analyzed. SCN^- ions, as a chaotropic ion, binds to hydrophobic cavity of PEOX and make carbonyl groups more available for stronger hydrogen bond formation. In the presence of chaotropic ions, when flat fibers were formed through electrostatic bridging of PEOX molecules (when pH of the solution is between two pKa values), repulsion between fibrous aggregates was reduced between negatively charged carboxylate ends of MA due to the screening effect. On the other hand, kosmotropic ions both dehydrate PEOX chains and attract protonated MA molecules. ITC experiments also confirmed the results that were obtained for the self-assembly process of PEOX and MA in the presence of sodium salt solutions.

Hollow structure of PEOX / MA fibers formed via self-assembly in aqueous solutions is promising in biomedical applications to be used as templates for the encapsulation and release of the functional cargo. Ciprofloxacin, a broad-spectrum antibiotic, was loaded into PEOX / MA fibers and released in physiological body conditions. Ciprofloxacin was loaded successfully into PEOX / MA fibers not only through physical adsorption but also interacting with the components of the fibers, PEOX and MA. The amount of loaded drug was directly correlated with the amount of PEOX in the fibers since PEOX and Ciprofloxacin interacts favorably as verified via ITC. High surface area of PEOX / MA fibers with their hollow structure resulted in higher loading amount of the drug compared to flat PEOX fibers. Release of the drug in physiological pH was also tested. While PEOX fibers released loaded drugs in a burst release manner, release from PEOX / MA fibers occurred either with diffusion limited or zero order release kinetics based on PEOX content in the fibers.

In summary, different forms of hydrogen bonded self-assembled structures consisting PEOX polymer were formed and their controlled release applications were shown studying them as model systems. For the first time, in Chapter 4, we have shown that LbL deposited multilayers restructure via manipulating film stability in conditions where films are still intact. In the prior studies, it has been acknowledged that in LbL deposited multilayers, adsorbed species relax and try to reach equilibrium via inter-diffusional movements. However, in this whole "rearrangement" process, films are stable on the surface. Thus, manipulating the stability of PEOX / TA films in a condition where H-bonds between PEOX and TA are still intact made possible to form pH responsive fibers via restructuring of film components and without disturbing the interactions. Thus, the results are motivating in terms of indicating potential usage of these fibers in biomedical applications since fibers have properties like being both pH/ temperature responsive and hollow structure. Since restructuring of LbL multilayers and manipulating their stability could be realized via exploiting the interaction between $H_2PO_4^-$ and PEOX molecules, the effect of Hofmeister series of sodium salts on LbL multilayers of PEOX and TA was investigated in the Chapter 5. Properties such as film thickness, pH stability and morphology of PEOX / TA multilayers could be tailored by treating them into salt solutions having different concentrations. It is well known that ions alter T_{cp} of thermo-responsive polymers via different mechanisms. There are also many studies which show film properties can be altered via salt-annealing in electrostatically bound multilayers. However, for the first time, we were able to demonstrate film properties can be modified and arranged during the preparation step by modifying the assembly conditions, specifically the type of salt solutions that was used. Thus, the importance of understanding the interaction mechanism between salt ions and polymers is underlined. In Chapter 6, PEOX / TA multilayers were used as a model system for being a release platform for small hydrophilic molecules. Literature work shows sustained release of hydrophobic drugs are possible by using micelles and incorporating drug loaded micelles into LbL multilayers. However, obtaining sustained release of hydrophilic drugs, especially with the zero-order release kinetics, is difficult for hydrophilic drugs due to the fast diffusion rate of them in aqueous environment. By using Rhodamine 6G as a model molecule and PEOX / TA or PNIPAM / TA films as release platforms, we were able to demonstrate that H-bonded LbL films are good choices for loading and sustained release of small hydrophilic molecules. Especially, reaching zero order release kinetics under defined conditions was crucial and PEOX / TA films are promising candidates for further research. In Chapter 7 of the thesis,

hollow fibers of PEOX and MA were formed through self-assembly process in aqueous solutions. For the first time, we have showed that formation of such fibers is possible with small molecules, a dicarboxylic acid in our case, through bridging effect in aqueous solutions and without using any electrospinning process. We were also able to demonstrate one of the beneficial biomedical application of hollow PEOX/ MA fibers: We used them for the encapsulation and release of a broad- spectrum antibiotic, Ciprofloxacin, at pH 7.4. Long lasting release of Ciprofloxacin at physiological pH of the body opens the possibility for further conducting release experiments in different pH or temperature conditions. With the completion of this thesis and contribution of the knowledge that was gained from the presented work, future studies can also be directed into various fields that can unite both polymer or surface chemistry and biomedical sciences.

BIBLIOGRAPHY

1. Gil, E.S. and S.M. Hudson, *Stimuli-reponsive polymers and their bioconjugates.* Progress in Polymer Science, 2004. **29**(12): p. 1173-1222.
2. Wei, M., et al., *Stimuli-responsive polymers and their applications.* Polymer Chemistry, 2017. **8**(1): p. 127-143.
3. Jeong, B. and A. Gutowska, *Lessons from nature: stimuli-responsive polymers and their biomedical applications.* Trends in Biotechnology, 2002. **20**(7): p. 305-311.
4. Alexander, C. and K.M. Shakesheff, *Responsive Polymers at the Biology/Materials Science Interface.* Advanced Materials, 2006. **18**(24): p. 3321-3328.
5. Kim, S., et al., *Engineered polymers for advanced drug delivery.* European Journal of Pharmaceutics and Biopharmaceutics, 2009. **71**(3): p. 420-430.
6. Alarcón, C.d.l.H., S. Pennadam, and C. Alexander, *Stimuli responsive polymers for biomedical applications.* Chemical Society Reviews, 2005. **34**(3): p. 276-285.
7. Bawa, P., et al., *Stimuli-responsive polymers and their applications in drug delivery.* Biomedical Materials, 2009. **4**(2): p. 022001.
8. Stuart, M.A.C., et al., *Emerging applications of stimuli-responsive polymer materials.* Nature Materials, 2010. **9**: p. 101.
9. Roy, I. and M.N. Gupta, *Smart Polymeric Materials: Emerging Biochemical Applications.* Chemistry & Biology, 2003. **10**(12): p. 1161-1171.
10. Mano, J.F., *Stimuli-Responsive Polymeric Systems for Biomedical Applications.* Advanced Engineering Materials, 2008. **10**(6): p. 515-527.
11. Mura, S., J. Nicolas, and P. Couvreur, *Stimuli-responsive nanocarriers for drug delivery.* Nature Materials, 2013. **12**(11): p. 991-1003.
12. Ganta, S., et al., *A review of stimuli-responsive nanocarriers for drug and gene delivery.* Journal of Controlled Release, 2008. **126**(3): p. 187-204.
13. Hu, J. and S. Liu, *Responsive Polymers for Detection and Sensing Applications: Current Status and Future Developments.* Macromolecules, 2010. **43**(20): p. 8315-8330.
14. Ma, M., et al., *Bio-Inspired Polymer Composite Actuator and Generator Driven by Water Gradients.* Science, 2013. **339**(6116): p. 186-189.
15. Hoffmann, J., et al., *Photopatterning of thermally sensitive hydrogels useful for microactuators.* Sensors and Actuators A: Physical, 1999. **77**(2): p. 139-144.
16. Khan, F. and M. Tanaka, *Designing Smart Biomaterials for Tissue Engineering.* International Journal of Molecular Sciences, 2018. **19**(1): p. 17.
17. Kocak, G., C. Tuncer, and V. Bütün, *pH-Responsive polymers.* Polymer Chemistry, 2017. **8**(1): p. 144-176.
18. Bazban-Shotorbani, S., et al., *Revisiting structure-property relationship of pH-responsive polymers for drug delivery applications.* Journal of Controlled Release, 2017. **253**: p. 46-63.
19. Dai, S., P. Ravi, and K.C. Tam, *pH-Responsive polymers: synthesis, properties and applications.* Soft Matter, 2008. **4**(3): p. 435-449.
20. Schmaljohann, D., *Thermo- and pH-responsive polymers in drug delivery.* Advanced Drug Delivery Reviews, 2006. **58**(15): p. 1655-1670.
21. Su, J., et al., *Catechol Polymers for pH-Responsive, Targeted Drug Delivery to Cancer Cells.* Journal of the American Chemical Society, 2011. **133**(31): p. 11850-11853.
22. Yang, X., et al., *Synthesis of pH-sensitive hollow polymer microspheres and their application as drug carriers.* Polymer, 2009. **50**(15): p. 3556-3563.

23. Liu, J., et al., *pH-Sensitive nano-systems for drug delivery in cancer therapy.* Biotechnology Advances, 2014. **32**(4): p. 693-710.
24. Cheung, C.Y., et al., *A pH-Sensitive Polymer That Enhances Cationic Lipid-Mediated Gene Transfer.* Bioconjugate Chemistry, 2001. **12**(6): p. 906-910.
25. Meyer, M., et al., *Breathing Life into Polycations: Functionalization with pH-Responsive Endosomolytic Peptides and Polyethylene Glycol Enables siRNA Delivery.* Journal of the American Chemical Society, 2008. **130**(11): p. 3272-3273.
26. Lee, K.S., I. In, and S.Y. Park, *pH and redox responsive polymer for antifouling surface coating.* Applied Surface Science, 2014. **313**: p. 532-536.
27. Mi, L., et al., *pH responsive properties of non-fouling mixed-charge polymer brushes based on quaternary amine and carboxylic acid monomers.* Biomaterials, 2010. **31**(10): p. 2919-2925.
28. Waziri, S.M., B.F. Abu-Sharkh, and S.A. Ali, *Protein Partitioning in Aqueous Two-Phase Systems Composed of a pH-Responsive Copolymer and Poly(ethylene glycol).* Biotechnology Progress, 2004. **20**(2): p. 526-532.
29. Ejima, H., J.J. Richardson, and F. Caruso, *Phenolic film engineering for template-mediated microcapsule preparation.* Polymer Journal, 2014. **46**: p. 452.
30. Shutava, T., et al., *pH Responsive Decomposable Layer-by-Layer Nanofilms and Capsules on the Basis of Tannic Acid.* Macromolecules, 2005. **38**(7): p. 2850-2858.
31. Xu, L.Q., K.-G. Neoh, and E.-T. Kang, *Natural polyphenols as versatile platforms for material engineering and surface functionalization.* Progress in Polymer Science, 2018. **87**: p. 165-196.
32. Rahim, M.A., et al., *Phenolic Building Blocks for the Assembly of Functional Materials.* Angewandte Chemie International Edition, 2019. **58**(7): p. 1904-1927.
33. Fan, H., et al., *Supramolecular Hydrogel Formation Based on Tannic Acid.* Macromolecules, 2017. **50**(2): p. 666-676.
34. Gandhi, A., et al., *Studies on thermoresponsive polymers: Phase behaviour, drug delivery and biomedical applications.* Asian Journal of Pharmaceutical Sciences, 2015. **10**(2): p. 99-107.
35. Hocine, S. and M.-H. Li, *Thermoresponsive self-assembled polymer colloids in water.* Soft Matter, 2013. **9**(25): p. 5839-5861.
36. Kim, Y.-J. and Y.T. Matsunaga, *Thermo-responsive polymers and their application as smart biomaterials.* Journal of Materials Chemistry B, 2017. **5**(23): p. 4307-4321.
37. Zhao, C., Z. Ma, and X.X. Zhu, *Rational design of thermoresponsive polymers in aqueous solutions: A thermodynamics map.* Progress in Polymer Science, 2019. **90**: p. 269-291.
38. Qiao, S. and H. Wang, *Temperature-responsive polymers: Synthesis, properties, and biomedical applications.* Nano Research, 2018. **11**(10): p. 5400-5423.
39. Scarpa, J.S., D.D. Mueller, and I.M. Klotz, *Slow hydrogen-deuterium exchange in a non-.alpha.-helical polyamide.* Journal of the American Chemical Society, 1967. **89**(24): p. 6024-6030.
40. Ward, M.A. and T.K. Georgiou, *Thermoresponsive Polymers for Biomedical Applications.* Polymers, 2011. **3**(3): p. 1215.
41. Roy, D., W.L.A. Brooks, and B.S. Sumerlin, *New directions in thermoresponsive polymers.* Chemical Society Reviews, 2013. **42**(17): p. 7214-7243.
42. Seuring, J. and S. Agarwal, *Polymers with Upper Critical Solution Temperature in Aqueous Solution.* Macromolecular Rapid Communications, 2012. **33**(22): p. 1898-1920.
43. Niskanen, J. and H. Tenhu, *How to manipulate the upper critical solution temperature (UCST)?* Polymer Chemistry, 2017. **8**(1): p. 220-232.
44. Seuring, J. and S. Agarwal, *Polymers with Upper Critical Solution Temperature in Aqueous Solution: Unexpected Properties from Known Building Blocks.* ACS Macro Letters, 2013. **2**(7): p. 597-600.

45. Xu, Z. and W. Liu, *Poly(N-acryloyl glycinamide): a fascinating polymer that exhibits a range of properties from UCST to high-strength hydrogels.* Chemical Communications, 2018. **54**(75): p. 10540-10553.
46. Higashi, N., R. Sonoda, and T. Koga, *Thermo-responsive amino acid-based vinyl polymers showing widely tunable LCST/UCST behavior in water.* RSC Advances, 2015. **5**(83): p. 67652-67657.
47. Zhang, Q., et al., *Thermoresponsive polymers with lower critical solution temperature: from fundamental aspects and measuring techniques to recommended turbidimetry conditions.* Materials Horizons, 2017.
48. Park, J.-S. and K. Kataoka, *Precise Control of Lower Critical Solution Temperature of Thermosensitive Poly(2-isopropyl-2-oxazoline) via Gradient Copolymerization with 2-Ethyl-2-oxazoline as a Hydrophilic Comonomer.* Macromolecules, 2006. **39**(19): p. 6622-6630.
49. Park, J.-S. and K. Kataoka, *Comprehensive and Accurate Control of Thermosensitivity of Poly(2-alkyl-2-oxazoline)s via Well-Defined Gradient or Random Copolymerization.* Macromolecules, 2007. **40**(10): p. 3599-3609.
50. Kempe, K., et al., *Responsive Glyco-poly(2-oxazoline)s: Synthesis, Cloud Point Tuning, and Lectin Binding.* Biomacromolecules, 2011. **12**(7): p. 2591-2600.
51. Hoogenboom, R., et al., *Tuning the LCST of poly(2-oxazoline)s by varying composition and molecular weight: alternatives to poly(N-isopropylacrylamide)?* Chemical Communications, 2008(44): p. 5758-5760.
52. Huber, S., N. Hutter, and R. Jordan, *Effect of end group polarity upon the lower critical solution temperature of poly(2-isopropyl-2-oxazoline).* Colloid and Polymer Science, 2008. **286**(14): p. 1653-1661.
53. Zhang, H., et al., *A new comonomer design for enhancing the pH-triggered LCST shift of thermosensitive polymers.* Polymer Chemistry, 2015. **6**(37): p. 6644-6650.
54. Gao, X., et al., *pH- and thermo-responsive poly(N-isopropylacrylamide-co-acrylic acid derivative) copolymers and hydrogels with LCST dependent on pH and alkyl side groups.* Journal of Materials Chemistry B, 2013. **1**(41): p. 5578-5587.
55. Weiss-Malik, R.A., F.J. Solis, and B.L. Vernon, *Independent control of lower critical solution temperature and swelling behavior with pH for poly(N-isopropylacrylamide-co-maleic acid).* Journal of Applied Polymer Science, 2004. **94**(5): p. 2110-2116.
56. Lanzalaco, S. and E. Armelin, *Poly(N-isopropylacrylamide) and Copolymers: A Review on Recent Progresses in Biomedical Applications.* Gels, 2017. **3**(4): p. 36.
57. Halperin, A., M. Kröger, and F.M. Winnik, *Poly(N-isopropylacrylamide) Phase Diagrams: Fifty Years of Research.* Angewandte Chemie International Edition, 2015. **54**(51): p. 15342-15367.
58. Guan, Y. and Y. Zhang, *PNIPAM microgels for biomedical applications: from dispersed particles to 3D assemblies.* Soft Matter, 2011. **7**(14): p. 6375-6384.
59. Schild, H.G., *Poly(N-isopropylacrylamide): experiment, theory and application.* Progress in Polymer Science, 1992. **17**(2): p. 163-249.
60. Dhara, D. and P.R. Chatterji, *Phase Transition in Linear and Cross-Linked Poly(N-Isopropylacrylamide) in Water: Effect of Various Types of Additives.* Journal of Macromolecular Science, Part C, 2000. **40**(1): p. 51-68.
61. Yan, Y., et al., *Concentration effect on aggregation and dissolution behavior of poly(N-isopropylacrylamide) in water.* Journal of Applied Polymer Science, 2015. **132**(12).
62. Wu, C. and S. Zhou, *Laser Light Scattering Study of the Phase Transition of Poly(N-isopropylacrylamide) in Water. 1. Single Chain.* Macromolecules, 1995. **28**(24): p. 8381-8387.
63. Wu, C. and S. Zhou, *First Observation of the Molten Globule State of a Single Homopolymer Chain.* Physical Review Letters, 1996. **77**(14): p. 3053-3055.

64. Bischofberger, I., et al., *Hydrophobic hydration of poly-N-isopropyl acrylamide: a matter of the mean energetic state of water.* Scientific reports, 2014. **4**: p. 4377-4377.
65. Liu, H. and S. Wang, *Poly(N-isopropylacrylamide)-based thermo-responsive surfaces with controllable cell adhesion.* Science China Chemistry, 2014. **57**(4): p. 552-557.
66. Schlaad, H., et al., *Poly(2-oxazoline)s as Smart Bioinspired Polymers.* Macromolecular Rapid Communications, 2010. **31**(6): p. 511-525.
67. Hoogenboom, R., *Poly(2-oxazoline)s: A Polymer Class with Numerous Potential Applications.* Angewandte Chemie-International Edition, 2009. **48**(43): p. 7978-7994.
68. Hoogenboom, R. and H. Schlaad, *Thermoresponsive poly(2-oxazoline)s, polypeptoids, and polypeptides.* Polymer Chemistry, 2017. **8**(1): p. 24-40.
69. Demirel, A.L., et al., *Revisiting the Crystallization of Poly(2-alkyl-2-oxazoline)s.* Journal of Polymer Science Part B-Polymer Physics, 2016. **54**(7): p. 721-729.
70. Weber, C., R. Hoogenboom, and U.S. Schubert, *Temperature responsive bio-compatible polymers based on poly(ethylene oxide) and poly(2-oxazoline)s.* Progress in Polymer Science, 2012. **37**(5): p. 686-714.
71. Lin, P., et al., *Solubility and miscibility of poly(ethyl oxazoline).* Journal of Polymer Science Part B: Polymer Physics, 1988. **26**(3): p. 603-619.
72. Hiroshi, U. and K. Shiro, *A Novel Thermo-Sensitive Polymer. Poly(2-iso-propyl-2-oxazoline).* Chemistry Letters, 1992. **21**(9): p. 1643-1646.
73. Sedlacek, O., et al., *Poly(2-Oxazoline)s – Are They More Advantageous for Biomedical Applications Than Other Polymers?* Macromolecular Rapid Communications, 2012. **33**(19): p. 1648-1662.
74. Meyer, M., M. Antonietti, and H. Schlaad, *Unexpected thermal characteristics of aqueous solutions of poly(2-isopropyl-2-oxazoline).* Soft Matter, 2007. **3**(4): p. 430-431.
75. Demirel, A.L., M. Meyer, and H. Schlaad, *Formation of Polyamide Nanofibers by Directional Crystallization in Aqueous Solution.* Angewandte Chemie International Edition, 2007. **46**(45): p. 8622-8624.
76. Guner, P.T., et al., *Self-assembled poly(2-ethyl-2-oxazoline) fibers in aqueous solutions.* Polymer Chemistry, 2012. **3**(2): p. 322-324.
77. Rettler, E.F.-J., et al., *Thermal, Mechanical, and Surface Properties of Poly(2-N-alkyl-2-oxazoline)s.* Macromolecular Chemistry and Physics, 2010. **211**(22): p. 2443-2448.
78. Luxenhofer, R., et al., *Structure-property relationship in cytotoxicity and cell uptake of poly(2-oxazoline) amphiphiles.* Journal of Controlled Release, 2011. **153**(1): p. 73-82.
79. Trachsel, L., et al., *Enzymatically crosslinked poly(2-alkyl-2-oxazoline) networks for 3D cell culture.* Journal of Materials Chemistry B, 2018. **6**(46): p. 7568-7572.
80. Li, T., H. Tang, and P. Wu, *Structural investigation of thermo-responsive poly(2-isopropyl-2-oxazoline) hydrogel across the volume phase transition.* Soft Matter, 2015. **11**(10): p. 1911-1918.
81. Hofmeister, F., *Zur lehre von der wirkung der salze.* Naunyn-Schmiedeberg's Archives of Pharmacology, 1888. **25**(1): p. 1-30.
82. Zhang, Y. and P.S. Cremer, *Interactions between macromolecules and ions: the Hofmeister series.* Current Opinion in Chemical Biology, 2006. **10**(6): p. 658-663.
83. Zhang, Y. and P.S. Cremer, *Chemistry of Hofmeister Anions and Osmolytes.* Annual Review of Physical Chemistry, 2010. **61**(1): p. 63-83.
84. Baldwin, R.L., *How Hofmeister ion interactions affect protein stability.* Biophysical journal, 1996. **71**(4): p. 2056-2063.
85. Klement, K., et al., *Effect of Different Salt Ions on the Propensity of Aggregation and on the Structure of Alzheimer's Aβ(1-40) Amyloid Fibrils.* Journal of Molecular Biology, 2007. **373**(5): p. 1321-1333.

86. Collins, K.D., *Ions from the Hofmeister series and osmolytes: effects on proteins in solution and in the crystallization process.* Methods, 2004. **34**(3): p. 300-311.
87. Arosio, P., et al., *On the role of salt type and concentration on the stability behavior of a monoclonal antibody solution.* Biophysical Chemistry, 2012. **168-169**: p. 19-27.
88. Okur, H.I., et al., *Beyond the Hofmeister Series: Ion-Specific Effects on Proteins and Their Biological Functions.* The Journal of Physical Chemistry B, 2017. **121**(9): p. 1997-2014.
89. Gibb, C.L.D. and B.C. Gibb, *Anion Binding to Hydrophobic Concavity Is Central to the Salting-in Effects of Hofmeister Chaotropes.* Journal of the American Chemical Society, 2011. **133**(19): p. 7344-7347.
90. Thormann, E., *On understanding of the Hofmeister effect: how addition of salt alters the stability of temperature responsive polymers in aqueous solutions.* RSC Advances, 2012. **2**(22): p. 8297-8305.
91. Deyerle, B.A. and Y. Zhang, *Effects of Hofmeister Anions on the Aggregation Behavior of PEO–PPO–PEO Triblock Copolymers.* Langmuir, 2011. **27**(15): p. 9203-9210.
92. Li, L., J.-H. Ryu, and S. Thayumanavan, *Effect of Hofmeister Ions on the Size and Encapsulation Stability of Polymer Nanogels.* Langmuir, 2013. **29**(1): p. 50-55.
93. Naini, C.A., et al., *Hofmeister Effect of Sodium Halides on the Switching Energetics of Thermoresponsive Polymer Brushes.* Macromolecular Rapid Communications, 2013. **34**(5): p. 417-422.
94. Freitag, R. and F. Garret-Flaudy, *Salt Effects on the Thermoprecipitation of Poly-(N-isopropylacrylamide) Oligomers from Aqueous Solution.* Langmuir, 2002. **18**(9): p. 3434-3440.
95. Zhang, Y., et al., *Specific Ion Effects on the Water Solubility of Macromolecules: PNIPAM and the Hofmeister Series.* Journal of the American Chemical Society, 2005. **127**(41): p. 14505-14510.
96. Shechter, I., et al., *Microcalorimetric Study of the Effects of a Chaotropic Salt, KSCN, on the Lower Critical Solution Temperature (LCST) of Aqueous Poly(N-isopropylacrylamide) (PNIPA) Solutions.* Macromolecules, 2010. **43**(1): p. 480-487.
97. Jhon, Y.K., et al., *Salt-Induced Depression of Lower Critical Solution Temperature in a Surface-Grafted Neutral Thermoresponsive Polymer.* Macromolecular Rapid Communications, 2006. **27**(9): p. 697-701.
98. Zhang, Y., et al., *Effects of Hofmeister Anions on the LCST of PNIPAM as a Function of Molecular Weight.* The Journal of Physical Chemistry C, 2007. **111**(25): p. 8916-8924.
99. Cho, Y., et al., *Effects of Hofmeister Anions on the Phase Transition Temperature of Elastin-like Polypeptides.* The Journal of Physical Chemistry B, 2008. **112**(44): p. 13765-13771.
100. Bloksma, M.M., et al., *The Effect of Hofmeister Salts on the LCST Transition of Poly(2-oxazoline)s with Varying Hydrophilicity.* Macromolecular Rapid Communications, 2010. **31**(8): p. 724-728.
101. Tatar Güner, P. and A.L. Demirel, *Effect of Anions on the Cloud Point Temperature of Aqueous Poly(2-ethyl-2-oxazoline) Solutions.* The Journal of Physical Chemistry B, 2012. **116**(49): p. 14510-14514.
102. Zajforoushan Moghaddam, S. and E. Thormann, *Hofmeister effect of salt mixtures on thermo-responsive poly(propylene oxide).* Physical Chemistry Chemical Physics, 2015. **17**(9): p. 6359-6366.
103. Song, W., L. Liu, and G. Liu, *Ion specificity of macromolecules in crowded environments.* Soft Matter, 2015. **11**(29): p. 5940-5946.
104. Lo Nostro, P. and B.W. Ninham, *Hofmeister Phenomena: An Update on Ion Specificity in Biology.* Chemical Reviews, 2012. **112**(4): p. 2286-2322.
105. Bauduin, P., et al., *Hofmeister effect on enzymatic catalysis and colloidal structures.* Current Opinion in Colloid & Interface Science, 2004. **9**(1): p. 43-47.

106. Munishkina, L.A., et al., *Role of Protein−Water Interactions and Electrostatics in α-Synuclein Fibril Formation.* Biochemistry, 2004. **43**(11): p. 3289-3300.
107. Grover, P.K. and R.L. Ryall, *Critical Appraisal of Salting-Out and Its Implications for Chemical and Biological Sciences.* Chemical Reviews, 2005. **105**(1): p. 1-10.
108. Lawrence, D.S., T. Jiang, and M. Levett, *Self-Assembling Supramolecular Complexes.* Chemical Reviews, 1995. **95**(6): p. 2229-2260.
109. Whitesides, G.M. and B. Grzybowski, *Self-Assembly at All Scales.* Science, 2002. **295**(5564): p. 2418-2421.
110. Yabu, H., T. Higuchi, and H. Jinnai, *Frustrated phases: polymeric self-assemblies in a 3D confinement.* Soft Matter, 2014. **10**(17): p. 2919-2931.
111. Stoffelen, C. and J. Huskens, *Soft Supramolecular Nanoparticles by Noncovalent and Host–Guest Interactions.* Small, 2016. **12**(1): p. 96-119.
112. Branco, M.C. and J.P. Schneider, *Self-assembling materials for therapeutic delivery.* Acta Biomaterialia, 2009. **5**(3): p. 817-831.
113. Palao-Suay, R., et al., *Self-assembling polymer systems for advanced treatment of cancer and inflammation.* Progress in Polymer Science, 2016. **53**: p. 207-248.
114. Motornov, M., et al., *Stimuli-responsive nanoparticles, nanogels and capsules for integrated multifunctional intelligent systems.* Progress in Polymer Science, 2010. **35**(1): p. 174-211.
115. He, Y., B. Zhu, and Y. Inoue, *Hydrogen bonds in polymer blends.* Progress in Polymer Science, 2004. **29**(10): p. 1021-1051.
116. Steiner, T., *The Hydrogen Bond in the Solid State.* Angewandte Chemie International Edition, 2002. **41**(1): p. 48-76.
117. Chen, S. and W.H. Binder, *Dynamic Ordering and Phase Segregation in Hydrogen-Bonded Polymers.* Accounts of Chemical Research, 2016. **49**(7): p. 1409-1420.
118. Sherrington, D.C. and K.A. Taskinen, *Self-assembly in synthetic macromolecular systems multiple hydrogen bonding interactions.* Chemical Society Reviews, 2001. **30**(2): p. 83-93.
119. Sijbesma, R.P. and E.W. Meijer, *Self-assembly of well-defined structures by hydrogen bonding.* Current Opinion in Colloid & Interface Science, 1999. **4**(1): p. 24-32.
120. Kuo, S.-W., *Hydrogen bond-mediated self-assembly and supramolecular structures of diblock copolymer mixtures.* Polymer International, 2009. **58**(5): p. 455-464.
121. Binder, W.H., *Polymeric Ordering by H-bonds. Mimicking Nature by Smart Building Blocks.* Monatshefte für Chemie / Chemical Monthly, 2005. **136**(1): p. 1-19.
122. Lee, H.-F., et al., *Hydrogen-Bonding Interactions Mediate the Phase Behavior of an A−B/C Block Copolymer/Homopolymer Blend Comprising Poly(Methyl Methacrylate-b-vinylpyrrolidone) and Poly(Vinylphenol).* Macromolecules, 2006. **39**(16): p. 5458-5465.
123. Lee, S.C., et al., *pH-Induced Reversible Complexation of Poly(ethylene glycol) and Poly(ε-caprolactone)-b-poly(methacrylic acid) Copolymer Micelles.* Macromolecules, 2005. **38**(22): p. 9291-9297.
124. Li, G., et al., *Formation of Complex Micelles with Double-Responsive Channels from Self-Assembly of Two Diblock Copolymers.* Angewandte Chemie International Edition, 2006. **45**(30): p. 4959-4962.
125. Parrish, D.A., L.J. Mathias, and K.M. Moore, *Supramolecular Materials from Multifunctional Pyroglutamic Acid Derivatives.* Macromolecules, 2003. **36**(12): p. 4250-4252.
126. Khutoryanskaya, O.V., et al., *Hydrogen-Bonded Complexes and Blends of Poly(acrylic acid) and Methylcellulose: Nanoparticles and Mucoadhesive Films for Ocular Delivery of Riboflavin.* Macromolecular Bioscience, 2014. **14**(2): p. 225-234.

127. Kozlovskaya, V., et al., *Polyphenolic Polymersomes of Temperature-Sensitive Poly(N-vinylcaprolactam)-block-Poly(N-vinylpyrrolidone) for Anticancer Therapy.* Biomacromolecules, 2017. **18**(8): p. 2552-2563.
128. Kozlovskaya, V., et al., *Responsive microcapsule reactors based on hydrogen-bonded tannic acid layer-by-layer assemblies.* Soft Matter, 2010. **6**(15): p. 3596-3608.
129. Wang, Y., T. Chou, and S.A. Sukhishvili, *Spontaneous, One-Pot Assembly of pH-Responsive Hydrogen-Bonded Polymer Capsules.* ACS Macro Letters, 2016. **5**(1): p. 35-39.
130. Stockton, W.B. and M.F. Rubner, *Molecular-Level Processing of Conjugated Polymers. 4. Layer-by-Layer Manipulation of Polyaniline via Hydrogen-Bonding Interactions.* Macromolecules, 1997. **30**(9): p. 2717-2725.
131. Kharlampieva, E., V. Kozlovskaya, and S.A. Sukhishvili, *Layer-by-Layer Hydrogen-Bonded Polymer Films: From Fundamentals to Applications.* Advanced Materials, 2009. **21**(30): p. 3053-3065.
132. Li, Y., X. Wang, and J. Sun, *Layer-by-layer assembly for rapid fabrication of thick polymeric films.* Chemical Society Reviews, 2012. **41**(18): p. 5998-6009.
133. Xiao, F.-X., et al., *Layer-by-layer assembly of versatile nanoarchitectures with diverse dimensionality: a new perspective for rational construction of multilayer assemblies.* Chemical Society Reviews, 2016. **45**(11): p. 3088-3121.
134. Zhang, S., M. Xing, and B. Li, *Biomimetic Layer-by-Layer Self-Assembly of Nanofilms, Nanocoatings, and 3D Scaffolds for Tissue Engineering.* International journal of molecular sciences, 2018. **19**(6): p. 1641.
135. Borges, J. and J.F. Mano, *Molecular Interactions Driving the Layer-by-Layer Assembly of Multilayers.* Chemical Reviews, 2014. **114**(18): p. 8883-8942.
136. de Villiers, M.M., et al., *Introduction to nanocoatings produced by layer-by-layer (LbL) self-assembly.* Advanced Drug Delivery Reviews, 2011. **63**(9): p. 701-715.
137. Ariga, K., J.P. Hill, and Q. Ji, *Layer-by-layer assembly as a versatile bottom-up nanofabrication technique for exploratory research and realistic application.* Physical Chemistry Chemical Physics, 2007. **9**(19): p. 2319-2340.
138. Guan, Y. and Y. Zhang, *Dynamically bonded layer-by-layer films: Dynamic properties and applications.* Journal of Applied Polymer Science, 2014. **131**(19).
139. Kozlovskaya, V., et al., *Multilayer-derived, ultrathin, stimuli-responsive hydrogels.* Soft Matter, 2009. **5**(21): p. 4077-4087.
140. Richardson, J.J., M. Björnmalm, and F. Caruso, *Technology-driven layer-by-layer assembly of nanofilms.* Science, 2015. **348**(6233).
141. Decher, G., J.D. Hong, and J. Schmitt, *Buildup of ultrathin multilayer films by a self-assembly process: III. Consecutively alternating adsorption of anionic and cationic polyelectrolytes on charged surfaces.* Thin Solid Films, 1992. **210**: p. 831-835.
142. Decher, G., *Fuzzy Nanoassemblies: Toward Layered Polymeric Multicomposites.* Science, 1997. **277**(5330): p. 1232-1237.
143. Kovacevic, D., et al., *Kinetics of Formation and Dissolution of Weak Polyelectrolyte Multilayers: Role of Salt and Free Polyions.* Langmuir, 2002. **18**(14): p. 5607-5612.
144. Karahan, H.E., et al., *pH-stability and pH-annealing of H-bonded multilayer films prepared by layer-by-layer spin-assembly.* European Polymer Journal, 2014. **56**: p. 159-167.
145. Yoo, P.J., et al., *Spontaneous assembly of viruses on multilayered polymer surfaces.* Nat Mater, 2006. **5**(3): p. 234-240.
146. Yoo, P.J., et al., *Controlling Surface Mobility in Interdiffusing Polyelectrolyte Multilayers.* ACS Nano, 2008. **2**(3): p. 561-571.

147. Dubas, S.T. and J.B. Schlenoff, *Swelling and Smoothing of Polyelectrolyte Multilayers by Salt.* Langmuir, 2001. **17**(25): p. 7725-7727.
148. Richardson, J.J., et al., *Innovation in Layer-by-Layer Assembly.* Chemical Reviews, 2016. **116**(23): p. 14828-14867.
149. Elbert, D.L., C.B. Herbert, and J.A. Hubbell, *Thin Polymer Layers Formed by Polyelectrolyte Multilayer Techniques on Biological Surfaces.* Langmuir, 1999. **15**(16): p. 5355-5362.
150. Das, B.P. and M. Tsianou, *From polyelectrolyte complexes to polyelectrolyte multilayers: Electrostatic assembly, nanostructure, dynamics, and functional properties.* Advances in Colloid and Interface Science, 2017. **244**: p. 71-89.
151. Gribova, V., R. Auzely-Velty, and C. Picart, *Polyelectrolyte Multilayer Assemblies on Materials Surfaces: From Cell Adhesion to Tissue Engineering.* Chemistry of Materials, 2012. **24**(5): p. 854-869.
152. Mendelsohn, J.D., et al., *Fabrication of Microporous Thin Films from Polyelectrolyte Multilayers.* Langmuir, 2000. **16**(11): p. 5017-5023.
153. Lavalle, P., et al., *Modeling the Buildup of Polyelectrolyte Multilayer Films Having Exponential Growth.* The Journal of Physical Chemistry B, 2004. **108**(2): p. 635-648.
154. Michel, M., et al., *Layer by Layer Self-Assembled Polyelectrolyte Multilayers with Embedded Phospholipid Vesicles Obtained by Spraying: Integrity of the Vesicles.* Langmuir, 2005. **21**(17): p. 7854-7859.
155. Bieker, P. and M. Schönhoff, *Linear and Exponential Growth Regimes of Multilayers of Weak Polyelectrolytes in Dependence on pH.* Macromolecules, 2010. **43**(11): p. 5052-5059.
156. Yoo, D., S.S. Shiratori, and M.F. Rubner, *Controlling Bilayer Composition and Surface Wettability of Sequentially Adsorbed Multilayers of Weak Polyelectrolytes.* Macromolecules, 1998. **31**(13): p. 4309-4318.
157. Shiratori, S.S. and M.F. Rubner, *pH-Dependent Thickness Behavior of Sequentially Adsorbed Layers of Weak Polyelectrolytes.* Macromolecules, 2000. **33**(11): p. 4213-4219.
158. Mauser, T., et al., *Microcapsules Made of Weak Polyelectrolytes: Templating and Stimuli-Responsive Properties.* Langmuir, 2006. **22**(13): p. 5888-5893.
159. Fery, A., et al., *Nanoporous Thin Films Formed by Salt-Induced Structural Changes in Multilayers of Poly(acrylic acid) and Poly(allylamine).* Langmuir, 2001. **17**(13): p. 3779-3783.
160. Zhang, L., et al., *Layer-by-Layer Assembly of Salt-Containing Polyelectrolyte Complexes for the Fabrication of Dewetting-Induced Porous Coatings.* Langmuir, 2011. **27**(4): p. 1346-1352.
161. Salomäki, M., et al., *The Hofmeister Anion Effect and the Growth of Polyelectrolyte Multilayers.* Langmuir, 2004. **20**(9): p. 3679-3683.
162. McAloney, R.A., V. Dudnik, and M.C. Goh, *Kinetics of Salt-Induced Annealing of a Polyelectrolyte Multilayer Film Morphology.* Langmuir, 2003. **19**(9): p. 3947-3952.
163. O'Neal, J.T., et al., *QCM-D Investigation of Swelling Behavior of Layer-by-Layer Thin Films upon Exposure to Monovalent Ions.* Langmuir, 2018. **34**(3): p. 999-1009.
164. Mjahed, H., et al., *Hole formation induced by ionic strength increase in exponentially growing multilayer films.* Soft Matter, 2009. **5**(11): p. 2269-2276.
165. Anandhakumar, S., P. Gokul, and A.M. Raichur, *Stimuli-responsive weak polyelectrolyte multilayer films: A thin film platform for self triggered multi-drug delivery.* Materials Science and Engineering: C, 2016. **58**: p. 622-628.
166. Tan, H.L., et al., *Temperature Dependence of Polyelectrolyte Multilayer Assembly.* Langmuir, 2003. **19**(22): p. 9311-9314.
167. Salomäki, M., I.A. Vinokurov, and J. Kankare, *Effect of Temperature on the Buildup of Polyelectrolyte Multilayers.* Langmuir, 2005. **21**(24): p. 11232-11240.

168. Tan, W.S., et al., *Temperature-Induced, Reversible Swelling Transitions in Multilayers of a Cationic Triblock Copolymer and a Polyacid.* Macromolecules, 2010. **43**(4): p. 1950-1957.
169. Kujawa, P., et al., *Effect of Molecular Weight on the Exponential Growth and Morphology of Hyaluronan/Chitosan Multilayers: A Surface Plasmon Resonance Spectroscopy and Atomic Force Microscopy Investigation.* Journal of the American Chemical Society, 2005. **127**(25): p. 9224-9234.
170. Sun, B., et al., *Assembly of Multilayered Films Using Well-Defined, End-Labeled Poly(acrylic acid): Influence of Molecular Weight on Exponential Growth in a Synthetic Weak Polyelectrolyte System.* Langmuir, 2007. **23**(16): p. 8452-8459.
171. Poptoshev, E., B. Schoeler, and F. Caruso, *Influence of Solvent Quality on the Growth of Polyelectrolyte Multilayers.* Langmuir, 2004. **20**(3): p. 829-834.
172. Wang, L., et al., *A new approach for the fabrication of an alternating multilayer film of poly(4-vinylpyridine) and poly(acrylic acid) based on hydrogen bonding.* Macromolecular Rapid Communications, 1997. **18**(6): p. 509-514.
173. Quinn, J.F., et al., *Next generation, sequentially assembled ultrathin films: beyond electrostatics.* Chemical Society Reviews, 2007. **36**(5): p. 707-718.
174. Kharlampieva, E. and S.A. Sukhishvili, *Hydrogen-Bonded Layer-by-Layer Polymer Films.* Journal of Macromolecular Science, Part C, 2006. **46**(4): p. 377-395.
175. Kharlampieva, E., et al., *Hydrogen-Bonded Multilayers of Thermoresponsive Polymers.* Macromolecules, 2005. **38**(25): p. 10523-10531.
176. Sundaramurthy, A., et al., *Hydrogen Bonded Multilayer Films Based on Poly(2-oxazoline)s and Tannic Acid.* Advanced Healthcare Materials, 2014. **3**(12): p. 2040-2047.
177. Sukhishvili, S.A. and S. Granick, *Layered, Erasable, Ultrathin Polymer Films.* Journal of the American Chemical Society, 2000. **122**(39): p. 9550-9551.
178. Sukhishvili, S.A. and S. Granick, *Layered, Erasable Polymer Multilayers Formed by Hydrogen-Bonded Sequential Self-Assembly.* Macromolecules, 2002. **35**(1): p. 301-310.
179. Such, G.K., A.P.R. Johnston, and F. Caruso, *Engineered hydrogen-bonded polymer multilayers: from assembly to biomedical applications.* Chemical Society Reviews, 2011. **40**(1): p. 19-29.
180. Erel, I., H. Schlaad, and A.L. Demirel, *Effect of structural isomerism and polymer end group on the pH-stability of hydrogen-bonded multilayers.* Journal of Colloid and Interface Science, 2011. **361**(2): p. 477-482.
181. Yang, S., et al., *The influence of pH on a hydrogen-bonded assembly film.* Soft Matter, 2007. **3**(4): p. 463-469.
182. Erel-Unal, I. and S.A. Sukhishvili, *Hydrogen-Bonded Hybrid Multilayers: Film Architecture Controls Release of Macromolecules.* Macromolecules, 2008. **41**(22): p. 8737-8744.
183. Erel-Unal, I. and S.A. Sukhishvili, *Hydrogen-Bonded Multilayers of a Neutral Polymer and a Polyphenol.* Macromolecules, 2008. **41**(11): p. 3962-3970.
184. Erel, I., et al., *Hydrogen-bonded layer-by-layer films of block copolymer micelles with pH-responsive cores.* Journal of Colloid and Interface Science, 2011. **355**(1): p. 61-69.
185. Quinn, J.F. and F. Caruso, *Facile Tailoring of Film Morphology and Release Properties Using Layer-by-Layer Assembly of Thermoresponsive Materials.* Langmuir, 2004. **20**(1): p. 20-22.
186. Zhuk, A., S. Pavlukhina, and S.A. Sukhishvili, *Hydrogen-Bonded Layer-by-Layer Temperature-Triggered Release Films.* Langmuir, 2009. **25**(24): p. 14025-14029.
187. Ma, J., et al., *Effect of temperature on the build-up and post hydrothermal processing of hydrogen-bonded PVPON/PAA film.* Soft Matter, 2011. **7**(19): p. 9435-9443.
188. da Fonseca Antunes, A.B., et al., *Hydrogen bonded polymeric multilayer films assembled below and above the cloud point temperature.* Chemical Communications, 2013. **49**(83): p. 9663-9665.

189. Yang, S., et al., *Water uptake behavior of hydrogen-bonded PVPON–PAA LBL film.* Soft Matter, 2006. **2**(8): p. 699-704.
190. Lee, H., et al., *Strategies for Hydrogen Bonding Based Layer-by-Layer Assembly of Poly(vinyl alcohol) with Weak Polyacids.* Macromolecules, 2012. **45**(1): p. 347-355.
191. Guan, Y., et al., *Fabry–Perot Fringes and Their Application To Study the Film Growth, Chain Rearrangement, and Erosion of Hydrogen-Bonded PVPON/PAA Films.* The Journal of Physical Chemistry B, 2006. **110**(27): p. 13484-13490.
192. DeLongchamp, D.M. and P.T. Hammond, *Highly Ion Conductive Poly(ethylene oxide)-Based Solid Polymer Electrolytes from Hydrogen Bonding Layer-by-Layer Assembly.* Langmuir, 2004. **20**(13): p. 5403-5411.
193. Quinn, J.F. and F. Caruso, *Thermoresponsive Nanoassemblies: Layer-by-Layer Assembly of Hydrophilic–Hydrophobic Alternating Copolymers.* Macromolecules, 2005. **38**(8): p. 3414-3419.
194. Lin, W., et al., *Salt-induced erosion of hydrogen-bonded layer-by-layer assembled films.* Soft Matter, 2009. **5**(4): p. 860-867.
195. Mehrotra, S., et al., *Time Controlled Protein Release from Layer-by-Layer Assembled Multilayer Functionalized Agarose Hydrogels.* Advanced functional materials, 2010. **20**(2): p. 247-258.
196. Kim, B.-S., S.W. Park, and P.T. Hammond, *Hydrogen-Bonding Layer-by-Layer-Assembled Biodegradable Polymeric Micelles as Drug Delivery Vehicles from Surfaces.* ACS Nano, 2008. **2**(2): p. 386-392.
197. Kharlampieva, E. and S.A. Sukhishvili, *Release of a Dye from Hydrogen-Bonded and Electrostatically Assembled Polymer Films Triggered by Adsorption of a Polyelectrolyte.* Langmuir, 2004. **20**(22): p. 9677-9685.
198. Liu, F., et al., *Encapsulation of anticancer drug by hydrogen-bonded multilayers of tannic acid.* Soft Matter, 2014. **10**(46): p. 9237-9247.
199. Wohl, B.M. and J.F.J. Engbersen, *Responsive layer-by-layer materials for drug delivery.* Journal of Controlled Release, 2012. **158**(1): p. 2-14.
200. Ding, Z., et al., *Layer-by-layer multilayer films linked with reversible boronate ester bonds with glucose-sensitivity under physiological conditions.* Soft Matter, 2009. **5**(11): p. 2302-2309.
201. Swiston, A.J., et al., *Surface Functionalization of Living Cells with Multilayer Patches.* Nano Letters, 2008. **8**(12): p. 4446-4453.
202. He, T., et al., *Stable pH responsive layer-by-layer assemblies of partially hydrolysed poly(2-ethyl-2-oxazoline) and poly(acrylic acid) for effective prevention of protein, cell and bacteria surface attachment.* Colloids and Surfaces B: Biointerfaces, 2018. **161**: p. 269-278.
203. Hendessi, S., et al., *Hydrogen bonded multilayers of poly(2-ethyl-2-oxazoline) stabilized silver nanoparticles and tannic acid.* European Polymer Journal.
204. Kotov, N.A., *The Fourth International Conference on Nanostructured Materials (NANO '98)Layer-by-layer self-assembly: The contribution of hydrophobic interactions.* Nanostructured Materials, 1999. **12**(5): p. 789-796.
205. Clark, S.L. and P.T. Hammond, *The Role of Secondary Interactions in Selective Electrostatic Multilayer Deposition.* Langmuir, 2000. **16**(26): p. 10206-10214.
206. Li, C., et al., *Controlling the growth behaviour of multilayered films vialayer-by-layer assembly with multiple interactions.* Physical Chemistry Chemical Physics, 2009. **11**(39): p. 8835-8840.
207. Serizawa, T., S. Hashiguchi, and M. Akashi, *Stepwise Assembly of Ultrathin Poly(vinyl alcohol) Films on a Gold Substrate by Repetitive Adsorption/Drying Processes.* Langmuir, 1999. **15**(16): p. 5363-5368.
208. Guyomard, A., G. Muller, and K. Glinel, *Buildup of Multilayers Based on Amphiphilic Polyelectrolytes.* Macromolecules, 2005. **38**(13): p. 5737-5742.

209. Zhao, J., et al., *Fabrication of Ultrathin Membrane via Layer-by-Layer Self-assembly Driven by Hydrophobic Interaction Towards High Separation Performance.* ACS Applied Materials & Interfaces, 2013. **5**(24): p. 13275-13283.
210. Le Tirilly, S., et al., *Interplay of Hydrogen Bonding and Hydrophobic Interactions to Control the Mechanical Properties of Polymer Multilayers at the Oil–Water Interface.* ACS Macro Letters, 2015. **4**(1): p. 25-29.
211. Wang, X., et al., *Biomaterial Coatings by Stepwise Deposition of Silk Fibroin.* Langmuir, 2005. **21**(24): p. 11335-11341.
212. Shchepelina, O., et al., *Silk-on-silk layer-by-layer microcapsules.* Advanced materials (Deerfield Beach, Fla.), 2011. **23**(40): p. 4655-4660.
213. Uhrich, K.E., et al., *Polymeric Systems for Controlled Drug Release.* Chemical Reviews, 1999. **99**(11): p. 3181-3198.
214. Ravi Kumar, M.N.V. and N. Kumar§, *Polymeric Controlled Drug-Delivery Systems: Perspective Issues and Opportunities.* Drug Development and Industrial Pharmacy, 2001. **27**(1): p. 1-30.
215. Lee, J.H. and Y. Yeo, *Controlled drug release from pharmaceutical nanocarriers.* Chemical Engineering Science, 2015. **125**: p. 75-84.
216. Dash, S., et al., *KINETIC MODELING ON DRUG RELEASE FROM CONTROLLED DRUG DELIVERY SYSTEMS.* Acta Poloniae Pharmaceutica, 2010. **67**(3): p. 217-223.
217. Kamaly, N., et al., *Degradable Controlled-Release Polymers and Polymeric Nanoparticles: Mechanisms of Controlling Drug Release.* Chemical Reviews, 2016. **116**(4): p. 2602-2663.
218. Pavlukhina, S. and S. Sukhishvili, *Polymer assemblies for controlled delivery of bioactive molecules from surfaces.* Advanced Drug Delivery Reviews, 2011. **63**(9): p. 822-836.
219. Berg, M.C., et al., *Controlled Drug Release from Porous Polyelectrolyte Multilayers.* Biomacromolecules, 2006. **7**(1): p. 357-364.
220. Macdonald, M., et al., *Release of a Model Protein from Biodegradable Self Assembled Films for Surface Delivery Applications.* Journal of controlled release : official journal of the Controlled Release Society, 2008. **131**(3): p. 228-234.
221. Zhou, L., et al., *Release of Polyphenolic Drugs from Dynamically Bonded Layer-by-Layer Films.* ACS Applied Materials & Interfaces, 2013. **5**(9): p. 3541-3548.
222. Tomita, S., K. Sato, and J.-i. Anzai, *Layer-by-layer assembled thin films composed of carboxyl-terminated poly(amidoamine) dendrimer as a pH-sensitive nano-device.* Journal of Colloid and Interface Science, 2008. **326**(1): p. 35-40.
223. Yuan, Q., et al., *Rhodamine loading and releasing behavior of hydrogen-bonded poly(vinylpyrrolidone)/poly(acrylic acid) film.* Colloids and Surfaces A: Physicochemical and Engineering Aspects, 2014. **456**: p. 153-159.
224. Bag, E., et al., *Hydrogen-Bonded Multilayers With Controllable pH-Induced Disintegration Kinetics for Controlled Release Applications From Surfaces.* Journal of Macromolecular Science, Part A, 2015. **52**(4): p. 286-298.
225. Erel, I., et al., *Hydrogen-bonded multilayers of micelles of a dually responsive dicationic block copolymer.* Soft Matter, 2012. **8**(3): p. 827-836.
226. Haktaniyan, M., et al., *pH- and temperature-induced release of doxorubicin from multilayers of poly(2-isopropyl-2-oxazoline) and tannic acid.* Polymer International, 2017. **66**(12): p. 1851-1863.
227. Zhao, Y.-N., et al., *Zero-order release of polyphenolic drugs from dynamic, hydrogen-bonded LBL films.* Soft Matter, 2016. **12**(4): p. 1085-1092.
228. Zhu, Z. and S.A. Sukhishvili, *Temperature-Induced Swelling and Small Molecule Release with Hydrogen-Bonded Multilayers of Block Copolymer Micelles.* ACS Nano, 2009. **3**(11): p. 3595-3605.

229. Zhu, Z., et al., *Temperature-triggered on-demand drug release enabled by hydrogen-bonded multilayers of block copolymer micelles.* Journal of Controlled Release, 2013. **171**(1): p. 73-80.
230. Paramasivam, G., et al., *Hydrogen bonded capsules by layer-by-layer assembly of tannic acid and poly(2-n-propyl-2-oxazoline) for encapsulation and release of macromolecules.* Journal of Materials Chemistry B, 2017. **5**(45): p. 8967-8974.
231. Palanisamy, A., V. Albright, and S.A. Sukhishvili, *Upper Critical Solution Temperature Layer-by-Layer Films of Polyamino acid-Based Micelles with Rapid, On-Demand Release Capability.* Chemistry of Materials, 2017. **29**(21): p. 9084-9094.
232. Kajdič, S., et al., *Electrospun nanofibers for customized drug-delivery systems.* Journal of Drug Delivery Science and Technology, 2019. **51**: p. 672-681.
233. Kim, K., et al., *Incorporation and controlled release of a hydrophilic antibiotic using poly(lactide-co-glycolide)-based electrospun nanofibrous scaffolds.* Journal of Controlled Release, 2004. **98**(1): p. 47-56.
234. Luong-Van, E., et al., *Controlled release of heparin from poly(ε-caprolactone) electrospun fibers.* Biomaterials, 2006. **27**(9): p. 2042-2050.
235. Zeng, J., et al., *Biodegradable electrospun fibers for drug delivery.* Journal of Controlled Release, 2003. **92**(3): p. 227-231.
236. Kenawy, E.-R., et al., *Release of tetracycline hydrochloride from electrospun poly(ethylene-co-vinylacetate), poly(lactic acid), and a blend.* Journal of Controlled Release, 2002. **81**(1): p. 57-64.
237. Tran, T., et al., *Temperature and pH Responsive Microfibers for Controllable and Variable Ibuprofen Delivery.* Advances in Materials Science and Engineering, 2015. **2015**: p. 6.
238. Thakur, R.A., et al., *Electrospun nanofibrous polymeric scaffold with targeted drug release profiles for potential application as wound dressing.* International Journal of Pharmaceutics, 2008. **364**(1): p. 87-93.
239. Huhtamäki, T., et al., *Surface-wetting characterization using contact-angle measurements.* Nature Protocols, 2018. **13**(7): p. 1521-1538.
240. Chiu, M.H. and E.J. Prenner, *Differential scanning calorimetry: An invaluable tool for a detailed thermodynamic characterization of macromolecules and their interactions.* Journal of pharmacy & bioallied sciences, 2011. **3**(1): p. 39-59.
241. Chiad, K., et al., *Isothermal Titration Calorimetry: A Powerful Technique To Quantify Interactions in Polymer Hybrid Systems.* Macromolecules, 2009. **42**(19): p. 7545-7552.
242. Adatoz, E.B., et al., *Restructuring of poly(2-ethyl-2-oxazoline)/tannic acid multilayers into fibers.* Soft Matter, 2018. **14**(19): p. 3849-3857.
243. Huang, C., et al., *Stimuli-responsive electrospun fibers and their applications.* Chemical Society Reviews, 2011. **40**(5): p. 2417-2434.
244. Myshakina, N.S., Z. Ahmed, and S.A. Asher, *Dependence of Amide Vibrations on Hydrogen Bonding.* The Journal of Physical Chemistry B, 2008. **112**(38): p. 11873-11877.
245. Liao, K.-S., et al., *Designing Surfaces with Wettability That Varies in Response to Solute Identity and Concentration.* Langmuir, 2009. **25**(1): p. 26-28.
246. Wong, J.E., et al., *Specific Ion versus Electrostatic Effects on the Construction of Polyelectrolyte Multilayers.* Langmuir, 2009. **25**(24): p. 14061-14070.
247. Liu, G., et al., *Specific Anion Effects on the Growth of a Polyelectrolyte Multilayer in Single and Mixed Electrolyte Solutions Investigated with Quartz Crystal Microbalance.* The Journal of Physical Chemistry B, 2010. **114**(31): p. 9987-9993.
248. Tang, K. and N.A.M. Besseling, *Formation of polyelectrolyte multilayers: ionic strengths and growth regimes.* Soft Matter, 2016. **12**(4): p. 1032-1040.

249. Zhang, L., H. Guo, and J. Sun, *Salt effects on the structural tailoring of layer-by-layer assembled polyelectrolyte complexes and salt-containing polyelectrolyte films.* Thin Solid Films, 2018. **653**: p. 258-266.
250. Kharlampieva, E., D. Pristinski, and S.A. Sukhishvili, *Hydrogen-Bonded Multilayers of Poly(carboxybetaine)s.* Macromolecules, 2007. **40**(19): p. 6967-6972.
251. Selin, V., J.F. Ankner, and S.A. Sukhishvili, *Nonlinear Layer-by-Layer Films: Effects of Chain Diffusivity on Film Structure and Swelling.* Macromolecules, 2017. **50**(16): p. 6192-6201.
252. Selin, V., J.F. Ankner, and S.A. Sukhishvili, *Ionically Paired Layer-by-Layer Hydrogels: Water and Polyelectrolyte Uptake Controlled by Deposition Time.* Gels, 2018. **4**(1): p. 7.
253. Ishida, N. and S. Biggs, *Salt-Induced Structural Behavior for Poly(N-isopropylacryamide) Grafted onto Solid Surface Observed Directly by AFM and QCM-D.* Macromolecules, 2007. **40**(25): p. 9045-9052.
254. Costa, E., et al., *Tannic Acid Mediated Suppression of PNIPAAm Microgels Thermoresponsive Behavior.* Macromolecules, 2011. **44**(3): p. 612-621.
255. Cho, Y., et al., *Effects of Hofmeister anions on the phase transition temperature of elastin-like polypeptides.* The journal of physical chemistry. B, 2008. **112**(44): p. 13765-13771.
256. Wang, C., et al., *Thermoresponsive polymeric nanoparticles based on poly(2-oxazoline)s and tannic acid.* Journal of Polymer Science Part A: Polymer Chemistry, 2018. **56**(14): p. 1520-1527.
257. Wang, Y. and S.A. Sukhishvili, *All-Aqueous Nanoprecipitation: Spontaneous Formation of Hydrogen-Bonded Nanoparticles and Nanocapsules Mediated by Phase Separation of Poly(N-Isopropylacrylamide).* Macromolecular Rapid Communications, 2017. **38**(16): p. 1700242.
258. Zeinali, E., V. Haddadi-Asl, and H. Roghani-Mamaqani, *Nanocrystalline cellulose grafted random copolymers of N-isopropylacrylamide and acrylic acid synthesized by RAFT polymerization: effect of different acrylic acid contents on LCST behavior.* RSC Advances, 2014. **4**(59): p. 31428-31442.
259. Zhou, J., M.V. Pishko, and J.L. Lutkenhaus, *Thermoresponsive Layer-by-Layer Assemblies for Nanoparticle-Based Drug Delivery.* Langmuir, 2014. **30**(20): p. 5903-5910.
260. Lei, L., et al., *Zero-order release of 5-fluorouracil from PCL-based films featuring trilayered structures for stent application.* European Journal of Pharmaceutics and Biopharmaceutics, 2011. **78**(1): p. 49-57.
261. Acharya, G. and K. Park, *Mechanisms of controlled drug release from drug-eluting stents.* Advanced Drug Delivery Reviews, 2006. **58**(3): p. 387-401.
262. Tang, Z., et al., *Biomedical Applications of Layer-by-Layer Assembly: From Biomimetics to Tissue Engineering.* Advanced Materials, 2006. **18**(24): p. 3203-3224.
263. Gentile, P., et al., *Layer-by-layer assembly for biomedical applications in the last decade.* Nanotechnology, 2015. **26**(42).
264. Zhang, X., H. Chen, and H. Zhang, *Layer-by-layer assembly: from conventional to unconventional methods.* Chemical Communications, 2007(14): p. 1395-1405.
265. Chung, A.J. and M.F. Rubner, *Methods of Loading and Releasing Low Molecular Weight Cationic Molecules in Weak Polyelectrolyte Multilayer Films.* Langmuir, 2002. **18**(4): p. 1176-1183.
266. Yuan, W. and C.M. Li, *Exponentially growing layer-by-layer assembly to fabricate pH-responsive hierarchical nanoporous polymeric film and its superior controlled release performance.* Chemical Communications, 2010. **46**(48): p. 9161-9163.
267. Burke, S.E. and C.J. Barrett, *pH-Dependent Loading and Release Behavior of Small Hydrophilic Molecules in Weak Polyelectrolyte Multilayer Films.* Macromolecules, 2004. **37**(14): p. 5375-5384.
268. Ritger, P.L. and N.A. Peppas, *A simple equation for description of solute release I. Fickian and non-fickian release from non-swellable devices in the form of slabs, spheres, cylinders or discs.* Journal of Controlled Release, 1987. **5**(1): p. 23-36.

269. Fujishige, S., K. Kubota, and I. Ando, *Phase transition of aqueous solutions of poly(N-isopropylacrylamide) and poly(N-isopropylmethacrylamide).* The Journal of Physical Chemistry, 1989. **93**(8): p. 3311-3313.
270. Futscher, M.H., et al., *The Role of Backbone Hydration of Poly(N-isopropyl acrylamide) Across the Volume Phase Transition Compared to its Monomer.* Scientific Reports, 2017. **7**(1): p. 17012.
271. Khutoryanskiy, V.V., *Hydrogen-bonded interpolymer complexes as materials for pharmaceutical applications.* International Journal of Pharmaceutics, 2007. **334**(1): p. 15-26.
272. Nurkeeva, Z.S., G.A. Mun, and V.V. Khutoryanskiy, *Interpolymer Complexes of Water-Soluble Nonionic Polysaccharides with Polycarboxylic Acids and Their Applications.* Macromolecular Bioscience, 2003. **3**(6): p. 283-295.
273. Staikos, G., K. Karayanni, and Y. Mylonas, *Complexation of polyacrylamide and poly(N-isopropylacrylamide) with poly(acrylic acid). The temperature effect.* Macromolecular Chemistry and Physics, 1997. **198**(9): p. 2905-2915.
274. Henke, A., et al., *The Structure and Aggregation of Hydrogen-Bonded Interpolymer Complexes of Poly(acrylic acid) With Poly(N-vinylpyrrolidone) in Dilute Aqueous Solution.* Macromolecular Chemistry and Physics, 2011. **212**(23): p. 2529-2540.
275. Vasile, C., et al., *Hydrogen-bonding interaction of an alternating maleic acid–vinyl acetate copolymer with poly(ethylene glycol), polyacrylamide and poly(N-isopropylacrylamide): a comparative study.* Polymer International, 2003. **52**(12): p. 1887-1891.
276. Hendessi, S., et al., *Hydrogen bonded multilayers of poly(2-ethyl-2-oxazoline) stabilized silver nanoparticles and tannic acid.* European Polymer Journal, 2017. **88**: p. 666-678.
277. Wilson, P., et al., *Poly(2-oxazoline)-based micro- and nanoparticles: A review.* European Polymer Journal, 2017. **88**: p. 486-515.
278. Altıntaş, Z., et al., *Self-assembled poly(2-ethyl-2-oxazoline)/malonic acid hollow fibers in aqueous solutions.* European Polymer Journal, 2019. **120**: p. 109222.
279. Curiel, D., M. Más-Montoya, and G. Sánchez, *Complexation and sensing of dicarboxylate anions and dicarboxylic acids.* Coordination Chemistry Reviews, 2015. **284**: p. 19-66.
280. Alderighi, L., et al., *Hyperquad simulation and speciation (HySS): a utility program for the investigation of equilibria involving soluble and partially soluble species.* Coordination Chemistry Reviews, 1999. **184**(1): p. 311-318.
281. Kim, C., et al., *Complexation of Poly(2-ethyl-2-oxazoline)-block-poly(ε-caprolactone) Micelles with Multifunctional Carboxylic Acids.* Macromolecules, 2002. **35**(1): p. 193-200.
282. Ambreen, J., et al., *Effect of carbon chain length of monocarboxylic acids on cloud point temperature of poly(2-ethyl-2-oxazoline).* Colloid and Polymer Science, 2013. **291**(4): p. 919-925.
283. Güner, P.T., et al., *Self-assembled poly(2-ethyl-2-oxazoline) fibers in aqueous solutions.* Polymer Chemistry, 2012. **3**(2): p. 322-324.
284. Shao, X., et al., *Vacuum FTIR observation on hygroscopic properties and phase transition of malonic acid aerosols.* Chemical Physics, 2017. **483-484**: p. 7-11.
285. Qiu, P. and C. Mao, *Biomimetic Branched Hollow Fibers Templated by Self-Assembled Fibrous Polyvinylpyrrolidone Structures in Aqueous Solution.* ACS Nano, 2010. **4**(3): p. 1573-1579.
286. Bizley, S.C., A.C. Williams, and V.V. Khutoryanskiy, *Thermodynamic and kinetic properties of interpolymer complexes assessed by isothermal titration calorimetry and surface plasmon resonance.* Soft Matter, 2014. **10**(41): p. 8254-8260.
287. Sundaramurthy, A., et al., *Hydrogen Bonded Multilayer Films Based on Poly(2-oxazoline)s and Tannic Acid.* Advanced Healthcare Materials, 2014. **3**(12): p. 2040-2047.
288. Caires, F.J., et al., *Thermal behaviour of malonic acid, sodium malonate and its compounds with some bivalent transition metal ions.* Thermochimica Acta, 2010. **497**(1): p. 35-40.

289. Campoli-Richards, D.M., et al., *Ciprofloxacin.* Drugs, 1988. **35**(4): p. 373-447.
290. Davis, R., A. Markham, and J.A. Balfour, *Ciprofloxacin.* Drugs, 1996. **51**(6): p. 1019-1074.
291. Koort, J.K., et al., *Sustained release of ciprofloxacin from an osteoconductive poly(DL)-lactide implant.* Acta Orthopaedica, 2008. **79**(2): p. 295-301.
292. Bentz, K.C. and D.A. Savin, *Hollow polymer nanocapsules: synthesis, properties, and applications.* Polymer Chemistry, 2018. **9**(16): p. 2059-2081.
293. Chen, Y., et al., *Hollow Core–Porous Shell Structure Poly(acrylic acid) Nanogels with a Superhigh Capacity of Drug Loading.* ACS Applied Materials & Interfaces, 2010. **2**(12): p. 3532-3538.